# Stability of Lithium doped Magnesium Oxide and Zinc Oxide Catalysts for the Conversion of Natural Gas

vorgelegt von
Diplom-Chemiker
Sebastian Arndt
geboren in Meiningen

Von der Fakultät II - Mathematik und Naturwissenschaften
der Technischen Universität Berlin
zur Erlangung des akademischen Grades
Doktor der Naturwissenschaften
Dr.rer.nat

genehmigte Dissertation

Promotionsausschuss:

Vorsitzender: Prof. Dr. rer. nat. Arne Thomas

Berichter: Prof. Dr. rer. nat. Reinhard Schomäcker

Berichter: Prof. em. Dr. rer. nat. Manfred Baerns

Tag der wissenschaftlichen Aussprache: 02.12.2010

Berlin 2010

D 83

**Zusammenfassung**

Der Hauptbestandteil von Erdgas ist Methan, dessen Reserven denen von Erdöl gleichkommen. Aufgrund der großen Erdgasreserven ist die Umwandlung von Methan in andere Produkte der chemischen Wertschöpfungskette von großem wirtschaftlichen Interesse. Die direkte Umwandlung von Methan ist schwierig und bisher noch nicht gelungen, da es der stabilste Kohlenwasserstoff ist. Ein möglicher Prozess ist die oxidative Kupplung von Methan, hierbei wird Methan, unter Abspaltung von Wasser, zu Ethan oder Ethylen verbunden.

Ein sehr intensiv untersuchter Katalysator für diese Reaktion ist Li-dotiertes MgO. Doch trotz der sehr intensiven Forschungen bleibt die Frage nach dem aktiven Zentrum und dessen Struktur, der Stabilität des Katalysators und der Beziehung zwischen Struktur und Reaktivität unbeantwortet.

In dieser Arbeit wird die bekannte Literatur zu Li/MgO ausführlich zusammengefaßt und kritisch bewertet. Detailliertes Literaturstudium zeigt, daß der bekannte Reaktionsmechanismus, vorgeschlagen von Lunsford *et al.*, nicht auf adäquaten experimentellen Beweisen fußt.

Ausführliche experimentelle Untersuchungen zur Stabilität von Li/MgO wurden durchgeführt. Die Präparation erfolgte auf vier verschiedenen Syntheserouten mit dem Ziel ein Material zu finden, daß unter den anspruchsvollen Reaktionsbedinungen der oxidative Methankupplung stabil ist. Zusätzlich wurde zu verschiedenen Zeitpunkten während der Reaktion eine detaillierte Strukturanalytik durchgeführt. Es zeigte sich, daß alle präparierten Li/MgO Katalysatoren instabil sind und deaktiviert, unabhängig von der Präparationsmethode und auch nach 40 Stunden im Reaktor wurde kein stationärer Zustand erreicht. Die Aktivität der verschiedenen Katalysatoren unterschied sich jedoch nach 40 Stunden nicht sehr stark, was darauf deutet, daß im stationären Zustand die Katalysatoren sich nicht mehr stark unterschieden. Aufgrund der starken Deaktivierung ist Li/MgO für eine industrielle Anwendung ungeeignet.

Als mögliche Alternative zu Li/MgO wird Zinkoxid in der Literatur erwähnt. Die Aktivität von ZnO, rein, Li-dotiert und geträgert auf kommerziellen Trägern für die Aktivierung von Propan, Ethan und Methan wurde untersucht. Auch hier zeigte sich, daß ungeträgertes ZnO unter den Reaktionsbedinungen der untersuchten Reaktionen nicht stabil ist. Die Trägerung führte ebenfalls zu keiner deutlichen Verbesserung der Stabilität, da das ZnO mit den Trägern reagierte und neue Verbindungen bildete.

**Schlagwörter:**
Oxidative Kupplung von Methan, Li/MgO, ZnO, Katalysatorstabilität

## Abstract

The main component of natural gas is methane, with known resources rivaling those of crude oil. A process, which could convert methane into value added products is therefore of big economical interest. Methane is the most stable hydrocarbon, hence, its direct conversion is difficult and has not been achieved yet. A possible process is the oxidative coupling of methane, in which methane is coupled to ethane or ethylene under the elimination of water.

An intensively investigated catalyst for this reaction is Li-doped MgO. The questions about the active center and its structure, the stability of the catalyst and the relationship between the structure and reactivity remain unanswered despite the intensive research.

In this work, the existing literature of Li/MgO is summarized in detail and critically assessed. Detailed literature studies revealed that the reaction mechanism, as proposed by Lunsford *et al.*, is not based on appropriate experimental evidence.

Detailed experimental investigations on the stability of Li/MgO were done. The preparation was carried out on four different synthetic routes with the aim to find a material which is stable under the harsh reaction conditions of the oxidative coupling of methane. Additionally, detailed structural analysis at different times of the reaction was performed. It was found that all Li/MgO materials are instable and deactivate irrespective of the preparation, and even after 40 hours time on stream no steady state was reached. However, after 40hours time on stream, the activity of the differently prepared samples did not differ strongly anymore, indicating that in steady state the samples are the same. Due to the severe deactivation, Li/MgO cannot be considered to be a candidate for an industrial application.

Zinc oxide is discussed in the literature as possible alternative for Li/MgO. The activity of ZnO, pure, Li-doped and supported on commercial supports for the activation of propane, ethane and methane was investigated. It was found, that unsupported ZnO is not stable under the reaction conditions of all three investigated reactions. Supporting ZnO did not lead to a significant improvement of the stability because ZnO reacts with the support materials to form new compounds.



**Keywords:**
Oxidative Coupling of Methane, Li/MgO, ZnO, Catalyst Stability

für Viktor und Haimanti

# Contents

# Chapter 1

# Introduction

The fossil fuels on the earth are coal (as lignite and anthracite), crude oil and natural gas. The proven reserves and the geological distribution is shown in Table 1.1 [1]. Coal has the largest proven reserves and it has the broadest global distribution. Only the Middle East has no significant resources of coal. The proven resources of natural gas and crude oil are much smaller compared to the ones of coal.

| Area | Coal | Crude Oil | Natural Gas |
|---|---|---|---|
| North America | 250,510 Mt | 9,500 Mt | 7,980 B cm |
| South & Central America | 16,276 Mt | 15,900 Mt | 7,730 B cm |
| Europe & Central Asia | 272,446 Mt | 8,500 Mt | 14,760 B cm |
| Russian Federation | 157,010 Mt | 10,900 Mt | 44,650 B cm |
| Middle East | 1,386 Mt | 102,900 Mt | 73,210 B cm |
| Africa | 49,605 Mt | 15,600 Mt | 14,580 B cm |
| Asia Pacific | 257,465 Mt | 5,400 Mt | 14,460 B cm |
| Total | 1,004,698 Mt | 168,700 Mt | 177,370 B cm |

Table 1.1: The geological distribution of the fossil fuels coal (as lignite and anthracite), crude oil and natural gas in the world (Mt = million tons, B cm = billion cubic meter.

The resources of crude oil are mainly concentrated in the Middle East, while natural gas is more widespread than crude oil. The big deposits of natural gas are still in the Middle East and the Russian Federation, but other parts of the world also have nameable reserves of natural gas. The distribution of natural gas is shown in more detail in Figure 1.1.

Crude oil is currently the main source for liquid fuels and basic materials for the chemical industry. However, the resources of crude oil are declining and will be depleted in foreseeable future. To avoid a monopole of countries in the Gulf

region, it is necessary to find alternatives for the production of fuels and basic materials.

The conversion of coal into liquid fuels and petrochemical materials is an option since the known reserves of coal are large. The drawbacks are that these processes are costly, energy-consumptive and not environmentally friendly. Because of the large resources of natural gas, there is a growing interest in converting it into value added products. Furthermore, the main component of natural gas is also available from biogenic sources, via the fermentation, making it literally endlessly available.

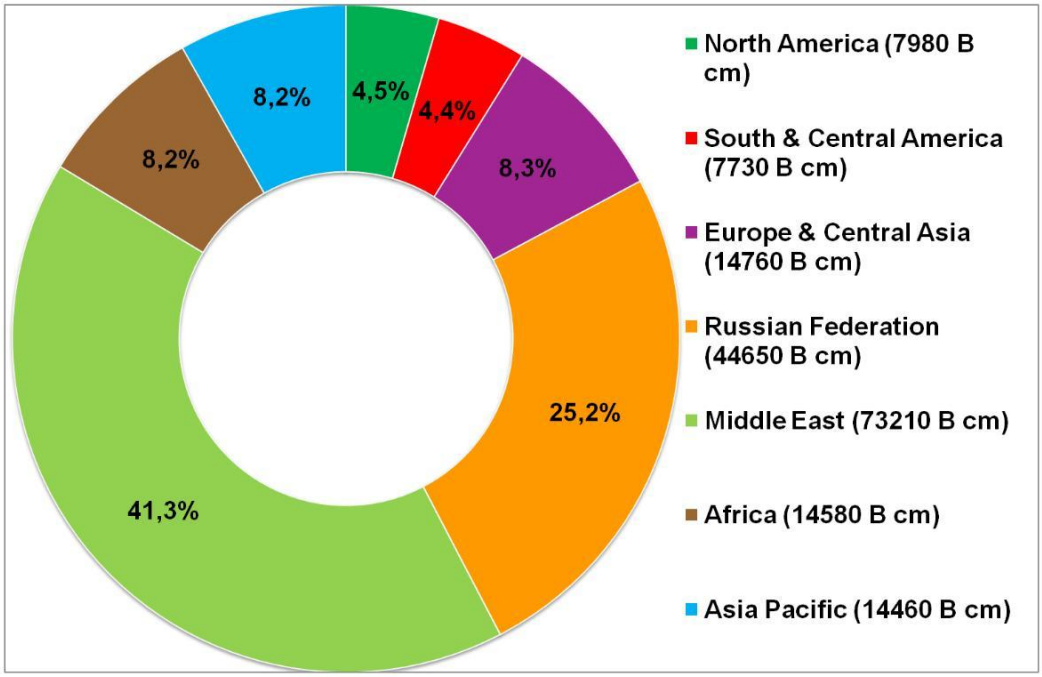


Figure 1.1: The distribution of the reserves of natural gas in the world. The number in brackets show the proven reserves in billion cubic meters (B cm) [1].

Methane is the main component of natural gas. The exact composition of natural gas depends on the geographical origin but the fraction of methane is usually above 90 %. Because of the large resources, a strong economic interest exists in converting methane into value added products. Currently methane is greatly underutilized, which is mainly due to two reasons. One is that much of the methane is found in remote areas, far away from the customers. The transport of gas requires pipelines, which are not always available and the liquification of natural gas is a costly process [2]. The other reason is that no economically attractive route for the conversion of methane in a large scale exists.

Two general strategies are possible for the conversion of methane [2]. In the indirect way, methane is first converted into synthesis gas, which is subsequently processed via Fischer Tropsch into the desired products. In the direct way, methane is directly converted into the desired compounds and the expensive and energy-consumptive synthesis gas step is circumvented. The possible direct ways are

1. the partial oxidation to methanol or formaldehyde,
2. the oxidative coupling to ethane and/or ethene,
3. and the non-oxidative conversion to aromatics.

The oxidative coupling of methane (OCM) has attracted much attention, since the first publications of Keller *et al.* [3] and Hinsen *et al.* [4]. Several books [5, 6], numerous reviews [7, 8, 9, 10, 11] and reams of articles have been published on this topic. Despite the intensive research, this process has not yet reached the stage of commercial application.

As methane is the most stable hydrocarbon, having the highest bond dissociation energy for the abstraction of a hydrogen [12, 13], the activation of methane and its conversion into value added products is difficult. Therefore, the required reaction temperatures are still too high and the catalysts are too unselective and unstable. The reaction mechanism, a mechanism with homogeneous and heterogeneous contributions, is also still not understood.

Li-doped MgO is a catalyst which has been the subject of intensive research in the OCM. The activity is reported to be relatively high, the preparation is reported to be simple and the system is suitable for surface science experiments and quantum chemical calculations. However, many contradictory results have been published and never been solved. Some of these contradictions are very severe, the reported well-understood catalyst Li-doped MgO can therefore be considered as not being understood.

This work is a contribution to the understanding of the function of Li-doped MgO and the quest for alternative catalysts. Due to the high number of publications dealing with Li-doped MgO, the available literature is comprehensively summarized and the contradictions and problems are shown. The detailed literature study revealed that the stability of the Li/MgO catalyst has been neglected in many studies, even so Li/MgO was discussed as a possible candidate for a commercial application. Therefore, the main aim of the experimental work regarding Li-doped MgO was the investigation of the stability and the reasons for the deactivation.

An alternative catalyst to Li/MgO could be ZnO, as it was found to be a suitable OCM catalyst, especially when doped with Li [14]. Moreover, it was proposed that the reaction mechanism and the active center of Li/MgO and Li/ZnO

are similar [15, 16]. However, not much is known about ZnO as catalyst for the C-H activation and the existing literature is scarce. The zinc oxide catalyst was investigated pure, Li-doped and supported on different commercial support materials for the appraisal of the usability as a catalyst for research and industrial purposes.

The investigation of catalysts requires large facilities for testing catalytic activities. Therefore a 6-fold parallel testing reactor was procured, started-up and test procedures were developed to manifold the testing facilities which were available at the beginning of this work.

# Chapter 2

# Li/MgO - The Drosophila Catalyst for Methane Oxidative Coupling. A Critical Assessment.

This work is being prepared for submission as: S. Arndt, G. Laugel, S. Levchenko, R. Horn, M. Baerns, M. Scheffler, R. Schlögl and R. Schomäcker, "Li/MgO - The Drosophila Catalyst for Methane Oxidative Coupling. A Critical Assessment." in Catalysis Reviews Science and Engineering.

## 2.1 Introduction

The resources of natural gas rival those of crude oil. The composition of natural gas depends on its origin, but the main component is always methane. Therefore, there is a large economical interest in making methane available as a carbon source for chemical industry.

A direct way for the conversion of methane into value added products is the oxidative coupling (OCM) to ethane or ethylene. The overall pathway is shown in Reaction 2.1. This reaction has attracted a lot of attention since the fundamental work of Keller *et al.* and Hinsen *et al.* [3, 4]. However, until now no economically viable process has been put into practice despite all efforts [5, 17, 18, 6].

$$\begin{aligned} CH_4 + 1/2 O_2 &\rightarrow 1/2 C_2H_4 + H_2O \\ \Delta_r H^{\ominus}(800^{\circ}C) &= -139 kJ/mol \\ \Delta_r G^{\ominus}(800^{\circ}C) &= -153 kJ/mol \end{aligned} \tag{2.1}$$

The coupling of methane without an oxidant is a highly endothermic reaction and due to thermodynamic constraint the conversion is limited. By introducing an

oxidizing agent, the process becomes exothermic and the thermodynamic restrictions can be overcome. However, from a thermodynamic point of view, the partial oxidation (Reaction 2.2) and the total oxidation (Reaction 2.3) are thermodynamically much more favored than the oxidative coupling of methane.

$$\begin{aligned} CH_4 + {}^3/_2 O_2 &\rightarrow CO + 2H_2O \\ \Delta_r H^{\ominus}(800^{\circ}C) &= -519 kJ/mol \\ \Delta_r G^{\ominus}(800^{\circ}C) &= -611 kJ/mol \end{aligned} \tag{2.2}$$

$$\begin{aligned} CH_4 + 2O_2 &\rightarrow CO_2 + 2H_2O \\ \Delta_r H^{\ominus}(800^{\circ}C) &= -801 kJ/mol \\ \Delta_r G^{\ominus}(800^{\circ}C) &= -801 kJ/mol \end{aligned} \tag{2.3}$$

To obtain reasonable yields of $C_2$ hydrocarbons ($C_2H_6$ and $C_2H_4$), the reaction must be controlled kinetically. For this, suitable catalysts are necessary. However, the known catalysts are not very active at low temperatures, thus the reaction requires temperatures between 700 - 900 $^{\circ}C$, which leads to low yields (due to consecutive $CO_x$ formation) and severe catalyst deactivation (due to decomposition or sintering, caused by the high reaction temperatures).

In the past, the research strategy was often characterized by random testing of catalysts with focus on maximization of the $C_2$ yield. This strategy has not led to a final break-through with respect to high selectivity and yield of $C_2$ hydrocarbons. Thus, studying only one catalytic system to understand the reasons for these limitations in detail is necessary. The outcome of this research may be the basis for further efforts in optimizing catalyst formulations and maximizing catalyst performance. At a later stage, high throughput testing of numerous different catalysts may be of advantage.

In the search for better catalysts hundreds of materials have been tested. Li-doped MgO showed higher performance than most other materials. Lunsford *et al.* were among the first to publish extensive details about this catalytic system [19, 20, 21]. Li-doped MgO was and still is the object of intensive studies for several research groups. Moreover, it is possible to perform quantum chemical studies and surface science experiments on Li-doped MgO, which is a rather difficult task for many other catalysts. Studies on MgO doped with other alkali metals did not lead to better catalysts [22, 23, 24, 25, 26, 27].

In spite of all the research which has been done, many aspects remain unclear. As it will be outlined in this review, the active center, the maximum solubility of Li in the MgO lattice, the position and nature of Li in the MgO, the stability of the

catalyst and many other questions are still not answered, despite the substantial amount of literature published on this topic. Therefore, identifying the points, that need further investigation is not easy. The aim of this article is to summaries the existing knowledge on Li/MgO and point out problems and unclarities which need further investigation.

This publication focuses on Li/MgO and where necessary on MgO. Further additives on Li/MgO are only discussed in Chapter 2.6.

## 2.2 Preparation of Li/MgO Catalysts

The preparation of the Li/MgO catalyst is crucial for its performance and many different methods have been used as described below.

### 2.2.1 Wet Impregnation

In the first publications from the Lunsford group [19, 20, 21], a suspension of $Li_2CO_3$ in deionized $H_2O$ was added to MgO. The slurry was stirred and heated until a thick paste remained, which was dried overnight at 140 °*C*. The obtained material was calcined for one to several hours at temperatures between 450 and 465 °*C* under flow of $O_2$.

Ross *et al.* synthesised Li/MgO via wet impregnation of MgO with an aqueous solution of LiOH [28]. The procedure was done under a stream of $CO_2$ for some samples. Afterwards, the samples were dried at 140 °*C*, calcined in air at various temperatures and then crushed and sieved.

Matsuura *et al.* prepared Li/MgO via adding $Li_2O$ to a suspension of ultra fine crystalline MgO in $C_2H_5OH$, followed by drying at 78 °*C* and calcination at 740 °*C* for 4 hours. The use of ultra fine crystalline MgO resulted in a catalyst with an exceptionally high activity for the OCM [29].

Choudhary and co-workers reported a highly stable Li/MgO, which showed no deactivation for 15 hours on stream (temperature: 750 °*C*, feed gas composition: $CH_4$:$O_2$ = 4:1, flow rate: 85 ml/min) [30]. This Li/MgO was prepared by impregnation of $Mg(CH_3COO)_2$ with aqueous $Li(CH_3COO)$ and subsequent calcination. The stability was attributed to the high content of $CO_2$, which reduced the loss of Li and improved the resistance against sintering of the catalyst.

The Li precursor was reported to play an important role in the nature of the surface species and the development of the specific surface of the Li/MgO catalyst [31, 32, 33]. Also the precursors for MgO (which was either obtained by thermal decomposition of hydroxy carbonates or the precipitation of nitrates) had an influence on the Li/MgO, indicating a “memory” effect of the catalyst with regard to the MgO precursor.

Choudhary *et al.* studied the influence of the precursors for $Li_2O$ and MgO for the surface and catalytic properties of Li/MgO in more detail [34]. They prepared the catalysts by thorough mixing of the precursor powders in deionized $H_2O$. The precursors for Li were nitrate, ethanoate and carbonate. For MgO, the precursors were nitrate, ethanoate, carbonate, oxide and hydroxides (MgO from $Mg(OH)_2$ was prepared using different Mg salts and precipitation agents). The amount of added water was just sufficient to form a thick paste. Subsequent drying at 120 $^{\circ}C$ for 4 hours and calcination at 750 $^{\circ}C$ for 6 hours followed. The $CH_4$ conversion, the $C_2$ yield ($C_2H_6$ + $C_2H_4$) and the $C_{2+}$ yield ($C_2H_6$ + $C_2H_4$ + higher hydrocarbons), comprising the formation of $C_2H_6$ and $C_2H_4$ for $C_2$ and the formation of all hydrocarbons in the case of $C_{2+}$, were reported for different temperatures, feed gas compositions and gas flows. In Figure 2.1 the reported data as described in Table 4 and 6 of reference [34] are plotted. The precursors for $Li_2O$ and MgO, had a strong effect on the surface area, the basicity, the $CO_2$ content and the catalytic performance, but a strong variation of the catalytic results was not observed. However, a direct relationship between these factors could not be observed. In agreement with other groups it was found, that catalysts with a high $CO_2$ content showed a better performance in the OCM.

Kuo and co-workers tried to increase the specific surface area of the Li/MgO via adding charcoal during the preparation (using a wet impregnation procedure of MgO with $Li_2CO_3$) and subsequent burning off during the calcination [35]. Indeed, the result was that the addition of charcoal did increase the surface area and it also modified the morphology of the Li/MgO, however no major improvement in terms of the yield was achieved.

### 2.2.2 Sol-Gel

López *et al.* prepared Li-doped MgO via a sol-gel method. They studied the effect of the pH value on the surface hydroxylation and characterized the prepared MgO [36]. It was found, that Li/MgO catalysts prepared via the sol-gel method had comparable activities to Li/MgO catalysts prepared by wet impregnation of commercial MgO, but significantly higher $C_2$ selectivities [37, 38].

Trionfetti and co-workers showed, that via sol-gel synthesis a high surface-area, nano-scale Li/MgO could be prepared, with low Li loadings [39, 40]. This procedure limited the formation of separate Li phases, therefore suppressing sintering and loss of surface area during thermal treatment. Furthermore, the application of high temperatures to incorporate Li into the MgO lattice could be avoided. It was reported that it had a strongly improved activity for the oxidative dehydrogenation (ODH) of $C_3H_8$ compared to Li/MgO prepared via wet impregnation.

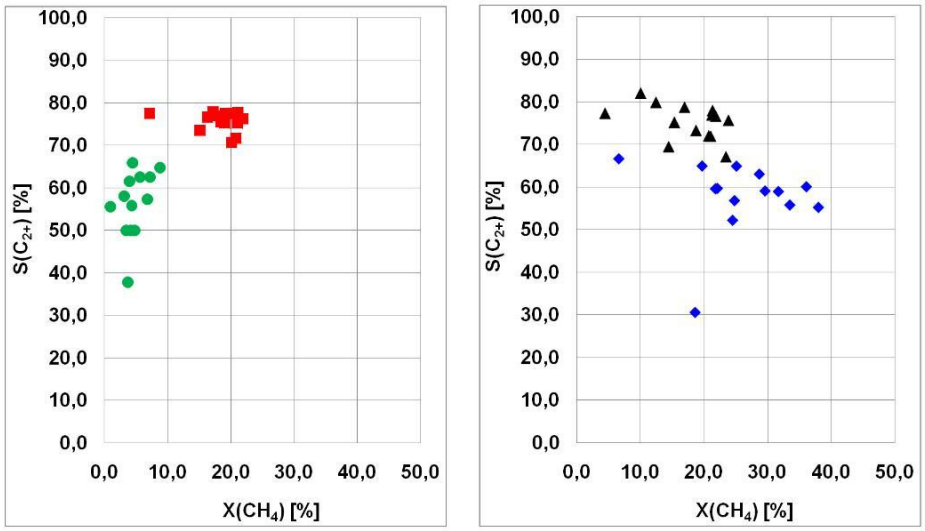


Figure 2.1: Left Part: The applied reaction conditions were 100 mg catalyst, $CH_4/O_2$ ratio 8.0 and a gas flow of 8.6 ml/min. The green circles were obtained at 650 $°C$, the red squares at 750 $°C$. The selectivity was calculated from the formula $S_{C_{2+}} = Y_{C_{2+}}/X_{CH_4}$. The plotted data are derived from Table 4 of [34]. Variations cannot be observed.
Right Part: The applied reaction conditions were 100 mg catalyst, temperature of 750 $°C$ and a gas flow of 17.1 ml/min. The blue diamonds were obtained at a $CH_4$ to $O_2$ ratio of 3.0 and the black triangles at a $CH_4$ to $O_2$ ratio of 8.0. The selectivity was calculated from the formula $S_{C_{2+}} = Y_{C_{2+}}/X_{CH_4}$. The plotted data are taken from Table 6 of [34]. Strong variations of the results can also not be observed.

### 2.2.3 Co-Precipitation

A precipitation procedure was described by Roussy and co-workers [41]. To an aqueous solution of $Mg(NO_3)_2$ and LiOH, oxalic acid was added until a pH of 2.2. The precipitate was obtained and dried at $120\,^{\circ}C$ and calcined at $750\,^{\circ}C$ under argon for 24 hours. The catalytic performance was compared for the cases of classical and micro-wave heating, showing a high improvement of the selectivity in case of micro-wave heating.

### 2.2.4 Organometallic

Chevalier *et al.* applied a surface organo-metallic approach for the preparation of Li/MgO [42]. The Li is introduced to the MgO surface via Li-neopentyl, as shown in Reaction 2.4.

$$Li\text{-}Neopentyl + Mg_{Surface}\text{-}OH \rightarrow Mg_{Surface}\text{-}O\text{-}Li + Neopentyl\text{-}H. \qquad (2.4)$$

In contrast to Lunsford, the applied preparation procedure led to a precursor catalyst, which did not contain anions such as carbonate species. The prepared catalyst was more active but less selective towards the formation of $C_2$ products than the Lunsford catalyst.

The group of Driess applied a single source precursors approach. They prepared magnesium alkoxide clusters, which were thermally decomposed. The substitution of a Mg atom for a Li atom in one corner of the cubane, led to the formation of Li/MgO [43, 44]. A reaction scheme of the cubane synthesis is shown in Figure 2.2. The prepared material was characterized in detail, however, its catalytic performance is presently under investigation.

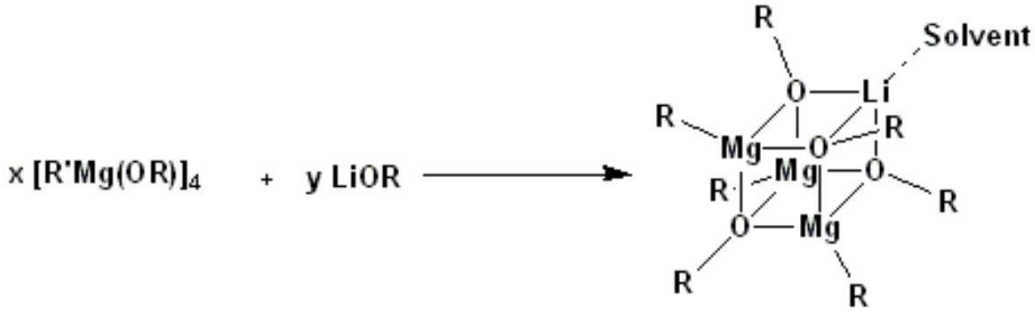


Figure 2.2: The preparation of heterobimetallic magnesium lithium alkoxide clusters, which are then thermally decomposed to Li/MgO. Changed Figure adapted from [43, 44].

### 2.2.5 Other Methods

Berger *et al.* applied chemical vapor deposition (CVD) for the preparation of Li-doped MgO nanoparticles [45].

The addition of $SiO_2$ to Li/MgO via hydrothermal treatment led to basic magnesium hydrosilicates. If the added amount of silica was not too large (Si/MgO ratio of 0.0 to 1.2), the catalyst became more active and selective towards $C_2H_4$, however, the overall $C_{2+}$ selectivity remained unchanged. The addition of $SiO_2$ reduced the evaporation of Li and increased the specific surface area, which resulted in a more stable catalyst [46].

Sarkas and co-workers prepared unsupported nanocrystalline Li/MgO using an inert gas condensation-based smoke source and applied it in the oxidative coupling of methane [47]. One sample showed total oxidation activity already at $300\,^{\circ}C$, a temperature where conventional catalysts are still not active.

Choudhary *et al.* synthesized Li/MgO supported on commonly used supports, such as $Al_2O_3$, $ZrO_2$, $HfO_2$, SiC and $SiO_2$ containing materials [48]. Conversion and selectivity were approximately reduced by a factor of 3, compared to unsupported Li/MgO. This observation was attributed to the reduction of the surface bascitiy, which could be an effect of a strong interaction of the supported material with the support. With $Al_2O_3$, $SiO_2$ and $ZrO_2$ the formation of mixed oxides containing Li or MgO was found, indicating that these materials are not suitable as inert carriers.

The gel-combustion technique, which was reported for Pt nanoparticles [49], was recently applied for the synthesis of Li-doped MgO [50]. A series of different Li loadings was prepared by thermal ignition of the metal nitrates in a mixture of glycerol and ethanol, with subsequent calcination in argon or air at $800\,^{\circ}C$ for 2 hours. Detailed catalytic data was not reported, since the study was focused on the structure and morphology.

### 2.2.6 Summary

A variety of preparation procedures including wet impregnation, sol-gel and organometallic approaches have been reported so far. The wet impregnation is by far the most applied procedure, used in more than 80 % of the publications. Compared to this, other important procedures like co-precipitation, solid state reactions, mixed milling or combustion synthesis are comparably underrepresented in the literature. Unfortunately a direct comparision of the catalytic performance of the differently synthesized materials is very difficult due to vastly varying testing conditions.

In studies on the active center, many publications follow the suggestions of Lunsford *et al.* that the active center is $[Li^+O^-]$ [21] (see also Chapter 2.5.4). However, the main preparative route in these publications has been wet impreg-

nation. In this approach it is necessary to calcine at high temperatures to enable the Li to diffuse into the MgO. But this also accelerates side reactions, like evaporation of Li or carbonate formation and decomposition. Moreover, some publications applied rather low calcination temperatures. It remains unclear if these temperatures are sufficient for the diffusion of Li into the MgO.

Other preparative routes, although they are more intricated and more sophisticated, should be more suitable for the preparation of $[Li^+O^-]$. However, they have hardly been applied.

For wet impregnation it was shown, that the properties of the obtained catalyst (surface basicity, surface area, $CO_2$ content, etc.) depend on the used precursors. A strong variation of the catalytic results was not observed and a correlation between the properties and the catalytic performance was not fond.

The realized studies on the preparation of Li/MgO could not reveal the essential factors determining the catalytic performance so far. A comparative study of differently prepared Li/MgO materials, applying the same reaction conditions for the catalytic tests, could therefore be useful.

## 2.3 Structural Characterisation

### 2.3.1 Basicity and Acidity

The effect of the basicity and acidity on the OCM has already been subject of discussion, including not only Li/MgO [51, 52] but also other OCM catalysts. However, as the following review shows, no consensus has been reached how basicitiy and acidity influence OCM performance.

#### 2.3.1.1 Pure MgO

Davydov and co-workers studied basic sites of various oxides used as catalysts in the oxidative coupling of methane via infrared spectroscopy (IR) of adsorbed molecules such as $CO_2$ [53, 54]. It was demonstrated that the basic sites can be titrated with $CO_2$. The correlation between the spectral behavior of the carbonates and the strength allowed a discrimination between the different sites. The presence and concentration of the strongest basic sites were reported to determine the catalytic activity.

Kuś *et al.* observed that both the presence or absence of impurities, such as Ca or Na, and the gas atmosphere during calcination also influenced surface basicity [55, 56].

Bailly and co-workers studied the nature of possible active sites of MgO by investigating the relationship between the thermodynamic Brønsted basicity and re-

activity of basic sites ($CH_3OH$ deprotonation and conversion of 2-methyl-3-butyn-2-ol (MBOH)) [57]. The relative distribution of low coordinated $O^{2-}$ was varied via different preparative routes and measured via photoluminescence. Moreover, the hydroxylation of clean MgO surfaces and its influence on the Brønsted basicity were studied. Hydroxylated surfaces were found to be more reactive, although they had a lower deprotonation ability than clean surfaces. The specific reactivity of OH groups, compared to low coordinated $O^{2-}$, was found to be determined by the variable stability of the resulting alcoholate intermediates. As OH groups are poor Brønsted bases, the number of alcoholate species is lower on clean surfaces, however, these intermediates were less stabilized and therefore more reactive.

Chizallet *et al.* used $^1$H Mas NMR (MAS - magic angle spinning, NMR - nuclear magnetic resonance) to distinguish between different OH groups that can exist on a defective MgO surface [58, 59]. They found a clear correlation between the area of NMR signals below -0.7 ppm chemical shift and the conversion of 2-methylbut-3-yn-2-ol (MBOH) to acetone and acetylene as test reaction. As these NMR signals $\leq$ -0.7 ppm could be identified as hydroxyl groups coordinated to surface $Mg^{2+}$ ions, these $O_{LC}$-H sites (LC - low coordination), with L = 1, 2, were reported as active sites. DFT (Density Functional Theory) calculations showed that nucleophilicity of the $O_{LC}$ groups rather than basicity of the surface oxygen ions determines reactivity towards MBOH conversion. No statement was made whether the same holds for reactivity and/or selectivity in methane oxidative coupling.

#### 2.3.1.2 Li/MgO

The surface basicity and acidity of MgO promoted with alkali metals (Li, Na, K, Rb and Cs), prepared via impregnation, was compared with the catalytic performance of these materials [27]. The surface properties strongly depended on the promoter and on the calcination temperature. The following order was found for the BET surface area after preparation: Li/MgO $\ll$ Na/MgO $\leq$ Rb/MgO $\leq$ K/MgO $\leq$ Cs/MgO. Acidic sites of different strength were found, and basic sites were found to be broadly distributed and strongly influenced by the promoter. A correlation between the density of the strongly basic sites and the formation of $C_2$ products per unit surface area was observed. In another study using other dopants ($Li_2O$, $Na_2O$, PbO, $La_2O_3$, $MgCl_2$, $CaCl_2$), the result was a significant increase in surface basicity, without significant correlation between basicity and $C_2$ yield [60]. This was considered as an indication, that further factors play an important role for the catalytic performance.

The acid-base properties and the base-catalyzed elimination reaction of 2-propanol, giving either acetone or propylene, was studied for MgO and alkali-doped MgO by Díez *et al.* [61]. The basic properties depended on the relative

concentration of certain surface species (OH groups, for instance). The addition of alkali metals, prepared via impregnation, increased the density of basic sites and also modifieded the strength. Dopants with a higher electron-donating strength led to the formation of stronger basic sites. The activity in the test reaction also increased with an increasing base strength.

### 2.3.2 Structure and Properties

The known literature about the morphological aspects of OCM catalysts, among them Li/MgO, is summarized in detail in a book chapter of Martin and Mirodatos [62]. The loss of Li, the phase organization of Li/MgO and the influence of the surface area and the structure on the OCM is discussed. In the present review, the aspects are discussed in the according chapters and paragraphs.

#### 2.3.2.1 Pure MgO

Zecchina and co-workers reviewed the research on the adsorption of CO on MgO, in the form of single crystals, films and powders [63]. CO was chosen as a test molecule, because it can react with both $Mg^{2+}$ and $O^{2-}$. Results obtained via IR and high-resolution transmission electron microscopy (HR-TEM) were considered in particular. However, the results of other techniques are described as well. It was shown that the gap between surface science experiments and powders, as typically used in catalysis, can be progressively bridged.

Choudhary and co-workers reported that the thermal decomposition of $MgCO_3$ leads to MgO, which was highly active in the OCM [64]. They found a strong influence of the preparation conditions on the thermal decomposition and the surface properties (surface area, total basicity, base strength distribution) [65, 66]. That the surface properties of MgO, prepared from $Mg(OH)_2$, also depends on the preparation and calcination conditions had been shown before [67].

Aridzzone *et al.* applied X-ray photoelectron spectroscopy (XPS) to study different precursors for MgO [68, 69]. Different defects were characterized and considered to be responsible for the activation step of $CH_4$ in the OCM. From the experimental data obtained at different temperatures, it had been shown that the chemical state and the basicity of MgO is a result of the competition of $O_2$, hydrocarbon and $H_2O$ for the different reactive surface sites.

Mellor and co-workers investigated the impact of the MgO structure on the heterolytic oxygen exchange with the surface [70]. Either the particle size or the termination plane was varied. The exchange was independent of the particle size, (particles with a (100) termination plane were used). The activity order of different planes were (111) or (110) *mean* surface planes $>$ (100) $>$ (111), indicating that low coordinated $Mg^{2+}O^{2-}$ pairs play a beneficial role.

#### 2.3.2.2 Li/MgO

Kimble and Kolts showed in thermogravimetric studies with different phases of Li/MgO that Li is present as LiOH, if prepared from $LiNO_3$ or as $Li_2CO_3$, if prepared from $Li_2CO_3$ [71]. They reported, that the LiOH exposed to the reaction gas at 700 $°C$ was converted to $Li_2CO_3$. Treating MgO with the same conditions, it did not gain weight, suggesting that no change took place. If treated at 775 $°C$ in a $N_2$ atmosphere, $Li_2CO_3$/MgO showed a partial decomposition of the carbonate. The decomposition was completed at 900 $°C$. Being exposed to the reaction mixture at 700 $°C$, it was converted back to $Li_2CO_3$. If $H_2O$ was added at 700 $°C$, the quantity of carbonate seemed to decrease. Kimble and Kolts assumed that in return the amount of hydroxides increased. Cycles of carbonate formation and decomposition did not effect the activity as a catalyst. It was assumed that in the presence of a mixture of $CO_2$ and $H_2O$ an equilibrium will be established, with carbonate as the predominant species [72]. A loss of Li during the calcination of the Li/MgO was reported. The loss of Li from the catalyst at high temperatures under reaction conditions was also reported by Kimble and Kolts[73]. Moreover, it was reported that the Li content was stabilized at approximately 1 % when supported on CaO. That limit for the maximum concentration of Li could exist, was underlined by these authors.

The chemistry of Li in Li/MgO during the OCM was investigated by Ross *et al.* [74]. Their conlcusions were:

1. Behavior of Li/MgO was found to depended strongly on the preparation procedure.

2. Passing $CO_2$ through the solution while impregnating MgO led to higher amounts of $Li_2CO_3$ and segregation of Li to the surface of the catalyst.

3. The optimum loading of Li in the fresh catalyst was reported to be 2 - 4 wt%.

4. The active site was formed on the surface by a gradual decomposition of $Li_2CO_3$ in the presence of $O_2$. The absence of $O_2$ had an adverse effect on the activity.

5. The active sites were found to be unstable. The deactivation was due to a loss of Li, via evaporating of the volatile LiOH or the formation of $Li_2SiO_3$, from Li and the quartz glass material of the reactor. $H_2O$ in the feed had therefore an adverse effect.

6. In hot spot areas the loss of Li was reported to occur most rapidly.

7. $CO_2$ in the feed was found to lead to:

   (a) reversible poisoning of the active site,

   (b) but also to stabilization of the active site against deactivation.

8. Measures for a stable catalyst points out that:

   (a) equilibrium between $Li_2CO_3$ and LiOH is necessary,

   (b) periodic reversal of the flow direction improves the stability,

   (c) application of an $Al_2O_3$ instead of a quartz glass reactor can improve the stability.

While investigating the reaction of $CO_2$ during the oxidative coupling of methane, Galuszka *et al.* found that a substantial amount of Li formed a carbonate, which was stable up to 800 $^\circ C$ [75]. The carbonate formation started at 400 $^\circ C$, as shown via Fourier Transform infrared spectroscopy (FT-IR), temperature programmed reaction (TPR) and temperature programmed desorption (TPD). Interestingly several hours of calcination at 800 $^\circ C$ were necessary to remove the $CO_2$ from the catalyst. There was no $CO_2$ on pure MgO above 600 $^\circ C$, therefore chemisorbed $CO_2$ on Li/MgO above 600 $^\circ C$ had to be attributed to the Li. Furthermore, different types of carbonates can be assumed, and they should have different properties and activities. However, the identification of surface species by IR has proven to be difficult [76, 77].

In the publication of Lunsford *et al.* the optimum loading of Li was reported to be 7 wt% [20]. In a later discussion it was noted that for achieving a monolayer of $Li^+$ on MgO ca. 0.2 wt% Li is required, which is a relativley low loading [78]. Therefore, Hutchings and co-workers reinvestigated the optimum loading of Li on MgO [79]. They found that a sub-monolayer loading, i.e. the above mentioned 0.2 wt% Li enhances the activation of $CH_4$ and the selectivity towards coupling products, indicating that the optimum loading of Li is much lower than reported in previous publications, e.g. 7 wt% reported by Lunsford *et al.* [20].

Hargreaves and co-workers investigated the morphology of Li/MgO and its relationship to catalytic performance [80, 81, 82, 83]. For pure MgO, it was demonstrated, that the morphology is an important factor for the catalytic performance in the oxidative coupling of methane. The addition of Li to MgO led to changes due to grain growth. It was concluded, that corner and edge sites did not significantly contribute to the catalytic activity. A special "bottom step" site was suggested to be the active center. For Li/MgO, immobile dislocations were detected in the bulk of these grains. It was suggested that pinning of these dislocations by Li, led to the formation of $[Li^+O^-]$, a frequently suggested candidate for the role of the active sites, as outlined in Chapter 2.5.4.

The results of Hargreaves *et al.* [80, 81, 82, 83] were confirmed via atomistic simulation techniques by Catlow's group [84]. They also showed that the presence

of Li increased the concentration of oxygen defects (in the form of $[Li^+O^-]$) and promoted their segregation to surface sites. $[Li^+O^-]$ centers were reported to be trapped in low coordinated surface sites, which should lead to a modified activity. They assumed that the activity of pure, undoped MgO was the result of more complex surface defects.

The relationship between surface morphology and reactivity was investigated by testing several differently prepared and well characterized MgO and Li/MgO catalysts by the group of Lunsford [85]. The comparison of the results showed that the surface area and the morphology did not have a significant impact on the OCM. However, small structural effects, which could have a strong catalytic impact, might have remained undetected.

Berger *et al.* observed the changes of the surface properties of MgO when small amounts of Li were introduced [45]. It was found that the addition of only 0.2 at% Li to pure MgO decreased already the thermal stability of the resulting material. After the Li seggregated to the surface, it changed the spectroscopic properties significantly (e.g. IR fingerprint of active hydroxyls and hydrides, surface-trapped electrons, and adsorbed oxygen radicals). It was concluded that Li preferentially moves to surface sites associated with low coordinated ions and higher surface reactivity.

Choudhary *et al.* investigated MgO, Li/MgO and MgO doped with other additives as catalysts for the oxidative coupling of methane [86]. The doping with Li led to a severe sintering of the MgO and therefore to lower specific surface areas. The selectivity obtained with the doped material, increased significantly. It was found that the $C_2$ selectivity increased nearly linearly with the decrease of the specific surface area. The involvement of lattice oxygen of the catalysts was investigated in a pulsed micro-reactor [87]. It was found that with increasing pulse number, in each pulse only $CH_4$ was dosed to the reactor, the conversion of $CH_4$ decreased sharply and the $C_2$ selectivity increased. It was concluded that lattice oxygen was involved.The re-oxidation of the catalysts after the pulses, led to a decrease of the $C_2$ selectivity as compared with fresh catalyst. The reason could be the formation of active chemisorbed species and/or restructuring of the catalyst surface.

Sinev *et al.* studied the redox properties of differing catalyst, among them Li/MgO [88]. Based on the results, a new mechanism for the catalyst re-oxidation was suggested, viz. that under steady state, the re-oxidation can proceed via the oxidative dehydrogenation of surface OH groups.

Taniewski and co-workers oxidized $C_2H_4$ over Li/MgO without co-feeding of $O_2$, to obtain information on the oxidation properties of Li/MgO [89]. Since large amounts of CO and $H_2$ were found, it was clearly demonstrated that Li/MgO exhibits a high oxygen mobility. After the reduction of the catalyst, it was possible to restore the activity by its re-oxidation with air. The results on the oxidation of

$C_2H_4$ can also be used to draw conclusions about the fate of $C_2H_4$ in the post-catalytic zone, being still in the reactor.

Anderson and Norby analysed the liquid phases in Li/MgO by means of thermoanalytical and electrical conductivity measurements and electron microscopy [90]. The results indicated that the solubility of Li in MgO increases with increasing oxygen activity, which is also predicted by the defect theory. At 700 $°C$ and in a $CO_2$-rich, oxidizing atmosphere, the solubility of Li in MgO was estimated to be in the order of magnitude of 0.1 mol%, respectively 0.02 wt%.

Pure MgO is a poor electronic conductor at low temperatures, however, doping with Li leads to *p*-type semiconductivity [91, 92]. Norby and Anderson studied the electrical conductivity of sintered Li/MgO at different temperatures ($\leq$ 1200 $°C$) and under different $O_2$ partial pressures. The effect of $H_2O$ and $CO_2$ was also investigated. It was found, that Li dissolves in MgO, such that an $Mg^{2+}$ is being substituted by $Li^+$, forming a negative defect and increasing *p*-type conductivity, which was dominating at near atmospheric $O_2$ partial pressures and high temperatures. Surface and/or grain boundary conductivity became important at intermediate temperatures ($\leq 700\,°C$), which was also probably mainly due to *p*-type conductivity. It was observed that Li readily evaporated from the surface at high temperatures and that Si containing impurities reacted with Li/MgO forming non-conducting silicate phases. Under ambient pressures of $H_2O$ or $H_2$, proton defects seemed to play a minor role [93].

When measuring the direct current (DC) conductivity of Li/MgO as a function of $H_2O$ vapor and $O_2$ partial pressure, Balint and Aika observed, that proton species dominated the conductivity at low temperatures (400 $°C$), *p*-type conductivity dominated at high temperates (800 - 900 $°C$); corresponding to the results of Norby *et al.* which indicated a mixed conduction mechanism at intermediate temperatures (500 - 700 $°C$) [94]. A mechanism was proposed, in which doping with Li leads to the formation of oxygen vacancies, which play an important role in the generation of $O^-$ sites. These oxygen vacancies were believed to be blocked by hydrogen defects at low temperatures.

Balint and Aika investigated the defect sites formed when MgO was doped with Li or Ti [95]. Pure MgO and Li/MgO always exhibited *p*-type conductivity, whereas Ti/MgO showed *n*-type conductivity. Doping with Li favored the formation of oxygen vacancies, while doping with Ti had the inverse effect. That showed, that the defect structure of MgO can be controlled via doping. Tardío and co-workers also determined *p*-type semiconductor properties of Li/MgO single crystals [96].

For MgO and Li/MgO, the dependency of DC conductivity on the partial pressures of $O_2$ and $H_2O$ was investigated at OCM temperature [97, 98]. The DC conductivity of Li/MgO increased with increasing $O_2$ pressures, indicating a *p*-type conductivity of this material. The effect of $H_2O$ was stronger on MgO than on

Li/MgO. A model for the defect generation due to $H_2O$ inclusion was proposed. Two different activation energies for DC conductivity were found, one at low temperatures (400 - 600 $^\circ C$) the other at high temperatures (700 - 900 $^\circ C$). Based on the pressure dependencies, different conductivity mechanisms were proposed. For the low temperature an OH-vehicle mechanism and at high temperature a *p*-type mechanism due to $O^-$ defects was proposed. TPD experiments showed the release of $H_2$ above 600 $^\circ C$. Therefore, a mechanism with O-H bond rapture for the formation of $O^-$ defects in the high temperature region was proposed

That the electronic semiconductor properties could be very important features of catalysts for the oxidative coupling of methane, has also been discussed in a review of Baerns and co-workers [18].

In 1971, Abraham and co-workers reported a variation of the carbon arc-fusion technique, which allowed them to grow highly pure MgO and CaO single crystals. This method was successfully applied for doping single crystals of MgO with a variety of different metals, Li for instance [99]. Electron paramagnetic resonance spectroscopy (EPR) experiments with a variety of different alkali earth metals with alkaline doping indicated the formation of $[Li^+O^-]$ centers. Schirmer provided evidence using EPR, that the Li substitutes an Mg in the MgO lattice [100]. Electron nuclear double resonance (ENDOR) experiments supported this finding [101, 102]. The formation of $[Li^+O^-]$ centers is favored by heavy electron irradiation and high temperature quenching, which were stable at room temperature. However, $\gamma$-radiation resulted in the formation of these centers, but they were not stable at room temperature. EPR and ENDOR experiments revealed that the defects produced via different ways had the same local configuration [101, 103]. The irradiation with neutrons did not lead to stable $[Li^+O^-]$ centers [104]. At high temperatures, a $Li_2O$ precipitate led to the formation of a so called "microgalaxy", i.e. a localized $[Li^+O^-]$-rich environment in the neighborhood of the precipitate. Diffusion in the MgO crystal and replacement of $Mg^{2+}$ or formation of vacancies followed [105]. The formation of stable $[Li^+O^-]$ centers strongly depended on the surrounding atmosphere, the presence of $O_2$ was inevitable for the thermal generation of the defects. The $[Li^+O^-]$ centers formed at higher temperatures were stable, however, the cooling procedure effected the stability. When a slow cooling took place, the Li, which had diffused into the MgO crystal, diffused back into the more stable Li-precipitates [106]. Since impurities, such as Fe and Cr, could not be avoided, the formation of $[Li^+O^-]$ centers was partly accompanied by a valence change of these metals [107]. Interestingly, the $[Li^+O^-]$ centers were also found in CaO [108]. From the investigation of current-voltage characteristics, it was concluded, that at oxidizing temperatures the crystals of Li/MgO had a significant effect on the $[Li^+O^-]$ concentration and the electrical conductivity, thermal aging did not seem to have a significant effect on these features [109]. For further information, the review of Chen and Abraham on trapped

hole centers in alkali earth oxides is recommended [110].

The solubility of hydrogen or deuterium was reported to be much higher in Li/MgO than in pure MgO [104, 111]. The mimium temperature for a diffusion of deuterium in pure MgO was reported to be 1477 $^{\circ}C$, for Li/MgO the mimimum temperature was reported to be 527 $^{\circ}C$, the higher diffusity was attributed to the presence of $Li_2O$ precipitates [111, 112]. Furthermore it was observed, that $D_2O$ adsorbs dissociatively on Li/MgO.

Matsuura *et al.* prepared Li/MgO using ultra fine crystaline MgO. A good correlation between the intensity of the photoluminescence signal (at $\lambda = 450\,\text{nm}$) and the activity was found, also indicating that lower coordinated surface sites, which were formed through the incorporation of Li into the (111) plane of MgO, are playing a significant role [29, 113].

Padró *et al.* studied Li/MgO with different Li loadings with x-ray diffraction (XRD), XPS and scanning electron microscopy (SEM) in order to characterize the surface and the catalytic behavior [114]. It was found that the catalytic behavior and the surface composition depend strongly on the Li loading. Furthermore, it was concluded that di-oxygen species, e.g. $O_2^-$ could be present at the surface and that a complex equilibrium between the surface oxygen species and the $O^-$ centers exists.

Aritani and co-workers characterized Li/MgO by means of XRD, XPS, Mg K-edge X-ray absorption near edge structure (XANES) and SEM techniques [115, 116]. It was found that for low Li loadings (2.5 wt%), Li ions tended to stay in the near surface region. Furthermore, the surface Li tended to form separate phases, without a strong effect on the surface MgO structure. For higher Li loadings (7.5 wt%), the Li was also found in the bulk. An effect of Li incorporation in the bulk was the reduction of the MgO crystallinity. The Li-atoms - being located in the near surface region and in the bulk - had an effect on the activity in the OCM. It was assumed that the near surface defects had a strong positive influence on the $CH_4$ conversion, while the bulk defects positivily influenced the $C_2$ selectivity.

The surface morphology of Li/MgO was investigated via low temperature infrared spectroscopy of adsorbed CO by Trionfetti *et al.* [117]. These authors demonstrated that the morphology and the defect structure was of great importance in the oxidative dehydrogenation of $C_3H_8$. Step sites were unselective sites and the major feature on the surface of pure MgO. When the MgO was doped with Li, which tended to occupy the surface step sites and to replace $Mg^{2+}$, a configuration as shown in Figure 2.3 was proposed. When the loading of Li was increased, the step sites were decorated with $Li^+$ and oxygen vacancies, leading to a higher reactivity. Li/MgO prepared via sol gel, had higher amounts of incorporated Li and they showed a higher selectivity in the ODH of $C_3H_8$ and the cracking of propane.

Myrach and co-workers recently tried to elucidate the role of Li in MgO, by

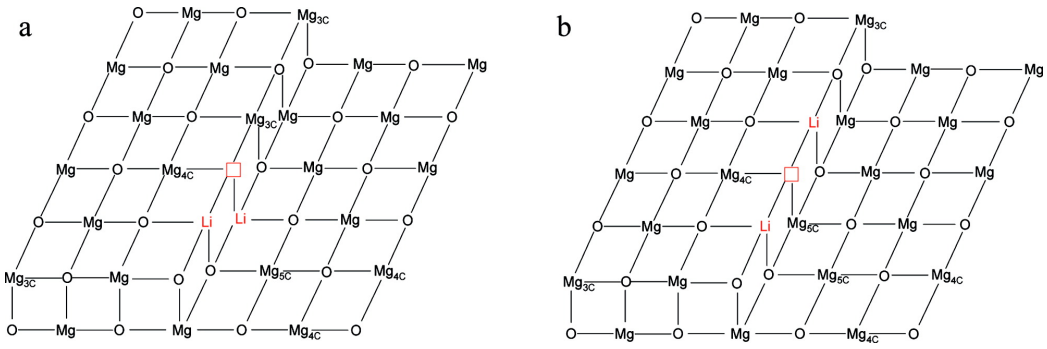


Figure 2.3: Proposed configurations for lithium ions and oxygen vacancy sitting at the step site on the surface of MgO. Figure unchanged form [117]. Reprinted from Langmuir, Vol. 24/15, C. Trionfetti, I.V. Babich, K. Seshan and L. Lefferts, Presence of Lithium Ions in MgO Lattice: Surface Characterization by Infrared Spectroscopy and Reactivity towards Oxidative Conversion of Propane, 8220-8228, Copyright (2008), with permission from American Chemical Society via the Copyright Clearance Center.

investigating two model systems: a MgO film - with and without Li-doping - on Mo(001) and powder samples prepared via calcination of the respective precursors in an $O_2$-atmosphere [118]. Their study mainly focused on the physical properties. It was found, that at low concentrations of Li, it most probably incorporates into the MgO together with oxygen vacancies, changing the optical properties of the system. Above 427 $^{\circ}C$, the segregation of Li towards the surface and the formation of irregular Li-enriched areas was observed. Above 777 $^{\circ}C$, Li desorbed from the MgO surface, leaving behind distinct defects. The Li was not completely removed by heating, very small amounts dissolve in the MgO, as indicated by different optical properties. The change of the optical properties is shown in Figure 2.4. The principle possibility to detect $[Li^{+}O^{-}]$ with EPR was demonstrated on Li/MgO single crystals from Oak Ridge National Laboratories. EPR signals which could be assigned to the $[Li^{+}O^{-}]$ center, proposed by Lunsford [21], which is often considered as the active center of this material (as outlined in Chapter 2.5.4), were not found neither on the Li/MgO films nor in the powder samples. The possible reasons are absence, low concentration or electron tunneling from the Mo(001) support into the hole centers. However, the results do not exclude the general possibility of the formation of $[Li^{+}O^{-}]$.

Recently, the preparation of Li/MgO from gel-combustion was reported [50]. Combined studies with transmission electron microscopy (TEM) and SEM were applied to characterize the structure and morphology. A hierarchical pore structure was found for samples with low loadings of Li. Calcination at 800 $^{\circ}C$ changed the morphology from cubic via truncated octahedral to platelet morphologies, de-

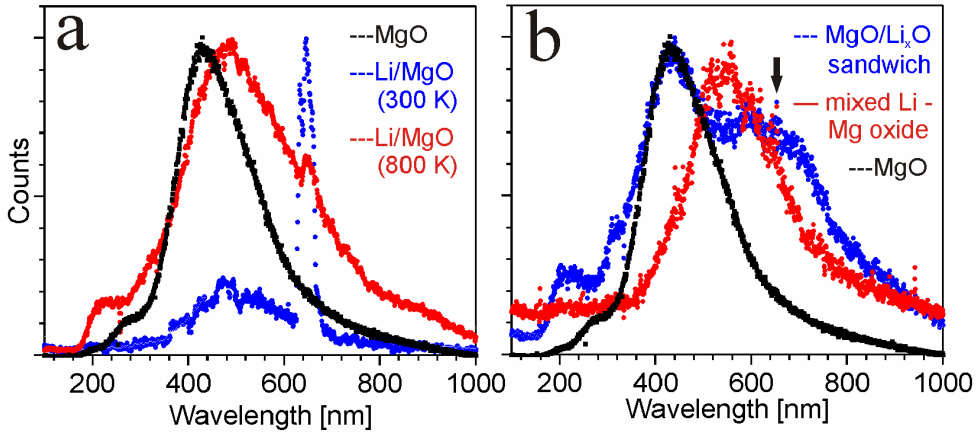


Figure 2.4: Photon-emission spectra of 12 ML MgO/Mo(001) (black), after deposition of 1 ML Li (blue) and after annealing to 800 K (red). The radiation was stimulated by the injection of 100 eV electrons at 1 nA current; b) Emission spectra of 12 ML MgO/Mo(001) (black), a layered MgO-Li$_x$O-MgO film annealed to 500 K (blue) and a Li-doped MgO film annealed to 700 K (red). The arrow indicates Li D-transitions. The spectral parameters are identical to those for (a). Figure unchanged from [118]. P. Myrach, N. Nilius, S.V. Levchenko, A. Gonchar, T. Risse, K.P. Dinse, L.A. Boatner, W. Frandsen, R. Horn, H.J. Freund, R. Schlögl and M. Scheffler: Temperature-Dependent Morphology, Magnetic and Optical Properties of Li-Doped MgO. ChemCatChem. 2010. 2. 854-862. Copyright Wiley-VCH Verlag GmbH & Co. KGaA. Reproduced with permission.

pending on the Li-loading. Indications were found that the Li enhances this transformation. Modifications in the primary morphology of the particles caused severe changes in the secondary structure. Edge-and-step structures and protrusions on flat terraces were found to be the two kinds of high-energy structures found in the micro-structure of the primary particles. It was reported that a relation between the transformation from cubic to complex terminated particles and the catalytic function for the OCM was existed.

### 2.3.3 Summary

Doping of MgO with Li results in more than a simple supported catalyst. Depending on loading, preparation conditions and contact to different atmospheres a variety of modifications of the MgO structure is caused by Li. Besides Li-rich phases supported on MgO bulk, surface defects are induced, causing characteristic changes in the physical and spectroscopic properties of the bulk material and the surface, as well as pronounced changes in the morphology of the MgO. Defects with different electronic structures as well as different oxygen species are considered to contribute to the catalytic performance of the Li/MgO. Different surface densities of the species will result in different ratios of selective and inselective reaction pathways in OCM. The strong dependence of the presence of the different surface species on preparation and operation conditions results in a complex picture of the mechanism of OCM and the difficulty to derive clear structure reactivity relation.

## 2.4 Catalytic Performance of Li/MgO based Catalysts

### 2.4.1 Stability of Li/MgO-based Catalysts

Lunsford *et al.* prepared Li/MgO catalysts with Li loadings of 1 to 26 wt%. All these prepared materials showed a catalytic activity. They found that $CH_4$ conversion and $C_{2+}$ selectivity increased with increasing reaction temperature up to approximately 700 $^{\circ}C$ [19, 20]. After the catalytic tests, the specific surface area of Li/MgO was considerably lower than the specific surface area of pure MgO. A separate experiment with high and low surface area MgO (34 $m^2$/g and 8 $m^2$/g), respectively, showed comparable conversions of 16 %, but different selectivities (5 % and 29 %). A deactivation experiment at 700 $^{\circ}C$ with 7 wt% Li/MgO was conducted. The catalyst was stable, after approximately 15 to 32 hours time on stream. However, the reaction conditions applied for this test were 1 g catalyst, 700 $^{\circ}C$, flow rate of 49.8 ml/min and a feed gas composition of $CH_4$:$O_2$:He =

3:1:21.3, being highly diluted. Lunsford *et al.* proposed that $C_2H_6$ forms via the coupling of two $CH_3\cdot$ radicals. It was also found, that $C_2H_4$ was formed via the oxidative dehydrogenation of $C_2H_6$.

Mirodatos *et al.* studied the deactivation of MgO and Li/MgO in detail, together with chemical and morphological changes [119]. Two kinds of sintering phenomena were found. At 727 °*C* (the melting point of $Li_2CO_3$ is 720 °*C*), the deactivation coincided with sintering of the solid, a loss of BET surface area (Brunauer Emmett Teller) and of Li. Nevertheless, at 634 °*C*, the deactivation coincided only with a reduction of the BET surface area, a loss of Li was not found. The stability of the surface area depended on the temperature treatment (the surface collapsed above 727 °*C*) and on the gas phase. In an $O_2$ atmosphere the surface was observed to be stable up to 634 °*C*, it started sintering when it was in contact with the reaction gas mixture. The formation of $Li_2CO_3$ significantly reduced the stability of the MgO surface area, this was also shown for other dopants and other supports [120, 121]. $Li_2CO_3$ was held responsible for the formation of $CO_x$ [122]; the increase of the $C_2$ selectivity with time on stream was therefore explained with the decomposition of $Li_2CO_3$.

Choudhary and co-workers reported a highly stable Li/MgO, which showed no deactivation for 15 hours on stream (temperature: 750 °*C*, 0.5 g catalyst, feed gas composition: $CH_4$:$O_2$ = 4:1, flow: 85.6 ml/min) [30]. The catalyst was prepared via impregnation of $Mg(CH_3CO_2)_2$ with aqueous $Li(CH_3CO_2)$ and subsequent calcination. The stability was attributed to the high content of $CO_2$ (determined via heating the catalyst in a $N_2$ flow), which reduced the loss of Li and improved the resistance against sintering of the catalyst.

In their study on the nature of the active site of Li/MgO, van der Wiele and co-workers compared the activity and deactivation of Li/MgO and $Li_2CO_3$ supported on $ZrO_2$ [123]. In terms of activity, for a 7 wt% "home made" Li/MgO an increase in $O_2$ conversion and $CH_4$ conversion is observed, until 16 hours time on stream, followed by a steady deactivation by a steady deactivation. The Li content decreased continuously throught the experiment. For 0.2 wt% Li/MgO, deactivation and loss of Li were observed from the beginning. However, $Li_2CO_3/ZrO_2$ suffered from a comparatively fast deactivation to nearly zero activity after approximately 15 hours time on stream. The working prinicple of the catalysts derived from these experiments is discussed in detail in 2.5.1. However, the increase in activity in the first hours times on stream has not been reported by other research groups, but the deactivation of the activity of Li/MgO has been reported.

The catalyst deactivated due to a loss of Li as volatile LiOH or as $Li_2SiO_3$, due to the fact that the laboratory reactors are made of quartz glass [123]. This result was confirmed by Ross and co-workers [28, 74]. A consequence is, that the use of experimental equipment made of quartz glass had a negative effect on the stability of Li/MgO. Figure 2.5 shows the result of deactivation experiment with and

without quartz dilution. It is evident, that without quartz the deactivation process is strongly retarded. After the experiment done by Ross *et al.* [28], the Li content had fallen to 0.1 wt%, which is significantly lower than previously described by other authors [73, 119]. The reason could be the higher reaction temperature.

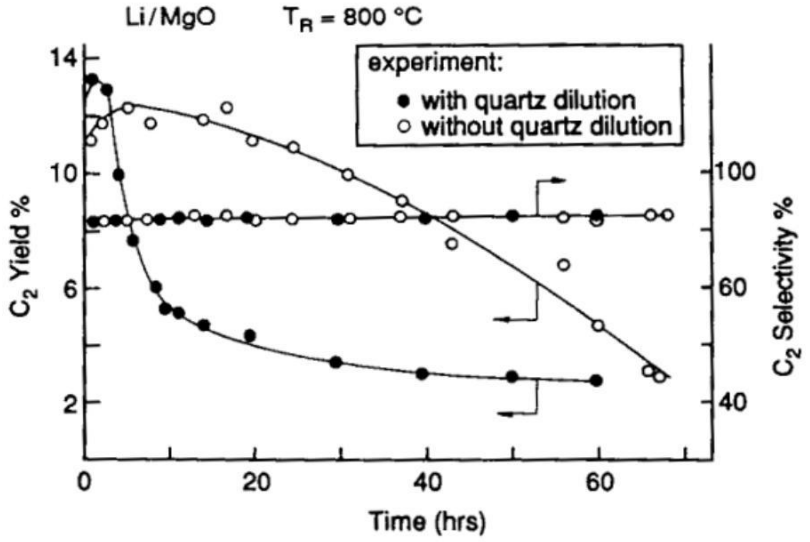


Figure 2.5: Aging experiments at $T_{Reaction\ Temperature}$ = 800 °$C$ with Li/MgO (ca. 3.1 wt% Li) ($T_{Calcination}$ = 850 °$C$), with and without quartz dilution. Figure unchanged from [28]. Reprinted from Catalysis Today, Vol. 2/5, S.J. Korf, J.A. Roos, N.A. de Bruijn, J.G. van Ommen and J.R.H. Ross, Oxidative Coupling of Methane over Lithium Doped Magnesium Oxide Catalysts, 535-545, Copyright (1988), with permission from Elsevier via the Copyright Clearance Center.

Rapid deactivation of Li/MgO was observed by Ross *et al.* [124]. They also showed that, if Li was still available, the catalyst could be regenerated by treatment with $CO_2$ under reaction conditions. The deactivation could be avoided if $CO_2$ was added to the reaction mixture in low concentrations. They furthermore concluded, that $CO_2$ temporarily poisoned the active site and simultaneously stabilized it against deactivation, the selectivity was not affected by the $CO_2$ addition [28, 124]. The selectivity did not change much in their long-term experiments, therefore the conclusion was that the nature of the active site had not changed much, but their number decreased. For Li/Nb/MgO, the prevention of deactivation by adding $CO_2$ could not be observed [125].

The addition of silica to Li/MgO via hydrothermal treatment led to basic magnesium hydrosilicates. If the added amount of silica was not too large, the catalyst became more active and selective towards $C_2H_4$, however, the overall $C_{2+}$ selectivity remained unchanged. Furthermore, silica addition reduced the evaporation

of Li and it increased the specific surface area, resulting in a more stable catalyst [46].

Ross and co-workers tested a series of different catalysts, such as Li/MgO and Pb-containing materials [126]. Li/MgO was found to be more stable than the Pb-containing ones. However, the Li- and Pb-containing materials seemed to have a superior catalytic performance compared to the other tested materials.

Galuszka showed that carbonate free Li/MgO initially showed a good activity, but it decreased after 20 minutes on stream. The deactivation, the appearance of $CO_2$ and the disappearance of $C_2H_4$ coincided. Furthermore, he found that a substantial amount of Li formed carbonate, which was stable until $800\,^{\circ}C$ [75].

Hutchings *et al.* compared $O_2$ and $O_3$ as oxygen source for the OCM over Li/MgO [127]. In their study, they observed that the catalysts steadily lost their activity, because of sintering and recrystallization.

Perrichon and Durupty investigated the thermal stability of Li, Na and K deposited on MgO, $SiO_2$, $Al_2O_3$ and $Cr_2O_3$ [121]. It was found, that on $SiO_2$, $Al_2O_3$ and $Cr_2O_3$ the alkali metals are rather stable, however, on MgO a loss of alkali metal was observed at calcination temperatures higher than $500\,^{\circ}C$. This effect increased from Li to K at $800\,^{\circ}C$, showing that the loss of alkali metals is not limited to li. A reason for this could be that MgO is not able to form stable compounds, unlike $SiO_2$, $Al_2O_3$ and $Cr_2O_3$ which can form silicates, aluminates and chromates. Supports impregnated with alkali metals always had a lower surface area, the temperature had no influence on this. This effect was explained with the formation of a conglomerate of alkali metal salt and support. Furthermore, it was assumed that the alkali metal phase, which was present at the interface between the support particles, underwent transformations, especially fusion during sintering. Therefore, it induced partial dissolution of the support and thus the growth of larger crystals.

Choudhary *et al.* observed the effect on the catalytic activity for the OCM of doping MgO and Li/MgO with Mn, Cd and Zn. The addition of the dopants caused a severe sintering of the MgO, resulting in a decreased specific surface area, but the selectivity also significantly increased. It was found that the $C_2$ selectivity increased nearly linearly with the decrease of the specific surface area. However, the Li-promoted catalysts suffered from heavy sintering during the catalytic experiments [86].

Al-Zahrani and co-workers studied the effect of $CO_2$, steam and liquid water treatment and the process conditions on the oxidative coupling of methane over Li/MgO [128, 129, 130]. It was shown that $CO_2$ has not only a poisoning effect on the formation rate of CO, $CO_2$ and $C_2$ products. However, the $C_2$ selectivity remained unaffected. $H_2O$ in the feed enhanced the deactivation rate. This is accelerated with increasing partial pressure of $H_2O$. Small amounts of $CO_2$ decreased the deactivation. The addition of liquid $H_2O$ into the catalyst bed in-

creased the $CH_4$ conversion. Due to the water treatment, it was reported that the Li content decreased and the specific surface area increased. It was also shown that the catalyst lost Li, by deposition on the reactor walls.

Taniewski and co-workers did research on the effective utilization of the catalyst bed, which deactivated during the reaction [131]. It was reported that a hot-spot area was the only working region of the bed and the place of catalyst aging. In a scaled-up laboratory reactor, it was shown that the deactivation could be attributed to a significant loss of Li, which led to the decrease of $C_2$ selectivity. Changing the feed inlet locations made it possible to involve successive layers of catalyst in the reaction. Furthermore, transformations of the bed, prepared from fresh and deactivated Li/MgO, led to the transport of Li from the fresh catalyst (deactivation) to the deactivated catalyst (regeneration).

### 2.4.2 Comparision of Catalytic Performance of several Li/MgO Catalysts

In Table 2.1 the different reaction conditions and catalytic results taken from different publications are presented. The applied reaction conditions vary significantly, often a large amount of inert dilutent was applied in the feed gas. The strong differences in the reaction conditions hinder a comparison of results, obtained by different research groups [9]; no correlation can be observed in the obtained results due to the strong variation.

### 2.4.3 Influence of Process Parameters

The required minimum temperature for $CH_4$ conversion is concordantly reported to be at approximately 600 $^\circ C$. The $CH_4$ conversion and the $C_2$ yield increase with increasing reaction temperature, reaching a maximum at ca. 750 $^\circ C$ to 800 $^\circ C$. However, since some authors reported Li/MgO to be an instable catalysts, the catalytic performance of different Li/MgO catalysts after several hours time on stream is questionable. Studies on this subject have not been published yet.

In 1994, Machocki showed that the OCM at temperatures below 700 $^\circ C$ could applied without the loss of effectiveness, via applying a much longer contact time. He showed, that the required contact times were much longer than previously reported in the majority of publications. Therefore, an extended contact time could lead to lower reaction temperatures, i.e. 600 $^\circ C$ to 650 $^\circ C$, even for catalysts that are regarded suitable for the high temperature range [137].

Asami and co-workers observed that the non-catalytic oxidative coupling of $CH_4$ was considerably enhanced under pressures up to 16 bar and in a temperature range between 650 $^\circ C$ and 800 $^\circ C$ [138].

Table 2.1: Overview of the reaction conditions and catalytic performance taken from selected publications. Usually the $C_2$ selectivity is reported, meaning the combined selectivity towards $C_2H_6$ and $C_2H_4$. However, in few publications the $C_{2+}$ selectivity, which also takes higher hydrocarbons into account is reported. The difference between $C_2$ and $C_{2+}$, which is usually small, has been neglected and reported as $C_2$.

| No. | Li-Content | Mass | $CH_4$:$O_2$:Dilutent | Temperature | Flow Rate [ml/min] | $X_{CH_4}$ [%] | $X_{O_2}$ [%] | $S_{C_2}$ [%] | $\frac{C_2H_6}{C_2H_4}$ | Comment | Ref. |
|---|---|---|---|---|---|---|---|---|---|---|---|
| 1 | 7 wt% | 4.0 g | 1.9:1:3.6 | 720 [$^\circ C$] | 49.8 | 37.5 | n.s. | 46.5 | 0.48 | - | [20] |
| 2 | 8 wt% | 0.8 g | 2.1:1:17.5 | 700 [$^\circ C$] | 55.2 | 22.6 | n.s. | 56.7 | n.s. | - | [22] |
| 3 | 4.8 wt% | 4.0 g | 5.1:1 6.2 | 700 [$^\circ C$] | 50.0 | 14.6 | n.s. | 57.4 | n.s. | after 10 h | [85] |
| 4 | 4.5 wt% | 4.0 g | 5.1:1:6.2 | 700 [$^\circ C$] | 50.0 | 13.0 | n.s. | 58.9 | n.s. | after 10 h | [85] |
| 5 | 5.5 wt% | 4.0 g | 5.1:1:6.2 | 700 [$^\circ C$] | 50.0 | 20.3 | n.s. | 59.6 | n.s. | after 10 h | [85] |
| 6 | 1.3 wt% | 2.0 g | 2:1:2 | 760 [$^\circ C$] | 50.0 | 37.0 | n.s. | 40.0 | 0.25 | - | [42] |
| 7 | 1.3 wt% | 2.0 g | 2:1:2 | 780 [$^\circ C$] | 50.0 | 37.0 | n.s. | 40.0 | 0.21 | - | [42] |
| 8 | 1.3 wt% | 2.0 g | 2:1:2 | 800 [$^\circ C$] | 50.0 | 37.0 | n.s. | 40.0 | 0.18 | - | [42] |
| 9 | 3.1 wt% | 0.1 g | 9.6:1:3.7 | 780 [$^\circ C$] | 25.2 | 13.3 | 100.0 | 73.0 | 0.72 | - | [132] |
| 10 | 0.63 wt% | 2.0 g | 5.5:1:5.5 | 750 [$^\circ C$] | - | 25.2 | 100.0 | 41.9 | 1.00 | - | [83] |
| 11 | 1 mol% | 0.1 g | 3:1:0 | 700 [$^\circ C$] | 50.0 | 38.5 | 94.8 | 49.0 | 0.52 | - | [29] |
| 12 | 3 mol% | 0.1 g | 3:1:0 | 700 [$^\circ C$] | 50.0 | 38.3 | 91.4 | 55.0 | 0.51 | - | [29] |
| 13 | 5 mol% | 0.1 g | 3:1:0 | 700 [$^\circ C$] | 50.0 | 30.4 | 68.4 | 54.1 | 0.54 | - | [29] |
| 14 | 10 mol% | 0.1 g | 3:1:0 | 700 [$^\circ C$] | 50.0 | 16.1 | 43.4 | 56.2 | 0.61 | - | [29] |
| 15 | 15 mol% | 0.1 g | 3:1:0 | 700 [$^\circ C$] | 50.0 | 5.8 | 12.8 | 54.0 | 0.67 | - | [29] |
| 16 | Li/Mg = 0.1 | 0.1 g | 3:1:0 | 750 [$^\circ C$] | 17.0 | 28.7 | n.s. | 63.1 | 0.91 | Code A | [34] |
| 17 | Li/Mg = 0.1 | 0.1 g | 3:1:0 | 750 [$^\circ C$] | 17.0 | 22.1 | n.s. | 59.7 | 1.25 | Code B | [34] |
| 18 | Li/Mg = 0.1 | 0.1 g | 3:1:0 | 750 [$^\circ C$] | 17.0 | 24.8 | n.s. | 56.9 | 1.25 | Code C | [34] |
| 19 | Li/Mg = 0.1 | 0.1 g | 3:1:0 | 750 [$^\circ C$] | 17.0 | 19.7 | n.s. | 65.0 | 1.25 | Code D | [34] |
| 20 | Li/Mg = 0.1 | 0.1 g | 3:1:0 | 750 [$^\circ C$] | 17.0 | 33.5 | n.s. | 55.8 | 0.71 | Code E | [34] |
| 21 | Li/Mg = 0.1 | 0.1 g | 3:1:0 | 750 [$^\circ C$] | 17.0 | 18.6 | n.s. | 30.6 | 2.00 | Code F | [34] |
| 22 | Li/Mg = 0.1 | 0.1 g | 3:1:0 | 750 [$^\circ C$] | 17.0 | 6.6 | n.s. | 66.6 | 3.33 | Code G | [34] |
| 23 | Li/Mg = 0.1 | 0.1 g | 3:1:0 | 750 [$^\circ C$] | 17.0 | 21.8 | n.s. | 59.6 | 1.43 | Code H | [34] |
| 24 | Li/Mg = 0.1 | 0.1 g | 3:1:0 | 750 [$^\circ C$] | 17.0 | 31.7 | n.s. | 59.0 | 0.63 | Code I | [34] |
| 25 | Li/Mg = 0.1 | 0.1 g | 3:1:0 | 750 [$^\circ C$] | 17.0 | 29.6 | n.s. | 59.1 | 0.77 | Code J | [34] |
| 26 | Li/Mg = 0.1 | 0.1 g | 3:1:0 | 750 [$^\circ C$] | 17.0 | 36.1 | n.s. | 60.1 | 0.59 | Code K | [34] |
| 27 | Li/Mg = 0.1 | 0.1 g | 3:1:0 | 750 [$^\circ C$] | 17.0 | 25.1 | n.s. | 64.9 | 0.77 | Code L | [34] |
| 28 | Li/Mg = 0.1 | 0.1 g | 3:1:0 | 750 [$^\circ C$] | 17.0 | 38.0 | n.s. | 55.3 | 0.42 | Code M | [34] |
| 29 | Li/Mg = 0.1 | 0.1 g | 3:1:0 | 750 [$^\circ C$] | 17.0 | 24.5 | n.s. | 52.2 | 1.25 | Code N | [34] |
| 30 | Li/Mg = 0.1 | 0.5 g | 4:1:0 | 700 [$^\circ C$] | 86.0 | 11.9 | n.s. | 50.0 | 3.33 | - | [27] |
| 31 | Li/Mg = 0.1 | 0.5 g | 4:1:0 | 750 [$^\circ C$] | 86.0 | 27.6 | n.s. | 64.0 | 1.18 | - | [27] |
| 32 | 0.66 wt% | 0.1 g | 10:1:0 | 780 [$^\circ C$] | 25.2 | 4.4 | 50 | 66.4 | 1.37 | - | [28] |
| 33 | 1.71 wt% | 0.1 g | 10:1:0 | 780 [$^\circ C$] | 25.2 | 10.0 | 75 | 75.1 | 75.1 | - | [28] |
| 34 | 2.47 wt% | 0.1 g | 10:1:0 | 780 [$^\circ C$] | 25.2 | 11.1 | 85 | 71.7 | 1.12 | - | [28] |
| 35 | 3.19 wt% | 0.1 g | 10:1:0 | 780 [$^\circ C$] | 25.2 | 11.4 | 88 | 72.0 | 1.24 | - | [28] |
| 36 | 0.02 wt% | 2.0 g | 3.7:1:17.4 | 650 [$^\circ C$] | 50.0 | 4.1 | n.s. | 7.6 | n.s. | - | [133] |
| 37 | 0.05 wt% | 2.0 g | 3.7:1:17.4 | 650 [$^\circ C$] | 50.0 | 6.2 | n.s. | 9.6 | n.s. | - | [133] |
| 38 | 0.10 wt% | 2.0 g | 3.7:1:17.4 | 650 [$^\circ C$] | 50.0 | 7.6 | 37.0 | 17.5 | n.s. | - | [133] |
| 39 | 0.15 wt% | 2.0 g | 3.7:1:17.4 | 650 [$^\circ C$] | 50.0 | 9.3 | 44.4 | 25.7 | n.s. | - | [133] |
| 40 | 0.20 wt% | 2.0 g | 3.7:1:17.4 | 650 [$^\circ C$] | 50.0 | 8.2 | 38.3 | 35.7 | n.s. | - | [133] |
| 41 | 0.25 wt% | 2.0 g | 3.7:1:17.4 | 650 [$^\circ C$] | 50.0 | 9.6 | 36.8 | 30.8 | n.s. | - | [133] |
| 42 | 1.00 wt% | 2.0 g | 3.7:1:17.4 | 650 [$^\circ C$] | 50.0 | 9.1 | 44.8 | 36.4 | n.s. | - | [133] |
| 43 | 5.00 wt% | 2.0 g | 3.7:1:17.4 | 650 [$^\circ C$] | 50.0 | 8.0 | 30.4 | 34.5 | n.s. | - | [133] |
| 44 | 7.00 wt% | 2.0 g | 3.7:1:17.4 | 650 [$^\circ C$] | 50.0 | 6.0 | 27.4 | 30.6 | n.s. | - | [133] |
| 45 | 10.00 wt% | 2.0 g | 3.7:1:17.4 | 650 [$^\circ C$] | 50.0 | 7.6 | n.s. | 35.6 | n.s. | - | [133] |
| 46 | 0.2 % | 4.0 ml | 3:1:0 | 700 [$^\circ C$] | 75.5 | 29.8 | 94.2 | 58.8 | 2.40 | - | [79] |
| 47 | 2.0 % | 4.0 ml | 3:1:0 | 700 [$^\circ C$] | 85.7 | 22.1 | 63.9 | 62.8 | 1.54 | - | [79] |
| 48 | 5.0 % | 4.0 ml | 3:1:0 | 700 [$^\circ C$] | 88.0 | 11.8 | 27.8 | 53.0 | 2.27 | - | [79] |
| 49.0 | 5 % | 4.0 ml | 3.3:1:0 | 720 [$^\circ C$] | 43.2 | 2.7 | n.s. | 65.4 | 0.65 | - | [134] |
| 50.0 | 5 % | 4.0 ml | 3.3:1:0 | 550 [$^\circ C$] | 43.2 | 1.6 | n.s. | 22.5 | 3.50 | - | [134] |
| 51.0 | 0.6 % | 1.25 ml | 2:1:7.1 | 680 [$^\circ C$] | 50.0 | 38.0 | n.s. | 35.0 | 0.59 | after 10 h | [135] |
| 52.0 | 1.2 % | 1.25 ml | 2:1:7.1 | 680 [$^\circ C$] | 50.0 | 30.0 | n.s. | 41.0 | 0.71 | after 10 h | [135] |
| 53.0 | 4 wt% | 3.0 ml | 2:1:6.3 | 700 [$^\circ C$] | 74.0 | 34.4 | n.s. | 46.7 | 0.46 | after 0.5 h | [136] |

Ekstrom *et al.* investigated the effect of pressure (range of 1 - 6 bar) on the OCM reaction [139]. They found that with increasing pressure the importance of the uncatalyzed reaction also increased significantly. This is in agreement with the results of Lane and Wolf [140]. The pressure dependency of the catalyzed and uncatalyzed reactions were different, at high pressures and low flow rates the uncatalyzed reactions were predominant. Moreover, they found that at high flow rates, the $C_{2+}$ selectivity decreased with increasing pressure. Pinabiau-Carlier *et al.* also investigated the effect of the pressure on the OCM, but not with a Li/MgO catalyst [141].

Edwards and co-workers studied the OCM in a fixed-bed and a fluidized-bed reactor [142]. They found that increasing the pressure in the fixed-bed reactor led to an increase in $CH_4$ conversion, but in a reduced $C_2$ selectivity.

Marin *et al.* studied the effect of pressure (up to 10 bar) on the oxidative coupling of methane in the absence of a catalyst [143]. The conversion of $CH_4$ and $O_2$ increased with pressure at constant temperature and residence time. Increasing pressure favored the oxidative route from $C_2H_6$ to $C_2H_4$ compared to the pyrolytic route. The methyl and the hydrogen peroxy radicals were reported to be the most abundant radicals, however, this was concluded on the basis of a model [143, 144].

Parida *et al.* found that the key factor of the OCM was a low specific surface area, however there should be an optimal surface area. Furthermore it was found, that the $C_2$ selectivity increased with an increasing basicity [145].

Aika *et al.* studied different alkali-doped MgO for the oxidative coupling of methane [23, 24, 120]. They found that a low surface area was a very important factor for a high $C_2$ yield. Also other researchers found that a low surface area was rather beneficial than detrimental for a high yield, for instance Lunsford *et al.* [85]. In an investigation with a series of metal oxides supported on $SrCO_3$, Aika and co-workers found that a decrease in catalyst surface led to an increase in the $C_2$ formation, concomitantly suppressing the total oxidation [146].

Rynkowski *et al.* reported on the influence of the calcination temperature on the surface area of $SiO_2$, $Al_2O_3$ and MgO, comparing this with the results obtained when these oxides were promoted with Li [147]. The addition of Li led to a significant decrease in the BET surface area after calcination, compared to the undoped sample.

Kuo *et al.* showed that the reduction of surface area, which is induced by the incorporation of Li, could be compensated by addition of activated charcoal at the start of the preparation procedure [35]. The charcoal was burned off in the calcination step. The surface area increased and the morphology was modified. The effect of the charcoal addition could be avoiding the formation of large MgO crystals. The conversion and selectivity of the catalysts (per unit surface area) was found to be nearly independent of the specific surface area. Therefore, Kuo and co-workers concluded, that the effect of the BET surface area on the activity,

reported in earlier studies, was probably influenced by the residence time and it is not a pure effect of the BET surface area. However, a correlation was found between the $CH_4$ conversion, the total surface area in the reactor and an inverse correlation between catalyst density and specific surface area of the catalyst. The variation of the BET surface are in these experiments was only between approximately 0.5 $m^2/g$ and 3.0 $m^2/g$.

The results of experiments with different catalysts indicate the idea that an optimal surface area, which is not too high, exists for the OCM [62]. However, the authors also argued, that more detailed work is necessary to substantiate this idea, is it cannot be excluded that the OCM is a structure sensitive reaction. For such a case, a heat treatment of the catalysts would not only lead to a reduced surface area, but also to a different surface morphology.

### 2.4.4 Summary

Deactivation of Li/MgO is due to a loss of Li as LiOH, which is formed from Li-compounds with the reaction product $H_2O$. Deactivation is partly suppressed by $CO_2$ transforming $Li_2O$ into the more stable $Li_2CO_3$. There seems to be a general trend that high carbonate containing materials are more stable and more selective towards $C_2$ formation then such with small carbonate content. The role of the LiOH vapor in the gas phase has not yet been investigated, although this problem has been mention by Martin and Mirodatos [62].

The rate of deactivation, in particular of sintering, depends on the gas composition around the catalyst. High $CH_4$ conversions, and therefore high partial pressures of $H_2O$, lead to a high deactivation. High amounts of dilutent in the feed gas seem to supress deactivation. Both is detrimental to an industrial application. Supporting Li/MgO on $SiO_2$, $Al_2O_3$ and $Cr_2O_3$ did not lead to any significant improvement with respect to catalyst stability.

Catalyst selectivity towards $C_2$ of Li/MgO increased by doping Li/MgO with certain dopants like Mn, Cd and Zn; however, activity was negatively affected. Operating conditions and the dimensions of the reactor also influence selectivity. Usually, temperatures in the range of 700 $^\circ C$ to 800 $^\circ C$ lead to the best selectivities while at lower as well as higher temperatures selectivity deteriorates due to total oxidation. High ratios of partial pressures of $CH_4$ to $O_2$ results in better selectivity than in the reversed case. Furthermore, the absolute pressure of $O_2$ is also a selectivity-determining factor: higher $O_2$ partial pressures favor total oxidation. Any excessive hotspots within the reactor as well as transport limitations should be avoided since selectivity is negatively affected.

At higher pressures non-catalytic gas phase oxidation reactions can occur leading also to some $C_2$ formation, even though small in comparison to $CO_x$. Even though typical OCM conditions mixtures are outside flammability limits at atmo-

spheric pressure, it cannot be excluded that gas phase reactions play also there an important role, as radicals released of the catalyst might initiate gas phase radical chain processes.

## 2.5 Mechanistic Studies

### 2.5.1 General Mechanistic Studies

Lunsford *et al.* conducted experiments with a series of differently doped Li/MgO catalysts. It was reported that their 7 wt% Li/MgO prepared catalyst reached a steady state after 15 hours time on stream and remained a stable performance until the end of the experiment, 32 hours time on stream [20]. The reaction conditions were 700 °*C*, 1 g of catalyst, feed gas composition: $CH_4$:$O_2$:He = 3:1:21.3, flow: 50 ml/min, which are typical laboratory conditions. It was proposed that the coupling of two $CH_3\cdot$ radicals lead to the formation of $C_2H_6$ and that $C_2H_4$ is formed via the oxidative dehydrogenation of $C_2H_6$. The measured EPR signals were in agreement with the ones Abraham and co-workers assigned to $[Li^+O^-]$ [148], suggesting the presence of this defect. Later the EPR technique was used to observe the formation of methyl radicals, when $CH_4$ was passed over pure MgO at 500 °*C* [21, 149]. Depending on the kind of pretreatment, significant differences in the initial activity were observed. Vacuum pretreatment did not lead to an increase in activity, while pretreatment in $O_2$ did increase the initial activity, observed as an improved formation of methyl radicals. The formation of $[Li^+O^-]$ centers in single crystals of MgO doped with Li at temperatures between 1000 to 1300 °*C* was reported and extensively studied before by the group of Abraham [101, 103, 106, 107, 108, 109, 148]. It was shown, that these centers also formed at temperatures between 500 - 1000 °*C* in an $O_2$ atmosphere, even if the intensity differed [21].

Yates and Zlotin observed that the uncatalyzed thermal reaction, in an empty reactor, contributed significantly to the oxidative coupling of methane [150]. The results obtained at 700 °*C* and 720 °*C* are shown in Table 2.2. It is evident, that in the applied reactor system, the blank reaction contributed significantly to the $CH_4$ conversion, however, the total oxidation was dominant. Moreover, the main contribution of the catalysts was the oxidation of CO to $CO_2$. Only Li/MgO showed an increase in $C_2H_4$ selectivity. Lunsford *et al.* had reported in their earlier study, that only 0.2 % conversion in the blanc reactor were observed [19, 20, 151], Yates and Zlotin explained the difference to their observed values with a difference in the reactor geometry. Remarkable, the obtained values for the reactor with catalysts did not differ so significantly. The authors concluded, that the function of Li/MgO in the OCM is extremely complex and that homogeneous *and* heteroge-

neous reaction is important.

Table 2.2: The applied reaction conditions were: flow rate 50.0 ml/min, composition: $CH_4$:$O_4$:Dilutent = 1.8:1:3.6 and 4.1 g catalyst. Table adopted from Table 3A in [150].

| Temperature | Catalyst | $X_{CH_4}$ | $S_{C_2}$ | Product Composition [mol%] | | | |
|---|---|---|---|---|---|---|---|
| | | | | CO | $CO_2$ | $C_2H_4$ | $C_2H_6$ |
| 700 °C | None | 22.3 % | 20.9 % | 73.9 | 14.4 | 6.9 | 4.8 |
| 700 °C | MgO | 34.6 % | 17.4 % | 15.2 | 75.5 | 6.0 | 3.2 |
| 700 °C | 3% Li/MgO | 39.4 % | 37.6 % | 2.1 | 74.8 | 15.8 | 7.3 |
| 720 °C | None | 26.8 % | 19.6 % | 73.0 | 16.0 | 7.1 | 3.8 |
| 720 °C | MgO | 35.0 % | 18.2 % | 13.7 | 76.3 | 7.1 | 2.9 |
| 720 °C | 3% Li/MgO | 39.2 % | 36.5 % | 2.1 | 75.7 | 15.6 | 6.6 |

In the ensuing discussion, Lunsford and co-workers argued that the variations in the results could be explained with differences in residence time [152]. The residence time in the experiments of Lunsford *et al.* was shown to be less than 5 seconds [19, 20, 151], whereas the set-up of Yates and Zlotin had a residence of above 20 seconds [152]. Furthermore, it was emphasized that the extent of the homogeneous reactions was also strongly influenced by the free volume, a factor which was also different in the works of Lunsford and Yates. Different $CH_4$ conversions were reported in case of an empty reactor or a reactor filled with fused-quartz rings and the question was raised, why Yates and Zlotin [150], but also Lane and Wolf [140], did not observe differences for such experiments. Regarding the $O_2$ conversion, it was argued, that under the conditions Yates and Zlotin applied, most of the $O_2$ had already been consumed before reaching the catalyst bed. Lunsford and co-workers concluded summarizingly, that in their experiments the homogeneous contribution was not significant and that it seemed unlikely that $C_2$ yield could be achieved purely by homogeneous reactions.

Yates and Zlotin replied [153], that they published a $Li_2B_4O_7$, which did not have any combustion activity and therefore did not produce significantly more $CO_2$ than the empty reactor [154]. It was critized, that Lunsford and co-workers did not cite this work. They also argued, that the $O_2$ conversion in their work and that of Lunsford, did not differ as significantly as argued by Lunsford, since the same reaction conditions were applied. This debate shows that several research groups can obtain different results, alone due to differences in the reactor set-up. Further detailed experiments under controlled and comparable conditions will be necessary to unreveal structure activity correlations.

It is reported that the contribution of the gas phase depends on the exact operating conditions (partial pressures of all compounds, temperature, residence time and free reactor volume) [155]. Yates and Zlotin and other researches did observe

significant contributions of gas phase reactions for the OCM. Therefore it can be concluded, that Lunsford *et al.* underestimated the importance of gas phase reactions, maybe due to their small scale experimental set-up and the applied the reaction conditions.

Hutchings and co-workers studied the partial oxidation of $CH_4$ at 5.85 kPa at higher temperatures, ca. 700 - 800 $°C$ with and without the presence of a catalyst [156]. The product yields were similar in the presence and absence of the catalyst, which indicated that a suitable catalyst is of secondary importance at this temperature, in agreement with the results of Yates and Zlotin [150].

Hutchings *et al.* compared the selectivities of Li/MgO and MgO in order to study the role of Li. Since Li/MgO showed higher selectivies for $C_2H_6$ they assumed that the role of Li could be the inhibition of the oxidative dehydrogenation activity of the MgO [157].

Ross and co-workers showed, that the active sites were formed as a result of the loss of carbonate species and that they were unstable under the reaction conditions of the OCM, namely reducing conditions. Catalysts with a high concentration of carbonate species produced more $C_2$ products, than catalysts with a lower concentration of these species. Because calcination at lower temperatures led to a higher residual $CO_2$ content of the catalysts, it also led to a higher catalytic activity. Furthermore, the formation of the active sites was suggested to be a direct result of the loss of carbonate species, which were unstable under the reaction conditions of the OCM, namely reducing conditions [28].

Ross and co-workers investigated the reaction pathway of the OCM over Li/MgO [158]. A recycle system was applied which behaves like a gradientless reactor with respect to the gas phase concentrations, a description can be found in [159]. It was found, that at 720 $°C$ the reaction followed a sequential reaction scheme, as shown in Reaction 2.5. Furthermore, they found that the presence of alkali carbonates and an excess of $CH_4$ decelerated the total oxidation of $C_2H_6$ and $C_2H_4$.

$$CH_4 \rightarrow C_2H_6 \rightarrow C_2H_4 \rightarrow CO_x \tag{2.5}$$

Van der Wiele and co-workers investigated the nature of the active compound of Li/MgO via comparison of the activity and the deactivation of Li/MgO catalysts and $Li_2CO_3$ supported on $ZrO_2$ [123]. The $O_2$ conversion of their 7 wt% Li/MgO increased during the first 16 hours, nearly to full conversion, followed by a steady deactivation. It was also shown, that the Li-content decreased during the whole time on stream. For 0.2 wt% Li/MgO, deactivation and loss of Li were observed from the beginning. However, the initial values of conversion were the same for both catalysts. It was concluded, that only a small amount of the Li was responsible for the activity. $Li_2CO_3$ alone supported on the inert carrier $ZrO_2$ revealed that $Li_2CO_3$ was also an active OCM catalyst, with a performance identical to Li/MgO, except for lower activity due to the lower specific surface area.

The activity lasted as long as $Li_2CO_3$ was present. It was shown that $Li_2ZrO_3$, which was also an active catalyst, was not the active phase here, as it was not present. From these information a working hypothesis of Li/MgO was developed, as shown in Figure 2.6. These results are in agreement with results published by Mirodatos and co-workers [119, 122].

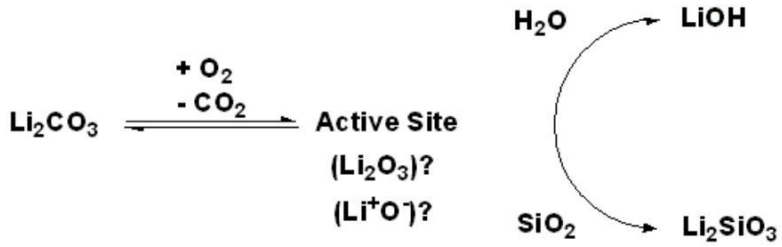


Figure 2.6: The working hypothesis of the Li/MgO catalysts, as proposed by van der Wiele *et al.* In the presence of $O_2$, $Li_2CO_3$ decomposes to form the active site, which reacts with $CH_4$. The deactivation proceeds through evaporation, reaction with $H_2O$ to LiOH, or the formation of $Li_2SiO_3$, reaction with $SiO_2$ from the quartz of the reactor material, which is being almost inert. Unchanged Figure adapted from [123]. Reprinted from Studies in Surface Science and Catalysis, Vol. 55, J.M.N. van Kasteren, J.W.M.H. Geerts and K. van der Wiele, Working Principle of Li Doped Mgo Applied For The Oxidative Coupling of Methane, 343-349, Copyright (1990), with permission from Elsevier via the Copyright Clearance Center.

Lunsford and co-workers studied the Reaction 2.6 over (LiCl+NaCl)/MgO [160]. With a matrix isolation system, methyl radicals were observed.

$$CH_4 + C_2H_4 \rightarrow C_3H_6 \tag{2.6}$$

However, vinyl radicals could not be detected. With isotopic experiments it was shown, that the methyl group, which was added to the alkene, derived from the $CH_4$.

## 2.5.2 Reactant Activation

### 2.5.2.1 Oxygen Activation

Nibbelke *et al.* showed that $O_2$ interacts strongly with the catalyst. It reversibly adsorbed dissociatively and an exchange between the surface and the bulk oxygen took place [161]. Doping with Li, even more with Sn, increased the oxygen diffusion coefficient, therefore, increasing the exchangeable amount of oxygen on the

catalyst. $CO_2$ interacted with the catalyst, in the absence of the reactants, only in the presence of Li.

Peil and co-workers used steady-state isotopic transient kinetic analysis (SSITKA) to investigate surface phenomena in the OCM over MgO and Li/MgO at temperatures up to 645 $^{\circ}C$ [162, 163, 164]. They found that the MgO and the Li/MgO catalysts could be divided into three regions:

1. physical surface where the oxygen exchange between gas phase and solid phase takes place,
2. several layers of subsurface oxygen atoms: that are readily available for exchanges,
3. and the bulk oxide.

The subsurface oxygen and the bulk oxygen were significant additional oxygen source. The investigation of the pathway of $CO_2$ suggested a multi-step oxidation pathway. Active sites which were involved in the coupling process were found to have a lower activity than active sites involved in the inselective processes [162, 163, 164].

Dahl *et al.* conducted characterization studies of Li/MgO in a pulse reactor, exposing the catalyst to pulses of air, $CH_4$ and air-$CH_4$ mixtures [165]. The results indicated that, the catalyst was active even with small amounts of $Li_2CO_3$ and $O_2$ may reversibly adsorb on the surface. Additionally, Li/MgO could act as an "oxygen reservoir".

Contradictory results to Peil and Nibbelke have been published by Choudhary *et al.* [166]. With pulse of $CH_4$, $C_2H_6$ and $C_2H_4$ in the presence and absence of gas phase $O_2$ over Li-, La- and Sm-promoted MgO, it was shown that the lattice oxygen of these catalysts did not have a significant role in the OCM and the presence of free $O_2$ is necessary for the OCM. The lattice oxygen is involved in the conversion of $C_2H_6$ and $C_2H_4$, however, the importance for the oxidation of $C_2H_4$ seemed to be more significant than for the oxidation of $C_2H_6$. Similar results were found for Li/MgO with additives [87] and for the oxidation of $C_2H_4$ over Li/MgO [89].

Keulks and co-workers studied the oxygen species with temperature programmed reactions in the oxidative coupling of methane over various catalysts, among them: Li/MgO [167]. Their results suggested that simple adsorbed oxygen species were not active for coupling, but for total oxidation. For simple oxide catalysts, such as Li/MgO, gas phase $O_2$ was necessary for the generation of the oxygen species active for the coupling reaction. Nevertheless, for multicomponent catalysts, the lattice oxygen regenerates the active oxygen species. The results of Bhumkar and Lobban also suggested that gas phase $O_2$ was involved in the regeneration of the active sites and in the $CO_2$ formation [168].

#### 2.5.2.2 Alternative Oxygen Sources

Nakamura and co-workers studied the decomposition of $N_2O$ on Li/MgO investigating the adsorbed oxygen species being formed [169]. It was demonstrated that a substantial amount of adsorbed oxygen species were formed. Moreover, the formed amount increased by doping MgO with Li. Experiments with molecular oxygen resulted in a much lower formation of adsorbed oxygen species. TPD experiments revealed two types of adsorbed oxygen species on Li/MgO, the $\alpha$-species desorbing between 400 - 420 $^{\circ}C$, the $\beta$-species at 480 - 495 $^{\circ}C$. In contrast, for pure MgO only a week $\alpha$-oxygen species was found. It was suggested that the $\alpha$-oxygen species was present on higher index faces of MgO, whereas the $\beta$-oxygen species was present at oxygen vacancies in the neighborhood of places where Li substituted Mg. The hydrolysis of the oxygen species, by soaking the samples in a solution of $H_2SO_4$, resulted in considerable amounts of $H_2O_2$, suggesting that they were mainly present as surface peroxides.

The use of different oxygen sources for the oxidative coupling of methane has been reviewed by Hutchings *et al.* [170, 171]. Only publications that refer to Li/MgO as a catalyst will be discussed in detail here.

Hutchings and co-workers investigated the role of surface $O^-$ in the selective oxidation of $CH_4$ using $N_2O$ as oxygen source [134, 172]. They showed that $O^-_{(s)}$ has two roles:

1. at low temperatures: hydrogen abstraction
2. at high temperatures: non-selective oxidation

Using $O_2$ as oxygen source, the $CH_4$ conversion was an order of magnitude higher than with $N_2O$. However, at comparable conversions, $N_2O$ led to higher selectivities than $O_2$.

In contrast to this, while studying the decomposition of $N_2O$ and the activation of $CH_4$ with $O_2$ and $N_2O$ over Li/MgO and MgO doped with alkaline earth oxides, Cunningham and McNamara found that $O_2$ was the more effective oxygen source; generally resulting in higher conversion and higher selectivities [173].

Later Hutchings *et al.* studied the OCM over Li/MgO in the presence of NO [174]. They found, that in the presence of NO, Li/MgO showed at least two different oxidizing species or oxidizing sites, which were significant. In the OCM over MgO and Li/MgO in the presence of different nitric oxides, different trends were observed for these two catalysts, therefore indicating different reaction mechanisms for MgO and Li/MgO [175].

In 1988, the same group did a comparative study of $O_2$, $O_3$ and $N_2O$ as oxygen source for the OCM over Li/MgO, MgO and $\gamma$-$Al_2O_3$ [127, 176]. Below 400 $^{\circ}C$, $O_3$ was more active and selective than $O_2$. The products under these conditions

were only $H_2$, $CO_2$ and CO. $H_2O$ could not be detected. The addition of $H_2O$ did not affect the product selectivity. $O_2$ and $O_3$ showed a similar performance at higher temperatures, while at low temperatures (200 - 300 $^\circ C$) $O_3$ showed higher performance. Nitrous oxides appeared to enhance the partial oxidation at low temperatures (550 $^\circ C$), while at higher temperatures (720 $^\circ C$), it increased the formation of total oxidation products. However, deactivation of the catalyst was observed.

The kinetic isotope effect during the oxidative coupling of methane over Li/MgO was studied by Shi and co-workers [177]. When using $O_2$ as oxygen source, it was found that a single rate limiting step did not exist. For $N_2O$, the rate limiting step was the incorporation of the oxygen into the crystal lattice of the Li/MgO.

Yamamoto *et al.* studied the OCM over Li/MgO with $N_2O$ as oxygen source [178]. The rate of oxygen incorporation into the catalyst was slower with $N_2O$ than with $O_2$. However, at the same $CH_4$ conversion levels, $N_2O$ led to higher selectivities than $O_2$, probably due to a decrease of surface reactions, which led to $CO_x$. Applying $N_2O$ as oxidant, pure MgO exhibits a much higher $CH_4$ conversion in comparison to Li/MgO, however, its $C_2$ selectivity was rather low.

#### 2.5.2.3 Methane Activation

Davydov *et al.* investigated the character of the primary $CH_4$ activation on MgO [179]. They observed, that the $CH_4$ activation on MgO formed $CH_3$-groups.

The effect of $CO_2$ on the selectivity of OCM and ODH of $C_2H_6$ over Li/MgO at temperatures below 650 $^\circ C$ was investigated by Lunsford and co-workers. It was found that secondary reactions of the methyl radicals on the catalyst surface are inhibited by $CO_2$ [180]. In this publication it was also commented that Korf *et al.* did not observe an effect of $CO_2$ on the $C_2$ selectivity [28]. The reason could be, that the reaction temperature in Korf's experiments was 780 - 800 $^\circ C$ and the selectivity of 78 %, was already high. The main source of $CO_2$ at this temperature was the total oxidation of $C_2H_6$ and $C_2H_4$ in the gas phase [181]. Thus the importance of surface phenomena, like secondary reactions of the methyl radicals, decreased, however, the formation of methyl radical still took place [180].

The effect of $CO_2$ on the activation energy for the $CH_3\cdot$ formation and the overall $CH_4$ consumption in the OCM over Li/MgO was investigated by Lunsford *et al.* [182]. They found that in the gas phase $CO_2$ increased the intrinsic activation energy for the $CH_3\cdot$ formation by 100 % with increasing partial pressure of $CO_2$. The activation energy approached a limiting value of 209 kJ/mol at $CO_2$ partial pressures higher than 0.001 bar, a value which is definitely being achieved under typical reaction conditions for the OCM. $CO_2$ acted as a catalyst poison, because it adsorbed at the basic oxygen ions, which were believed to be responsible for the activation of $CH_4$. At lower temperatures more active sites were poisened than at

higher temperatures.

Coulter and Goodman showed that the rate-limiting step of the OCM depended on the $CO_2$ coverage of the catalyst. Their results indicated that at low partial pressures of $CO_2$, the C-H bond cleavage is the rate determining step, while at high partial pressures of $CO_2$ the desorption of $CO_2$ is the rate determining step [183].

Cant *et al.* observed that the rate of conversion of $CH_4$ over Li/MgO is 1.5 times larger than the rate of $CD_4$, indicating that the C-H bond breaking is the rate determining step [184].

Lapszewicz and Jiang studied the relationship between activity, selectivity and basicity and the ability of C-H and O-O bond scission of $\gamma$-$Al_2O_3$, MgO and monoclinic or cubic $Sm_2O_3$ [185]. Isotopic exchange rates were measured to determine the ability of these materials to activate the reactants of the OCM. Since a correlation was not found, it was concluded that the formation of the methyl radical cannot be explained simply by a one-step mechanism.

## 2.5.3 Reaction Network

### 2.5.3.1 Reaction Intermediates

Bhumkar and Lobban observed *in situ* the surface features of Li/MgO and its interactions with adsorbates at steady state and transient conditions, applying diffuse reflectance Fourier transform infrared spectroscopy (DRIFTS) [168]. Under reaction conditions adsorbed $CO_2$, strongly bonded to OH-groups and carbonate was found. $CO_2$ in the gas phase reduced the catalytic activity, due to adsorption and reaction to carbonate. However, $H_2O$ had a positive effect on the carbonate decomposition.

The presence of carbene during the OCM reaction was shown by Martin and Mirodatos [186]. They introduced $C_2H_4$ into the reactor, which was transformed into cyclopropane. Later this was confuted by Mims and co-workers [187].

Mirodatos *et al.* studied the heterogeneous and homogeneous processes involved in the OCM over Li/MgO [188]. They compared the conversion, selectivities and yields of $CH_4/O_2$ and $C_2H_6/O_2$ mixtures. The observed differences were likely to be due to the much shorter lifetime of the $C_2H_5\cdot$ radical, preventing subsequent heterogeneous deep oxidation. $CH_4$ mixed with other hydrocarbons led to cross coupling products, if the C-H bond strength is relatively small (for example propene and toluene in contrast to benzene). Cross-coupling of $CH_4$ and $C_2H_4$ was also observed by Lunsford [160].

Nibbelke investigated the heterogeneous steps of the OCM over Li/MgO and Li/Sn/MgO. As mentioned above, for a fully satisfying explanation of the obtained results, a methoxy species was postulated, which was the only carbon containing intermediate leading to the formation of $CO_2$ [161].

#### 2.5.3.2 Product Formation

Van der Wiele and co-workers investigated the individual reaction steps in the oxidative coupling of methane over Li/MgO, studying the oxidation of $C_2H_6$, $C_2H_4$ and CO separately [189]. It was found, that the conversion of $C_2H_6$ to $C_2H_4$ was faster than the total oxidation of $C_2H_6$, irrespective of the catalyst. The conversion of $C_2H_6$ proceeded much faster than the conversion of $CH_4$. The combustion proceeds mainly via $C_2H_4$, which would be a serious constraint for the maximal achievable yield.

Campbell and Lunsford investigated the contribution of the gas phase radical coupling in the oxidative coupling of methane. They found a good agreement between the yield and the methyl radical formation. The $CO_2$ partial pressure was also found to be an important variable [190].

Van der Wiele *et al.* used low pressure experiments to discriminate between the homogeneous and the heterogeneous reactions [191]. The Li/MgO in the OCM was proposed to activate $CH_4$ and to produce of methyl radicals, which couple in the gas phase, in case a sufficient amount of third bodies are available. Furthermore, it was shown that Li/MgO was involved in the total oxidation of $C_2H_6$, $C_2H_4$ and CO.

This is in agreement with the work of Campbell *et al.* [192], concluding that at least 40 - 45 % of the $C_2$ molecules were the product of gas phase coupling. That no significant hydrogen exchange was observed indicates, that the C-H breaking is an irreversible step.

In studies of the OCM with Li/MgO with a reactant mixture of $CH_4$, $CD_4$ and $O_2$ [193, 194, 195], no significant hydrogen exchange between $CH_4$ and $CD_4$ was detected. The only detected reaction products were:

1. Saturated Products:
   (a) $C_2H_6$
   (b) $CH_3CD_3$
   (c) $C_2D_6$
2. Unsaturated Products:
   (a) $C_2H_4$
   (b) $CH_2CD_2$
   (c) $C_2D_4$.

Depending on the concentration of the reactants, the relative concentration of the different products could be predicted. Based on these results, it was proposed that the formation of $C_2H_6$ occurred via the gas phase coupling of methyl

radicals and the oxidative dehydrogenation of $C_2H_6$ in the gas phase was the source of $C_2H_4$. However, the absence of hydrogen exchange is remarkable, because over pure MgO it has been reported to take place for $C_2$ hydrocarbons at 300 °*C* and for $CH_4$ at 400 °*C* [196] and the activation energy was determined to be 193 kJ/mol ± 14 kJ/mol [197]. Even so taking place at elevated temperatures, other researchers also reported the exchange between $CH_4$ and $D_2$ over MgO [185, 198]. Balint and Aika could observe an isotopic exchange between $CD_4$ and the hydroxyl groups of the 1 wt% Li/MgO at room temperature [199].

Mims *et al.* also investigated the oxidative coupling of methane with $CH_4/CD_4$ mixtures [187]. The results were in agreement with Nelson *et al.* [193, 194, 195]. The OCM reaction mechanism via methylene, which was proposed by Martin and Mirodatos [186], could be excluded, because the only products formed, are $C_2H_6$, $CH_3CD_3$ and $C_2D_6$.

A close relationship between the formation rate of $C_2H_6$ per unit surface area and the density of strong basic sites on the surface was observed by Choudhary *et al.* [27].

#### 2.5.3.3 Consecutive Reaction: Ethane to Ethylene

$C_2H_6$ is the primary $C_2$ product in OCM, but already below the temperature required for the $C_2H_6$ formation the oxidative dehydrogenation of $C_2H_6$ to $C_2H_4$ proceeds. Therefore it is important not only to consider the coupling of methyl radicals to $C_2H_6$, but also the ODH of $C_2H_6$, to produce the desired product $C_2H_6$.

Morales and Lunsford reported that 3 wt% Li/MgO was an effective catalyst for the ODH of $C_2H_6$ [181]. They also showed that $CO_x$ species were produced from the total oxidation of $C_2H_6$ as well as $C_2H_4$. They could further show that above temperatures of 675 °*C* the gas phase reactions became predominant. It was assumed that even the ODH of $C_2H_6$ reaction involved the generation of radicals, $C_2H_5\cdot$ radicals in case of the ODH of $C_2H_6$ .

Chevalier and co-workers also observed that under reaction conditions of the OCM (800 °*C*), $C_2H_6$ was non-oxidatively dehydrogenated to $C_2H_4$ [42].

The importance of consecutive reactions was studied over the Li/MgO catalyst by van der Wiele *et al.* [200]. The experiments were carried out at low pressures (0.0001 - 0.015 bar). It was found that $C_2H_6$ was converted 4 times faster than $CH_4$, mostly to $C_2H_4$. $C_2H_4$ was still oxidized 2.6 times faster than $CH_4$. The conclusion was, that there should be an upper limit of the $C_{2+}$ yield, which can be achieved with Li/MgO.

#### 2.5.3.4 Consecutive Reaction: Total Oxidation

Reviewing the study of the single steps of the OCM reactions, van der Wiele *et al.* found that the main reaction pathway for the combustion proceeded via $C_2H_4$ [189]. In the absence of a catalyst, the main combustion product was CO, while in the presence of a catalysts $CO_2$ dominated. Similar results were observed by Mirodatos and co-worker. $C_2H_6$ was oxidized to CO already at $600\,^{\circ}C$ in the gas phase. At this temperature the oxidative coupling was still very limited. This was identified as one of the biggest problems of the oxidative coupling of methane [201].

Ross and co-workers also compared the reaction pathways of $C_2H_6$ and $C_2H_4$ over Li/MgO and Ca/$Sm_2O_3$ [202]. None of the molecules were found to be stable under reaction conditions. The total oxidation of $C_2H_6$ and $C_2H_4$ contributed significantly to the overall reaction network. Since Ca/$Sm_2O_3$ was the most active catalyst, its total oxidation activity for $C_2H_6$ and $C_2H_4$ was at least partially responsible for its lower selectivity compared to Li/MgO.

Nelson and Cant studied the kinetic isotope effect and the contribution of the oxidation of the $C_2$ products to the $CO_2$ formation with isotopic tracer experiments over Li/MgO with isotopic reactant mixtures [184, 193, 194, 195, 203, 204]. They could show that above $740\,^{\circ}C$ 30-80 % of the $CO_2$ derived from the oxidation of the $C_2$ hydrocarbons, while below $700\,^{\circ}C$, they were responsible for less than 10 % of the $CO_2$ formation. Two pathways for the $C_2$ oxidation were possible:

1. competition of the $C_2$ products with $CH_4$ for $O_2$ in surface promoted reaction,

2. and competition for $CH_3\cdot$ by abstraction and combination, leading to the formation of $CO_x$.

Furthermore their experiments showed that an exchangeable pool of $CO_2$ existed in the catalyst, indicating that $Li_2CO_3$ is present during the reaction. Besides, it was also found that the first step of activation was the bond breaking of a C-H bond.

In 1994, Mims and co-workers traced the secondary reactions of $C_2H_4$ with computer models and isotopic experiments [205]. The oxidation of $C_2H_4$ had only little effects on the $CH_4$ conversion, even at comparable partial pressures. From the comparison with computer models, the surface was seen to quantitatively quench much of the oxidative gas phase radical chemistry. The $C_3$ and $C_4$ yield and the isotopic distributions agreed well with the described gas phase pathways.

The origin of $CO_2$ in the OCM was investigated with isotope experiments by the group of Lunsford [206]. The results showed that the rate of $CO_x$ formation

from $C_2$ products was several times larger than the $CO_x$ formation from $CH_4$, even for Li/MgO at temperatures below 700 $^{\circ}C$. The rate constants for the formation of $CO_x$ from $CH_4$ and from $C_2H_4$ depended on several factors like type of catalyst, reaction temperature, $CH_4$ to $O_2$ ratio and type of oxidant. Under the studied reaction conditions, the ratio of $CO_x$ formed from $CH_4$ and from $C_2H_4$, the $C_2$ selectivity and the $C_2$ yield tended to increase with increasing temperature. This suggested that the amount of $CH_4$ being converted to $CO_x$ decreased.

#### 2.5.3.5 Consecutive Reactions: Formation of Hydrogen, Reforming and Water Gas Shift Reaction

Hargreaves and co-wokers studied the formation of $H_2$ in the OCM over MgO [207]. $H_2$ had an unexpectedly high selectivity in the OCM reaction. The source was the water gas shift reaction but also thermal cracking of $C_2H_6$. However, the partial oxidation became more dominant at higher flow rates and low oxygen conversions.

Kinetic and mechanistic aspects of the ODH of $C_2H_6$ on Li/MgO were studied by Ross *et al.* [208]. The results indicated that $H_2$ and CO are unlikely to be the product of steam reforming, $CO_2$ reforming of $C_2H_6$ or the water gas shift reaction. $H_2$ and CO are most likely produced by the decomposition of ethoxy species on the surface.

Balint and Aika investigated the water gas shift reaction and the methane steam reforming over 1 % Li/MgO with temperature programmed reactions and isotope labeled compounds [199]. The experimental results suggested, that the contribution of water gas shift reaction to the amounts of $CO_2$ and $H_2$ formed in the oxidative coupling of methane was important, which is in contradiction to the results of Ross *et al.* [208]. Steam reforming of methane could not be observed. However, an isotopic exchange between $CD_4$ and the OH groups of the Li/MgO was observed at room temperature.

### 2.5.4 Debate about the Active Center

#### 2.5.4.1 Defect Sites with Lithium and Oxygen

In their EPR experiments, Lunsford *et al.* found an EPR signal, which was in agreement with the signal Abraham *et al.* assigned to $[Li^+O^-]$ [148]. The methyl radical formation was correlated with the relative intensity of EPR signals, which were assigned to the concentration of the $[Li^+O^-]$ centers, shown in Figure 2.7. Depending on this correlation it was concluded that the active center is $[Li^+O^-]$ [21]. They suggest, that methyl radicals are formed via a hydrogen abstraction from $CH_4$ by the $[Li^+O^-]$ centers. The mechanism proposed by Lunsford *et al.* is

shown in Figure 2.8. An alternative pathway for the regeneration may also be possible, with an electron trapped in an oxygen ion vacancy [20].

However, no direct proof, e.g. by ENDOR, was given, that the observed signal at g = 2.054 was indeed caused by $[Li^+O^-]$. Furthermore, the signal was never detected directly upon quenching from OCM conditions but only upon quenching after heating in air or pure $O_2$. It is therefore highly questionable whether the correlation observed in Figure 2.8 is indicative of the mechanism - suggested by Lunsford *et al.*.

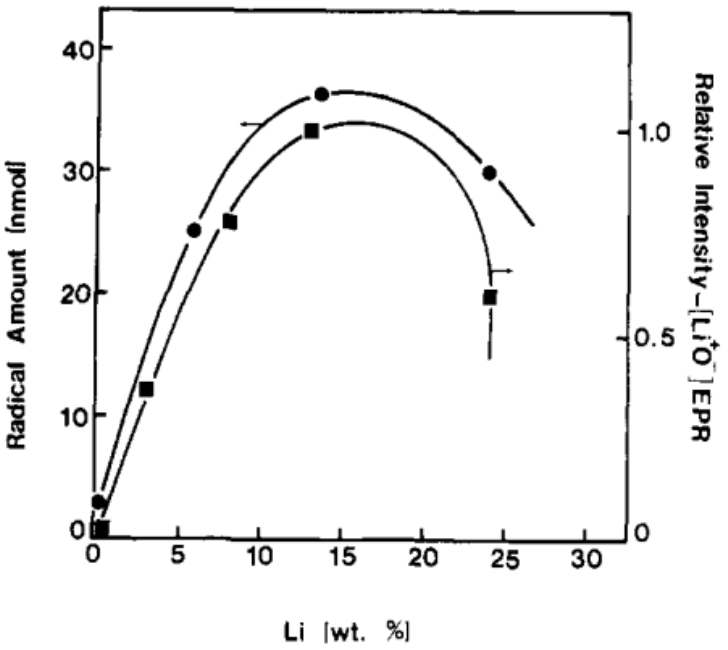


Figure 2.7: The amount of radicals and $[Li^+O^-]$ centers formed as a function of lithium doping into MgO (Aldrich Gold Label). All reactions were carried out under the following conditions: T = 500 °*C*, collection period, 25 min (after 4 h on line), 0.50 g of catalyst, argon flow 3.8 $cm^3min^{-1}$, $CH_4$ flow 1.14 $ccm^3min^{-1}$, $O_2$ flow 0.023 $cm^3min^{-1}$. Preconditioned at 450 °*C*, 2.5 h, 300 $cm^3min^{-1}$ $0_2$. The samples were quenched in liquid nitrogen after a 2 h exposure to air at 700 °*C*. Figure unchanged from [21]. Reprinted from Journal of the American Chemical Society, Vol. 107/1, D.J. Driscoll, W. Martir, J.X. Wang and J.H. Lunsford, Formation of gas phase methyl radicals over magnesium oxide, 58-63, Copyright (1985), with permission from the American Chemical Society via the Copyright Clearance Center.

In 1986, the $[Li^+O^-]$ centers in Li/MgO were characterized by Wang and Lunsford [209]. They found indications, that these centers were formed at isolated

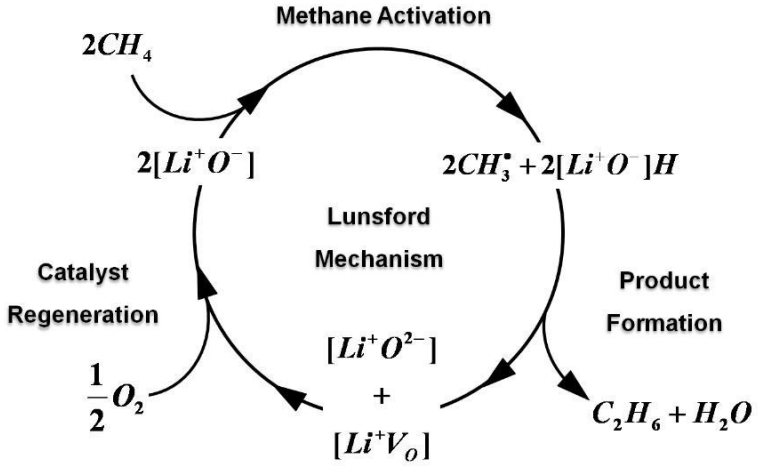


Figure 2.8: The mechanism of the $CH_4$ activation over Li/MgO and the regeneration of the active center as proposed by Lunsford and co-workers.

substitutional $Li^+$ ions. These defects were believed to be responsible for the activation of $CH_4$.

Peng and co-workers investigated the surface composition and the reactivity of Li/MgO with kinetic and XPS measurements [133]. Under reaction conditions, they observed two Li containing phases in Li/MgO, namely $[Li^+O^-]$ and $Li_2CO_3$. The O(1s) XPS peaks were assigned to the surface $[Li^+O^-]$ and its concentration. Due to the correlation of the $CH_4$ conversion and the concentration of surface $[Li^+O^-]$, it was demonstrated that the $[Li^+O^-]$ species is the active center. Moreover, they determined that the concentration of the $[Li^+O^-]$ species seemed to be saturated at a Li loading of 0.2 wt%. They presumed that Li in excess to this, evaporated from the surface and/or diffused into the MgO. This value is in agreement with the discussion on the optimal loading of Li [78] and the experiments for the re-appraisal of the Li loading of Hutchings and co-workers [79].

However, Myrach *et al.* could not detect EPR signal compatible with $[Li^+O^-]$ [118].

#### 2.5.4.2 F-Center

Goodmann *et al.* investigated the OCM over model catalysts of MgO and Li/MgO with combined surface science techniques under ultra high vacuum (UHV) conditions and kinetic measurements at elevated pressures. Their results indicated that the $[Li^+O^-]$ centers were not responsible for the activation of $CH_4$, but in fact the formation of F-type centers in the near surface region [210, 211, 212, 213]. The formation of $C_2H_6$ could be correlated with the F-type defects, determined by spectroscopic methods [212, 214]. The effect of the pretreatment on the active

site of MgO and Li/MgO was also investigated [215]. The $C_2$ product formation over MgO increased with increasing pretreatment temperature indicated that the active site for the $CH_4$ activation was most probably an F-type defect. This was in agreement with the thin film model [214]. The formation of these defects was postulated as the rate determining step. However, for Li/MgO the rate determining step depended on the reactant gas mixture, namely whether $O_2$ was present or absent. Li is considered to be a promoter for the F-type defects, which could explain, that in Li/MgO the rate determining step was different compared to MgO. It was suggested, that in the presence of $O_2$, the decomposition of $Li_2CO_3$ was the rate determining step and in the absence of $O_2$ it was the H abstraction from $CH_4$ [215].

Nelson and Tench studied the chemisorption of $O_2$ on MgO. The experiments showed that in an $O_2$ atmosphere, the F-centers disappeared at 350 $^\circ C$ [216]. However, statistical thermodynamics predicts, that at higher temperatures, more F-centers should be formed. If the F-centers are stable under OCM conditions is unknown.

#### 2.5.4.3 Mobile Lithium Carbonate Film

The deactivation of the Li/MgO catalysts was investigated in detail by Mirodatos and co-workers [119]. It was found, that a tight interface between $Li_2CO_3$ and MgO phases enabled an optimal catalytic performance. This was the case after a treatment, which allowed the liquefaction of the alkali salt. However, the static model of Li substitution, proposed by Lunsford and co-workers [20, 21, 217], does not agree exactly with the model of the mobile $Li_2CO_3$-film coating the MgO [119]. The role and the fate of the surface active site of Li/MgO was also studied [122]. Uncarbonated MgO was reported to have a very poor activity for coupling and total oxidation. However, for Li/MgO, the total oxidation activity was reported to depend on the accessible surface area of $Li_2CO_3$, and the coupling activity was suggested to require an association of Li and Mg phases, being enhanced after high temperature treatment. Under reaction conditions, the total oxidation selectivity was reported to decrease, due to the decomposition of $Li_2CO_3$.

### 2.5.5 Pure MgO

Aika and Lunsford investigated the dehydrogenation of alkanes by $O^-$ on MgO, with EPR and catalytic experiments [218]. The formation of alkenes was observed at 25 $^\circ C$, the maximum was reached at 300 $^\circ C$. For the reaction with alkanes, an alkoxide intermediate was proposed. For $CH_4$, a methoxide group was proposed, which decomposed at 450 $^\circ C$, to form mainly $H_2$.

Iwamoto and Lunsford studied the oxidation of alkanes and alkenes by $O_2^-$ on MgO, using EPR and catalytic experiments [219]. Stochiometric reactions were observed with simple hydrocarbons at 175 $^\circ C$, resulting in oxygenates, hydrocarbons and $CO_2$. It was proposed that the first step for the reaction of hydrocarbons with $O_2^-$ is the abstraction of a hydrogen atom. Garrone and co-workers discussed in a note the formation of $O_2^-$ on MgO in more detail [220].

Takita and Lunsford investigated the oxidation of alkanes by $O_3^-$ on MgO, using EPR and catalytic experiments [221]. The evidence suggested a direct reaction of the $O_3^-$ with the hydrocarbons, rather than a dissociation of the $O_3^-$ with subsequent reaction.

Ito *et al.* observed the activation of $CH_4$ on MgO at lower temperatures by means of TPD and ESR (electron spin resonance) experiments [222]. It was found that the C-H bond was easily activated on the MgO surface, even below room temperature. Furthermore, the nature of the active site was discussed and it was shown, that on MgO in low coordinated states the $CH_4$ adsorbs in the heterolytically dissociated state.

Hargreaves and co-workers reported the structural effects of the oxidative coupling of methane on two samples of MgO [80]. MgO obtained via the thermal decomposition of carbonates was found to show higher $C_2$ selectivities than MgO obtained via burning Mg. The two MgO samples had different morphologies, which demonstrated that the morphology of MgO was an important factor for the OCM.

Zhen *et al.* characterized and studied the catalytic properties of MgO obtained from different preparation procedures [223]. The used MgO materials were, pure commercial MgO, prepared via decomposition of $MgCO_3$ and the decomposition of $Mg(NO_3)_2$. The structural data and the catalytic performance were correlated and the important factors for the catalytic performance, namely temperature and specific surface area, were discussed.

Aika and Karasuda scrutinized MgO and its active site [224, 225, 226]. It was proposed that the active site in MgO was an electron-deficient oxygen source, $O^-$ for instance [224]. Oxygen exchange experiments confirmed this [225]. Later they proposed, that the adsorption of $H_2O$ could be responsible for the generation of the active site [226]. Figure 2.9 shows a model for the flux of oxygen atoms for different types of oxygen in MgO-based catalysts.

Hutchings and co-workers studied the oxidative coupling of methane in the presence of nitric oxides over MgO and Li/MgO [175]. Since different trends for these two catalysts were observed, it was suggested that the reaction mechanism for the OCM over MgO and Li/MgO is different.

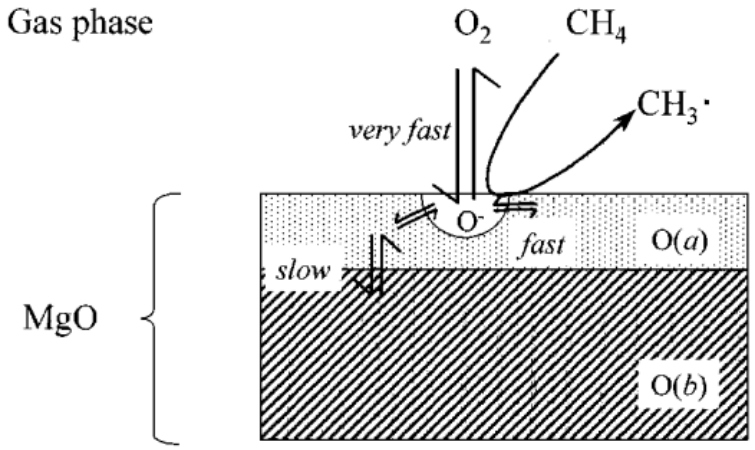


Figure 2.9: Model for oxygen atom flux in MgO-based catalysts, as proposed by Karasuda *et al*. Figure unchanged from [225]. Reprinted from Journal of Catalysis, Vol. 171/2, T. Karasuda and K. Aika, Isotopic Oxygen Exchange between Dioxygen and MgO Catalysts for Oxidative Coupling of Methane, 439-448, Copyright (1997), with permission from Elsevier via the Copyright Clearance Center.

### 2.5.6 Summary

Abraham *et al.* reported the presence of $[Li^+O^-]$ defects in Li-doped MgO single crystals. The formation of this defect requires high temperatures and oxidative conditions, with subsequent thermal quenching [101, 103, 106, 107, 108, 109, 148]. That the oxidative conditions are necessary can be seen when this formation is written in Kröger Vink notation (see Reaction 2.7). Due to the monovalent nature of $Li^+$ compared to $Mg^{2+}$, excess gas phase $O_2$ is required for charge compensation.

$$Li_2O + 2Mg_{Mg}^X + 1/2O_2 \rightarrow 2Li_{Mg}^{'} + 2O_O^{\cdot} + 2MgO \tag{2.7}$$

Abraham and his group provided evidence for the presence of $[Li^+O^-]$ using EPR *and* ENDOR spectroscopy. Lunsford *et al.* attributed the the EPR signal at $g = 2.054$ to $[Li^+O^-]$ [20, 21, 209], according to the work of Abraham. But in his works, the EPR measurements were done after calcination of the catalyst in air or $O_2$ followed by quenching in liquid $O_2$ or liquid $N_2$. However, the reaction conditions in the OCM are reducing as $CH_4$ is present in excess and $H_2$ occurs as reaction product. In fact, the EPR signal at $g = 2.054$ was never reported after quenching from reaction conditions. Moreover, the proof via ENDOR has also never been published.

The correlation between the loading of Li, the intensity of the EPR signal, measured after calcination for 2 hours in air, and the formed amount of $CH_3\cdot$ radicals, is no proof, that $[Li^+O^-]$ is the active center.

At OCM temperatures, considerable amounts of $C_2H_6$ and $C_2H_4$ can be formed, without the presence of a catalyst, as shown by Yates and Zlotin (Table 2.2). So, it is not surprising that $CH_3\cdot$ radicals can be detected at the end of a reactor at high temperatures by a technique as sensitive as EPR. There is no doubt, that Li/MgO and other catalyst have an influence on the OCM, however, the exact role is unclear.

In experiments with mixtures of $CH_4/CD_4$ conducted by Mims *et al.* and other, only symmetrically labeled $C_2$ products were found, pointing to radicals as precursors for the $C_2$ products. The positive isotope effect indicates that the cleavage of the C-H bond is the rate determining step. Other researchers reported H-D scrambling at rather low temperatures over MgO. The only way to combine these contradictory results is that the first C-H breaking occurs in the gas phase and not at the surface of Li/MgO. Attributing most of the OCM chemistry to reactions in the gas phase could explain also many chemically different materials catalyze the OCM with similar performance at temperatures of $750\,^{\circ}C$, but not why Li/MgO and other materials enhance $C_2$ selectivity.

## 2.6 Ternary Systems

### 2.6.1 Effect of Metal Oxides on Li/MgO

Li/MgO has been treated with different dopants; a general overview is shown in Table 2.3. The main idea of doping Li/MgO was to prevent the loss of Li, either by modification of the solid phase or by change the reaction conditions towards milder conditions.

In an early study, Bi *et al.* investigated the OCM reaction over a series of alkali, alkaline earth and rare earth metal oxides, prepared by an impregnation method. $SiO_2$, $Al_2O_3$ and several different MgO materials were used as support material. MgO was found to be the most promising support and Li/Ce/MgO to be the most promising catalyst [136].

Ross *et al.* observed the effect of additives, various oxides of transition metal oxides and rare earth oxides, on Li/MgO in the oxidative coupling of methane [228]. A number of dopants, for instance, Sn, Dy, Ti and Tb, did not effect the $C_2$ selectivity, however, the temperature required to achieve the optimal yield was lowered. An explanation could be that the formation of the active oxygen species is favored. Other additives showed minor improvements without an effect on the selectivity (La, Ni) or lowered the required temperature to reach a certain conversion (Co,

Table 2.3: Summary of different dopants of Li/MgO and the according to the references.

| No. | Dopant | Reference |
|---|---|---|
| 1 | Na | [208, 227] |
| 2 | Ca | [228] |
| 3 | Ti | [228] |
| 4 | V | [228] |
| 5 | Cr | [229] |
| 6 | Mn | [86, 87, 228, 229, 230, 231, 232, 233, 234] |
| 7 | Fe | [229] |
| 8 | Co | [228, 227] |
| 9 | Ni | [228, 235] |
| 10 | Zn | [86, 87, 228, 229, 230] |
| 11 | Zr | [227, 236, 237] |
| 12 | Nb | [125, 227] |
| 13 | Mo | [228] |
| 14 | Cd | [86, 87] |
| 15 | Sn | [228, 161, 227, 236, 238, 239, 240, 241] |
| 16 | La | [228, 136] |
| 17 | Ce | [136, 242, 243, 244, 245, 246] |
| 18 | Pr | [136] |
| 19 | Nd | [136] |
| 20 | Sm | [136] |
| 21 | Tb | [228] |
| 22 | Dy | [228] |
| 23 | Pb | [228] |
| 24 | Bi | [228, 247, 248] |

Mn, Pb, Bi). A comparison of the different additives showed that Li/Sn/MgO is a very promising system.

Ross and co-workers studied various promoted Li/MgO in the ODH of $C_2H_6$ [249]. Li/Na/MgO showed a $C_2H_4$ selectivity of 86 % at a $C_2H_6$ conversion of 38 %. Thermal investigations showed that an eutectic melt of $LiNaCO_3$ is formed at 490 $^\circ C$, which exists as a molten phase. This was probably the reason for the improved selectivity. Lercher *et al.* found a similar effect for the cracking and the ODH of $C_2H_6$ and $C_2H_8$ over Li/Dy/MgO [250].

Choudhary *et al.* investigated the effect of Mn, Cd and Zn oxides on pure MgO and Li/MgO in the oxidative coupling of methane [86]. Doping led to sintering of the MgO but also to an increase in $C_2$ selectivity. The involvement of lattice oxygen in the coupling reaction was shown by experiments in a pulsed microreactor.

Larkins and Nordin reported the effect of doping Li/MgO with different metal oxides, such as Fe, Mn, Zn and Cr [229]. The catalytic activity could be attributed to the physico-chemical properties of the catalyst, in particular to the presence of reducible sites on the surface. Especially Cr, but also Mn, seemed to favour the formation of total oxidation products, while Zn and Fe led to higher $C_2$ selectivities, probably due to the absence of reducible sites. The presence of these dopants was also involved in changes of the surface morphology.

Larkins and Nordin tested the performance of MgO, with and without $Li_2CO_3$ being present in the preparation, loaded with different amounts of ZnO and Mn oxides, in the oxidative coupling of methane [230]. If no $Li_2CO_3$ was present, the total oxidation of $CH_4$ dominates. At a reaction temperature of 805 $^\circ C$, the Zn containing catalysts resulted in $CH_4$ conversion higher than 25 % and a $C_2$ selectivity of around 60 %, however, this catalysts was not better than the undoped $Li_2CO_3$/MgO. For low loadings of Mn, the $CH_4$ conversion was higher than 35 % with a $C_2$ selectivity of around 50 %. Increasing the loading of Mn, resulted in a decrease of conversion and $C_2$ selectivity.

Studying the structural features of Li/Mn/MgO [231], the group of Fierro found that the incorporation of Li inhibited certain reactions of the Mn-MgO phases, resulting in a higher Mn dispersion.

Later Kanno and Kobayashi observed the different modification effects of Li on two Mn/MgO samples, one with lower and one with higher Mn content [232]. They discriminated between the different lattice oxygen species of Mn/MgO involved in the OCM [233]. The oxygen of MgO was found to be active for the methyl radical formation, while the oxygen of Mn-MgO was found to be active for the oxidative dehydrogenation of $C_2H_6$.

Zhang *et al.* studied the role of Li in Li/Mn/MgO with atomic absorption spectroscopy (AAS), XRD and infrared-photoacoustic spectroscopy [234]. Catalysts from which the Li had been washed off showed a lower $C_2$ selectivity, indicating

that the presence Li is important.

Since Li/Sn/MgO was considered being a very promising catalytic system [228], the mechanism of the oxidative coupling of methane on this system was investigated in detail [238]. The results were in agreement with a Langmuir Hinshelwood mechanism and it was concluded that the rate determining step involves the reaction of an adsorbed $CH_4$ with an adsorbed diatomic oxygen species.

The particular role of Sn in the Li/Sn/MgO was investigated by Ross *et al.* [239]. It was shown that the addition of Sn to Li/MgO stabilized the catalytic activity, Li was retained on the support under reaction conditions and therefore suppressed deactivation. On adding larger amounts of Sn, $Li_2Mg_3SnO_6$ was formed as a new phase. Pure $Li_2Mg_3SnO_6$ was also active for the oxidative coupling of methane. The $C_2$ yield versus time was also shown, with a decline of 12 % to 7 % over 150 hours time on stream.

Nibbelke *et al.* scrutinized the heterogeneous steps of the OCM over MgO, Li/MgO and Li/Sn/MgO [161]. They observed, that doping with Li, even more the addition of Sn, led to an increase of the oxygen diffusion and to an increase in the amount of exchangable oxygen.

Mallens and co-worker did TAP experiments (temporal analysis of products) with Sn/Li/MgO [251]. From these experiments, they concluded that methyl radicals were produced at the surface and combined in the gas phase. $C_2H_4$ was formed from $C_2H_6$ via the oxidative dehydrogenation in the gas phase. Both $C_2$ products could be converted into CO, which could further be oxidized to $CO_2$. $C_2H_6$ and $CH_4$ could be directly converted into $CO_2$ by adsorbed $O_2$. However, lattice oxygen could also play a role in this. For the non selective reactions of $C_2H_6$, gas phase and lattice oxygen seemed to play a role. The addition of Sn to Li/MgO increased the amount of reactive oxygen, in the uppermost lattice [240].

The group of Aika reported on the effect of Sn on Li/MgO [241]. They proposed two active centers. One was $O^-$, a surface oxide ion with an electron deficit, being generated when small amounts of Sn (less than 1 mol%) were added to Li/MgO. Another one was the $O^{2-}$ of a complex oxide, containing Sn, which was formed when large amounts of Sn were added. A redox cycle of $Sn^{4+}$ and $Sn^{2+}$ could be formulated involving $O^{2-}$. Furthermore it was shown, that the addition of Sn reduced the formation of $Li_2CO_3$, which covered the surface of the catalyst.

Ross and co-workers explored the importance of mixed oxides in the catalytic behavior of Li/MgO doped with Sn or Zr [236]. Doped with Sn, the phase, which was responsible for the improved properties, seemed to be $Li_2Mg_3SnO_6$, with a cubic structure like MgO. Doping with Zr resulted in various mixed oxides with different properties.

Zr-doped Li/MgO was studied in more detail by Ross *et al.* [237]. It was found that increasing the Li loading led to a decrease in the initial activity, while the selectivity was unaffected. The life-time of Li/Zr/MgO was depending on

the Li loading, increasing amounts of Li extended the life-time. The presence of $Li_2MgZrO_4$ increased the stability of the catalyst, while $Li_2Mg_3ZrO_6$ was an active and selective phase, but not stable under reaction conditions.

McNamara *et al.* investigated the effect of adding Nb and Zr to Li/MgO and Li/Na/MgO [227]. For comparison Sn and Co promoted Li/MgO and Li/Na/MgO were used. The resulting catalysts were more active and selective than the unpromoted Li/MgO, furthermore, the optimum yield could be obtained at lower temperatures. A similar effect was observed for Li/Na/MgO.

Ross *et al.* observed the effect of Nb on Li/MgO in the OCM and ODH of $C_2H_6$ [125]. In the OCM, at 600 $°C$ reaction temperature, a catalyst with 16 wt% Nb showed an activity 10 times higher than undoped Li/MgO. However, for the ODH of $C_2H_6$, only a slight improvement was found. Generally Li/Nb/MgO produced more $CO_2$, it had therefore a lower selectivity to the desired $C_2$ products. Two phases with Li and Nb were found, however, the active phase remained unclear. The loss of Li from Li/Nb/MgO was comparable to that of pure Li/MgO. The addition of Nb increased the specific surface area. Above the melting point of $Li_2CO_3$, the catalyst deactivated, the specific surface area decreased and the amount of the two Li/Nb phases sharply decreased. The addition of $CO_2$, which had previously been reported to avoid deactivation of Li/MgO [124], did not suppress the deactivation of Li/Nb/MgO.

Bartsch *et al.* studied the kinetics of the oxidative coupling of methane over Ce/Li/MgO [243, 244, 245]. Later, Dittmeyer and Hofmann made a kinetic analysis of these data and simulated reactor performance over this catalyst [242].

Ramasamy *et al.* reported the influence of important reaction parameters, such as temperature, feed gas composition and space velocity, for the oxidative coupling of methane over Li/Ni/MgO [235]. Catalyst deactivation was observed, the authors suggested as probable reasons a loss of Li and coke deposition.

Tiwari and co-workers studied the OCM over Li/Ce/MgO and Li/Ce/MgO-CaO [246]. Li/Ce/MgO-CaO showed a drastically improved $C_2$ selectivity, compared to Li/Ce/MgO.

### 2.6.2 Effect of Chlorine on Li/MgO

That $Cl^-$ containing catalysts improved the selectivity in the oxidative dehydrogenation as had already been shown by different researchers, among others Otsuka *et al.* and citations therein [252].

Burch and co-workers injected pulses of chlorinated compounds ($CH_2Cl_2$ and $CHCl_3$) during the reaction, using Li/MgO and other catalysts [253]. The chlorinated compounds drastically increased the $C_2$ selectivity. This effect was explained with the suppression of the total oxidation by the chlorine containing promoters. Moreover, it was observed, that these promoters enhanced the ODH of

$C_2H_6$ reaction. It was concluded that using gaseous chlorinated compounds could be an alternative to alkali doping of metal oxides.

Later, Burch *et al.* found that the role of chlorine over MgO was the modification of the catalyst surface to enhance the selectivity to $C_2H_4$ and $C_2H_6$ [254]. That the response of $C_2H_4$ and $C_2H_6$ on the introduction of $CH_2Cl_2$ was different, was taken as evidence, that the dehydrogenation of $C_2H_6$ is not due to gas phase reactions involving chlorine radicals. The surface concentration of chlorine at the catalyst surface was observed to be 3 %.

Conway and Lunsford showed that the addition of $Cl^-$ to Li/MgO significantly improved the yield in the ODH of $C_2H_6$ [255]. Under their reaction conditions, they observed that $Cl^-$ was slowly lost from the catalyst. The $Cl^-$ reduces the uptake of $CO_2$, which was actually a poison for the Li/MgO. They also assumed, that the presence of $Cl^-$ could change the form of oxygen on the surface, necessary for the activation. Their results demonstrated, that the activation of $CH_4$, forming methyl radicals, was the main pathway for the formation of $CO_x$, and not the total oxidation of $C_2H_4$ or $C_2H_6$. For Li/MgO without chlorine, Ross [158] and van der Wiele [189] obtained contrary results.

By doping Cl/Li/MgO with different metal oxides (Sn, La, Nd, and Dy) further improved the performance [255]. Dy is the best dopant, since the reaction temperature could be lowered to 570 - 585 $^\circ C$, hereby suppressing the non-selective gas phase reaction.

Hinson *et al.* showed that the preparation of Cl/Li/MgO, via a sol-gel synthesis, resulted in a stable and active catalyst [256].

Ruckenstein and Khan studied bi-alkali promoted Cl/MgO [247, 248]. Compared to mono-alkali MgO, the $CH_4$ and $O_2$ conversion and the $C_2$ selectivity was improved (60 hours time on stream).

Lunsford *et al.* examined the effect of $Cl^-$ on Li/MgO in the OCM [257]. The catalyst drastically changed its behavior at an $Cl^-$ to $Li^+$ ratio of nearly 1. The $C_2H_4/C_2H_6$ ratio became large, due to the improved activity towards ODH of $C_2H_6$. Adding amounts of $Cl^-$ reduced the strong basicity of the catalyst, it therefore did not react with $CO_2$ anymore, because the $Cl^-$ inhibited the formation of $Li_2CO_3$. The activity for methyl formation was the same for $Cl^-$-doped and pure Li/MgO only after poisoning with $CO_2$, otherwise Li/Cl/MgO had a lower activity. Under typical reaction conditions (650 $^\circ C$), chlorine left the catalyst as HCl, small amounts of $CH_3Cl$ were also detected. The decay of $CH_4$ conversion and $C_2H_4$ productivity was different, this indicated that these reactions were catalyzed by two different active centers.

A realted study considered the role of chlorine in OCM process over MgO and Li/MgO catalysts. Lewis and Catlow [258] investigated the effects of adding chloride ions on the (001) surface of pure and Li-doped MgO. They concluded that chloride in MgO segregates to the surface and especially to low coordinate sites.

This segregation induces modification in the activity of any active sites located at or near these surface sites. In the case of Li/MgO catalyst, the surface chloride competed with oxygen holes for Li and leads to the formation of a stable [$Li^+Cl^-$] defect cluster. The presence of this cluster influences the catalytic properties such as selectivity for $C_2H_4$.

### 2.6.3 Summary

Doping of Li/MgO with metal oxides led partially to improved catalytic performance and stability. The most frequent used dopants with a positive effect are Ce, Sn, Zr and Mn. The structural analysis indicates that together with Li and MgO new multi-metal-oxide phases are formed. Some experiments also showed that the doping of Li/MgO with certain metal oxides increased the oxygen diffusion in the catalyst material. The mechanism and the active center of these materials may very well be different from Li/MgO.

The addition of chlorine, either to the catalyst during preparation or as chlorine containing compounds in the feed, improve the yield, especially in the oxidative dehydrogenation of $C_2H_6$. When chlorine was added to the catalysts, it was slowly lost during the reaction, probably as HCl. The effect of the chlorine addition seemed not to be due the involvement in the gas phase reactions, the actual effect remains unclear.

The doping of Li/MgO, either with metal oxides or with chlorine, leads to an improved catalysts, the requirements for an industrial application are still not met. The main aim: reducing the loss of Li has not been achieved and the systems are too complex for a fundamental understanding of the role of the catalyst in the oxidative coupling of methane.

## 2.7 Engineering Aspects

In 1988, Ross *et al.* discussed the process conditions and catalyst requirements [132]. They concluded that a good catalyst is a basic material, which cannot provide larger amounts of lattice oxygen and which contains defects on the surface, with an electronic or structural nature. High gas velocities in a fixed bed reactor should result in better conversions and selectivities.

Chen *et al.* studied the OCM with a co-feed of $C_2H_6$ in the presence and absence of Li/Sn/MgO as catalyst [259]. They found an increase in the feed conversion in the absence of catalyst. It was concluded that this was due to an increase in the concentration of radicals. Co-feeding in the presence of the catalysts resulted in a small increase in $O_2$ conversion and a decrease in the $CH_4$ conversion. The later one probably occurred due to a competition with $C_2H_6$ for the active

site. The rate determining step was determined to be the regeneration of the active center. However, a beneficial effect of co-feeding $C_2H_6$ in the presence of the catalyst was not found. Based on this result, it was reasoned, that for the upgrade of natural gas the $C_2H_6$ should be separated beforehand.

The oxidative coupling of methane over Li/MgO in a fixed- and fluidized-bed reactor was studied by Edwards and co-workers [142]. In the fixed-bed reactor the $CH_4$ conversion was limited to 15 %, otherwise strong hot-spots were generated. The fluidized-bed reactor, however, gave 40 % $CH_4$ conversion, using no diluents. If the Li content of the catalyst was above 0.4 wt%, agglomeration caused problems. The presence of $CO_2$ reduced the activity of the Li/MgO.

The effect of the process conditions on the oxidative coupling of methane was studied by Ross *et al.* [260]. The three main conclusions were:

1. Increasing concentration of $O_2$ in the feed gas had an adverse effect on the selectivity.

2. As the products, $C_2H_6$ and $C_2H_4$, were susceptible to further oxidation, plug flow conditions are necessary to reach the optimal selectivity.

3. The non-selective gas phase reactions must be minimized in order to obtain the optimum $C_2$ yield.

Slagtern and co-workers tested different reactor materials ($Al_2O_3$, $Al_2SiO_5$ and $ZrO_2$ (stabilized with Ca) with Li/MgO as catalyst at 700 $^\circ C$ [261]. An alonized steel reactor was tested as a potential industrial reactor. Among the investigated materials only $Al_2O_3$ seemed a suitable material. It generally seems to be a problem to find a material, which is inert against the Li, which is highly mobile under OCM reaction conditions.

Alonized 316 stainless steal reactors were used for life tests of Li/MgO in the OCM by Phillips and Eastman [262]. Severe corrosion of reactor parts being in contact with the catalyst, loss of physical integrity and leaching of Cr from the stainless steel alloy onto the catalyst was found, demonstrating that alonized 316 stainless steal was not a suitable reactor material for the oxidative coupling of methane.

Santos *et al.* studied the OCM on Li/MgO in a fluidized bed reactor and a special type of membrane reactor [263]. They could show that the reactor design and the operation could significantly improve the yield. Later they tested Li/Sn/MgO in the fluidized bed reactor and at low gas velocities [264]. For undiluted $CH_4/O_2$ mixtures, a hydrocarbon yield of 20 % was obtained, a very high value.

Miguel and co-workers tested the oxidative coupling of methane also in a ceramic membrane reactor with Li/MgO and other alkali doped catalysts [265]. At the same conversion levels, the membrane reactor provided higher selectivities than a fixed bed reactor.

Taniewski *et al.* studied the effect of dilution of the catalyst bed in a fixed bed reactor on the heat transfer characteristics [266]. Dilution with limited amounts of dilutent ($SiO_2$ or $\alpha$-$Al_2O_3$) led to lower and wider local temperature peaks (hot spots). For short contact times, no changes in conversion, selectivity and yield was observed. It was found that $SiO_2$ enhanced the deactivation of Li/MgO, which is in agreement with the results of Korf *et al.* [28, 74, 124, 228], however, $\alpha$-$Al_2O_3$ was found to be inactive for several hours.

Later, Taniewski and co-workers investigated the effective utilization of the catalyst bed, which deactivated during the reaction [131]. It was confirmed that a hot-spot area was the only working region of the bed and the place of catalyst aging. In a scaled-up laboratory reactor it was shown, that the deactivation could be attributed to a significant loss of Li, which led to the decrease of $C_2$ selectivity. Changing of the feed inlet locations made it possible to involve successive layers of catalyst into the reaction. Furthermore, transformations of the bed, prepared from fresh and deactivated Li/MgO, led to the transport of Li from the fresh catalyst (deactivation) to the deactivated catalyst (regeneration).

Amin and Pheng investigated the influence of the process parameters and the optimization of the $C_2H_4$ yield in the OCM over Li/MgO [267]. They reported that their models were adequate for the description of $CH_4$ conversion and the yield of $C_2H_4$. The optimum temperature was determined as 839.51 $^\circ C$.

## 2.8 Miscellaneous

Roussy and co-workers investigated the effect of microwaves on the OCM over Li/MgO and $BaBiO_{3-x}$ [41]. Especially over Li/MgO an improved $C_{2+}$ selectivity was observed. Quenching of the output gas was a consequence of micro wave heating, because the reactor walls were not heated. Over Li/MgO this probably led to a decrease of the oxidation of methyl radicals in the gas phase of the post-catalytic zone.

Dai and co-workers tried to characterize Li/MgO by means of positron annihilation studies [268].

Aigler and Lunsford studied the oxidative coupling of methane over MgO and Li/MgO monoliths [135]. Pure MgO was more active but less selective for the formation of $C_2$ products, than Li/MgO. This high activity of pure MgO was at least partly attributed to $Ca^{2+}$ impurities, which were concentrated at the surface.

The group of Lunsford tested melts of $Li_2CO_3$ and talc ($3\,MgO \times 4\,SiO_2 \times H_2O$) for the OCM. It was shown that it was possible in principle, however, the obtained conversions and selectivities were not improved compared to fixed bed reactors [269].

## 2.9 Summary

The mechanism for the oxidative coupling of methane over Li/MgO, as shown in Figure 2.8 was proposed by the group of Lunsford. Based on a series of their papers [19, 20, 22, 149, 209], this mechanism proposes the formation of methyl radicals over $[Li^+O^-]$, which is the active center, their desorption and coupling in the gas phase. It has become widely accepted in the literature and is considered as a fact. However, a close look at the literature reveals, that the proof that $[Li^+O^-]$ is present in Li-doped MgO has only been provided by Abraham *et al.* applying EPR *and* ENDOR experiments [101, 103, 106, 107, 108, 109, 148]. All other publications use the EPR signal at g = 2.054 as proof for the presence of $[Li^+O^-]$. The absolute proof with ENDOR experiments has not been reported by other groups, except that of Abraham. However, this signal is not biunique and it has only been observed after calcination in air or $O_2$ followed by quenching in liquid $O_2$ or liquid $N_2$. The reaction conditions of the OCM are reducing and indeed, the EPR signal at g = 2.054 has never been detected after quenching from reaction conditions.

Moreover, the contribution of the gas phase reaction without a catalyst can be large. Experiments with isotopic labeled reactants showed no mixed reaction products, but an H/D exchange was observed at temperatures below reaction conditions. Together, these facts put a question mark on the exact role of the catalyst in the oxidative coupling of methane. In fact, reams of other catalyst, with different chemical and physical properties, catalyze the oxidative coupling of methane at high temperatures (approximately 750 $^\circ C$) making it very unlikely that a specific center such as $[Li^+O^-]$ is required to activate $CH_4$. Other catalysts, $La_2O_3$ for instance, which do not contain $Li^+$, $Na^+$ or $K^+$, were also found to be active OCM catalysts.

The facts on Li/MgO, that can be consider as being proven are:

1. Loss of surface area up Li-addition.
2. Loss of Li during time on stream.
3. Strong influence of gas phase reactions. The latter are a function of temperature, residence time, gas phase composition, free gas phase volume to surface area ratio and possibly the nature of the surface.
4. Pure MgO, Li/MgO and $Li_2CO_3$ are active OCM catalysts with comparable performance.
5. Positive isotope exchange effect.
6. Carbene mechanism is unlikely.

7. Irreversible C-H activation (no isotope scrambling), as H,D scrambling is observed on MgO. It could be that $C_2$ formation is a pure gas phase process.

8. Li/MgO active for ODH of $C_2H_6$ to $C_2H_4$.

9. Gas phase oxidation product is CO, surface oxidation product is $CO_2$.

10. Gas phase $O_2$ necessary for $C_2$ formation.

There is no doubt that the OCM consist of homogeneous and heterogeneous contributions, with the radicals as key intermediates. However, that $[Li^+O^-]$ is the active center lacks any solid experimental evidence.

The stability of Li/MgO is often not addressed or large amounts of inert diluent were used. But the publications dealing with the stability, reported deactivation, irrespective of the initial preparation, due to a loss of Li. Therefore it is questionable, if Li/MgO is a good "Drosophila Catalyst", as any measured data, for kinetics or characterization, is only a snapshot on one point on the deactivation trajectory. The transient nature of Li/MgO coupled to parallel occurring gas phase reactions which in turn are sensitive to temperature, pressure, surface to gas phase volume, dilution with inert gases etc. make mechanistic OCM studies extremely difficult. Therefore, it seems doubtful, if Figure 2.8 represents the real reaction mechanism, as the real mechanism seems to be much more complicated.

# Chapter 3

# Laboratory Reactors for Catalytic Tests

## 3.1 Single Reactor Set-up

For the investigation of the catalytic activity a single reactor set-up was available. The piping and instrumentation diagram is shown in Figure 3.1 and an image shown in Figure 3.2.

The mass flow controllers (MFC), Brooks 5850 TR Series are used to feed gas into the reactor. A series of manual valves before the MFCs is used to connect several different gases to each one of the MFCs, keeping the set-up highly flexible and allowing an extremely broad range of experimental conditions. All tubes from the MFCs until the ventilation are heated to a temperature above $180\,^{\circ}C$ to avoid the condensation of $H_2O$ and other liquid reaction products, e.g. oxygenates.

For the experiments described in chapter 5 a fluidized sand bed was applied for heating, ensuring isothermal conditions. A gas chromatograph (GC Satochrom 5873), equipped with a flame ionization detector, a thermal conductivity detector, a fused Poraplot Q and a Molsieve 5 column, was used to analyze the reaction products. The analyzed reaction products were $O_2$, $N_2$, CO, $CO_2$ and hydrocarbons. For this GC, suitable methods for the detection of the reaction products of the OCM and the ODE had to be developed at the beginning of this work.

For all other experiments the fluidized sand bed was replaced by an electric furnace, LK 1000-20-310-1 from HTM Reetz. An Agilent 7890A GC replaced the Satochrom 5873. The Agilent 7890A is equipped with a HP-Molesieve column and an HP-Plot/Q column. Suitable methods including temperature programs and switching times for the available detectors had to be developed for the detection of the reaction products of the OCM, ODE and ODP. A construction with a needle valve was designed to obtain the same GC signals at different flow rates (see

Figure 3.1).

To improve the utilization ratio, Mr. Torsten Otremba developed a software to control the MFCs, the valves, the electric furnace (including heating rate and waiting time) and the GC, allowing an automatic operation mode. The electric furnace was connected to an emergency shut-down to avoid accidents in case of any malfunctions. Together, it allows the safe accomplishments of experiments over extended periods of time, necessary for stability experiments.

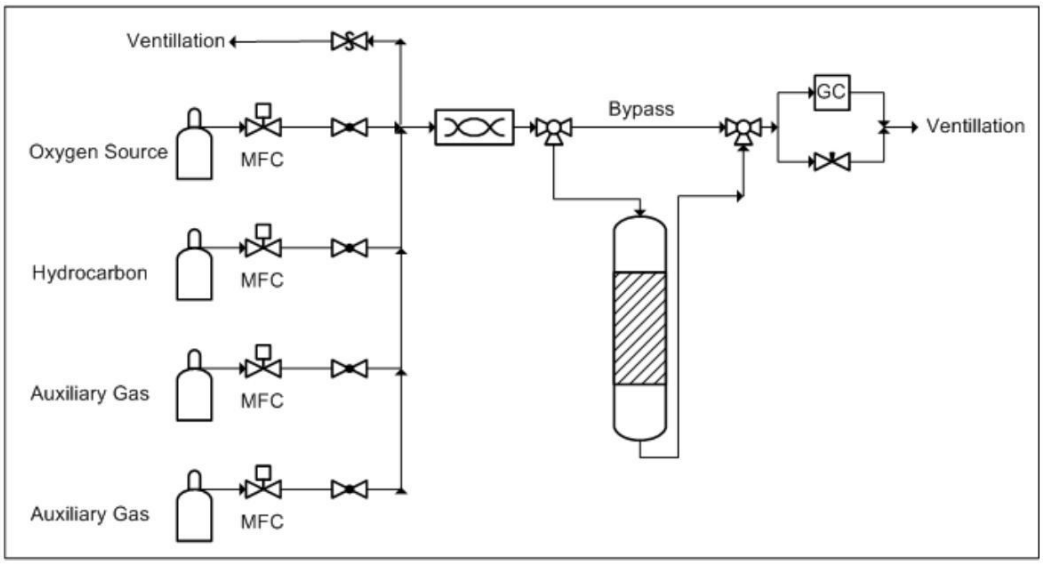


Figure 3.1: Piping and instrumentation diagram of the single reactor set-up used for the determination of the catalytic activity. The gas is supplied via the mass flow controller and it passes a pre-heater before entering the reactor. After the reactor, the gas flow is being split, one part is directly connected to the ventilation via a needle valve the other part passes through the sample loop of the gas chromatograph.

## 3.2 Parallel Testing Reactor

To manifold the testing capacities, the requirement profile for a parallel testing reactor was developed. The planning and construction was done by ILS (Integrated Lab Solutions, Berlin) and Premex Reactor AG, Lengnau. The piping and instrumentation diagram is not shown due to legal reasons and the protection of intellectual property.

The set-up is made of two parts. A kinetic part with two large reactors for tests with larger amounts of catalyst and for experiments under elevated pressures. This


Figure 3.2: Image of the single reactor set-up.

part is shown in Figure 3.3.

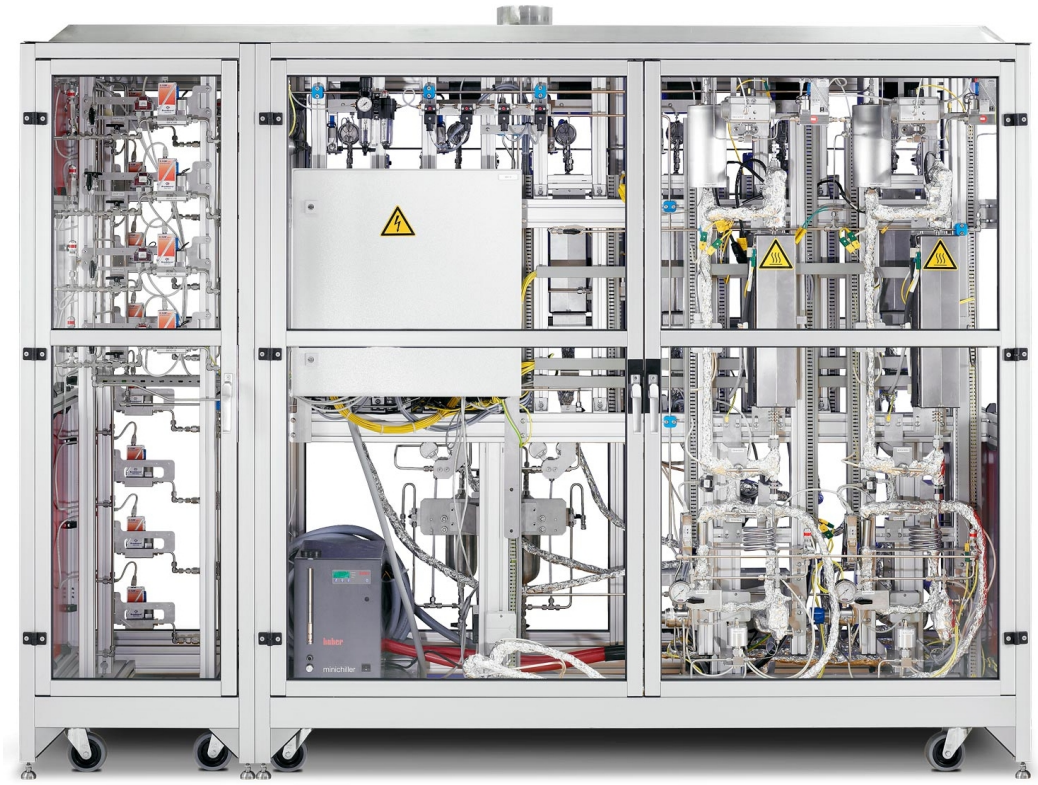

Figure 3.3: The kinetic part with 2 big reactors for tests of larger amounts of catalysts and experiments under elevated pressures.

The screening part, which was started up in this work, has 6 parallel tubular reactors, made of quartz glass, for parallel screening of a vast number of catalysts, see Figure 3.4. In this part 4 MFCs are used to fill a pressure vessel, one MFC for the oxygen source ($O_2$ or synthetic air), two MFCs for hydrocarbons and one MFC for $N_2$. Being feed from the pressure vessel, each reactor has one MFC to feed the mixed gas from the pressure vessel into the reactor. It is also possible to feed liquids, $H_2O$ for instance, into the reactor. The reactors are individually heated with electric furnaces from HTM Reetz, with maximum operation temperature of 800 $°C$. Figure 3.5 shows the ovens of the screening part and a fitted reactor. It is possible, to adjust a different feed gas composition for different experiment, however, being the same for all 6 reactors. The exact flow rate and reaction temperature can be adjusted for each reactor individually. The outlet gas is lead to the gas chromatograph. A special construction is used to obtain the same GC signals at different flow rates.

For parallel experimentation, a fast analysis of the reaction products is manda-

tory. An Agilent 7890A gas chromatograph from Agilent was purchased, especially designed for a fast analysis of the permanent gases, hydrocarbons and oxygenated compounds.

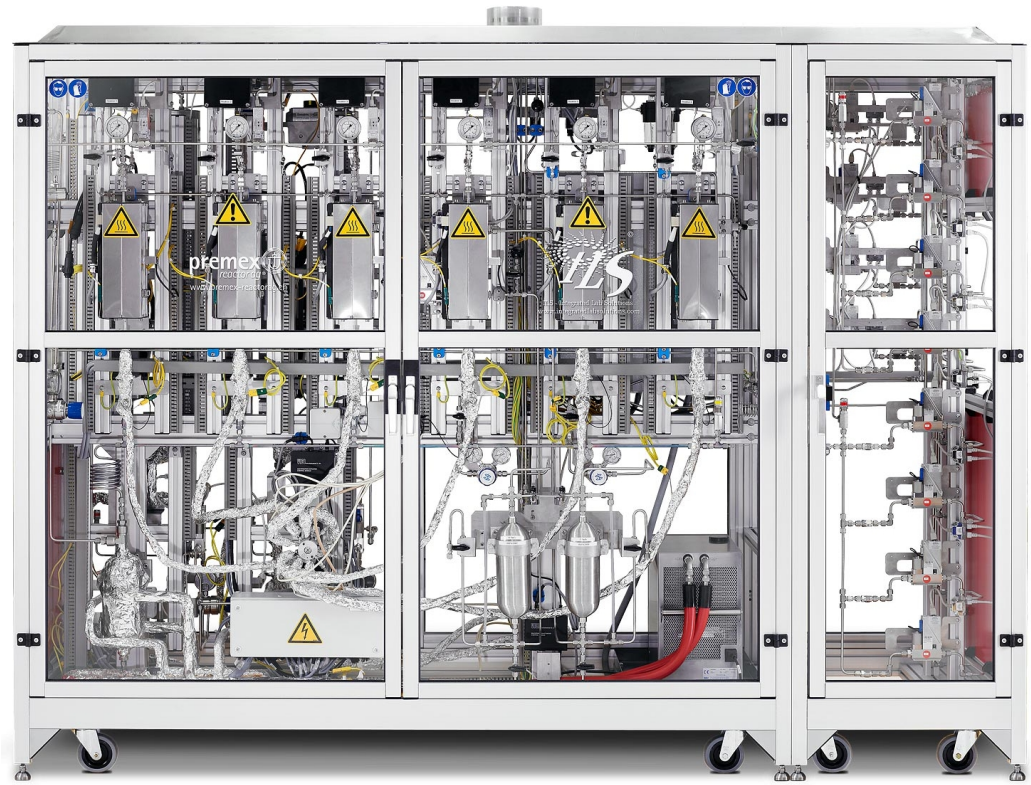


Figure 3.4: The parallel part with 6 parallel reactors of the parallel testing reactor.

In the start-up procedure, suitable analysis methods were developed together with Agilent for the reaction products of the OCM, ODE and ODP. The required time for the detection of compounds until $C_2H_6$ is 6 minutes and for the detection of compounds until $C_3H_8$ is 8 minutes. The gas chromatograph, the mass flow controllers and the electric furnaces were calibrated. Several problems due to unavoidable leakages and malfunctions were tracked and solved. The reliability of the unit had to be improved at the beginning to ensure continuous operations.

For an optimal use of the high parallel testing reactor, the same result should be obtained when the same catalyst is tested under the same reaction conditions. For this test, the oxidative coupling of methane was used as test reaction and Na-Mn-W-$SiO_2$ was used as catalyst with the following reaction conditions: temperature 700 $^\circ C$, 500 mg catalyst, undiluted, with a particle size of 250 - 500 $\mu$m, gas flow 60 ml/min and a feed gas composition of $CH_4$:$O_2$:$N_2$ = 4:1:4. The reaction conditions were in the kinetically controlled range, the conversion of $CH_4$ and

Figure 3.5: The ovens of the screening part and a fitted reactor are shown. The insertion for the introduction of liquids can be seen in the upper part of the reactor.

$O_2$ is limited, allowing the observation of possible changes and differences. For comparison, the same experiment was conducted in the single reactor set-up under identical conditions. For the 6 different reactors of the parallel testing reactor and the single reactor set-up, the $O_2$ conversion is shown in Figure 3.6, the $CH_4$ conversion in Figure 3.7, the $C_2$ selectivity in Figure 3.8 and the ratio of $C_2H_6$ to $C_2H_4$ in Figure 3.9. The ratio of $CO_2$ to CO is not discussed, as no CO was detected in experiments with the Na-Mn-W-$SiO_2$ catalyst. A comparison of the values at approximately 15 hours time on stream is shown in Table 3.1.

| | $X_{O_2}$ [%] | $X_{CH_4}$ [%] | $S_{C_2}$ [%] | $\frac{C_2H_6}{C_2H_4}$ |
|---|---|---|---|---|
| Reactor 1 | 35.6 | 5.3 | 47.5 | 4.3 |
| Reactor 2 | 36.8 | 5.8 | 50.7 | 3.9 |
| Reactor 3 | 38.1 | 5.9 | 48.8 | 3.9 |
| Reactor 4 | 35.6 | 5.5 | 51.1 | 4.0 |
| Reactor 5 | 47.2 | 7.3 | 44.3 | 3.5 |
| Reactor 6 | 42.6 | 6.4 | 44.6 | 4.0 |
| Single Reaktor Set-Up | 22.9 | 3.9 | 44.0 | 5.2 |
| Statistical Analysis for the 6 Reactos of the Screening Unit | | | | |
| Average Value | 39.3 | 6.0 | 47.8 | 3.9 |
| absolute Standard Deviation | 4.7 | 0.7 | 2.9 | 0.2 |
| relative Standard Deviation [%] | 11.8 | 12.2 | 6.1 | 6.2 |

Table 3.1: Comparison of the results obtained at approximately 15 hours time on stream. For the screening reactor set-up, the average value and the absolute and relative standard deviation is calculated.

The comparison of the 6 reactors of the parallel unit shows, that the obtained catalytic results are within a narrow range. Reactor 1 to 4 do not exhibit significant differences, only reactor 6 and especially reactor 5 show a higher performance. However, the variation is still within an acceptable range, as the oxidative coupling of methane is strongly depended on the reaction temperature. The statistical analysis shows, that the relative standard deviation is approximately 12 % for the $O_2$ and $CH_4$ conversion. The selectivities obtained for all 6 reactors can be considered approximately the identical. In summary, the reactors of the parallel testing reactor give approximately identical results within an acceptable range of experimental errors. Now, this unit is ready for operation to perform any kind of comparative experiments as well as long term stability experiments.

Comparing the obtained results for the parallel testing reactor and the single reactor set-up, it becomes evident, that the single reactor set-up has a significantly lower conversion of $CH_4$ and $O_2$ compared to the screening unit. The reason could be differences in the real residence times or channeling. However, the selectivities

of the screening unit and the single reactor set-up are comparable. The only major difference is that the ratio of $C_2H_6$ to $C_2H_4$ is higher for the single reactor set-up. Therefore, it can be concluded, that the empty reactor volume of second half of the U-shaped reactor of the single reactor has nearly no influence on the selectivity.

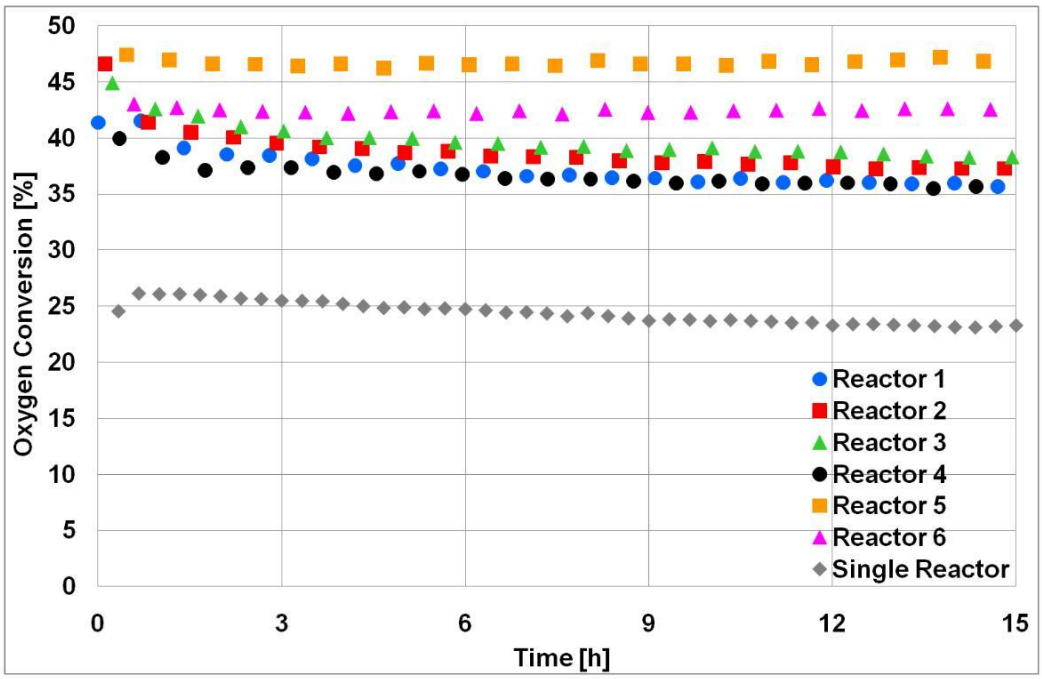


Figure 3.6: The $O_2$ conversions for the single and the screening reactor set-up. Reaction conditions: temperature 700 $°C$, 500 mg catalyst, feed gas: 60 ml/min.

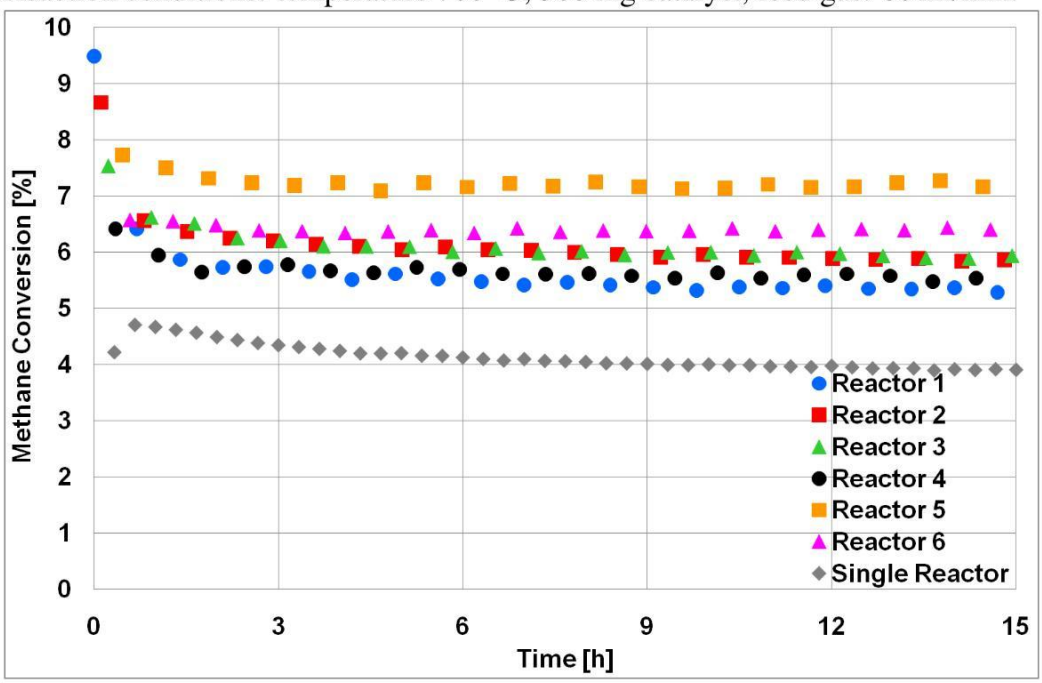


Figure 3.7: The $CH_4$ conversions for the single and the screening reactor set-up. Reaction conditions: temperature 700 $°C$, 500 mg catalyst, feed gas: 60 ml/min.

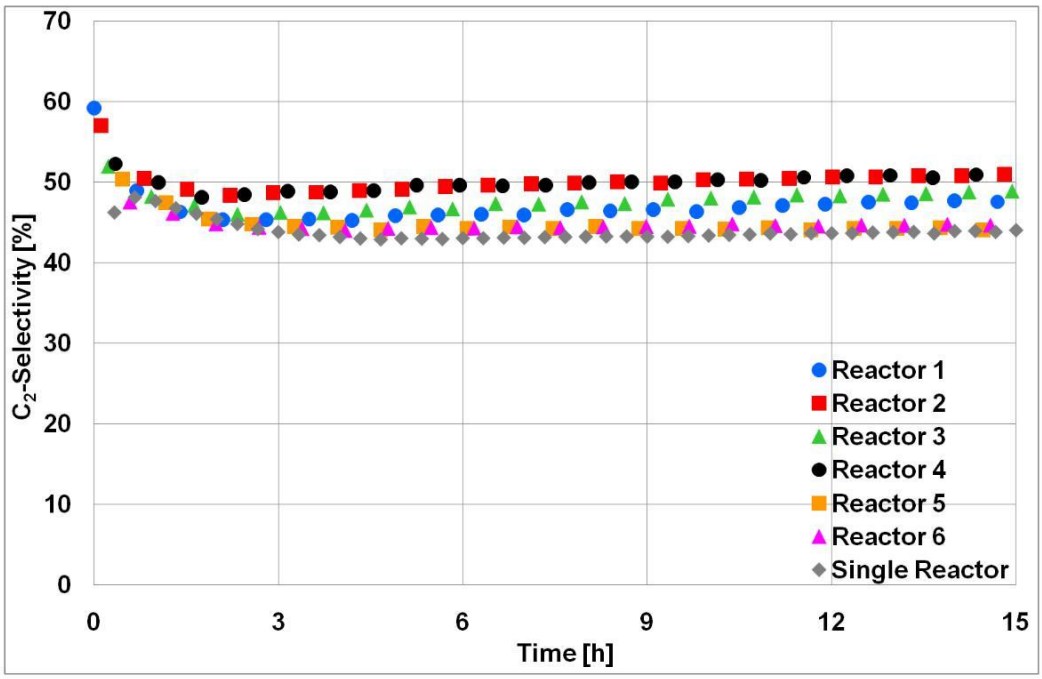


Figure 3.8: The $C_2$ selectivities for the single and the screening reactor set-up. Reaction conditions: temperature 700 °*C*, 500 mg catalyst, feed gas: 60 ml/min.

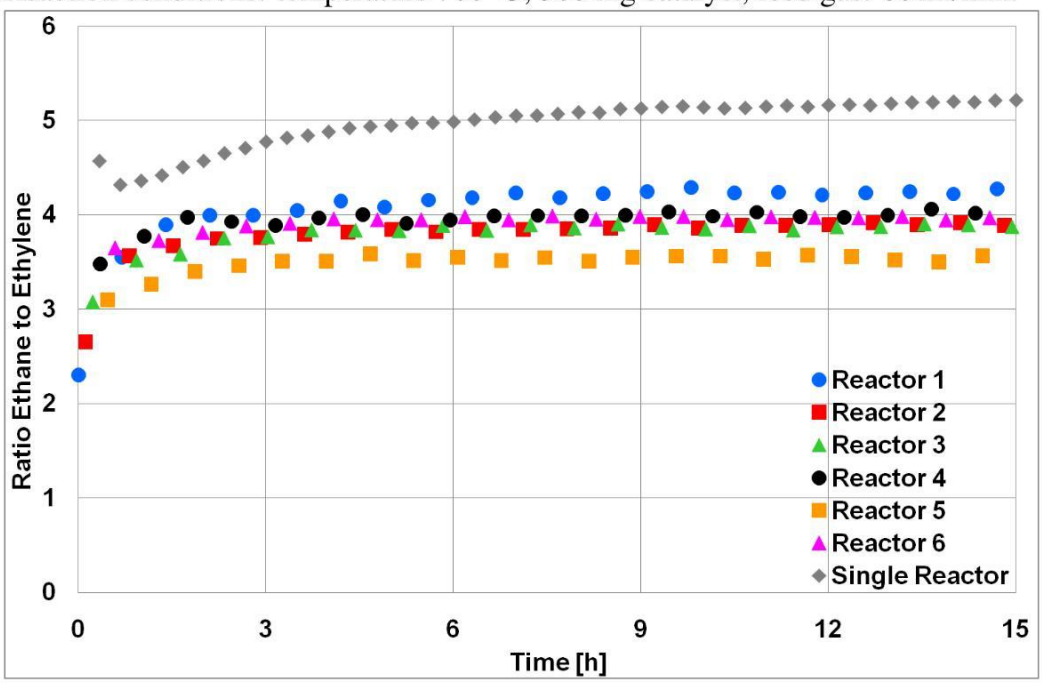


Figure 3.9: The ratio $C_2H_6$ to $C_2H_4$ for the single and the screening reactor set-up. Reaction conditions: temperature 700 °*C*, 500 mg catalyst, feed gas: 60 ml/min.

# Chapter 4

# Li-doped MgO From Different Preparative Routes For The Oxidative Coupling Of Methane

This work has been submitted as: S. Arndt, U. Simon, S. Heitz, A. Berthold, B. Beck, O. Görke, J.-D. Epping, T. Otremba, Y. Aksu. E. Irran, G. Laugel, M. Driess, H. Schubert and R. Schomäcker, "Li-doped MgO From Different Preparative Routes For The Oxidative Coupling Of Methane" in Topics in Catalysis.

## 4.1 Introduction

The known resources of natural gas are large [1]. The exact composition depends on the origin, but the main component of natural gas is always methane. However, methane is highly underutilized, due to two problems:

1. Conversion into value added products is difficult, because $CH_4$ is the most stable hydrocarbon and therefore difficult to activate.

2. Difficulties in transporting natural gas from the source to the consumer.

The oxidative coupling of methane (OCM), shown in equation 4.1, could overcome these problems and therefore, it is a reaction of great industrial interest.

$$CH_4 + O_2 \rightarrow C_2H_6 \text{ or } C_2H_4 + H_2O \tag{4.1}$$

However, this reaction has still not been put into practical application due to some drawbacks. The main ones are the high temperature at which this process runs and connected problems like the lack of active and selective catalysts and the thermal stability of possible candidates.

Li/MgO is a catalyst for this reaction which has been the subject of intensiv research, nevertheless, many aspects remain unclear, e.g. the active center, structure activity relationship and the stability of the catalyst.

Lunsford and co-workers correlated electron paramagnetic resonance (EPR) signals with the methyl radical formation rate, concluding that a $[Li^+O^-]$ defect is the active center [19, 20, 21]. It has become a widely accepted fact, even so contradictory results exist in the literature. Mirodatos *et al.* found that a tight interface between $Li_2CO_3$ and MgO is necessary for a good catalytic performance but it only occurs after pretreatment at temperatures allowing the liquefaction of $Li_2CO_3$ [119, 122]. Later, Goodmann and co-workers provided evidence that F-centers are the active center and that Li is a promoter for the formation of F-centers [210, 213, 212, 211].

The stability of the Li-doped MgO catalysts is often not adressed in the literature and/or large amounts of inert dilutent are used in the feed gas avoiding strong deactivation. However, Kimble and Kolts showed that Li is lost from the catalysts after calcination at 850 $^\circ C$ [73]. Moreover, and Mirodatos and co-workers showed that Li-doped MgO suffers from severe deactivation due to sintering and loss of Li [119].

Li-doped MgO was found to deactivate rapidly by Ross *et al.* [124]. They also showed that, if Li is still available, the catalyst can be regenerated by treatment with $CO_2$ under reaction conditions. The deactivation can be avoided if $CO_2$ is added to the reaction mixture in low concentrations. They furthermore concluded that $CO_2$ temporarily poisons the active site and simultaneously stabilises it against deactivation [124, 28]. The selectivity did not change so much in their long-term experiments, therefore the conclusion was that the nature of the active site has not changed much but the number decreased.

Another important finding was that the use of experimental equipment made of quartz glass is detrimental to the stability of Li-doped MgO [28, 74]. It was shown that the catalyst deactivates due to a loss of Li as the volatile LiOH or as $Li_2SiO_3$, due to the fact that many laboratory reactors are made of quartz glass. However, this is not limited to quartz devices, the Li caused problems in reactors made of alonized steel, $Al_2O_3$, $Al_2SiO_5$ and $ZrO_2$ (stabilized with Ca) [261, 262]. Generally, it seems a problem that currently no material exist which is stable against the highly mobile Li.

Perrichon and Durupty investigated the thermal stability of Li, Na and K deposited on MgO, $SiO_2$, $Al_2O_3$ and $Cr_2O_3$ [121]. It was found that on $SiO_2$, $Al_2O_3$ and $Cr_2O_3$ the alkali metals are rather stable, however, on MgO a loss of alkali metal was observed at calcination temperatures higher than 500 $^\circ C$. This effect increased from Li to K at 800 $^\circ C$. A reason for this could be that MgO is not able to form stable compounds, unlike $SiO_2$, $Al_2O_3$ and $Cr_2O_3$ which can form silicates, aluminates and chromates. Supports impregnated with alkali metals al-

ways had a lower surface area, and the temperature had no influence on this. That effect was explained with the formation of a conglomerate of alkali metal salt and the support. Furthermore, it was assumed that the alkali metal phase, which was present at the interface between the support particles, underwent transformations, especially fusion, during sintering. Therefore, it induced partial dissolution of the support and thus the growth of larger crystals.

A detailed discussion of the development and the stability of Li/MgO can be found in chapter 6 of reference [5]. In this reference the morphological aspects of Li/MgO and other catalysts and their influence on the OCM are discussed too (chapter 10 of [5]).

Many different procedures for the synthesis of Li-doped MgO have been reported with different results regarding the catalytic performance, though, a comparision is usually difficult because the applied test conditions vary strongly. However, this is a common problem in research on OCM catalysts [9]. It is well known that the catalytic activity depends on the preparation procedure. Choudhary and co-workers studied the influence of the precursors for $Li_2O$ and MgO on the surface and catalytic properties. The applied preparation procedure was wet impregnation [34]. They reported that the catalytic activity and other characteristics of the catalysts strongly depended on the precursors used for the preparation, however, deactivation was not considered in their publication.

Up to our knowledge, no detailed comparison of Li-doped MgO prepared on different routes exists. Furthermore, a detailed structural investigations after different times on stream for different catalysts has also not been reported so far.

In this publication, we present the results of a study of Li-doped MgO from different preparative routes and with Li loadings of 0, 0.5, 1, 2, 4 and 8 wt%. The applied preparative routes and the denomination of the catalysts are shown in Table 4.1. This comparison was performed in order to find a synthetic route that produces the most stable catalyst.

Since the Li-doped MgO system has been shown to be unstable [119, 124, 28, 74], time on stream experiments were used to determine the development of the catalytic activity. After the determination of the catalytic activity and the stability, one Li loading from each preparation route was chosen and structural analysis at different times on stream were done to observe the changes of the catalysts during the course of reaction. Moreover, the impact factors on the catalyst stability, such as a the flow rate and temperature, were studied with time on stream experiments.

## 4.2 Experimental Part

### 4.2.1 Catalyst Preparation

In this publication, the loading of Li is calculated from the equation 4.2.

$$\text{Li [wt\%]} = \frac{\text{Mass of Li [g]}}{\text{Mass of Li [g] + Mass of MgO [g]}} \times 100\% \tag{4.2}$$

The amount of the determined impurities is calculated with equation 4.3.

$$\text{Impurity [wt\%]} = \frac{\text{Mass of Impurity [g]}}{\text{Mass of Li [g] + Mass of MgO [g]}} \times 100\% \tag{4.3}$$

Four different preparation routes have been applied for the synthesis of Li-doped MgO. The routes and their denomination is shown in Table 4.1, disregarding of their actual Li content.

Table 4.1: The applied preparative routes and the denomination as used in this manuscript.

| No. | Preparation | Abbreviation |
|---|---|---|
| 1 | Single Source Precursors | Li@MgO |
| 2 | Wet Impregnation | Li/MgO |
| 3 | Precipitation | Li-MgO |
| 4 | Mixed Milling | Li+MgO |

#### 4.2.1.1 Li@MgO

The preparation of solid catalysts via the decomposition of single source precursors [270, 271] has recently been developed and already applied to Li-doped ZnO [272, 273, 274]. This procedure allows a reproducible synthesis of solid materials with controlled stoichiometry.

The Li@MgO is prepared via the thermal decomposition of alkyl-Mg-alkoxides and Li-Mg-alkoxides. In Figure 4.1 the reaction is shown schematically. The procedure for MgO and Li-doped MgO has been described in detail, including analytic data, by Heitz *et al.* [43, 44]. Since the prepared materials were a nanopowder, they were not crushed and sieved.

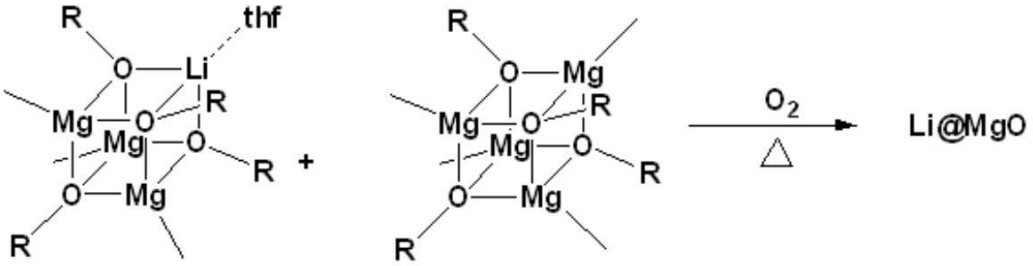


Figure 4.1: The thermal decomposition of Li-Mg alkoxides cubanes leads to a very pure and reproducible preparable Li-doped MgO.

#### 4.2.1.2 Li/MgO

The preparation of Li/MgO via wet impregnation is a well-known and common procedure, which has also been used by Lunsford and co-workers [19, 20, 21]. However, it remains unclear if this procedure is suitable to insert Li into the MgO lattice and to produce reasonable amounts of $[Li^+O^-]$, which corresponds to the active center for some researchers. In the vast majority of the literature dealing with Li-doped MgO, wet impregnation has been used as preparation procedure. In favor of this simple route, all other synthetic routes have been neglected, even so they should be more suitable for the preparation of $[Li^+O^-]$.

MgO (Alfa Aesar, 99.99 %) and $Li_2CO_3$ (Fluka $\geq$99.0 %) were mixed in distilled water. The water was evaporated until only a thick paste remained. The samples were dried over night at 140 $^\circ C$ and then calcinated in air at 465 $^\circ C$ for 1 hour. The materials were crushed and sieved, to obtain only particles $\leq 200\,\mu$m for catalytic studies.

#### 4.2.1.3 Li-MgO

Aqueous solutions of $Mg(NO_3)_2$ were prepared by dissolving $Mg(NO_3)_2 \times 6\,H_2O$ (p.A., Merck) in distilled $H_2O$. The nitrate solution was slowly added to stirred ammonia solution while keeping the pH value above 11. The gelatinous precipitated magnesium hydroxide was rinsed with distilled $H_2O$ and mixed with aqueous LiOH solution ($LiOH \times H_2O$ p.A., Riederl de Haen) with appropriate Li concentrations of 0, 0.5, 1, 2, 4 and 8 wt% in a tubular mixer. Finally, the solution was quick-frozen by using liquid $N_2$. Afterwards, iit was freez-dried over 72 hours using a freeze-dryer (Gamma 2-20 (Christ)). After calcination at 900 $^\circ C$ for 1 hour in MgO crucibles, Li-MgO powders were produced. The samples with a Li content of 0 wt% and 0.5 wt% were too fluffy, therefore, they were pressed at 100 bar for 10 minutes and subsequently crushed and sieved. All samples were sieved and only the fraction $\leq 200\,\mu$m was used for testing.

#### 4.2.1.4 Li+MgO

We also chose mixed milling to prepare Li-doped MgO, as this route could be applied to produce this catalysts fast and easy in larger amounts, which is of interest with respect to an industrial application.

$LiNO_3$ (Fluka, purity $\geq 99\,\%$) and MgO (Sigma Aldrich, 325 mesh, purity 99+ %) were milled in a centrifugal ball mill (Retsch S 100) for 1 hour at 400 rounds per minute with alternating directions. The grinding jar and the grinding balls were made of stainless stell, material number 1.4034. The data sheet names the main components as Fe 82.925 %, Cr 14.500 %, Mn 1.000 % and Si 1.000 %. Afterwards, the prepared samples were calcinated at 400 $^\circ C$ for 3 hour. The materials were crushed and sieved, only particles $\leq 200\,\mu$m were used.

### 4.2.2 Catalytic Tests

The catalytic experiments were carried out in a packed-bed, U-shaped, tubular reactor made of quartz glass. The outer diameter was 8 mm and the inner diameter 6 mm. For each catalytic run, 100 mg catalyst were diluted with approximately 1.5 ml quartz sand (quartz sand: purchased from Merck, it has already washed with HCl and calcined, ca. 60 % of the particles have the size 0.2 - 0.8 mm) for proper heat transfer. The reactor behaves like a plug flow tubular reactor (PFTR). The length of the catalytic bed was ca. 50 - 55 mm. Below and above the catalyst bed, a small amount of pure quartz sand was put to ensure proper heat transfer. The particle size of the catalyst was below 200 $\mu$m in each experiment to exclude internal mass transfer effects.

The gas was fed to the reactor using mass flow controllers of Brooks 5850 TR series. Methane and synthetic air, as oxygen source, were fed into the reactor with a flow rate of 60 ml/min and a feed gas composition of $CH_4$:$O_2$:$N_2$ = 4:1:4. Before entering the reactor, the reactants passed a pre-heater, heated to 180 $^\circ C$. The reactor was heated with an electric furnace (LK 1000-20-310-1 from HTM Reetz Berlin); isothermal conditions were insured. Under reactant gas flow, the reactor was heated to 750 $^\circ C$ with a heating rate of 20 K/min. 19 minutes after reaching the 750 $^\circ C$, the first data point was measured. After reaching the reactor temperature of 750 $^\circ C$, each catalyst was tested for at least 40 hours time on stream, counting from the time when the reactor temperature was reached. The same test protocol was applied for every experiment.

To investigate the dependence on the residence time, the flow rates were set to 30, 60, 120 and 180 ml/min, respectively, and the catalytic activity was recorded for at least 18 hours time on stream under otherwise identical experimental conditions. For the investigation of the temperature dependence, the experiments with a reaction temperature of 650, 700, 750 and 800 $^\circ C$ and a flow rate of 60 ml/min

were conducted, with otherwise identical experimental conditions.

The analysis was performed with a gas chromatograph Agilent 7890 A, equipped with a flame ionization detector (FID), a thermal conductivity detector (TCD), a HP-PLOT/Q and a HP Molsieve column. The analyzed compounds were $O_2$, $N_2$, CO, $CO_2$ via TCD, $CH_4$, $C_2H_4$ and $C_2H_6$ via FID. $N_2$ was used as internal standard. The reproducibility of conversion (X) and selectivity (S) is sufficient. The conversion and selectivity is calculated with a mass balance based on the inlet and outlet concentration of reactants and products, see Equations 4.4 and 4.5. The carbon balance was always well above 95 %.

$$X = \frac{\sum(\text{Reaction Products})}{\sum(\text{Reaction Products}) + \text{unconverted Reactant}} \tag{4.4}$$

$$S = \frac{\text{Product}}{\sum(\text{Reaction Products})} \tag{4.5}$$

The desired reaction products of the oxidative coupling of methane are $C_2H_4$ and $C_2H_6$. The selectivity of these two products is discussed as a sum, the $C_2$-selectivity. Higher reaction products, especially $C_3H_8$ and $C_3H_6$, have not been detected, although the applied method was suitable for their detection.

In order to determine the degree of thermal conversion of $CH_4$, blank experiments with pure quartz sand, with quartz balls with a particle size of 0.4 mm $\pm$ 0.1 mm (Quarzglas QCS, Maintal, Germany) and with an empty reactor were conducted under the above described reaction conditions. The importance of the homogeneous gas phase reaction in the OCM is significant [155], therefore, the obtained results for $CH_4$ conversions and the according selectivities are shown in detail in Table 4.2. At 700 $^\circ C$ and below the contribution of the thermal reaction is negligible in the applied experimental set-up. At 750 $^\circ C$ and 800 $^\circ C$, a contribution of the thermal reaction is observed. However, since the $CH_4$ conversion was rather small the influence of the thermal reaction has been neglected. The degree of contribution of the gas phase reaction strongly depends on several different factors, such as partial pressures of all compounds, temperature, residence time, free reactor volume et cetera [155]. Therefore, it is not surprising that different $CH_4$ conversions are observed in a reactor which is empty, filled with quartz sand or quartz balls.

### 4.2.3 Sample Preparation for Structural Analysis

For a structural analysis after the reaction it is necessary to retrieve the catalysts. With the applied quartz sand this is not possible, as its particle size distribution is too large and it overlaps with the particle size of the catalysts. Thus, quartz balls with a particle size of 0.4 mm $\pm$ 0.1 mm (Quarzglas QCS, Maintal, Germany) and

Table 4.2: Contribution of the homogeneous gas phase reaction to the oxidative coupling of methane, in reactors with different inert fillings. At 750 $^{\circ}C$ and below the contribution of the thermal reaction is small and therefore negligible.

| Reaction Conditions | | Quartz Balls | | | Quartz Sand | | | Empty Reactor | | |
|---|---|---|---|---|---|---|---|---|---|---|
| Temperature [$^{\circ}C$] | Flow [ml/min] | $X_{O_2}$ [%] | $X_{CH_4}$ [%] | $S_{C_2}$ [%] | $X_{O_2}$ [%] | $X_{CH_4}$ [%] | $S_{C_2}$ [%] | $X_{O_2}$ [%] | $X_{CH_4}$ [%] | $S_{C_2}$ [%] |
| 700 | 30 | - | - | - | 2.7 | 0.1 | 100.0 | - | - | - |
| 700 | 60 | - | - | - | - | - | - | - | - | - |
| 700 | 90 | - | - | - | - | - | - | - | - | - |
| 700 | 120 | - | - | - | - | - | - | - | - | - |
| 700 | 180 | - | - | - | - | - | - | - | - | - |
| 750 | 30 | 0.9 | 0.1 | 100.0 | 3.5 | 0.4 | 100.0 | 2.3 | 0.3 | 100.0 |
| 750 | 60 | - | - | - | 1.4 | 0.2 | 100.0 | 0.9 | 0.1 | 100.0 |
| 750 | 90 | - | - | - | 1.1 | 0.1 | 100.0 | 0.5 | 0.1 | 100.0 |
| 750 | 120 | - | - | - | 1.0 | 0.1 | 100.0 | - | - | - |
| 750 | 180 | - | - | - | 0.8 | 0.1 | 100.0 | - | - | - |
| 800 | 30 | 3.5 | 0.6 | 100.0 | 8.6 | 2.5 | 52.8 | 9.0 | 2.8 | 54.5 |
| 800 | 60 | 1.3 | 0.2 | 100.0 | 4.3 | 0.7 | 100.0 | 3.3 | 0.6 | 100.0 |
| 800 | 90 | 0.5 | 0.1 | 100.0 | 3.2 | 0.5 | 100.0 | 1.9 | 0.3 | 100.0 |
| 800 | 120 | 0.5 | 0.1 | 100.0 | 2.5 | 0.4 | 100.0 | 1.2 | 0.2 | 100.0 |
| 800 | 180 | 0.5 | 0.1 | 100.0 | 2.3 | 0.3 | 100.0 | 0.8 | 0.1 | 100.0 |

a very narrow particle size distribution were used instead of quartz sand as inert dilutent, enabling a separation of catalysts and inert material after the reaction by sieving. The reaction conditions for the sample preparation are identical to those described in paragraph 4.2.2. For the separation of catalyst and dilutent, a 200 $\mu$m sieve was used.

The contribution of the gas phase reaction is different when quartz sand or quartz balls are used, as shown in Table 4.2. Therefore, it could be that the catalytic behavior and the deactivation process of the reaction with quartz sand and quartz balls is not absolutely identical. However, the general trends should still be observable in a reliable manner.

### 4.2.4 Catalyst Characterization

#### 4.2.4.1 Atomic Absorption Spectroscopy

The Li content of the different samples was quantified via atomic absorption spectroscopy (AAS), using a AAS NovAA 400 G device from Analytik Jena via flame and graphite furnace. Furthermore, Fe, Cr, Mn, Ca and Cu were determined as possible impurities.

#### 4.2.4.2 BET

The specific surface area was determined by a Micromeritics Gemini III 2375 Surface Area Analyzer, using $N_2$ adsorption at -196 $^\circ C$. Before measuring, the samples were degassed at 300 $^\circ C$ and 0.15 mbar at least for 30 minutes. The surface areas were calculated by the method of Brunauer, Emmett and Teller (BET).

#### 4.2.4.3 X-Ray Diffraction

Powder X-Ray diffractograms (XRD) were obtained (CuK$\alpha$1 radiation - wavelength 0.154 nm) using Bruker AXS D8 ADVANCE X-ray diffractometer. The diffractorgramms were analyzed with the program STOE WinXPOW. The lattice parameter were determined with the algorithm of Werner and the particle size with the Scherrer equation.

#### 4.2.4.4 Solid State NMR

The solid state MAS (magic angle spinning) NMR (nuclear magnetic resonance) measurements were carried out at a Bruker Avance 400 spectrometer operating at 155.5 MHz for $^7$Li using a Bruker 4 mm double-resonance probehead operating at a MAS spinning rate of 12 kHz. TPPM (two pulse phase modulation) proton

decoupling was applied during the acquisition. The $^{7}$Li spectra were referenced to a 1 M solution of LiCl in water using solid LiCl as a secondary reference.

#### 4.2.4.5 Scanning Electron Microscopy

Scanning electron microscopic (SEM) studies were applied to characterize surface morphologies by using a Cross Beam Microscope (ESB 1540, Zeiss, Germany) with integrated energy dispersive X-ray Spectroscopy (Thermo Fisher Scientific, Germany). The specimen were bonded on conducting carbon pads and finally covered with a thin carbon layer via evaporating to avoid charging.

#### 4.2.4.6 Transmission Electron Microscopy

Transmission electron microscopic (TEM) images have been recorded on a Tecnai $G^2$ 20 S-TWIN (operating at 10 keV) with an energy dispersive X-ray spectrometer (EDAX, r-TEM SUTW) located at the ZELMI, Technical University Berlin.

## 4.3 Results

### 4.3.1 General Characterization

The Li-content for all catalysts is shown in Table 4.3. No Li was detected for pure MgO. For most catalysts there is a discrepancy between the target loading of Li and the actual loading. This is due to a loss during the calcination process, which has already been described in the literature [119, 73]. The Li-loading of 0.04 wt% for the 0.5 wt% Li-MgO can be attributed to the very high calcination temperature of 900 $^{\circ}C$. The general trend is, that with higher loadings of Li, the difference between the target and the actual loadings increases. The target loading of Li is used for denomination, to avoid any confusion.

Table 4.3: Lithium contents in wt% of the differently prepared Li-doped MgO materials.

| Loading | Li@MgO | Li/MgO | Li-MgO | Li+MgO |
|---|---|---|---|---|
| 0.0 | 0.00 | 0.00 | 0.00 | 0.00 |
| 0.5 | 0.41 | 0.49 | 0.04 | 0.51 |
| 1.0 | 0.61 | 0.92 | 0.84 | 0.97 |
| 2.0 | 1.33 | 2.09 | 1.71 | 1.69 |
| 4.0 | 2.24 | 4.04 | 2.76 | 2.48 |
| 8.0 | 5.99 | 7.43 | 6.15 | 3.66 |

The results for the BET experiments for all prepared catalysts are shown in Table 4.4. The specific surface area depends on the preparation procedure and the applied calcination temperature, albeit the highest BET values are observed for pure MgO. Upon Li-addition, the specific surface area decreases and with increasing loadings of Li, the BET surface area decreases. The strongest reduction of the specific surface area upon Li-addition is observed for Li/MgO and Li-MgO.

Table 4.4: The table shows the BET surface area in $m^2/g$ for all preparation routes and Li-loadings.

| wt% | Li@MgO | Li/MgO | Li-MgO | Li+MgO |
|---|---|---|---|---|
| 0.0 | 99.3 | 120.7 | 34.4 | 67.8 |
| 0.5 | 81.7 | 6.3 | 27.3 | 23.2 |
| 1.0 | 73.4 | 5.4 | $\leq 1$ | 16.7 |
| 2.0 | 26.3 | 5.6 | $\leq 1$ | 20.6 |
| 4.0 | 7.5 | 3.4 | $\leq 1$ | 24.0 |
| 8.0 | $\leq 1$ | 5.1 | $\leq 1$ | 14.5 |

Li can not be detected via XRD, SEM and TEM. Therefore, these results are not described here. However, the characterization of the catalysts after different times on stream still leads to useful data, which will be discussed in the according paragraphs.

## 4.3.2 Time on Stream Experiments

### 4.3.2.1 Li@MgO

Figure 4.2 shows the development of the $CH_4$ conversion and the $C_2$ selectivity during 40 hours time on stream for the Li@MgO catalyst with different loadings of Li. In the first 3 to 5 hours, a strong deactivation is observed. With higher Li loadings, the deactivation rate increases. For 0.5 wt% and 1 wt% Li@MgO, the strong deactivation is followed by a reactivation. For 0 wt%, 0.5 wt% and 1 wt% Li@MgO, the $CH_4$ conversion seems to approach the same residual value. The strong scattering of the trajectories for 4 wt% and 8 wt% is due to the small conversion. They are too small for an exact determination of the reaction products and therefore, for an exact calculation conversion and selectivity. The gap at 6.7 hours in the trajectory of 8 wt% Li/MgO can be explained that at low conversions the concentration of one of the reaction products (usually $CO_2$) falls below the detection limit of the TCD detector. The selectivity of these two catalysts is therefore not being discussed, because the conversion and the selectivity can not exactly be determined. The $C_2$ selectivity decreases with time on stream and approaches

a residual value. However, for 2 wt% Li, this decrease is much slower than for lower Li loadings. The catalytic performance of 0.5 wt% and 1 wt% is similar. Compared to materials prepared on other synthetic routes, the 0 wt% Li@MgO has a rather high $C_2$ selectivity.

#### 4.3.2.2 Li/MgO

Figure 4.3 shows the development of the $CH_4$ conversion and the $C_2$ selectivity during 40 hours time on stream for the Li/MgO catalyst with different loadings of Li. A strong and constant decrease in the $CH_4$ conversion can be observed. The deactivation rate increases with higher Li loadings, 0 wt% Li/MgO exhibit the slowest deactivation. The high initial $CH_4$ conversion falls below 4 % after 40 hours time on stream. The gap in the trajectory at 7 hours and 8 hours for 4 wt% and 8 wt% Li/MgO, respectively, occurs due to the same reasons like for Li@MgO. The selectivity is therefore not being discussed. There is no significant difference for the $C_2$ selectivity for 0.5 wt%, 1 wt% and 2 wt% Li/MgO. However, as already reported by other researchers, the catalysts without Li shows a very low $C_2$ selectivity.

#### 4.3.2.3 Li-MgO

Figure 4.4 shows the development of the $CH_4$ conversion and the $C_2$ selectivity during 40 hours time on stream for the Li-MgO catalyst with different loadings of Li. All materials with a Li-loading higher than 0.5 wt% drastically deactivate within 5 hours time on stream. However, the loss in activity for 0 wt% Li-MgO and 0.5 wt% Li-MgO is rather low compared to other materials. For 0.5 wt% Li-MgO, it might very well be due to the rather low actual Li content compared to the other preparation routes. The gap in the trajectory at 3 hours and 6.3 hours for 4 wt% and 8 wt% Li-MgO, respectively, can be explained by a low conversion and therefore a low concentration of one of the reaction products (usually $CO_2$), which then falls below the detection limit of the TCD detector. The selectivity of these two catalysts is also not being discussed. The $C_2$ selectivity remains constant for 0 wt% MgO and it is constant after an initial deactivation time for 0.5 wt% Li-MgO with time on stream. It is evident, that 0.5 wt% Li-MgO has the higher $CH_4$ conversion as well as the higher $C_2$ selectivity.

#### 4.3.2.4 Li+MgO

Figure 4.5 shows the development of the $CH_4$ conversion and the $C_2$ selectivity during 40 hours time on stream for the Li+MgO catalyst with different loadings

of Li. The catalysts, with higher loadings of Li, deactivate quickly and their residual activity is rather low. The difference between 0.5 wt% Li+MgO (red) and 1 wt% Li+MgO (green) is very distinct. However, the difference between 0 wt% MgO (milled) and the unmilled commercial MgO is remarkable. The unmilled material has a residual $CH_4$ conversion of 6.0 % and a $C_2$ selectivity of 22.3 %. When the material is milled, the residual $CH_4$ conversion is 15.6 % and the $C_2$ selectivity is 29.0 %. Moreover, the deactivation of the milled MgO seems to be retarded compared to unmilled commercial MgO. The $C_2$ selectivity decreases for all materials at the beginning of the experiment, however, for some materials the $C_2$ selectivity becomes stable, while for others the selectivity reduction proceeds, i.e. for commercial MgO. The commercial MgO and the 8 wt% Li+MgO catalyst exhibit a very poor $C_2$ selectivity. All other catalysts show a $C_2$ selectivity which is between 30 and 35 %.

#### 4.3.2.5 Summary of Time on Stream Experiments

The data for the residual activity for all catalysts is summarized in Table 4.5. Generally, the activity is rather low, disregarding of the preparation procedure and the Li-loading.

Figure 4.6 is a conversion selectivity diagram, containing all catalysts with the initial activity (small data points) and the residual activity (large data points). The initial activity shows a strong scattering for the different materials. However, after 40 hours time on stream, the activity is significantly reduced. Moreover, the catalytic data for the differently prepared Li-doped MgO catalysts do not differ so strong anymore. Since none of the catalysts reached a stable state, it can be expected that this scattering will be further reduced when the time on stream is extended, disregarding of the preparation.

### 4.3.3 Structural Analysis for Different Times on Stream

From each preparation procedure the samples with a loading of Li of 0.5 wt% were chosen. Samples were taken from the reactor after 1, 3, 7, 14 and 24 hours time on stream and structural analysis was performed. The obtained catalytic results, such as $O_2$ conversion, $CH_4$ conversion, $C_2$ selectivity, $C_2$ yield, and the ratios of $C_2H_6$ to $C_2H_4$ and $CO_2$ to CO of these 4 materials are shown in detail in Figure 4.7 for 24 hours time on stream.

#### 4.3.3.1 AAS

Figure 4.8 shows the Li content after different times on stream for all 0.5 wt% Li-doped MgO samples. The most significant reduction is observed within the

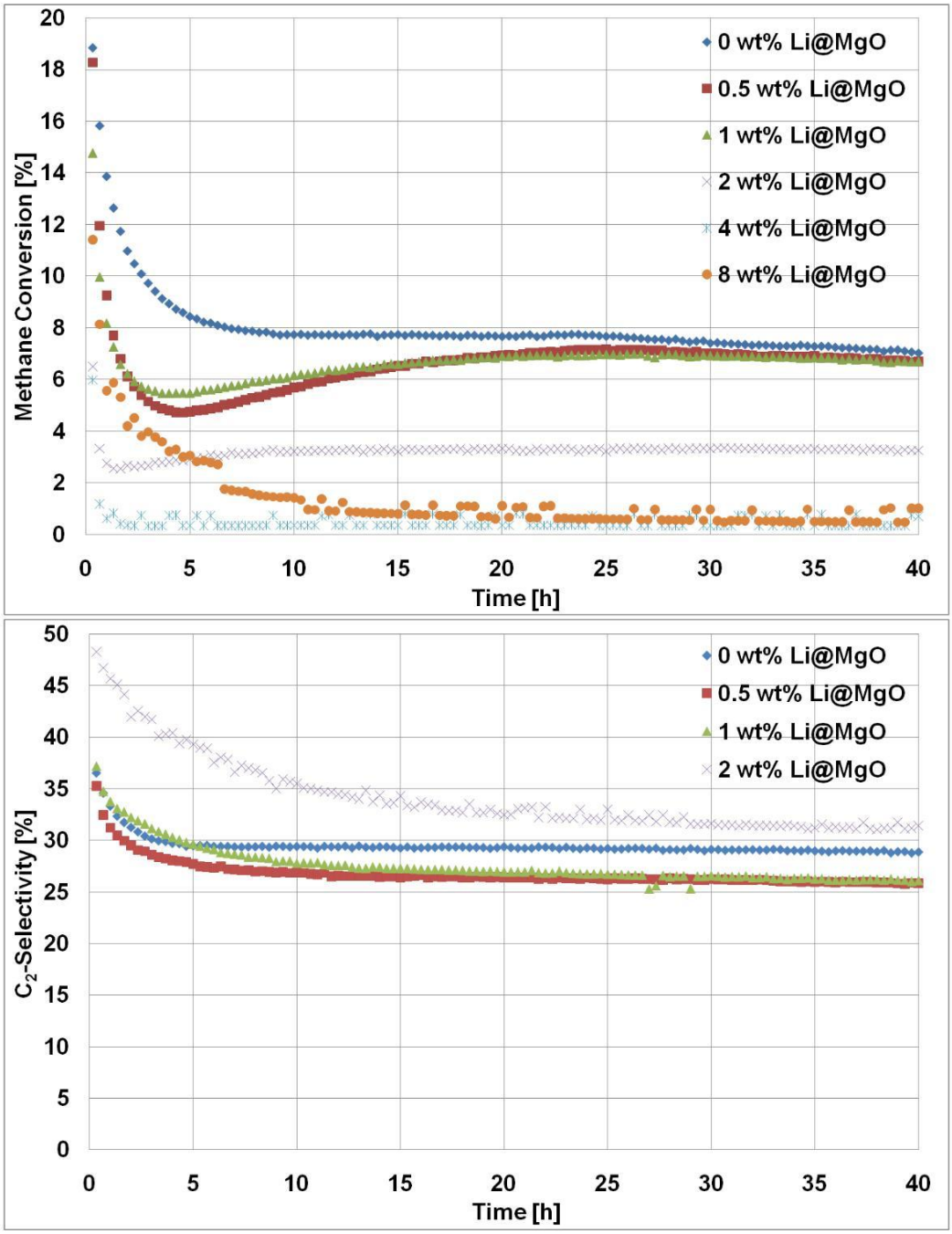


Figure 4.2: $CH_4$ conversion (above) and $C_2$ selectivity (below) of Li@MgO as function of time on stream.

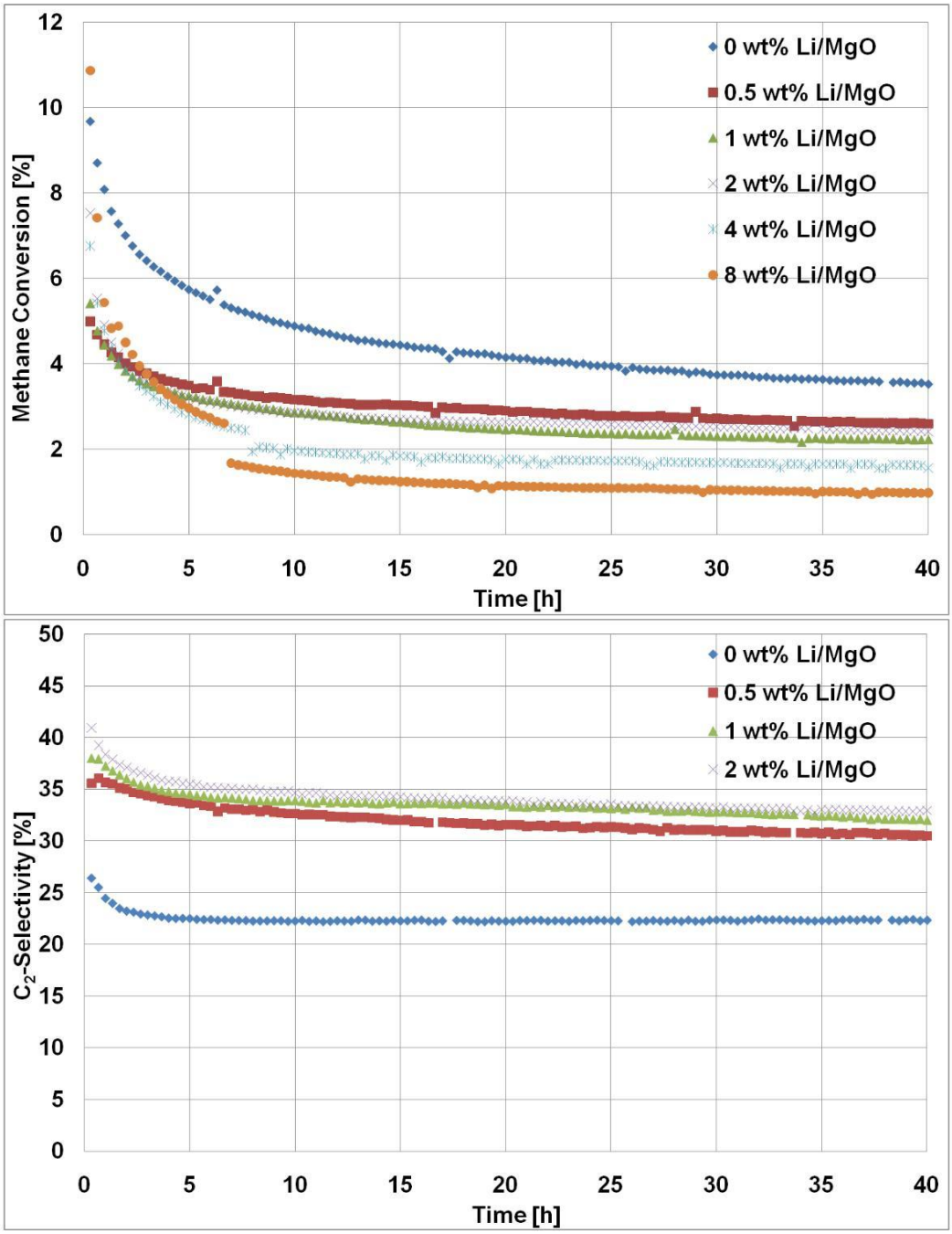


Figure 4.3: $CH_4$ conversion (above) and $C_2$ selectivity (below) of Li/MgO as function of time on stream.

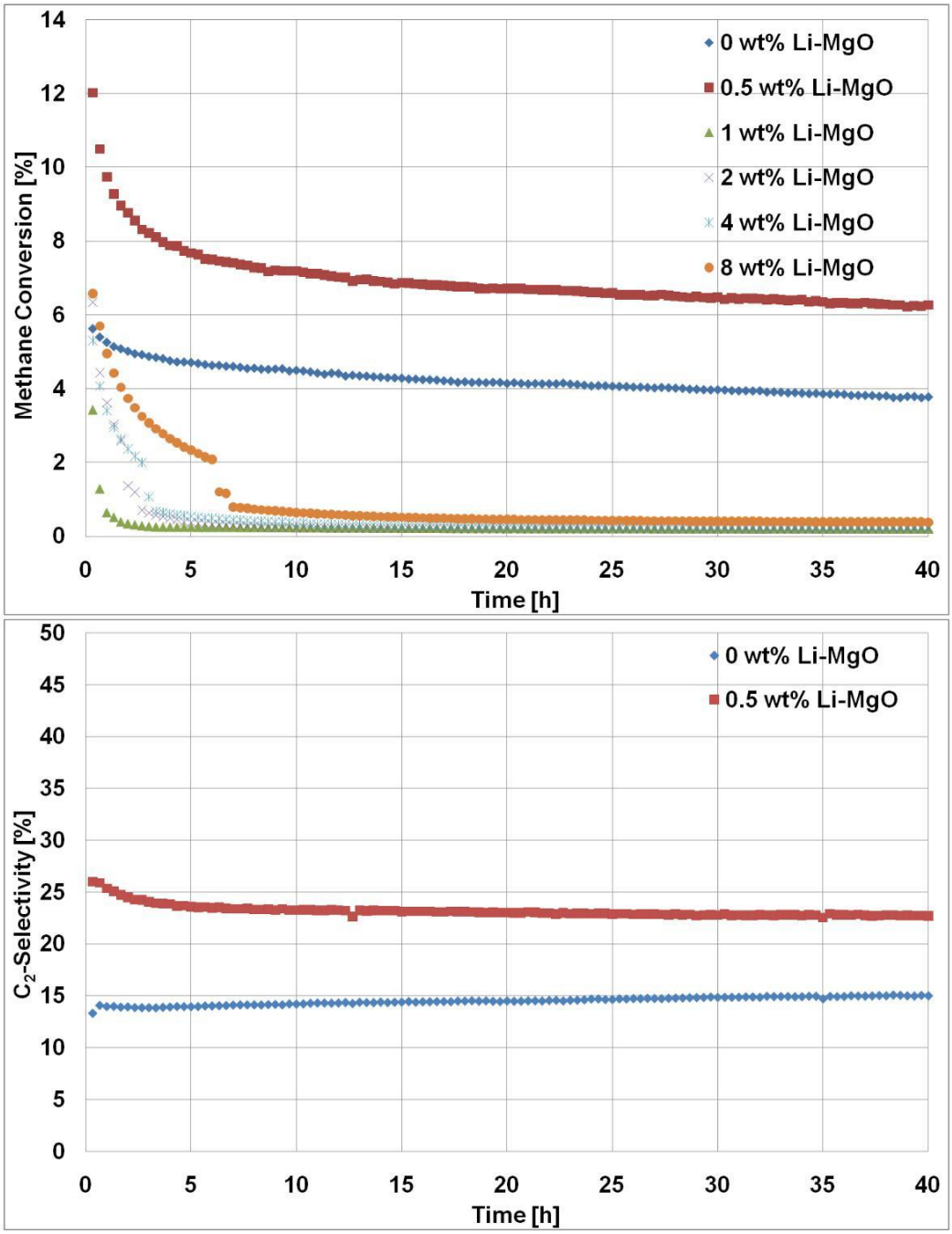


Figure 4.4: $CH_4$ conversion (above) and $C_2$ selectivity (below) of Li-MgO as function of time on stream.

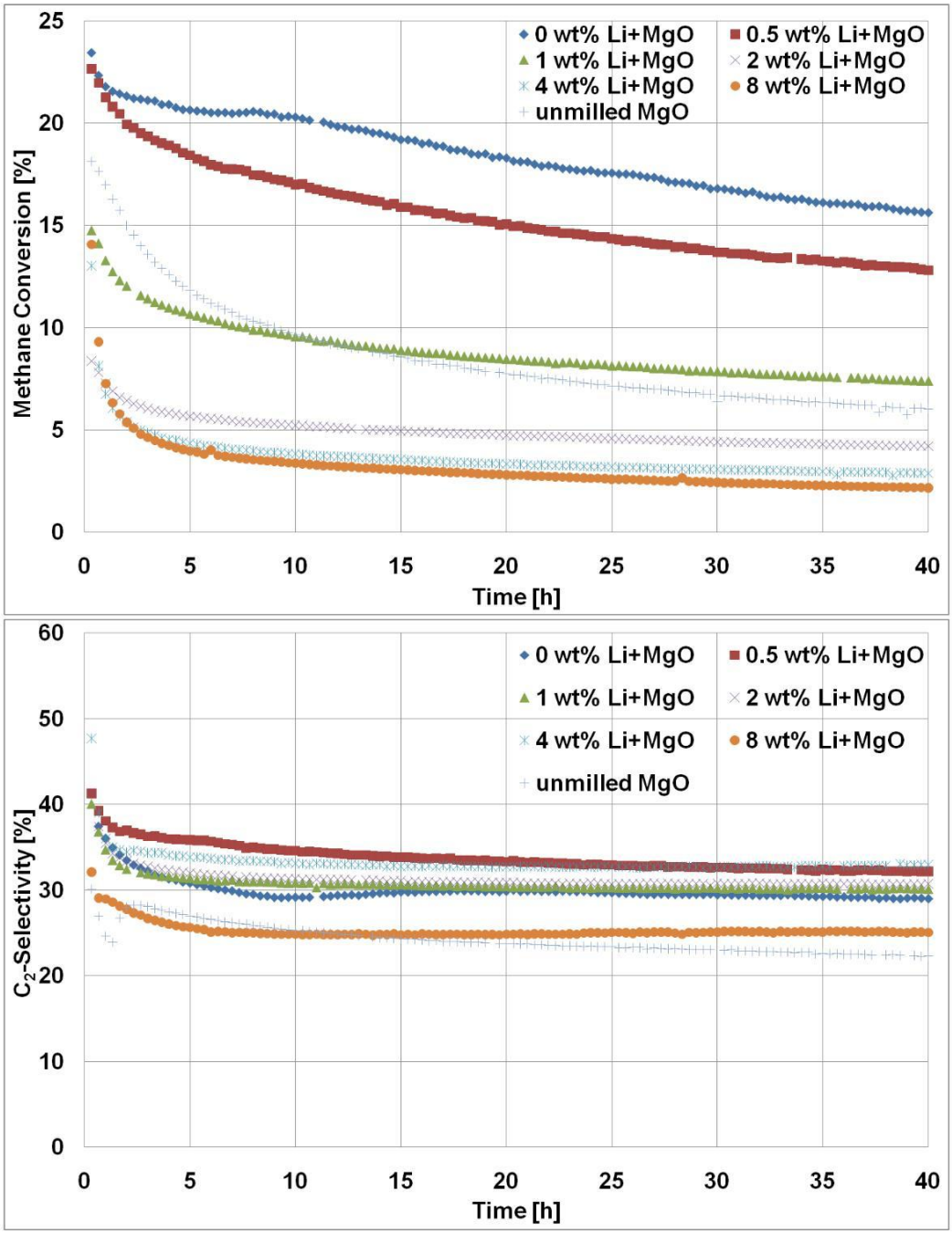


Figure 4.5: $CH_4$ conversion (above) and $C_2$ selectivity (below) of Li+MgO as function of time on stream.

Table 4.5: Summary of the residual activity ($O_2$ and $CH_4$ conversion, $C_2$ selectivity and the ratios of $C_2H_6$ to $C_2H_4$ and $CO_2$ to CO after 40 hours time on stream for the prepared catalysts. If the conversion was too low and the selectivity was not discussed, then the according values are replaced with a "-". The data in this table is also shown in a conversion selectivity diagram in Figure 4.6.

| **Single Source Precursor** | | | | | | |
|---|---|---|---|---|---|---|
| Catalyst | 0 wt% Li@MgO | 0.5 wt% Li@MgO | 1 wt% Li@MgO | 2 wt% Li@MgO | 4 wt% Li@MgO | 8.7 wt% Li@MgO |
| $X_{O_2}$ | 26.0 % | 24.9 % | 24.6 % | 10.7 % | 2.6 % | 2.1 % |
| $X_{CH_4}$ | 7.0 % | 6.7 % | 6.7 % | 3.2 % | 0.7 % | 1.0 % |
| $S_{C_2}$ | 28.9 % | 25.8 % | 26.1 % | 31.4 % | 47.9 % | 45.8 % |
| $C_2H_6/C_2H_4$ | 3.0 | 3.5 | 3.3 | 5.4 | - | 8.3 |
| $CO_2/CO$ | 0.3 | 0.3 | 0.3 | 0.2 | - | - |
| **Wet Impregnation** | | | | | | |
| Catalyst | 0 wt% Li/MgO | 0.5 wt% Li/MgO | 1 wt% Li/MgO | 2 wt% Li/MgO | 4 wt% Li/MgO | 8 wt% Li/MgO |
| $X_{O_2}$ | 13.7 % | 9.5 % | 9.5 % | 9.0 % | 6.6 % | 4.1 % |
| $X_{CH_4}$ | 3.5 % | 2.6 % | 2.2 % | 2.4 % | 1.6 % | 1.0 % |
| $S_{C_2}$ | 22.3 % | 30.5 % | 32.0 % | 32.9 % | 43.8 % | 59.3 % |
| $C_2H_6/C_2H_4$ | 5.2 | 5.5 | 6.9 | 5.8 | 60.1 | 9.0 |
| $CO_2/CO$ | 0.3 | 0.3 | 0.4 | 0.3 | 0.0 | - |
| **Precipitation** | | | | | | |
| Catalyst | 0 wt% Li-MgO | 0.5 wt% Li-MgO | 1 wt% Li-MgO | 2 wt% Li-MgO | 4 wt% Li-MgO | 8 wt% Li-MgO |
| $X_{O_2}$ | 15.8 % | 25.5 % | 1.1 % | 1.3 % | 1.7 % | 2.9 % |
| $X_{CH_4}$ | 3.8 % | 6.3 % | 0.2 % | 0.2 % | 0.2 % | 0.4 % |
| $S_{C_2}$ | 15.0 % | 22.7 % | - | - | - | - |
| $C_2H_6/C_2H_4$ | 4.6 | 3.3 | - | - | - | 7.5 |
| $CO_2/CO$ | 0.3 | 0.3 | - | - | - | - |
| **Mixed Milling** | | | | | | |
| Catalyst | unmilled MgO | milled MgO | 0.5 wt% Li+MgO | 1 wt% Li+MgO | 2 wt% Li+MgO | 4 wt% Li+MgO | 8 wt% Li+MgO |
| $X_{O_2}$ | 25.4 % | 69.8 % | 52.0 % | 29.2 % | 15.2 % | 8.9 % | 10.2 % |
| $X_{CH_4}$ | 6.0 % | 15.6 % | 12.8 % | 7.4 % | 4.2 % | 2.9 % | 2.2 % |
| $S_{C_2}$ | 22.3 % | 29.0 % | 32.2 % | 30.1 % | 30.7 % | 33.0 % | 25.1 % |
| $C_2H_6/C_2H_4$ | 3.3 | 1.4 | 1.6 | 2.6 | 4.0 | 5.5 | 6.1 |
| $CO_2/CO$ | 0.7 | 1.8 | 1.1 | 0.6 | 0.4 | 0.3 | 0.8 |

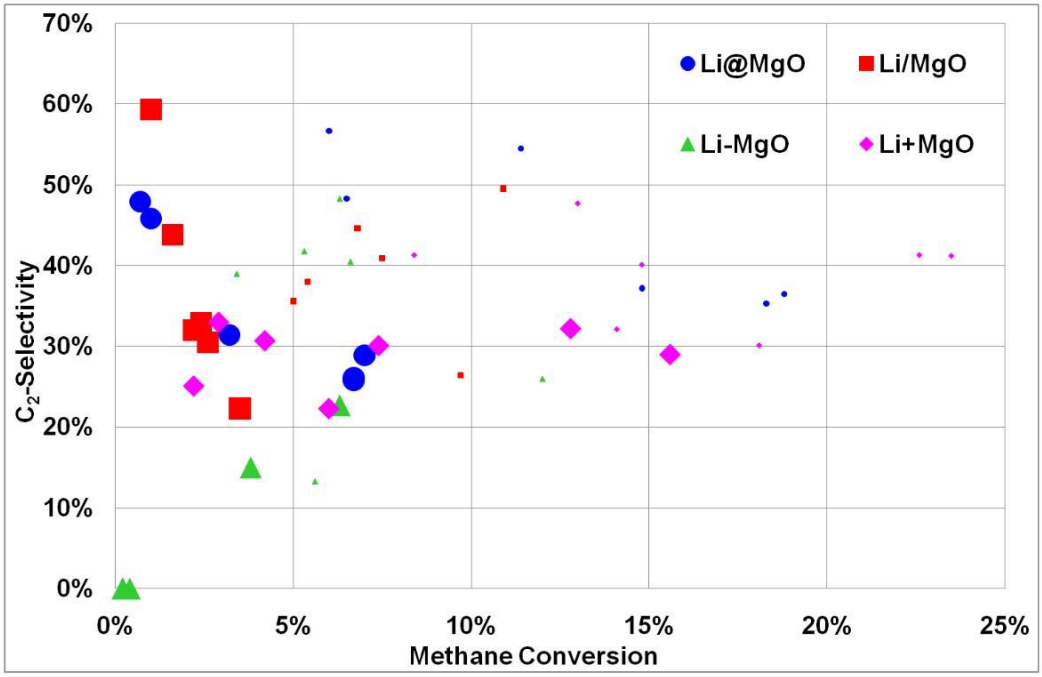


Figure 4.6: The initial activity (small data points) and residual activity (large data points) for all catalysts of Table 4.5 is shown as a conversion selectivity diagram. While the initial activity scatters, the residual activity and the scattering is strongly reduced, irrespective of the Li-loading or of the preparation procedure.

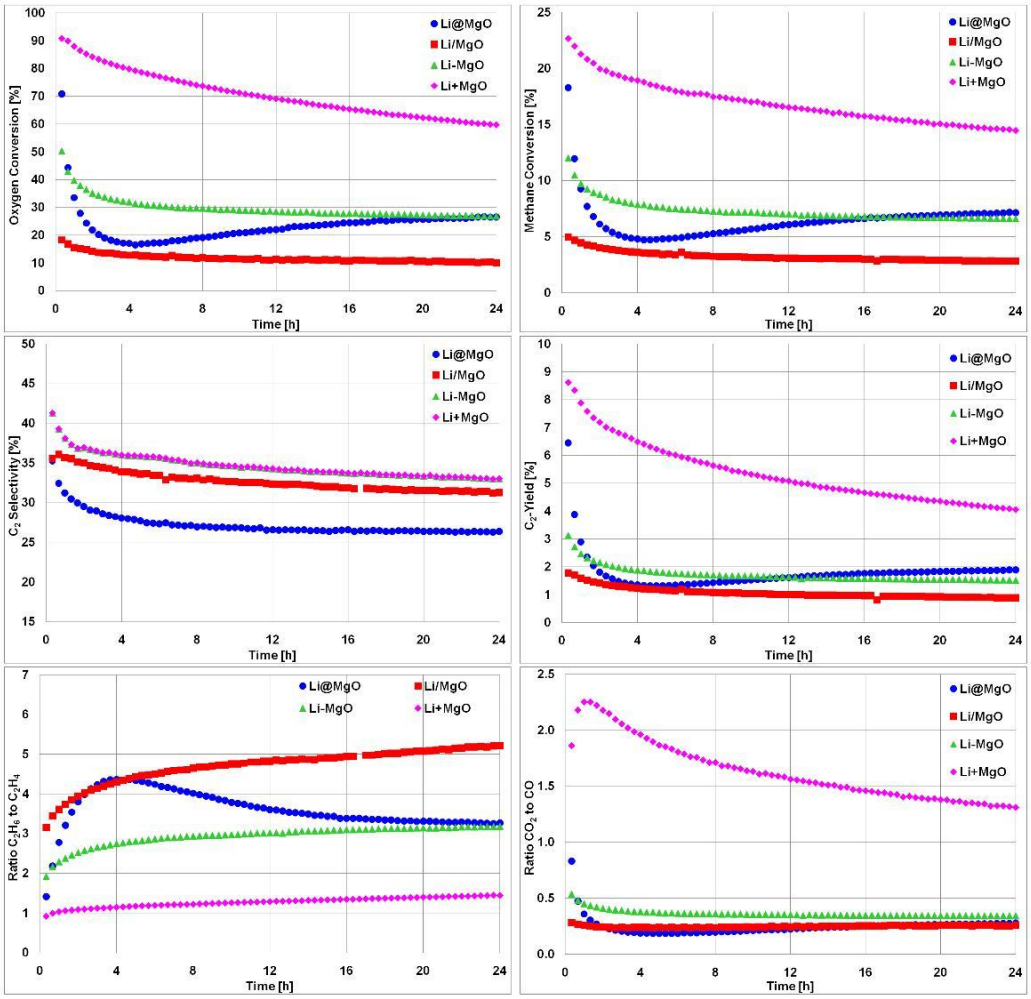


Figure 4.7: Comparision of the $O_2$ conversion, $CH_4$ conversion, $C_2$ selectivity, $C_2$ yield, and the ratios of $C_2H_6$ to $C_2H_4$ and $CO_2$ to CO for the differently prepared 0.5 wt% Li-doped MgO samples.

first hour under reaction conditions, irrespective of the preparation procedure. Afterwards, the further reduction is still signifcant, but small. After approximately 7 hours time on stream, the amount of Li in the catalyst is not significantly reduced anymore. Disregarding of the exact initial Li-loading and the preparation procedure, the residual Li-content approaches the same, or at least similar value, which lies between 0.01 and 0.03 wt%.

Moreover, possible impurities such as, Fe, Cr, Mn, Ca and Cu were determined via AAS before the reaction and after 24 hours time on stream. The results are shown in Table 4.6. Considerable amounts of Fe and Ca were found. Cr, Mn and Cu were also be determined, though in smaller amounts. For Li/MgO, Mn was found, even so in rather small amounts. Li+MgO contains the highest amount of impurities, which is probably due to the milling. The measured amounts of impurities did not change significantly after the reaction. The strong increase in Ca for Li/MgO is probably an outlier. The amounts of impurities seem to be relatively stable under reaction conditions.

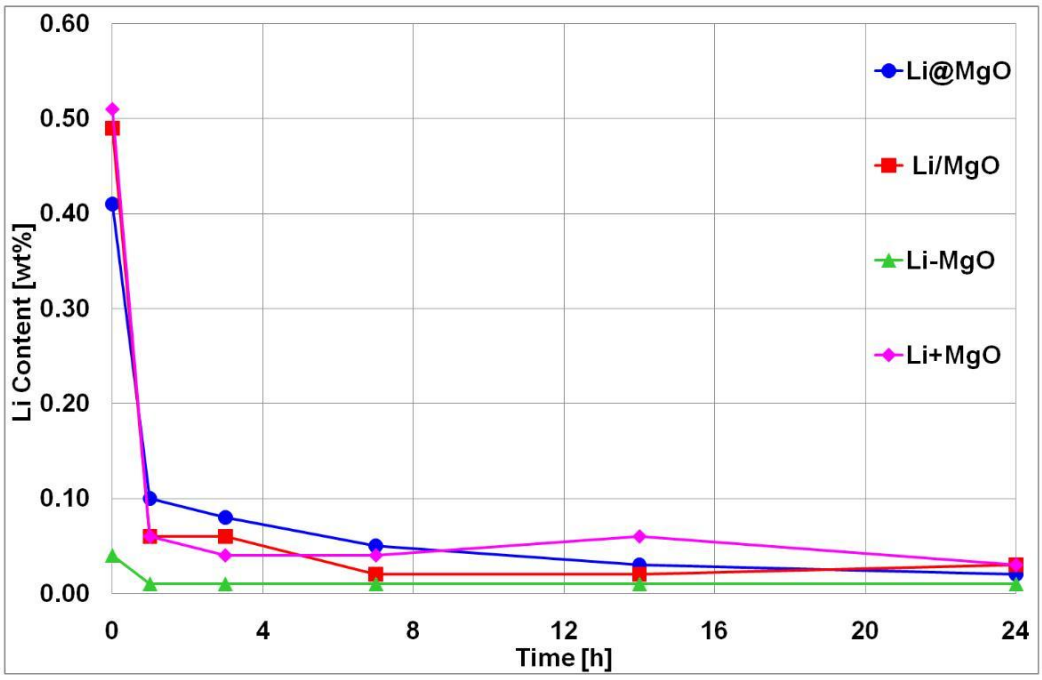


Figure 4.8: Decrease of the Li content of the differently prepared Li-doped MgO catalysts as a function of time on stream.

Table 4.6: Amount of the determined impurities in wt% before and after the reaction for the different 0.5 wt% Li-doped MgO.

| Catalyst | 0 h | 24 h |
|---|---|---|
| | Fe | |
| Li@MgO | 0.014 | 0.011 |
| Li/MgO | 0.011 | 0.014 |
| Li-MgO | 0.012 | 0.009 |
| Li+MgO | 0.13 | 0.122 |
| | Cr | |
| Li@MgO | 0.006 | 0.007 |
| Li/MgO | 0.006 | 0.007 |
| Li-MgO | 0.007 | 0.006 |
| Li+MgO | 0.006 | 0.008 |
| | Mn | |
| Li@MgO | 0.001 | 0.001 |
| Li/MgO | 0.000 | 0.000 |
| Li-MgO | 0.001 | 0.000 |
| Li+MgO | 0.006 | 0.005 |
| | Ca | |
| Li@MgO | 0.049 | 0.014 |
| Li/MgO | 0.041 | 0.942 |
| Li-MgO | 0.017 | 0.014 |
| Li+MgO | 0.939 | 0.452 |
| | Cu | |
| Li@MgO | 0.002 | 0.001 |
| Li/MgO | 0.002 | 0.005 |
| Li-MgO | 0.002 | 0.001 |
| Li+MgO | 0.002 | 0.002 |

#### 4.3.3.2 BET

The change of the BET surface area with time on stream is shown in Table 4.7 and the relative change is shown in Figure 4.9. It is evident, that the Li@MgO, prepared via the decomposition of single source precursors, had the highest BET surface area at the beginning of the experiment, but it also showed the strongest reduction. The Li/MgO, prepared via wet impregnation, did not have a high BET surface at all, but after 1 hour time on stream, the BET surface area fell below the detection limit of the used Micromeritics Gemini III 2375 Surface Area Analyzer. Therefore, after 3 hours time on stream, the specific surface has not been determined anymore. The Li-MgO, prepared via precipitation, suffered from a loss of BET surface area only within the 1 hour time on stream. After that no change was observed anymore. For Li+MgO, a strong decrease was observed after 1 hour time on stream and after that only a comparatively small reduction was observed. From 7 hours time on stream until the end of the experiment, no change was observed.

Table 4.7: The table shows the change of the BET surface area in $m^2/g$ with time on stream of the different 0.5 wt% Li-doped MgO.

| Time | Li@MgO | Li/MgO | Li-MgO | Li+MgO |
|---|---|---|---|---|
| 0 h | 81.7 | 6.3 | 27.3 | 23.2 |
| 1 h | 3.1 | $\leq 1$ | 20.9 | 14.5 |
| 3 h | 3.8 | $\leq 1$ | 20.0 | 14.9 |
| 7 h | 5.2 | n.d. | 22.8 | 10.0 |
| 14 h | 4.3 | n.d. | 21.4 | 11.1 |
| 24 h | 2.6 | n.d. | 20.5 | 11.0 |

#### 4.3.3.3 XRD

The XRD diffractograms show the reflexes for MgO. Small reflexes for $Li_2CO_3$ were found for the samples of Li/MgO and Li@MgO, before reaction. $Li_2O$ was not found in any sample. The Li@MgO samples showed small reflexes which are probably due to carbon containing materials, shown in Figure 4.10. Moreover the reflexes of Li@MgO were rather broad, indicating that they either have a rather low degree of crystallinity and/or have a small grain size. With time on stream the width of the reflexes decreased, indicating a higher regularity or crystallinity of the particles.

The lattice parameters were determined before reaction and after 24 hours time on stream. The values are in the range of the theoretical lattice parameter for MgO of 4.217 Å. The differences are insignificant and do not exhibit an evident trend.

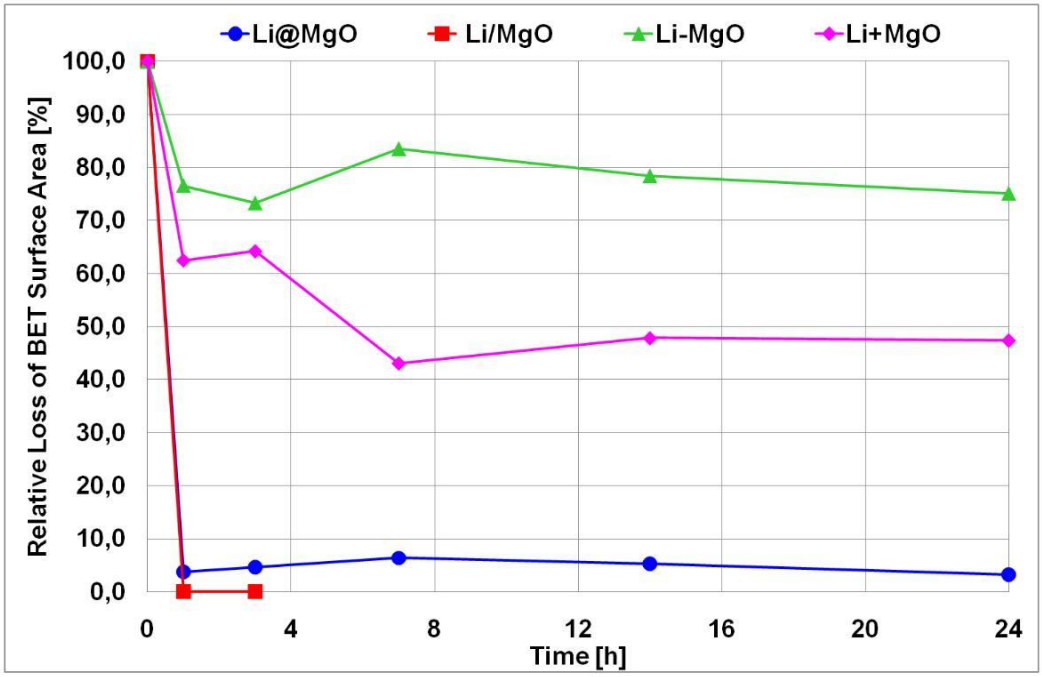


Figure 4.9: Relative loss of BET surface area with time on stream. The data of Table 4.7 is plotted in this Figure. A strong reduction is observed for Li@MgO and Li/MgO, while Li-MgO and Li+MgO remain constant after an initial reduction period.

However, the change in grain size was more significant. The change is shown in Figure 4.11. The freshly prepared materials had a relatively low grain size. All materials, except Li-MgO, showed a drastic increase in the grain size within the first 3 hours time on stream. After that, no significant change was observed. However, Li@MgO showed an increase in the grain size after 14 hours time on stream, which was concomitant to a small increase in the catalytic activity. The Li-MgO sample did not show any significant change in the particle size with time on stream.

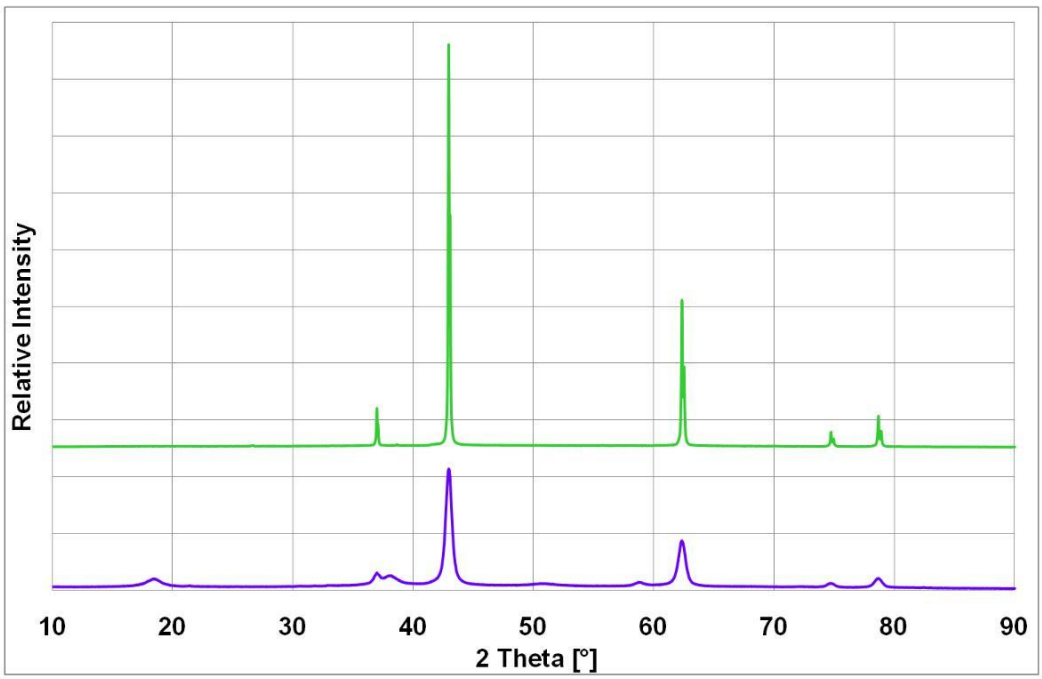


Figure 4.10: The blue graph (below) represents the XRD pattern of Li@MgO recorded before reaction. The reflexes are relatively broad and at angles of approximately 18 $\theta$, 38 $\theta$ and 58 $\theta$, they are most probably due to carbon contamination from the preparation. The green graph (above) represents the XRD of Li@MgO recorded after 24 hours time on stream. The reflexes for the carbon containing compounds disappeared and the MgO reflexes have become narrower, indicating a higher degree of crystallinity and/or a larger particle size.

#### 4.3.3.4 Solid State NMR

Solid state $^{7}$Li MAS NMR measurements have been carried out for all four Li-doped MgO catalysts before reaction and after 1, 3, 7, 14 and 24 hours time on stream. All samples before reaction show a single resonance at 0 ppm, with the

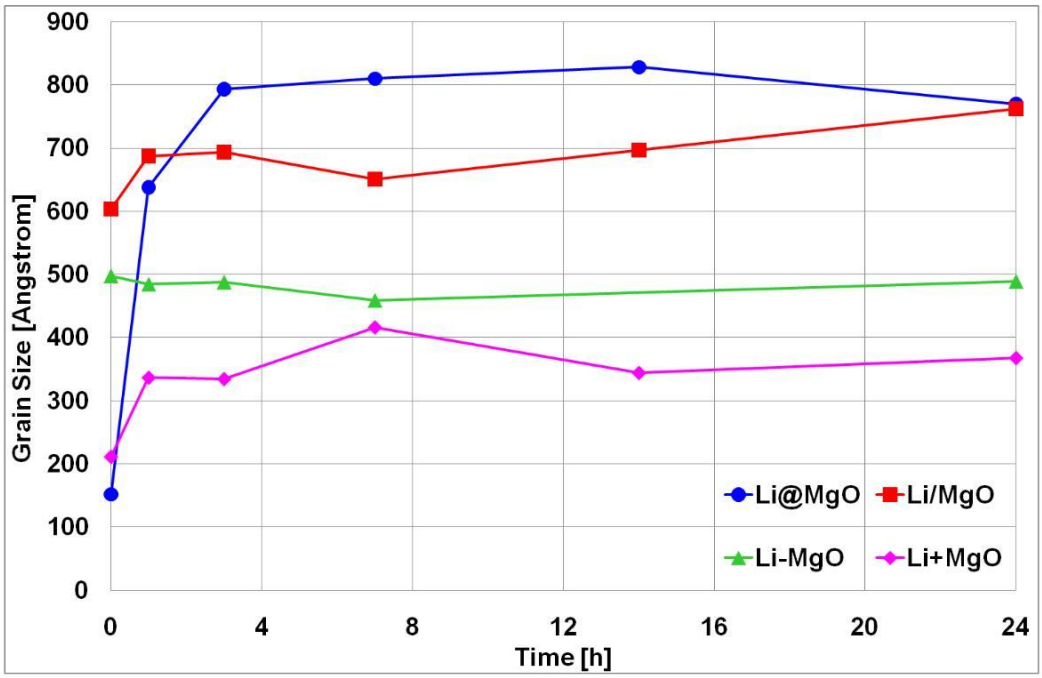


Figure 4.11: The change of the grain sizes for the different Li-doped MgO catalysts. The Li-MgO did not show an increase in particle size, while the other samples exhibited a drastic increase in grain size within the first 3 hours time on stream.

Li/MgO sample showing a slight shoulder at 1.4 ppm. It has to be noted that no signals at 3.2 ppm which would be indicative of $Li_2O$ were found in any of the samples. The $^7$Li resonance peaks of the four samples before reaction exhibit different line widths (full width at half height - fwhh) of 380 Hz, 285 Hz, 200 Hz and 190 Hz for Li/MgO, Li+MgO, Li@MgO and Li-MgO, respectively. The narrow lines in the latter samples indicate a higher degree of cristallinity and uniformity in the latter samples.

In the samples measured after different reaction times no significant shift in the $^7$Li signal is observed for any of the samples, indicating that the chemical environments of the $^7$Li nuclei are not changed dramatically during the reaction. In the Li-MgO material a small resonance at 1.5 ppm is emerging after 1 h of reaction time and slightly increasing up to 24 hours which can be explained by the formation of lithium silicates, but the dominant $^7$Li signal (90 % of Li signal intensity) remains at 0 ppm.

However, in all four materials the $^7$Li NMR line width is significantly decreased after reaction yielding resonances as narrow as 250 Hz, 70 Hz, 85 Hz and 100 Hz (fwhh) after 24 hours time on stream for Li/MgO, Li+MgO, Li@MgO and Li-MgO, respectively, indicating a significantly higher degree of order (i.e. a higher crystallinity) after the reaction. For example, Figure 4.12 shows the $^7$Li MAS NMR spectra of material Li+MgO before reaction and after 1 h, 3 h, 7 h, 14 h and 24 h on stream. Interestingly, the line width has already narrowed to 85 Hz (fwhh) after 1 hour on stream and no further narrowing is observed after 3 hours of reaction time. Similar results are observed for the other three materials. In summary, the $^7$Li MAS NMR measurements of the materials indicate that while no significant change in the chemical environment of $^7$Li nuclei can be observed during the catalytic reactions, a significant increase in the cristallinity of the $^7$Li environments is observed.

The Li-signal at 24 hours time on stream is smaller than at 0 hours time on stream. It can not be excluded, that the signal which is present at 24 hours is already present at 0 hours, but being overlapped due to the broadness of that peak.

#### 4.3.3.5 SEM

The SEM images for Li@MgO are shown in Figure 4.13. After 24 hours time on stream, restructuring is observed. Moreover, particle coarsening up to 500 nm and sintering effects such as neck growth and the loss of sharp edges are found.

The images for Li/MgO are shown in Figure 4.14. Similar to Li@MgO restructuring, extensive inhomogeneous particle coarsening up to 1 $\mu$m and sintering effects such as neck growth and the loss of sharp edges are discerned.

For Li-MgO, see Figure 4.15, the agglomerates have a fine and acicular grain structure, with a grain size $\leq$ 100 nm, which is in accord with grain size calculated

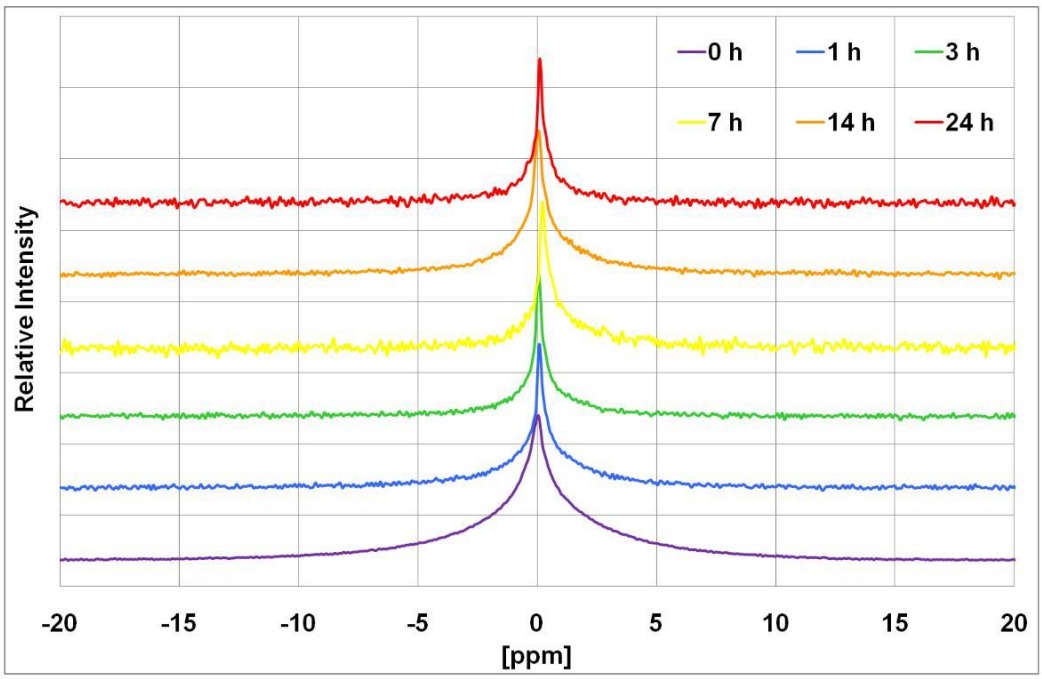


Figure 4.12: $^{7}$Li MAS NMR spectra of 0.5 wt% Li+MgO recorded before reaction and after 1, 3, 7, 14, and 24 hours time on stream.

via XRD. After 24 hours time on stream, homogeneous grain coarsening and sintering effects such as neck growth and the loss of sharp edges are discerned.

The images for Li+MgO are shown in Figure 4.16. The primary grain size is ca. 200 nm. After the reaction, alike for the other materials, homogeneous grain coarsening and sintering effects such as neck growth and the loss of sharp edges are noted.

#### 4.3.3.6 TEM

The TEM images before the reaction and after 24 hours time on stream for Li@MgO are shown in Figure 4.17, Li/MgO in Figure 4.18, Li-MgO in Figure 4.19 and Li+MgO in Figure 4.20. Generally, the agglomerates consist of irregularly shaped nanocrystals, which is in accord with the results obtained by XRD and SEM. The Li@MgO sample has the smallest particle size, this coincides with the observations of the XRD, as shown in Figure 4.11. However, after 24 hours time on stream crystal growth is observed for all Li-doped MgO materials.

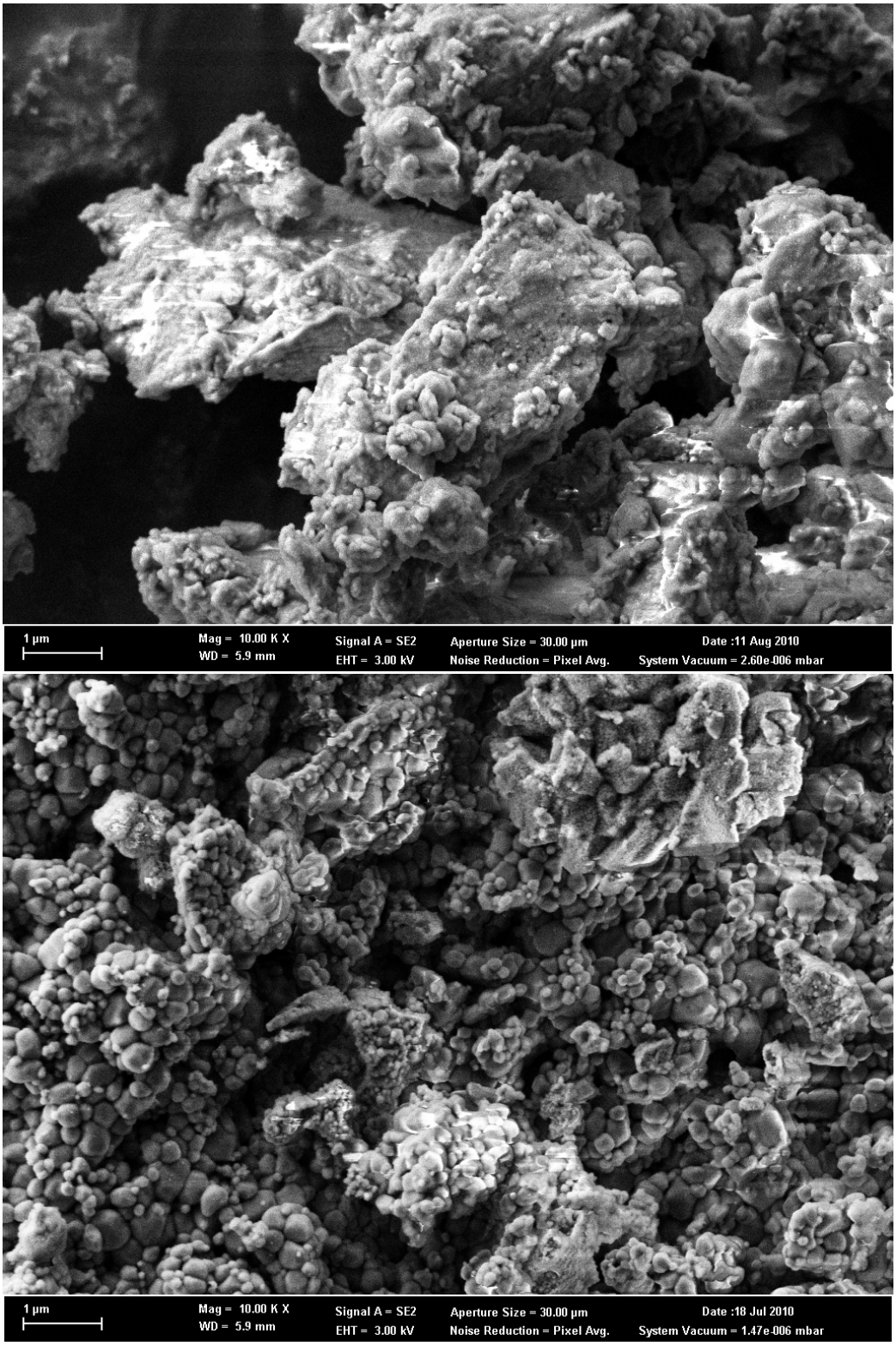


Figure 4.13: SEM imgages for Li@MgO, before reaction (above) and after 24 hours time on stream (below).

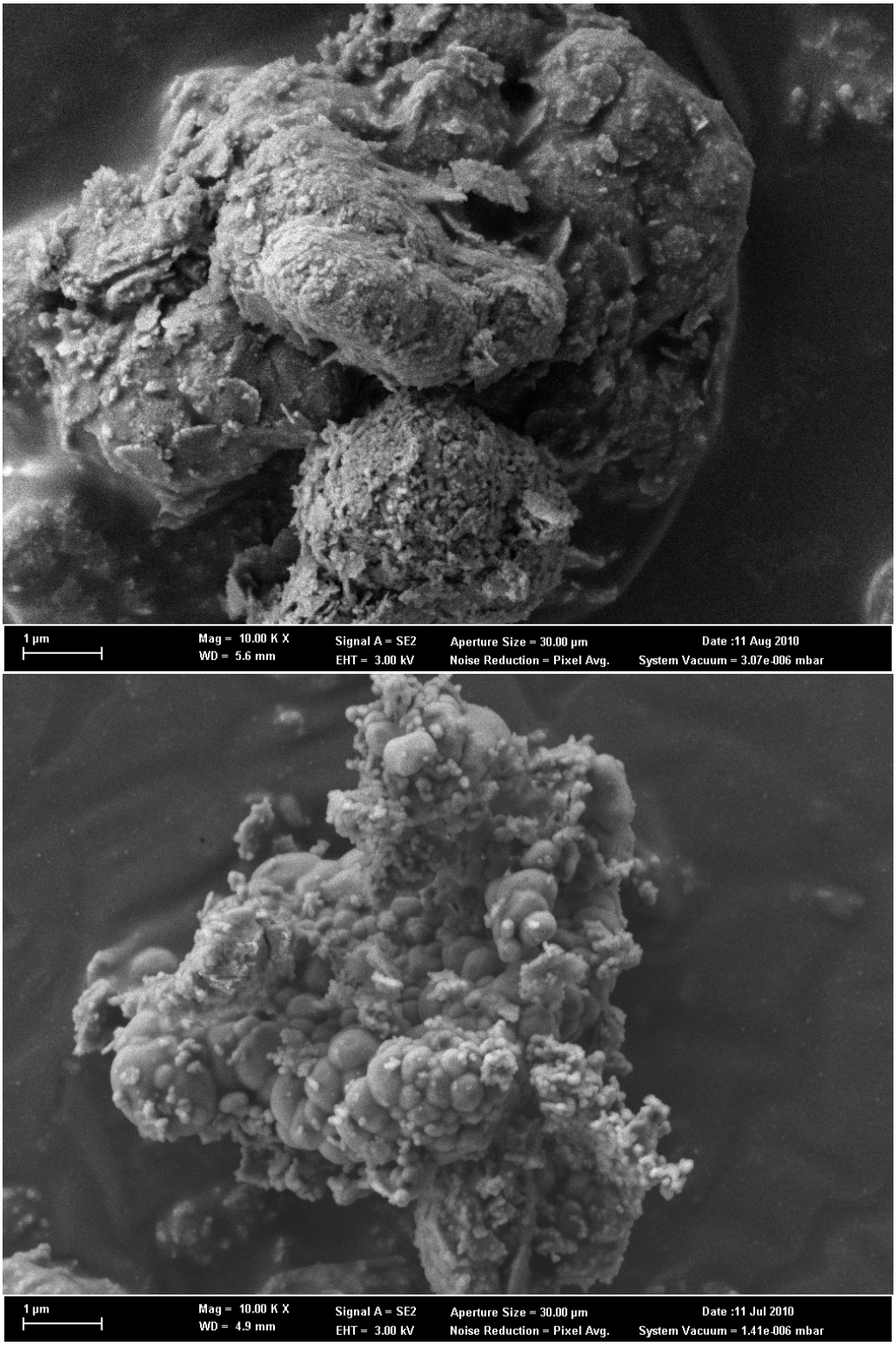


Figure 4.14: SEM imgages for Li/MgO, before reaction (above) and after 24 hours time on stream (below).

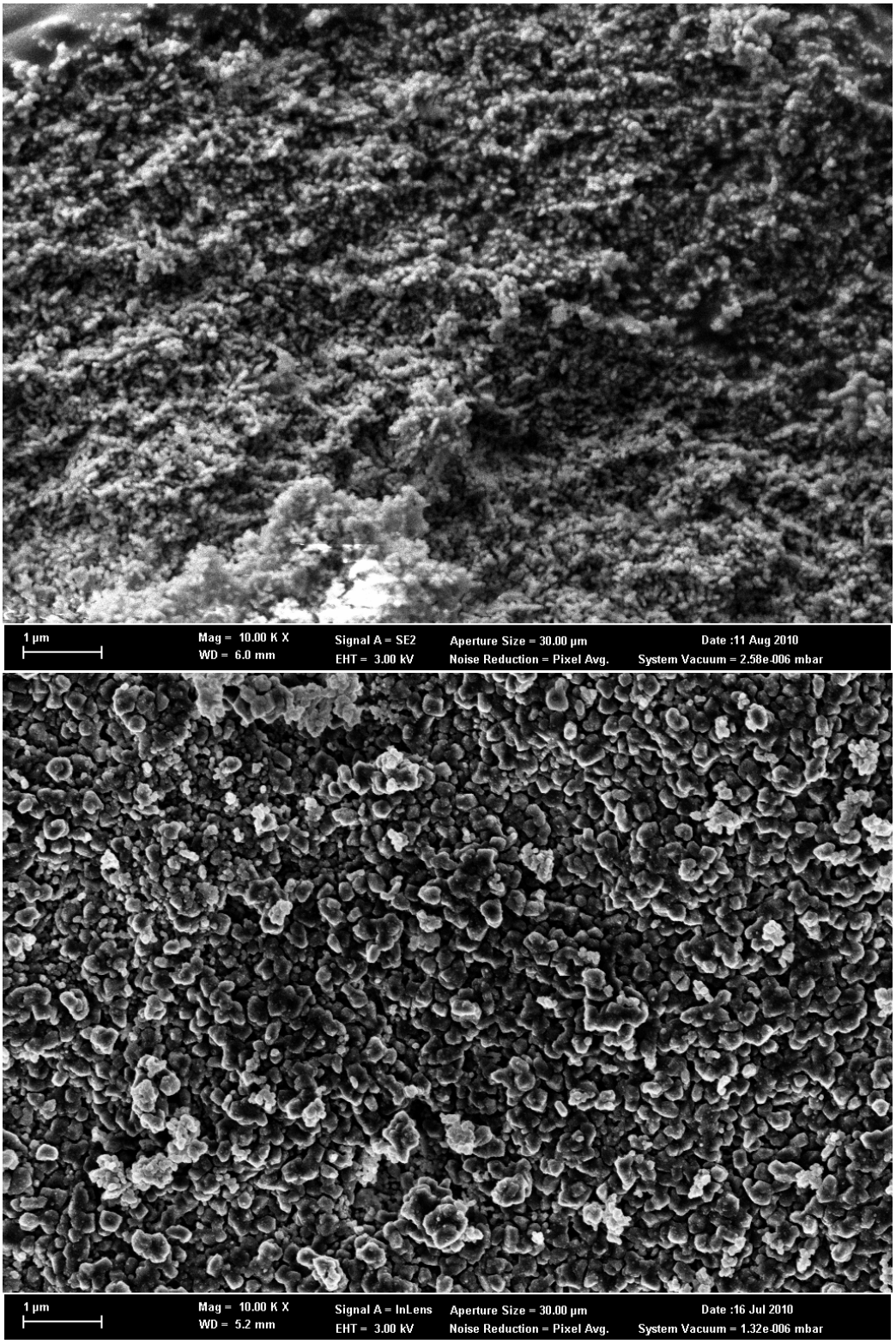


Figure 4.15: SEM imgages for Li-MgO, before reaction (above) and after 24 hours time on stream (below).

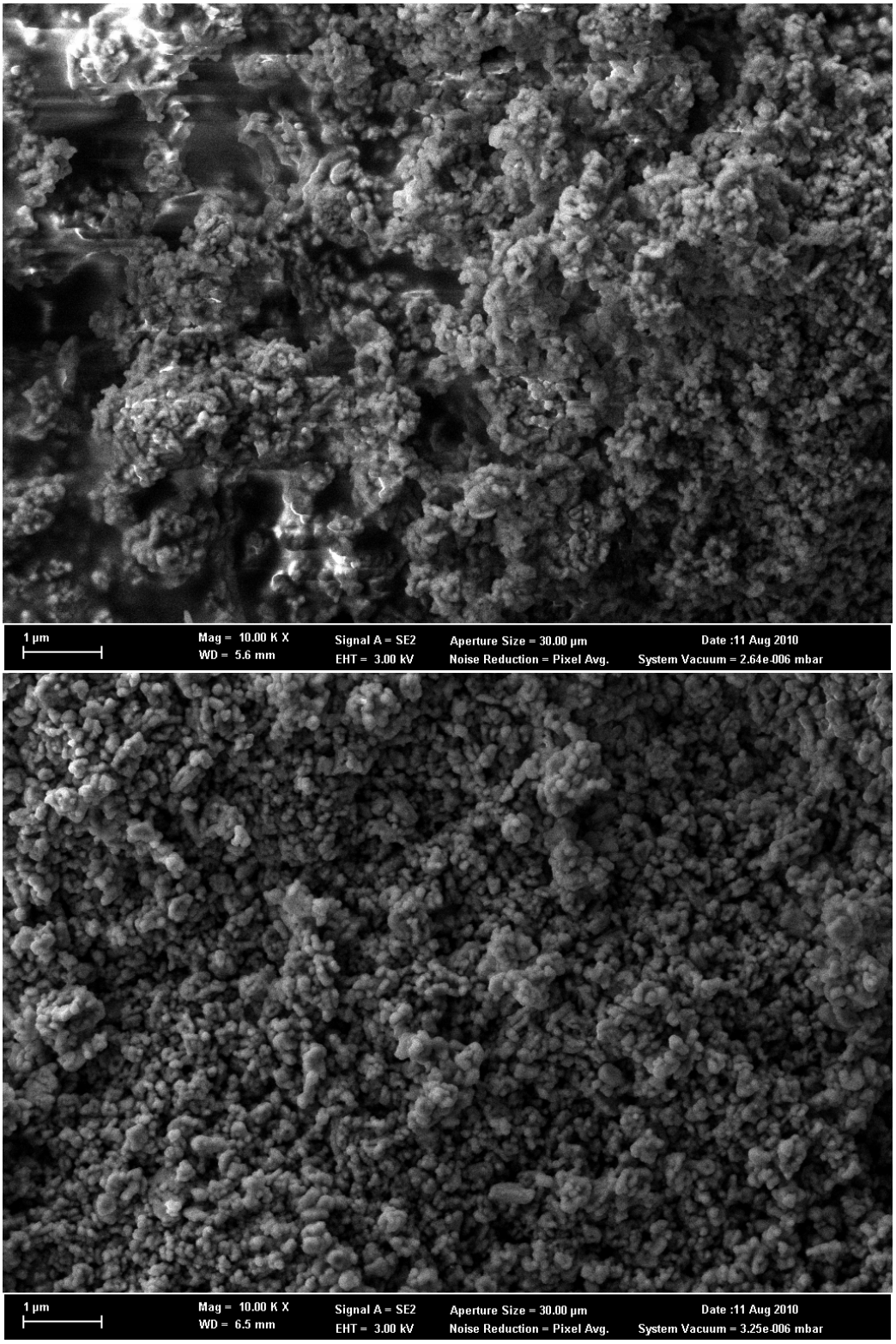


Figure 4.16: SEM imgages for Li+MgO, before reaction (left) and after 24 hours time on stream (right).

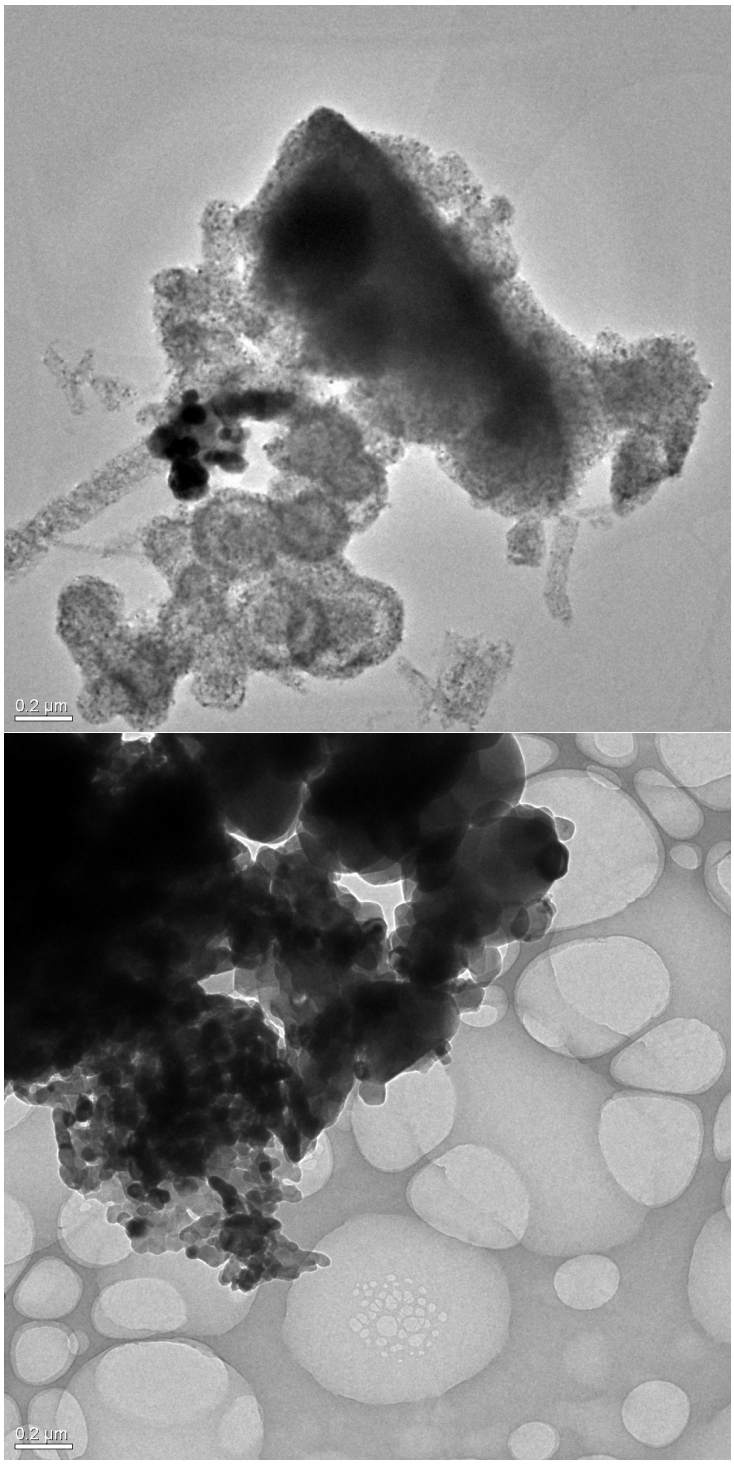


Figure 4.17: TEM imgages for Li@MgO, before reaction (above) and after 24 hours time on stream (below).

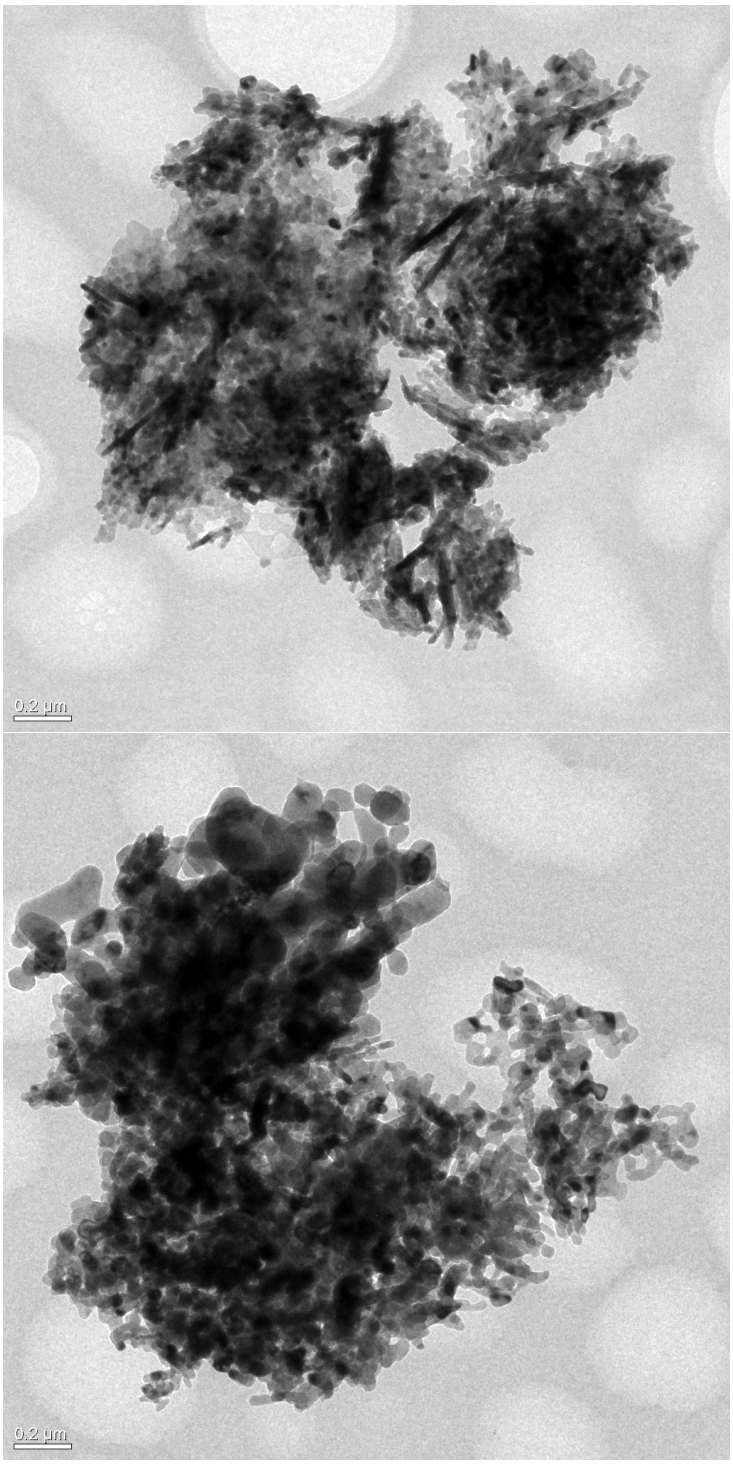


Figure 4.18: TEM imgages for Li/MgO, before reaction (above) and after 24 hours time on stream (below).

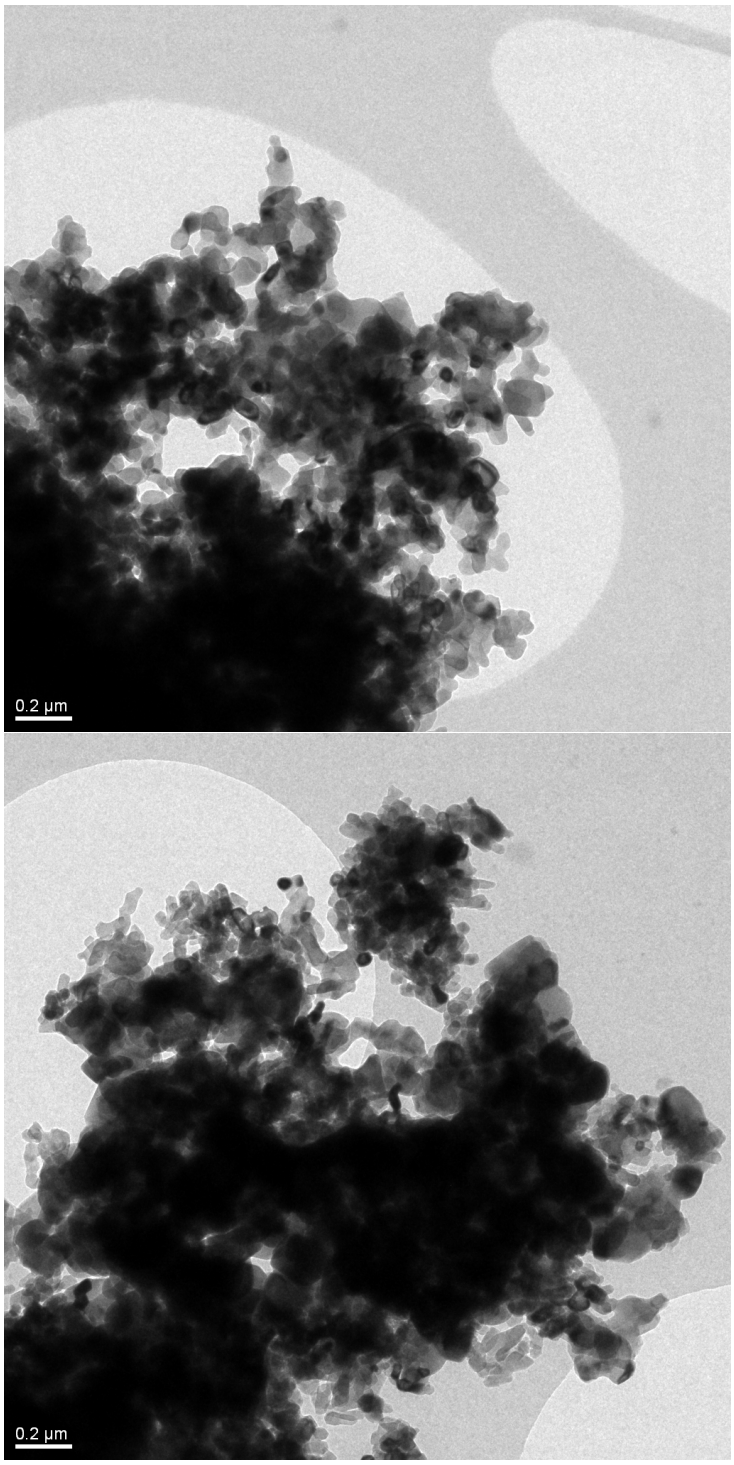


Figure 4.19: TEM imgages for Li-MgO, before reaction (above) and after 24 hours time on stream (below).

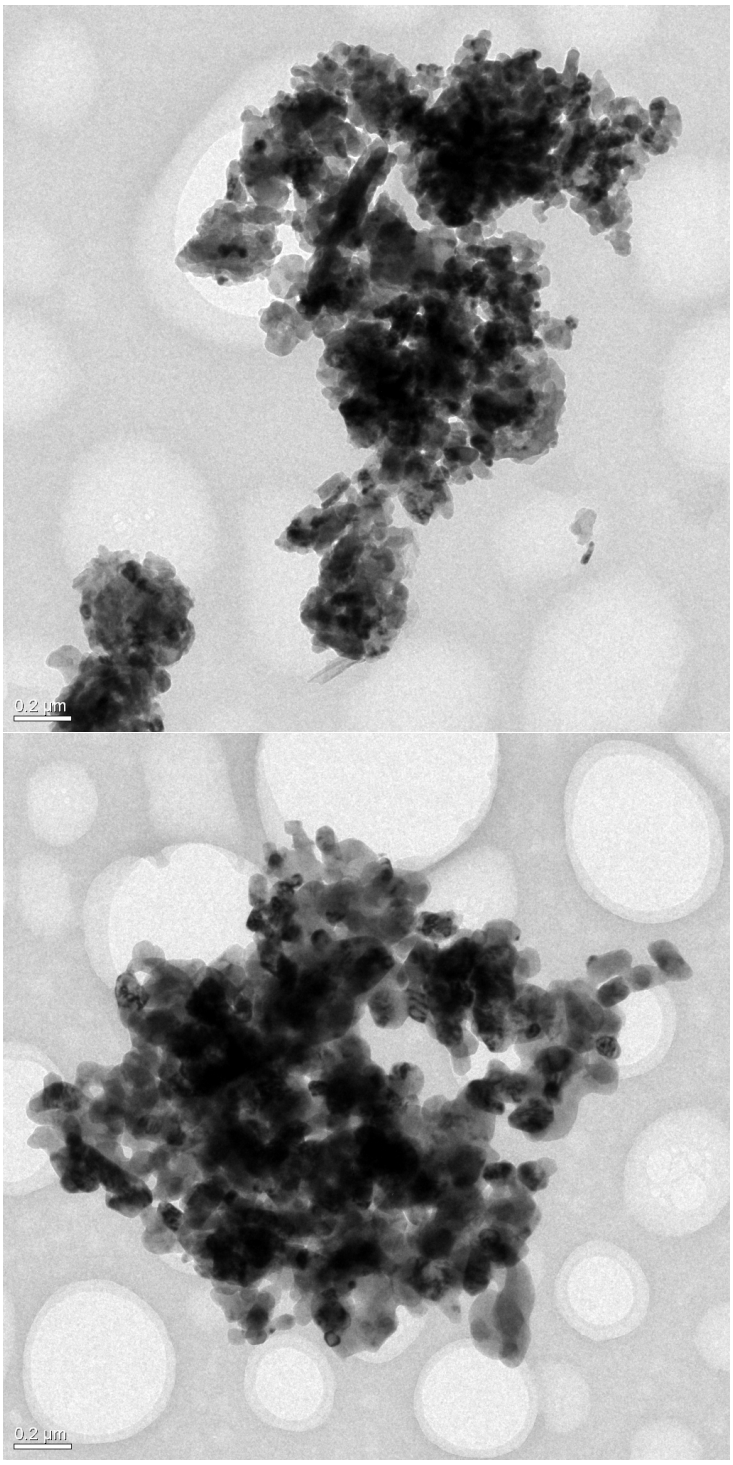


Figure 4.20: TEM imgages for Li+MgO, before reaction (above) and after 24 hours time on stream (below).

### 4.3.4 Main Deactivation Parameters

These parameters were also determined for the 0.5 wt% Li-doped MgO prepared via the four described preparation procedures. For all four Li-doped MgO samples the same trends were observed, however, Li+MgO exhibited the most distinct behavior. Therefore, it has been chosen to show the influence of the different deactivation parameters: temperature and flow rate.

A direct comparison of the deactivation at different flow rates and temperatures is not possible. Therefore, the relative $CH_4$ conversion is used. The first recorded data point is used for normalization, so that the relative decay can be compared for different reaction conditions.

#### 4.3.4.1 Flow Rate

Figure 4.21 shows the absolute and the relative $CH_4$ conversion (first data point equals to 100 %) and the $C_2$ selectivity for different flow rates as a function of time on stream for the catalyst Li+MgO, recorded at 750 $^\circ C$. The strong deactivation correlates with the flow rate, it is distinct that with increasing flow rates the deactivation rate increases. At a flow rate of 30 ml/min, the catalyst loses only 20 % activity within 18 hours time on stream. The $C_2$ selectivity also decreases with time on stream, but it remains approximately the same for 60, 120 and 180 ml/min. For the flow rate of 30 ml/min, a much lower $C_2$ selectivity is observed, which seems to increase towards the end of the experiment. The deactivation is accelerated at higher flow rates. This is remarkable, as usually the opposite is the case. An explanation has to be searched in the interaction of different process parameters.

The Li content was determined after the reaction, the results are shown in Table 4.8. The residual Li-loading after the experiment is independent of the applied flow-rate. In fact, the result is similar to the residual loadings of Li, obtained in paragraph 4.3.3.1.

Table 4.8: Li content in wt% after the end of the reaction, conducted with different flow rates at 750 $^\circ C$.

| 30 ml/min | 60 ml/min | 120 ml/min | 180 ml/min |
|---|---|---|---|
| 0.02 wt% | 0.03 wt% | 0.03 wt% | 0.03 wt% |

#### 4.3.4.2 Temperature

In Figure 4.22, the $CH_4$ conversion, the relative $CH_4$ conversion and the $C_2$ selectivity are shown. It has been reported in detail, that the $CH_4$ conversion and the $C_2$ selectivity increase with increasing reaction temperature. This was also the case

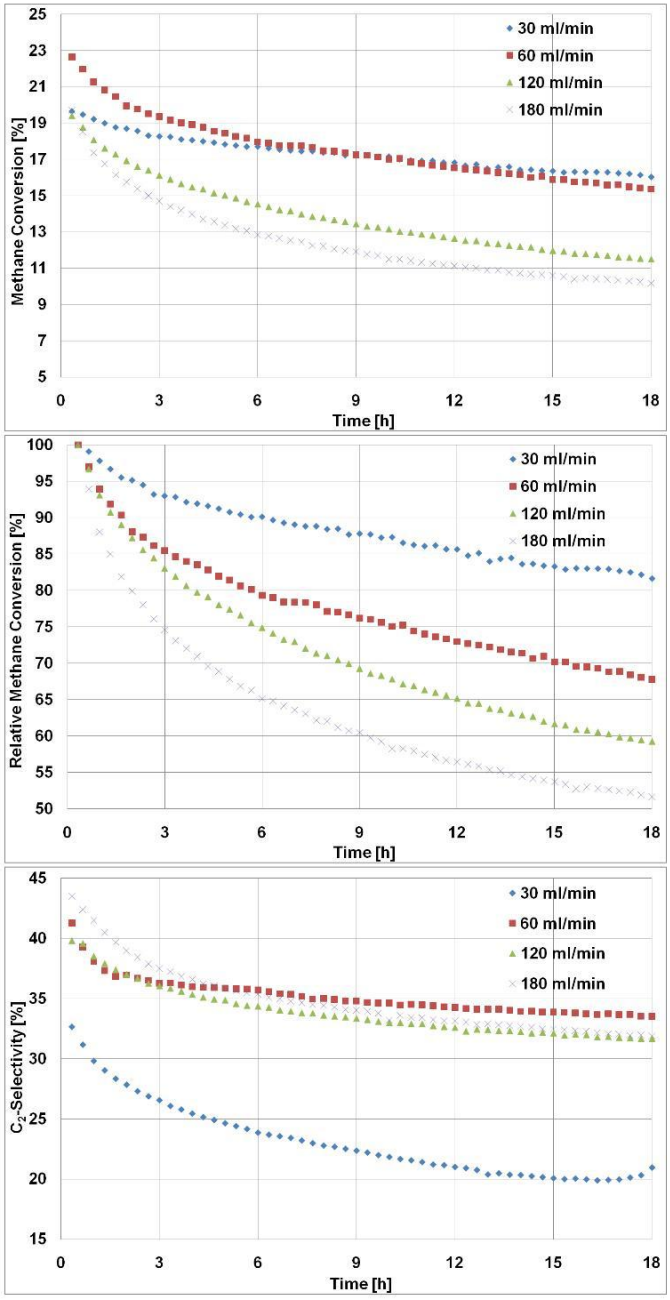


Figure 4.21: The absolute $CH_4$ conversion (above), the relative $CH_4$ conversion (middle) and the $C_2$ selectivity (below) of Li+MgO as function of the flow rate and time on stream, recorded at 750 $°C$. The deactivation increases with increasing flow rates, the differences are distinct. The $C_2$ selectivity increases with time on stream and the $C_2$ selectivity for the flow rate of 30 ml/min is much lower than for the other flow rates.

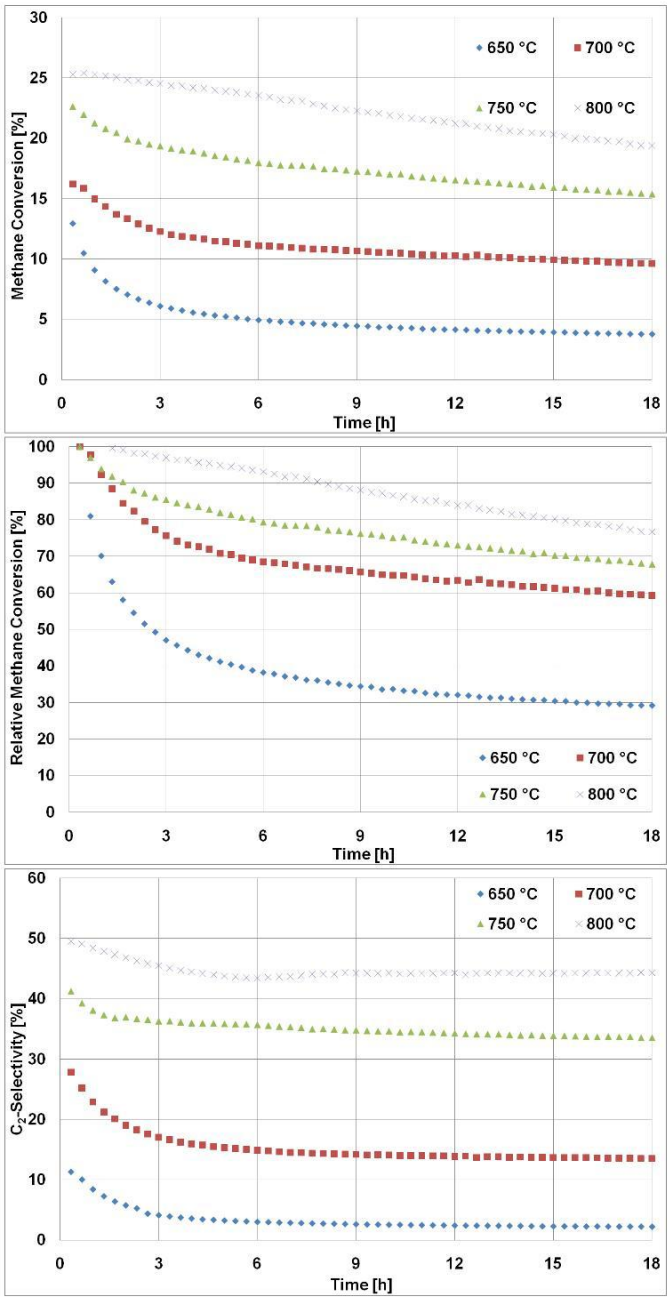


Figure 4.22: The absolute $CH_4$ conversion (above), the relative $CH_4$ conversion (middle) and the $C_2$ selectivity (below) of Li+MgO at 60 ml/min as function of the reactor temperature and time on stream. The $CH_4$ conversion and the $C_2$ selectivity increase with increasing temperature, which is according to the literature. The deactivation decreases at increasing temperature, the differences are distinct. The highest temperature exhibited the lowest deactivation and vice versa.

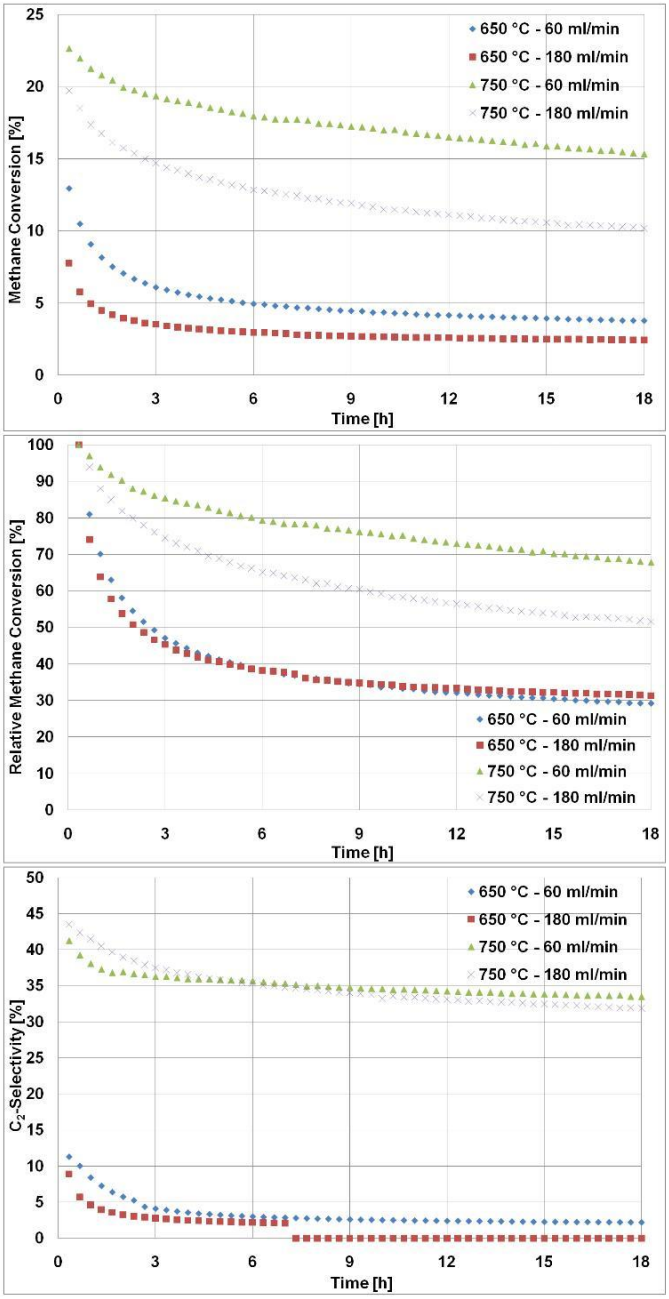


Figure 4.23: The absolute $CH_4$ conversion (above), the relative $CH_4$ conversion (middle) and the $C_2$ selectivity (below) of Li+MgO as function of the reator temperature, the flow rate and time on stream. The decrease in $CH_4$ conversion was independent of the flow rate at 650 $°C$. However, at 750 $°C$, the reduction depended on the flow rate.

for Li+MgO. However, the relative $CH_4$ conversion shows that the reduction of $CH_4$ conversion was more severe at lower temperatures. At 650 $°C$, the catalysts showed only 30 % of its inital $CH_4$ conversion, meaning a loss of 70 %. At higher temperatures the activity loss was reduced, for 800 $°C$ the loss accounted only to 20 %.

Like in paragraph 4.3.4.1, the Li content was determined at the end of the experiment. The results are shown in Table 4.9. At 650 °, a higher residual Li content was found. Above this temperature, the amount of Li was found to be 0.03 wt%, irrespective of the applied reaction temperature.

Table 4.9: Li content after the end of the reaction, conducted at different reaction temperatures and a flow rate of 60 ml/min.

| 650 $°C$ | 700 $°C$ | 750 $°C$ | 800 $°C$ |
|---|---|---|---|
| 0.07 wt% | 0.03 wt% | 0.03 wt% | 0.03 wt% |

#### 4.3.4.3 Temperature and Flow Rate

Due to the unexpected behavior, experiments were conducted with different flow rates at different temperatures. Like in the paragraphs 4.3.4.1 and 4.3.4.2, all tested materials show the same behavior. The results of 0.5 wt% Li+MgO are presented, since this material showed the most distinct trends. In Figure 4.23, the $CH_4$ conversion, the relative $CH_4$ conversion and the $C_2$ selectivity are shown. The $CH_4$ conversion depended on the flow rate, but the $C_2$ selectivity did not show changes at different flow rates.

After 18 hours time on stream, at 650 $°C$ the relative $CH_4$ conversion showed the same decrease at 60 ml/min and at 180 ml/min. For 750 $°C$, this was not the case. Here, a reduction of $CH_4$ conversion of 30 % for 60 ml/min was observed and of 50 % for 180 ml/min. The degree of reduction depended on the flow rate, but only at high temperatures.

The Li content after the experiment was determined and the results are shown in Table 4.10. At 650 $°C$, the residual loading of Li was determined to be 0.07 wt% at a flow rate of 60 ml/min and 0.08 wt% at a flow rate of 180 ml/min. However, for 750 $°C$, the same Li content was found, irrespective of the flow rate.

## 4.4 Discussion

The stability of the catalytic performance for different Li-doped MgO catalysts has been tested for 40 hours time on stream. Until now, these kind of life time

Table 4.10: Li content after the end of the reaction, conducted with two different reaction temperatures and flow rates.

| | 650 °C | 750 °C |
|---|---|---|
| 60 ml/min | 0.07 wt% | 0.03 wt% |
| 180 ml/min | 0.08 wt% | 0.03 wt% |

tests are not reported in the literature of Li-doped MgO. None of the prepared Li-doped MgO or pure MgO catalysts was found to be stable. The catalysts did not reach a stable range within 40 hours time on stream. Furthermore, the impression of stability at long times on stream are only due to the scaling of the axis. As shown in Figure 4.5, the residual activity does not scatter strongly anymore after 40 hours time on stream. For even longer times on stream, it can be expected that the scattering is further reduced, approaching a common activity. Therefore, it can be concluded that the preparation procedure has an influence on the initial activity, but not on the activity in a steady state, being reached after several hours time on stream.

Li@MgO and Li/MgO exhibit the trend that with increasing loading of Li, the residual conversion is reduced but the residual selectivity is increased. However, on a consecutive reaction pathway, the selectivity decreases with increasing conversion following a single trajectory. Figure 4.24 shows a conversion selectivity diagram for the residual values of Li@MgO and Li/MgO. It is obvious that the points for each catalyst lie on a separate trajectory, indicating different catalytic behavior within the OCM reaction network.

It has to be criticized that in many publications concerning Li-doped MgO, the stability is not reported or considered and only catalytic results which are obtained within a few hours time on stream are reported. But this kind of catalytic data can only be a snapshot on the deactivation trajectory of the Li-doped MgO catalysts.

All catalysts lose the majority of their initial Li content within the first hour time on stream, as shown in Figure 4.8. For higher Li-loadings, the decrease in Li content might be retarded. The Li content of 0.01 wt% to 0.03 wt% at 24 hours time on stream, is independent of the preparation procedure. Furthermore, this value is accordance with the estimation of Anderson and Norby for the maximum solubility of Li in MgO [90].

A significant loss of BET surface and an increase in grain size and crystallinity are also observed. The changes of these parameters seem to depend strongly on the applied preparation method. However, it can not be excluded that impurities play a significant role for the change of surface area and grain size.

In order to find a correlation between deactivation and physical properties a comparison of the relative changes of $CH_4$ conversion, $C_2$ yield, Li content, BET surface area and grain size (with inverse values for better comparability) for the

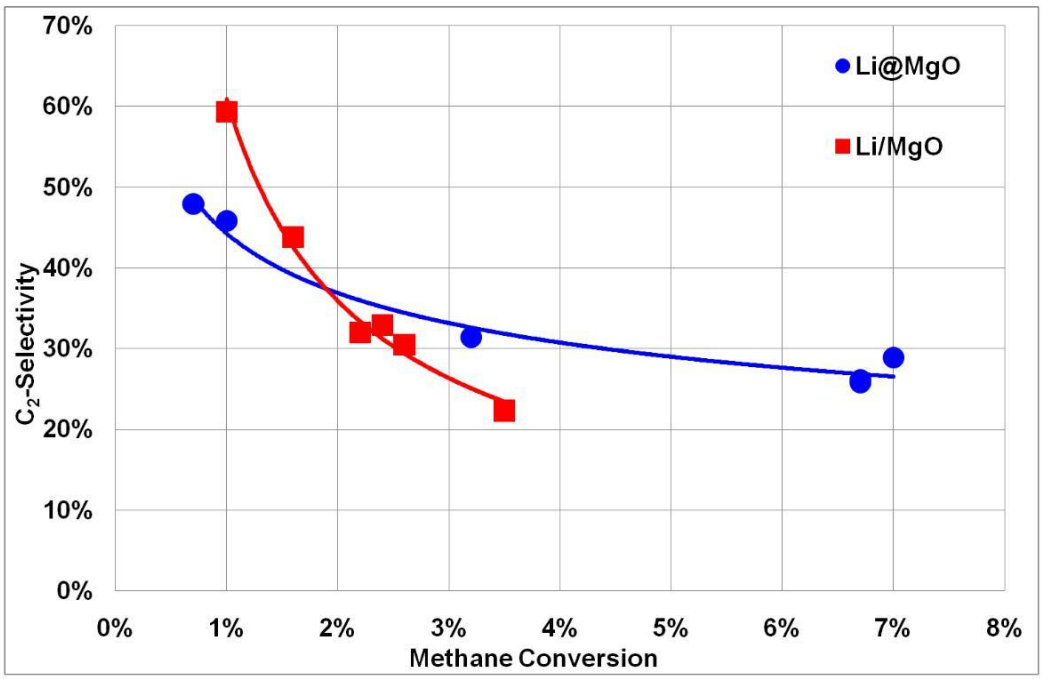


Figure 4.24: Conversion selectivity diagram for the Li@MgO and Li/MgO. For each material the data points lie on one single trajectory.

four different Li-doped MgO samples is done in Figure 4.25 and Figure 4.26. The loss of BET surface area, increase in grain size and loss of Li content correlate, this is well in agreement with the results of Mirodatos *et al.* [119, 122]. It becomes evident that the decline of $CH_4$ conversion and $C_2$ yield does not correlate with any of the other determined features. This fact gains further support, when the deactivation as a function of flow rate and temperature is considered. A high flow rate and a low temperature resulted in a high deactivation rate, while under a low flow rate and high temperatures the $CH_4$ conversion does not decline so strongly. Moreover, the reduction of the $CH_4$ conversion is the same at $650\,^{\circ}C$, irrespective of the flow rate, but not at $750\,^{\circ}C$. This observation indicates two different sintering phenomena, which is consistent with the results of Mirodatos and co-workers [119]. The Li content differed only with different temperatures, not with a different flow rate. Therefore, it can be concluded, that the influence of the Li content on the catalyst activity is much lower than previously thought.

The apparent activation energy was calculated for 0.3 and 24 hours time on stream. This was not possible for Li/MgO due to the fast deactivation. The calculated apparent activation energies are reported in Table 4.11 and the Arrhenius plot for Li+MgO is presented in Figure 4.27. There is a strong increase in the apparent activation energy with time on stream. The determined values for the apparent

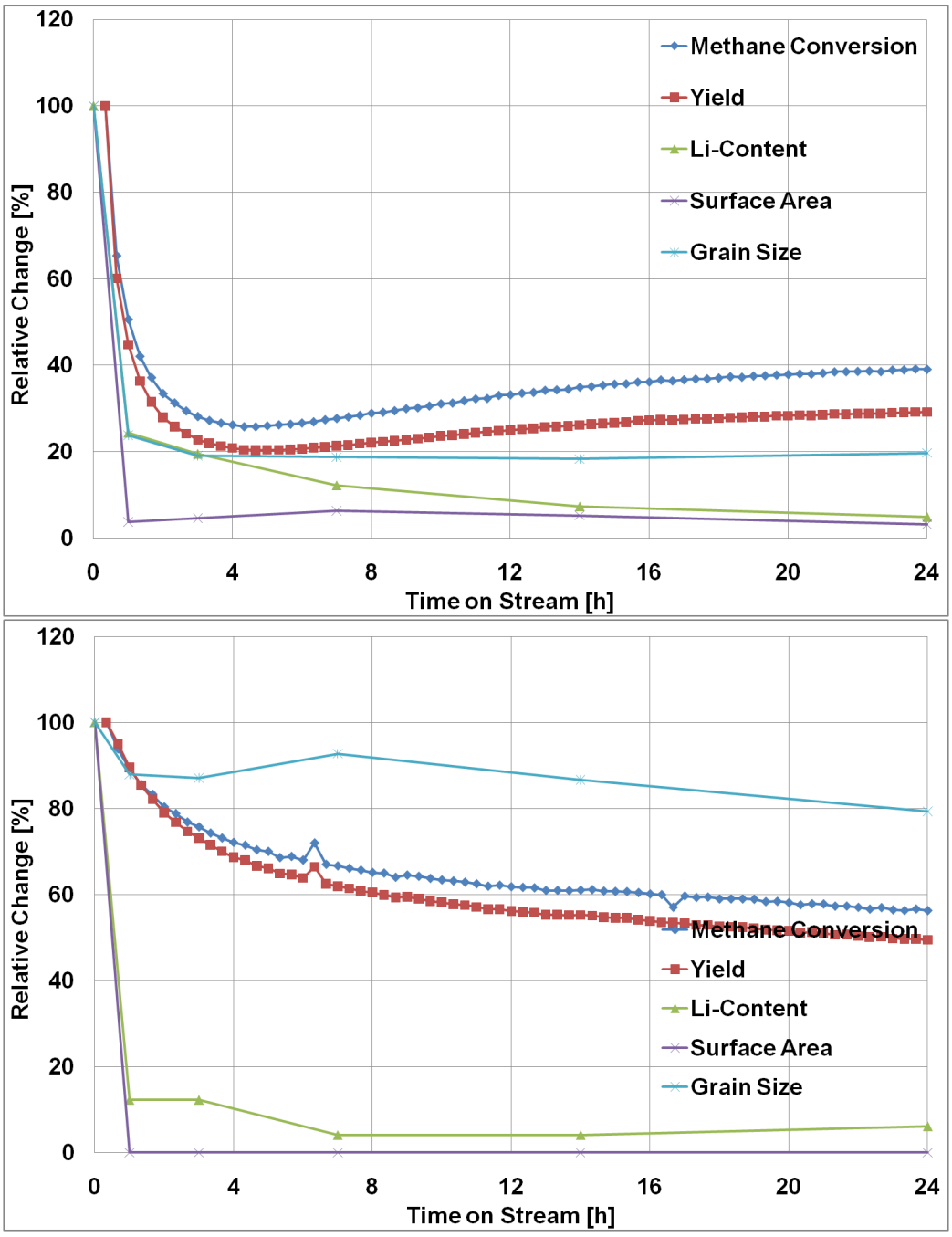


Figure 4.25: Relative changes of $CH_4$ conversion, $C_2$ yield, Li content, BET surface area and grain size for Li@MgO (above) and Li/MgO (below). The values for the gain size are inverse to improve the comparability.

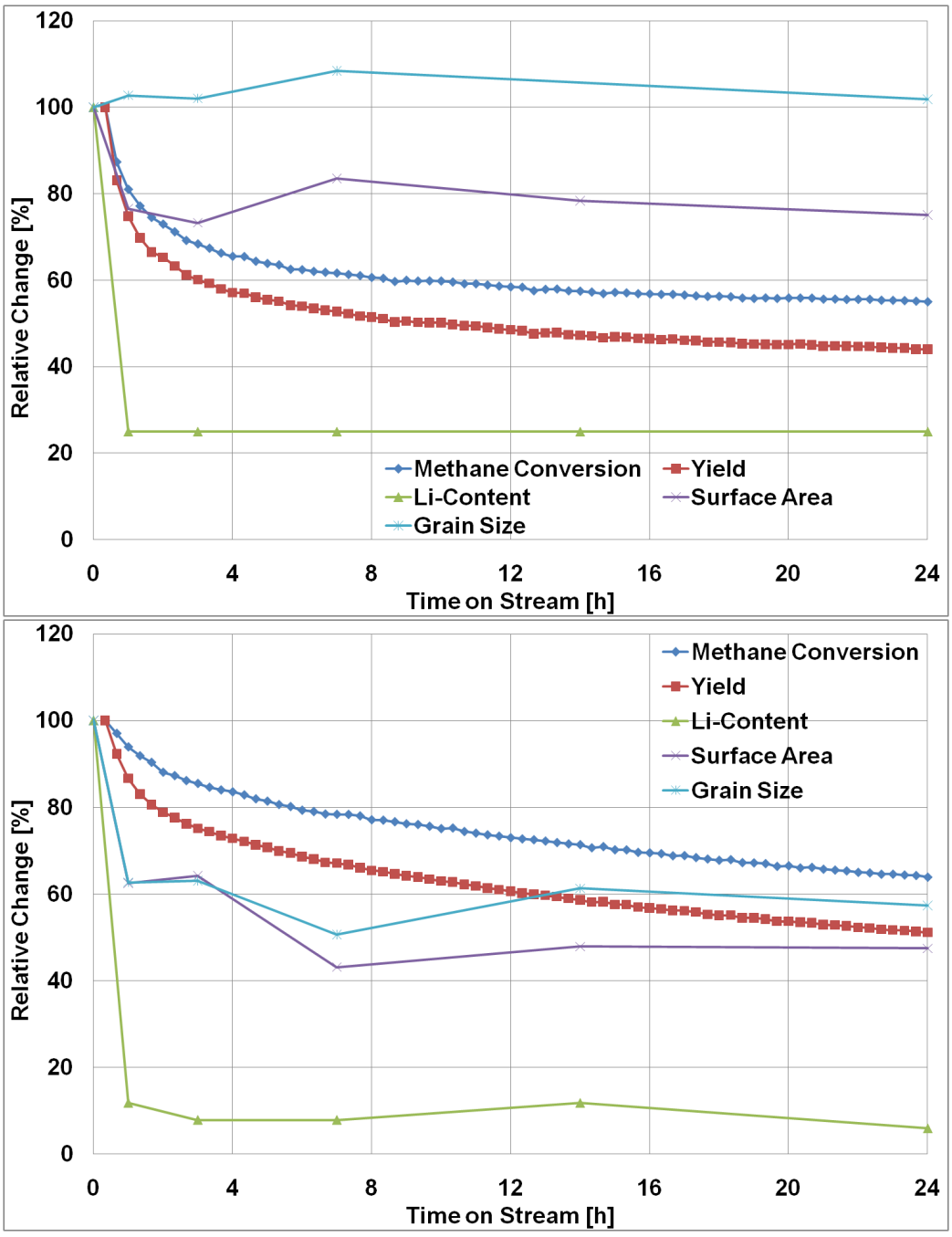


Figure 4.26: Relative changes of $CH_4$ conversion, $C_2$ yield, Li content, BET surface area and grain size for Li-MgO (above) and Li/+MgO (below). The values for the gain size are inverse to improve the comparability.

activation energy after 24 hours time on stream are within the range of experimentally determined values of 90 kJ/mol [88] and 235 kJ/mol [190], reported by other research groups, while at 0.3 hours time on stream, they are considerably lower. This observation indicates a substantial change in the catalytic performance of the material, rather than only a depletion of active sites.

Table 4.11: Apparent activation energies for Li@MgO, Li-MgO and Li+MgO in kJ/mol.

| Catalyst | 0.3 h | 24 h |
|---|---|---|
| Li@MgO | 40 | 160 |
| Li-MgO | 68 | 89 |
| Li+MgO | 47 | 98 |

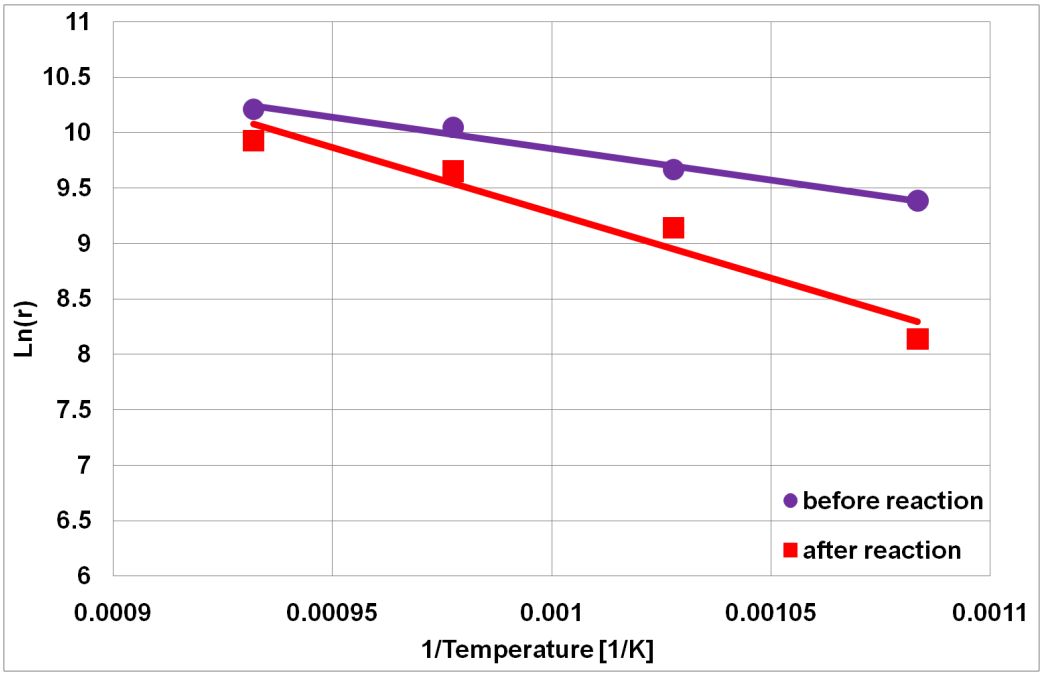


Figure 4.27: Arrhenius plots for Li+MgO for the determination of the apparent activation enery.

The impurities that were determined seem to be stable under reaction conditions, their concentration did not change significantly. Li+MgO has the highest is the catalyst with the highest initial and residual activity and it shows a relatively slow deactivation, however, it also has the highest concentration of impurities. The determined list of impurities is not complete, there could be even other impurities of considerable amounts in the Li-doped MgO catalysts.

We would also like to comment on the debate on the active center of Li-doped MgO. Lunsford *et al.* suggested [$Li^+O^-$] to be the active center [21]. This proposal is based on the following experiments: EPR spectra of the prepared Li/MgO were recorded, but they were not measured *in situ*, giving rise to signal at g = 2.054. The relative intensity of this signal was reported to increase with Li-loading of the catalyst. Moreover, the formation of methyl radicals was reported to increase with an increasing Li-loading. These two trajectories exhibited a very good correlation. The group of Abraham and Schirmer also found that signal with EPR and electron spin resonance (ESR) when studying Li-doped MgO single crystals [99, 100]. However, because this signal is not univocal, Abraham *et al.* and Rius *et al.* measured ENDOR spectra (electron nuclear double resonance spectroscopy), proving the existence of [$Li^+O^-$] [101, 103, 102]. In the works of Lunsford, this prove is missing. Furthermore, the problem of stability, based on loss of Li and the effect of impurities are not considered. A recent study by Myrach *et al.* could not detect [$Li^+O^-$], though the capability of their equipiment was demonstrated with Li-doped MgO single crystals [118]. Moreover, the finding of methyl radicals at the outlet of the reactor, could also be an effect of gas phase reactions; as described by Yates and Zlotin, who found a significant conversion and a medium $C_2$ selectivity in blank reactor studies [150].

To question the contribution of either Li, transition metals or further candidates for the active site 1 wt% Li/MgO was subjected to a pretreatment with $H_2S$, a well-known poison for transition metals. Thre pretreatment consisted in submitting the catalyst for 2 hours in 100 % $H_2S$ flow at 450 °*C*. The Li content was determined to be the same before and after the pretreatment. The 150 mg catalysts were tested for 15 hours time on stream at 700 °*C*. The other experimental conditions are as described in Paragraph 4.2.2. The result is shown in Figure 4.28. It is outstanding that with $H_2S$ pretreatment, the catalyst does not show any OCM activity anymore. Moreover, the activity could not be retained via calcination of the pretreated catalysts at 700 °*C* in air. The poisoning effect of $H_2S$ on the activity of Li/MgO is a strong indication that not the Li is the essential component of the active site, because it does not form stable sulfur components.

## 4.5 Summary and Conclusion

It has been shown that the Li-doped MgO is unstable, irrespective of the preparation procedure. The different catalysts are unstable over the tested time period of 40 hours, without the prospect of a range with stable activity. The most drastic changes occur during the first hour time on stream and the measured Li content reaches the proposed limit of Li solubility in MgO after approximately 14 hours time on stream.

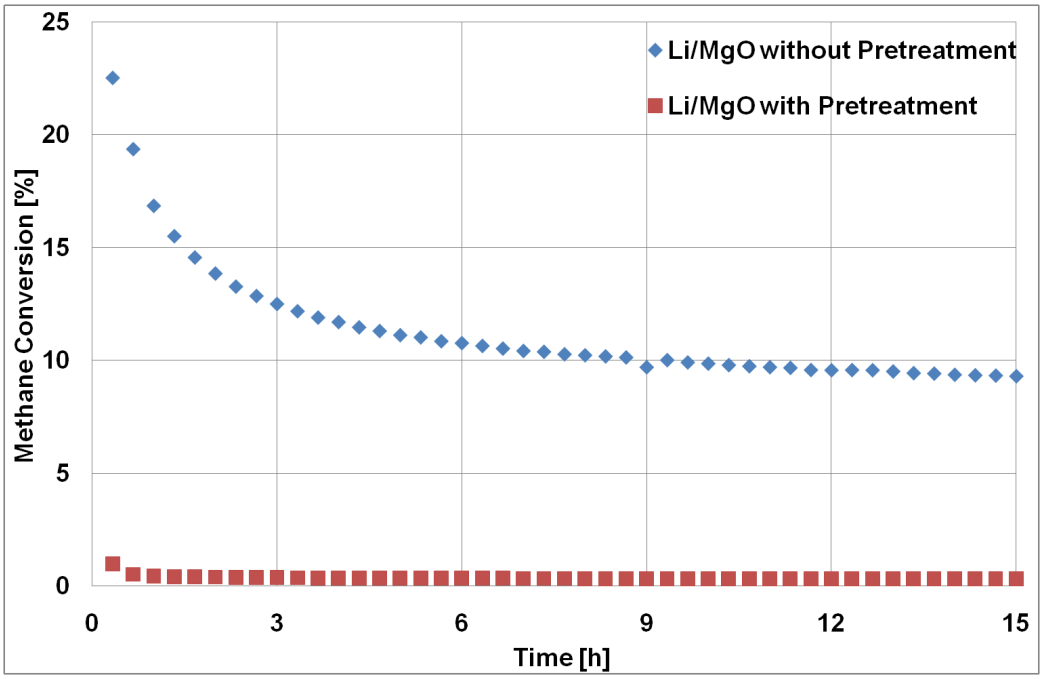


Figure 4.28: Poisoning effect of $H_2S$ on 1 wt% Li/MgO. After pretreatment (for 2 hours in 100 % $H_2S$ flow at 450 $^{\circ}C$), the 1 wt% Li/MgO catalyst does not show any activity anymore.

Since no correlation between the catalytic activity and the Li-loading, specific surface area and grain size was found, it was concluded that these are not the main deactivation factors. The deactivation is most probably due to a very complicated process, influenced by several different factors. However, at lower temperatures ($650\,^{\circ}C$) and at elevated temperatures ($750\,^{\circ}C$), different deactivation mechanism are predominant.

Due to the strong deactivation and the loss of Li and its effect on reactor materials, we do not see Li-doped MgO as a potential candidate for an industrial application of the oxidative coupling of methane.

Depending on our own results and the results published in the literature, it is concluded that there is no proof for $[Li^{+}O^{-}]$ being the active center. This is further supported by the poisoning effect $H_2S$ has on Li/MgO. Since Li does not form stable sulfides, it is most probably not part of the active center.

# Chapter 5

# The Catalytic Activity of Zinc Oxides from Single Source Precursors with Additives for the C-H Acitivation of lower Alkanes

This work has been published as: S. Arndt, Y. Aksu, M. Driess and R. Schomäcker, "The Catalytic Activity of Zinc Oxides from Single Source Precursors with Additives for the C-H Activation of Lower Alkanes" in Catalysis Letters, 131 (**2009**) 258-265. Reprinted with permission from Springer via the Copyright Clearance Center.

## 5.1 Introduction

The C-H activation in saturated alkanes is the crucial step for their functionalisation and combustion [275, 276]. Among the light alkanes methane is the most stable compound and therefore the most difficult molecule to activate. The activation of ethane and propane is less demanding and therefore lower reaction temperatures are necessary. The conversion of methane into value added products is of high interest for the chemical industry, as methane is the major constituent of natural gas, whose reserves are expected to be much higher than those of crude oil [7]. Ethane and propane are also available in large amounts from natural gas and other sources. Currently these gases are mostly used for the production of energy and heat. Their usage as a carbon source for the chemical industry is limited, as no process has yet been fully developed. In principle there are two ways of converting them, especially methane, into value added products [2]. In the indirect way, they are converted into synthesis gas and then being processed via

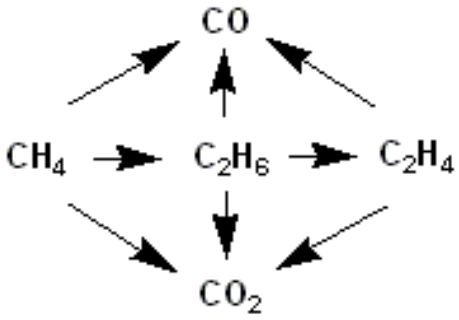


Figure 5.1: The reaction network of the oxidative coupling of methane.

Fischer Tropsch (FT). This process is well known, but very energy consumptive. An alternative route is the direct way, therein the synthesis gas step is evaded and the gases are directly converted into the desired products, like the oxidative coupling of methane (OCM), in which methane is coupled to ethane and/or ethene (see Figure 5.1 for the reaction network). Since the first publications by Keller *et al.* [3] and Hinsen *et al.* [4], a lot of research was done, which recently has been reviewed [7, 2]. As methane is so difficult to activate, the OCM reaction is performed at high temperatures, where many catalysts suffer from severe stability and selectivity problems.

The reactions for the conversion of methane, ethane and propane to the corresponding olefins are:

1. the oxidative coupling of methane (OCM)
   $2\ CH_4 + \frac{1}{2}$ or $1\ O_2 \rightarrow C_2H_6$ or $_4 + 1$ or $2\ H_2O$
2. the oxidative dehydrogenation of ethane (ODE)
   $C_2H_6 + \frac{1}{2}\ O_2 \rightarrow C_2H_4 + H_2O$
3. the oxidative dehydrogenation of propane (ODP).
   $C_3H_8 + \frac{1}{2}\ O_2 \rightarrow C_3H_6 + H_2O$

The structures of methane, ethane and propane are similar. The oxidative dehydrogenation of alkanes has only recently been reviewed [277]. Due to the structural similarity, one catalyst should be able to catalyze the C-H activation of all three molecules. However, the energy required for the activation of a C-H bond is different for each reaction, consequently the ODP, ODE and OCM reactions run at very different temperatures. Therefore catalytic testing over a broad temperature range is necessary.

Pure and Li doped zinc oxides are compounds which could be suitable catalysts for the C-H activation of alkanes, but in the literature not much is described

about this. In the first publication on this topic, Matsuura *et al.* investigated the activity of alkali doped zinc oxides for the OCM reaction and found that ZnO doped with Li is the most active catalyst [14]. Zhang *et al.* reported that the mechanism of the OCM reaction on Li doped zinc oxide is similar to the one proposed for Li doped MgO [15]. In 1990, Giusti *et al.* published results showing that $Li_2CO_3$ segregates to the surface of the ZnO and reduces the oxide active surface that is available for the gas phase reaction [278]. Wang and co-workers later investigated the effect of $Cl^-$ in Li doped ZnO in the OCM and ODE reaction [279]. The oxidative dehydrogenation of ethane has so far not been reported in the literature. The ODP was reported for supported zinc oxide [280].

Recently the synthesis of pure and doped zinc oxides via single source precursors has been developed and published [281, 273]. This method allows the synthesis of solid compounds with reproducible characteristics controlled on a molecular level, for instance it allows a real Li doping of ZnO. A series of pure and lithium doped zinc oxides, with different Li content were tested for the oxidative coupling and the combustion of methane and the oxidative dehydrogenation of ethane and propane. In this publication we report the results and discuss the prospects of pure and lithium-doped zinc oxide as a catalyst for the activation of C-H bonds in lower alkanes.

## 5.2 Experimental Part

### 5.2.1 Catalyst Preparation

The zinc oxides from different precursors are denominated as follows:

1. Li@ZnO - from single source precursors
2. Li+ZnO - from mixed milling

The pure ZnO was prepared from single source precursors via the thermal decomposition of zinc cubanes. Lithium doped zinc oxide was synthesized via the thermal decomposition of mono-lithium zinc cubanes with the molecular formula of $[Li(tetrahydrofurane)(MeZn)_3(OR)_4]$ prepared in a one-pot procedure by the reaction of $Me_2Zn$, lithiumalkoxide and water. Figure 5.2 shows the reaction in principle, a detailed description of the synthesis and characterization is found in the literature [281, 273]. The prepared zinc oxides had lithium contents of 0, 1, 3 and 7 wt%, respectively.

Li+ZnO with lithium contents of 1, 3 and 7 wt% were prepared via mixed milling for 1 hour of commerical zinc oxide (Fluka) and lithium hydroxide (FERAK Berlin), with subsequent calcination for 6 hours at 350 $^\circ C$.

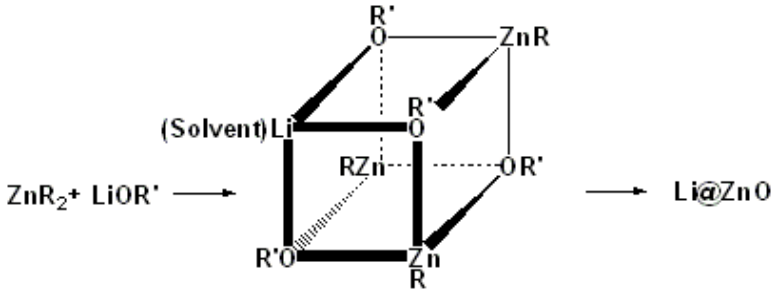


Figure 5.2: The synthesis of Li doped ZnO via single source precursors. The preparation of pure ZnO follows the same procedure.

The lithium contents were determined by atomic absorption spectroscopy (AAS). The results of the analytic are shown in Table 5.1.

| Catalyst | Li Content |
|---|---|
| 1 wt% Li@ZnO | 1.0 wt% |
| 3 wt% Li@ZnO | 3.0 wt% |
| 7 wt% Li@ZnO | 7.0 wt% |
| 1 wt% Li+ZnO | 1.5 wt% |
| 3 wt% Li+ZnO | 2.1 wt% |
| 7 wt% Li+ZnO | 7.2 wt% |

Table 5.1: Lithium contents of the different doped zinc oxides.

The specific surface area was determined by a Micromeritics Gemini III 2375 Surface Area Analyzer, using nitrogen adsorption at -196 $^{\circ}C$. Before measuring, the samples were degassed at 120 $^{\circ}C$ and 0.15 mbar at least for 30 minutes. The surface areas were calculated by the method of Brunauer, Emmett and Teller (BET).

### 5.2.2 Catalytic Tests

The catalytic experiments were carried out in a quartz glass packed bed tubular reactor. In each experiment 150 mg catalyst were diluted with approximately 1.9 g quartz sand to ensure a proper heat transfer and plug flow behavior of the reactants. The particle size was between 200 to 300 $\mu$m.

Synthetic air was used as an oxygen source (20.5 % $O_2$ in $N_2$). Therefore, the feed gas consisted of synthetic air and gaseous alkane ($CH_4$, $C_2H_6$ or $C_3H_8$). The exact composition of the feed gas is shown in Table 5.2. Before entering the reactor the mixture passed a static mixer and was preheated to 180 $^{\circ}C$. The reac-

tor was heated by a fluidized sand bed or an electric furnace. Nearly isothermal reaction conditions were ensured.

The reaction conditions are shown in Table 5.2 in detail. The temperature was varied in 50 K steps. After a temperature change a sufficient waiting time for re-establishing steady state conditions was ensured.

| Reaction | Alkane : $O_2$ : $N_2$ | Temperature | Gas Flow |
|---|---|---|---|
| OCM | 4 : 1 : 4 | 550 - 700 $°C$ | 60 - 180 ml/min |
| ODE | 2 : 1 : 4 | 500 - 650 $°C$ | 30 - 180 ml/min |
| ODP | 2 : 1 : 4 | 450 - 650 $°C$ | 30 - 180 ml/min |
| Total oxidation | 1 : 16 : 83 | 250 - 750 $°C$ | 100 ml/min |

Table 5.2: The reaction conditions for the different catalytic test reactions.

A gas chromatograph (GC Satochrom 5873), equipped with a flame ionization detector, a thermal conductivity detector, a fused Poraplot Q and a Molsieve 5 column was used to analyses the reaction products. The analyzed reaction products were CO, $CO_2$, $H_2O$, alkanes and alkenes.

Nitrogen was used as an internal standard. The reproducibility of conversion and selectivity measurement is sufficient.

Conversion X (see Equation 5.1) and selectivity S (see Equation 5.2) were calculated based on the inlet and outlet concentration of the alkanes.

$$X = \frac{c_{Reactant,0} - c_{unconverted\ Reactant}}{c_{Reactant,0}} \tag{5.1}$$

$$S = \frac{c_{Product}}{c_{converted\ Reactant}} \tag{5.2}$$

For the oxidative coupling of methane, the selectivities of the main products ethane and ethene are discussed as a sum, the $C_2$-selectivity. Higher products, if formed, appeared in a negligible amount and are therefore not being discussed.

The $CO_x$ selectivity and the selectivity towards the desired product (propane for ODP, ethene for ODE or $C_2$ for OCM) always sum up near to 100 %, therefore in the results only the selectivity towards the desired product is shown.

In order to determine the degree of thermal dehydrogenation, blanc experiments with pure quartz sand were conducted under reaction conditions. For methane and propane no conversion was observed. For ethane the thermal dehydrogenation was 0.3 % ethane conversion at 74 % ethene selectivity.

## 5.3 Results

### 5.3.1 Oxidative Coupling of Methane

At 650 °*C* the pure zinc oxides are active catalysts, while the lithium doped zinc oxides do not show any activity, while pure and doped zinc oxides are active at 700 °*C*. Figure 5.3 shows the results of the experiments of the oxidative coupling of methane at 700 °*C*, 150 mg catalyst and a gas flow of 60 ml/min. The undoped and non calcinated zinc oxide with defects lead to full conversion of oxygen, but its conversion of methane and the $C_{2+}$-selectivity of about 20 % is poor. The activity and selectivity of the commercial ZnO is similar.

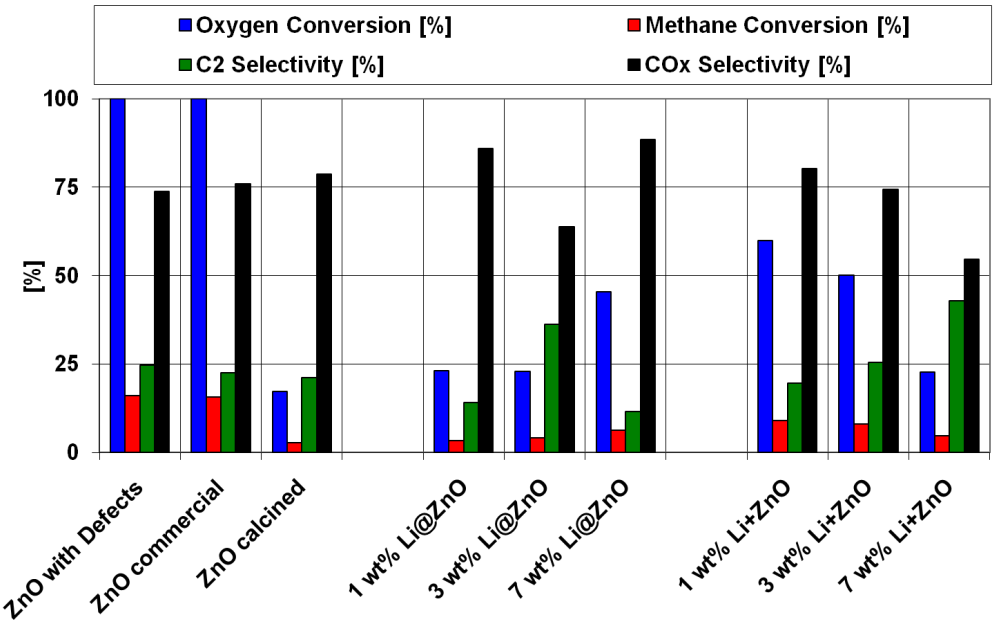


Figure 5.3: Results of the OCM experiments at 700 °*C*, 150 mg catalyst and a gas flow of 60 ml/min. For feed composition see Table 5.2.

The calcined ZnO was treated at 1100 °*C* for 6 hours. In the catalytic tests its oxygen and methane conversion is significantly lower, while the $C_2$ selectivity is comparable to those of the two untreated zinc oxides. All Li@ZnO show a much lower conversion of oxygen and methane and even lower $C_2$ selectivities. However, with an increasing lithium content, the conversion of oxygen and methane increases, while the $C_2$-selectivity has a maximum at a Li content of 3 wt%. The Li+ZnO catalysts showed an inverse behaviour. With higher Li content the oxygen conversion decreases while the $C_2$ selectivities increases and therefore the $CO_x$ selectivity decreases.

### 5.3.2 Oxidative Dehydrogenation of Ethane

The results for the oxidative dehydrogenation of ethane at 600 °*C*, 150 mg catalyst and 30 ml/min are shown in Figure 5.4. Under these reaction conditions all tested materials showed catalytic activity. The commercial zinc oxide and the one with defects show full oxygen conversion. The ethane conversion and the ethene selectivity is approximately 20 %. The results for the commercial zinc oxide and the one with defects can be considered being equal. The catalytic activity of calcinated commercial zinc oxide is very low, but it shows a much higher selectivity, these results represent obviously the thermal dehydrogenation.

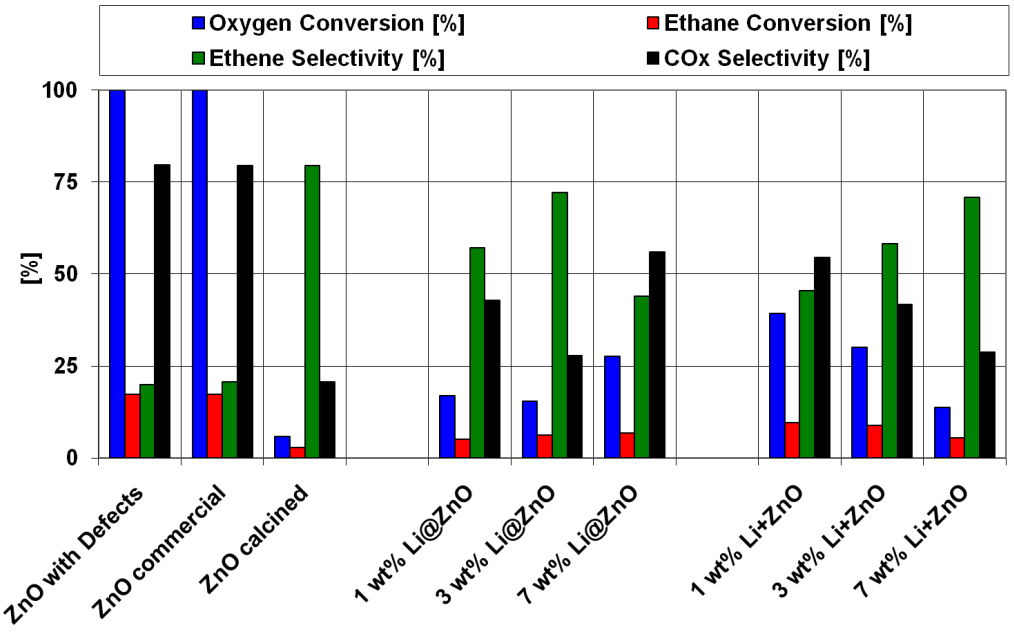


Figure 5.4: Results of the ODE experiments at 600 °*C*, 150 mg catalyst and a gas flow of 30 ml/min. For feed composition see Table 5.2.

The lithium doped zinc oxides from single source precursors show only around 20 % oxygen conversion, and the ethane conversion is around $^2/_3$ lower in comparison to the pure zinc oxides. However, all three Li@ZnO show a distinct increase in the ethene selectivity compared to the pure zinc oxides. The oxygen conversion slightly increases with a higher lithium loading, while the ethene selectivity shows a maximum at 3 wt%. The Li+ZnO also have a lower conversion of oxygen and ethane than the pure zinc oxides, the oxygen conversions are slightly higher than those of Li@ZnO, but the ethane conversion and ethene selectivity is comparable. For Li+ZnO the oxygen and ethane conversion decreases with increasing Li content, while the selectivity increases.

### 5.3.3 Oxidative Dehydrogenation of Propane

At 450 °*C* all catalysts show activity for the oxidative dehydrogenation of propane, except the calcinated zinc oxide. The results at 450 °*C*, 150 mg catalyst and 30 ml/min are shown in Figure 5.5. The commercial zinc oxide and the defective zinc oxide have 34 % and 47 % oxygen conversion and 3.7 % and 5.1 % propane conversion, respectively, at very low propene selectivities. As in the parts 5.3.1 and 5.3.2 described, the results for the commercial zinc oxide and the defective one can be considered approximately the same. Pure calcinated ZnO does not show any activity. The lithium doped zinc oxide from single source precursors shows a substantial decrease of oxygen and propane conversion at similar propene selectivites. The Li+ZnO catalysts prepared by milling show even lower oxygen and propane conversions, however the propene selectivity is five-fold and it decreases with increasing lithium content.

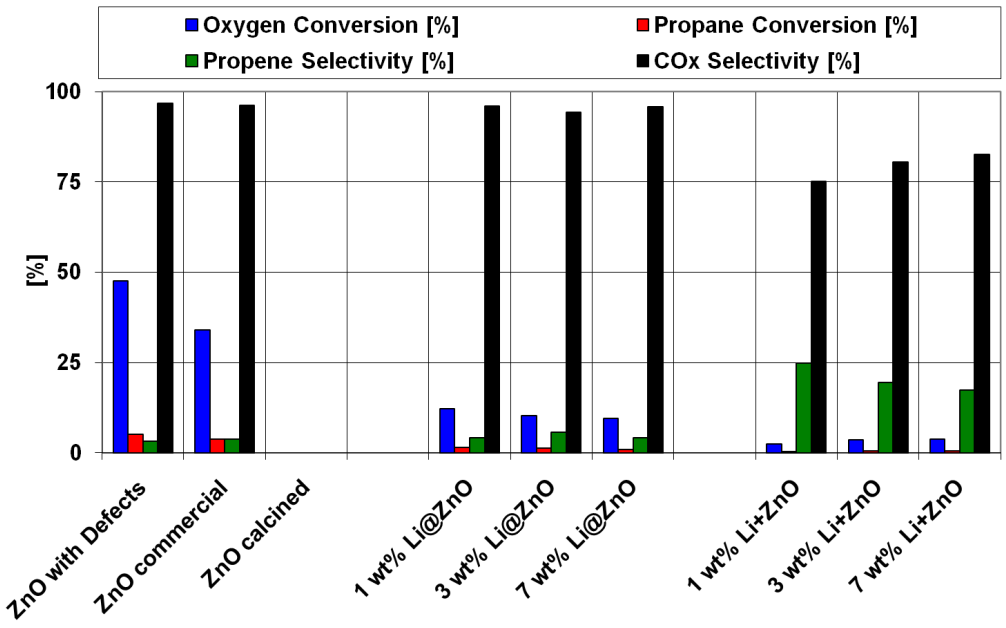


Figure 5.5: Results of the ODP experiments at 450 °*C*, 150 mg catalyst and a gas flow of 30 ml/min. For feed composition see Table 5.2.

### 5.3.4 Total oxidation

Already at very low conversion of propane, the propene selectivity is really low and therefore the $CO_x$ selectivity is high. This fact indicates the propane is converted to CO and $CO_2$ directly and not the propene, i.e. the catalysts is actually

active for total oxidation.

The results for the experiments for the total oxidation of methane with 150 mg catalyst are shown in Figure 5.6. The catalysts start showing combustion activity for $CH_4$ from 550 $°C$ upwards. As the calcined ZnO has already a very low activity, thus it was not tested for the total oxidation of methane. The pure zinc oxide from a single source precursor shows the highest combustion activity. The difference to commercial zinc oxide is distinct. At 650 $°C$ commercial zinc oxide converts 50 % of the methane, whereas with the zinc oxide with defects from single source precursors nearly 70 % of the methane are consumed.

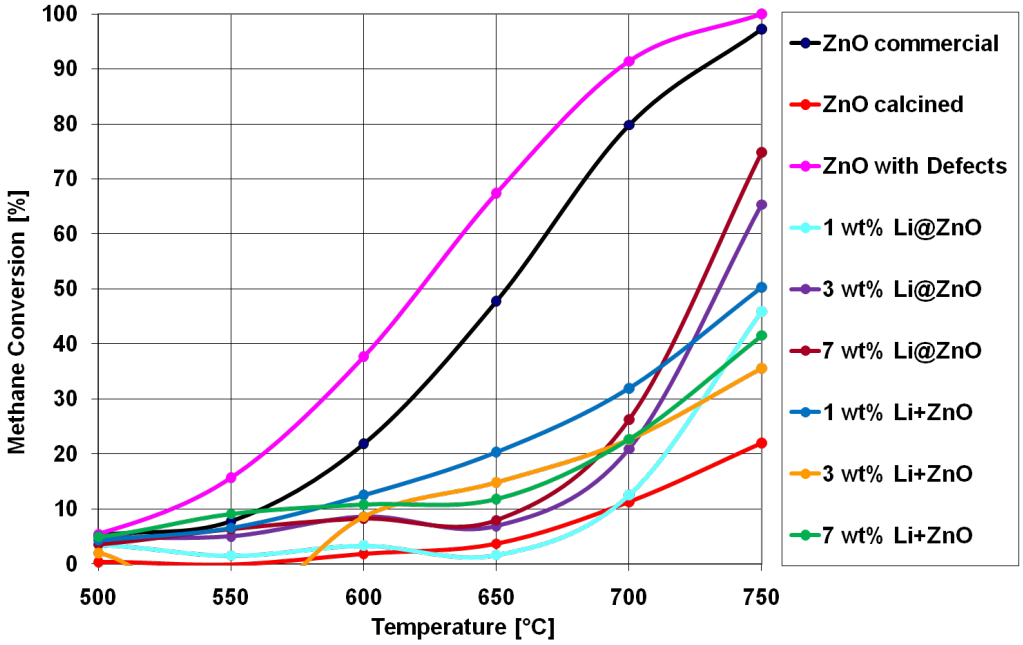


Figure 5.6: The conversion of methane in experiments for total oxidation with 150 mg catalyst. For feed composition see Table 5.2.

Alike for the OCM, ODE and ODP reaction, doping with Li leads to a sever decrease of the catalytic activity. Li@ZnO with the highest Li content of 3 wt% and 7 wt% is more active than with 1.5 wt% or the Li+ZnO catalysts.

### 5.3.5 Stability of Zinc oxide

In Table 5.3 the BET specific surface areas of the catalysts before and after OCM reaction are shown. The specific surfaces of pure and doped zinc oxides from single source precursors are distinctly higher than the commercial ZnO and the Li+ZnOs.

| Catalyst | before OCM | after OCM |
|---|---|---|
| ZnO with Defects | 27.0 $m^2/g$ | $\leq 1$ $m^2/g$ |
| ZnO commercial | 5.8 $m^2/g$ | $\leq 1$ $m^2/g$ |
| ZnO calcinated | $\leq 1$ $m^2/g$ | $\leq 1$ $m^2/g$ |
| 1 wt% Li@ZnO | 71.0 $m^2/g$ | $\leq 1$ $m^2/g$ |
| 3 wt% Li@ZnO | 24.7 $m^2/g$ | $\leq 1$ $m^2/g$ |
| 7 wt% Li@ZnO | 8.8 $m^2/g$ | $\leq 1$ $m^2/g$ |
| 1 wt% Li+ZnO | 4.3 $m^2/g$ | $\leq 1$ $m^2/g$ |
| 3 wt% Li+ZnO | 4.1 $m^2/g$ | $\leq 1$ $m^2/g$ |
| 7 wt% Li+ZnO | 4.8 $m^2/g$ | $\leq 1$ $m^2/g$ |

Table 5.3: The specific surface areas of the catalysts before and after the OCM reaction at 700 $°C$.

After the OCM reaction the BET surfaces were measured again, but for all catalysts, doped and undoped, the specific surface was below 1 $m^2/g$.

In order to determine the onset of the thermal sintering of ZnO, commercial zinc oxide was calcined for 6 hours at different temperatures. Afterwards the BET surface areas were measured again. The result is shown in Figure 5.7.

The increase in specific surface area between 100 to 200 $°C$ is due to the removal of water, hydroxides and other volatile impurities. Between 400 and 800 $°C$ there is a nearly linear decline in the BET area until a not detectable surface area.

For Li-doped ZnO the sintering ability is expected to be even higher than for undoped zinc oxide [282]. Therefore it can be assumed, that the decrease in the specific surface area occurs at even lower temperatures.

## 5.4 Discussion

All tested catalysts show activity for the OCM and the total oxidation of methane. The doping with Li reduces the oxidation activity significantly for all catalysts in all reactions studied, that is the conversion decreases while the selectivity increases.

With different lithium doping Li@ZnO and Li+ZnO show two different trends in OCM and ODE reaction. Li@ZnO shows:

1. an increasing oxygen and alkane conversion with increasing Li content
2. a maximum of product selectivity at a Li content of 3 wt%,

while Li+ZnO shows

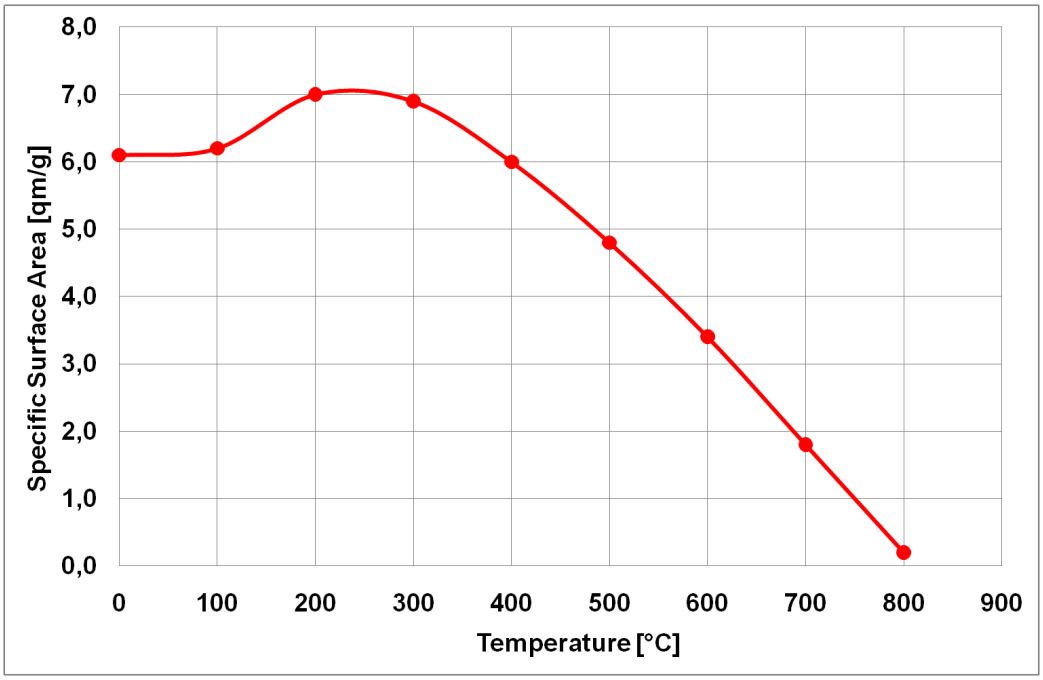


Figure 5.7: The specific surface areas of commercial ZnO depending on the calcination temperature.

1. a decreasing oxygen and alkane conversion with increasing Li content
2. a increasing product selectivity with increasing Li content

As the trends for oxygen and methane conversion and the product selectivity is the same in the OCM and ODE reaction for different catalysts, it could be assumed that the active centers for the activation of methane and ethane are the same. The same trend is observed for Li@ZnO and Li+ZnO for the ODP reaction.

Generally speaking, on a single reaction pathway, the selectivity decreases with increasing conversion following a single trajectory and vice versa. Some catalysts allow more than only one reaction pathway for one reaction. If doping of a catalyst only decreases the conversion and therefore increases the selectivity, or when doping opens new reaction pathways this can be seen if there is more than one trajectory in the conversion selectivity diagram. In Figure 5.8 the conversion selectivity diagrams for the oxidative coupling of methane and the oxidative dehydrogenation of ethane and propane for the different catalysts are shown. It can be seen that for the oxidative dehydrogenation of ethane and propane most likely only one trajectory exists, respectively, therefore it can be presumed that doping with lithium leads to a decreased conversions at increased selectivities controlled by a constant ratio of the rate constants of the involved reactions. However, for the

oxidative coupling of methane it is obvious that there is more than only one trajectory. It can be followed that doping with Li opens new reaction pathways, with different kinetic parameters of the involved reactions in comparison to undoped ZnO.

For the ODE and ODP it can not be expected that this type of catalyst can be further improved, as doping with lithium does not change the reaction pathway. For the OCM reaction however, doping does lead to different reaction pathways, therefore tuning the doping could allow to find a catalysts that opens a reaction pathway with higher conversions at higher selectivities.

Comparison of the Li@ZnO and the Li+ZnO catalysts shows that generally the later ones are more active and selective, as they usually show higher oxygen and alkane conversions and higher product selectivities. An exception is the oxidative dehydrogenation of propane where the Li@ZnO catalysts have a significantly higher propane conversion than the Li+ZnOs. A reason for the higher activity of Li+ZnO is the higher fraction of Li atoms at the surface, due to the preparation by milling, while for the Li@ZnO catalysts most of the Li atoms are probably hidden in the bulk phase as the synthesis via single source precursors ensures a real doping.

Generally, the conversion and the selectivities of the tested reactions are not satisfactory for industrial applications. The reason for the low activity is the deactivation of the catalyst by sintering. Reactions at lower temperatures like the oxidative dehydrogenation of ethane and propane do not show an improved activity either. A reason could be that the loss in activity starts already at $400\,^{\circ}C$ for commercial pure ZnO, with sintering of the material. This explains that no distinct difference for commercial ZnO and ZnO from single source precursors for the OCM, ODE and ODP can be observed. For lithium doped zinc oxides the sintering and therefore the deactivation should occur at even lower temperatures [283, 284, 282]. But below $400\,^{\circ}C$ no catalyst showed any activity for the activation of a C-H bond. However, for the total oxidation of methane a difference between commercial and single source precursor zinc oxide can be seen, a reason could be that the deactivation process has not been completed under the chosen conditions.

## 5.5 Summary and Conclusion

Pure and Li doped zinc oxides from single source precursors and from mixed milling were tested for their catalytic activity in the oxidative dehydrogenation of propane and ethane, the oxidative coupling of methane and its total oxidation. The catalysts showed usually poor activity in alkane conversion and their selectivity towards the desired olefins was low. The experiments for the total oxidation of

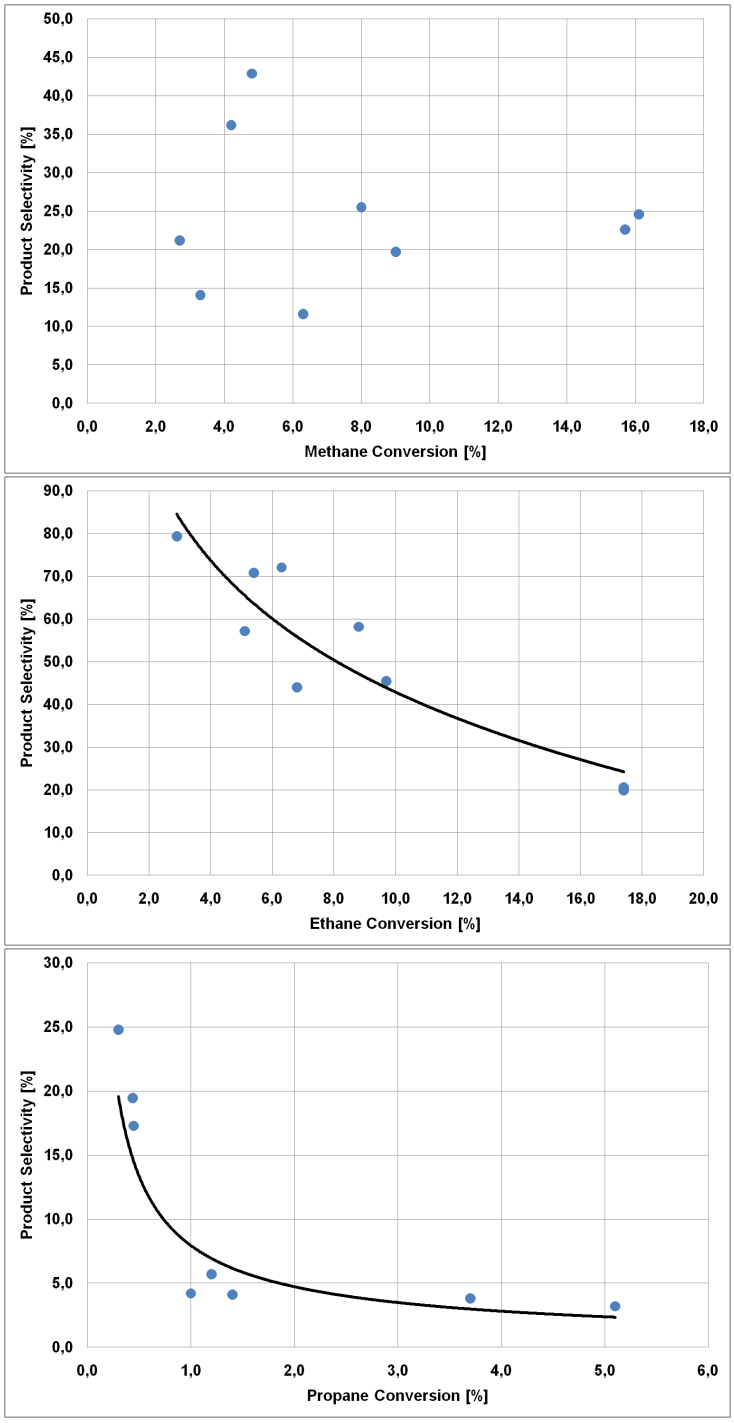


Figure 5.8: Conversion selectivity diagramm for the OCM, ODE and ODP reaction. As it can be seen, the points do not lie on a single curve. Therefore different reaction pathways are existent for different loadings of Li.

methane revealed that even the activity for total oxidation was low, because the catalysts are deactivated at temperatures above 400 $^{\circ}C$.

Therefore these catalysts are only suitable for substrates that can be activated at even lower temperatures. The application of the single source precursor strategy towards thermally more stable catalysts, and therefore the preparation of catalysts which do not suffer from sever sintering, with subsequent improving their catalytic performance could be a big step forward in the C-H activation of lower alkanes.

# Chapter 6

# ZnO on Different Support Materials for the C-H Activation of Methane, Ethane and Propane

This work is being prepared for submission as: S. Arndt, B. Uysal, A. Berthold, T. Otremba, Y. Aksu, M. Driess and R. Schomäcker, "ZnO on Different Supports Materials for the C-H Activation of Methane, Ethane and Propane" in Applied Catalysis A: General.

## 6.1 Introduction

The first step of functionalisation or combustion of alkanes is the activation of a C-H bond [275, 276]. The lower alkanes propane, ethane and especially methane are relatively stable compounds, therefore, their activation is difficult. Since methane is the most stable hydrocarbon, its activation is most difficult. However, methane is the major compound in natural gas, with resources rivaling those of crude oil [7]. Thus, there is a big economical interest in converting natural gas into value added products.

For the conversion of methane, two possible routes exist [2]. On the indirect route, methane is converted into synthesis gas, which is further processed in the Fischer Tropsch process. In the direct route, methane is directly converted into the desired products, circumventing the energy-consumptive syn-gas step. A possible reaction for this is the oxidative coupling of methane. Since the first publications in this field [3, 4], extensive research has been done. However, this process has not yet reached the stage of commercial application. Since methane is so difficult to activate, high reaction temperatures are necessary, at which many catalysts suffer from severe stability and selectivity problems.

The other two main compounds of natural gas are ethane and propane. The desired reaction for their conversion is the oxidative dehydrogenation. The reactions for the conversion of methane, ethane and propane to the corresponding olefins are:

1. the oxidative coupling of methane (OCM)
   $2\ CH_4 + {}^1/_2$ or $1\ O_2 \rightarrow C_2H_6$ or $_4 + 1$ or $2\ H_2O$
2. the oxidative dehydrogenation of ethane (ODE)
   $C_2H_6 + {}^1/_2\ O_2 \rightarrow C_2H_4 + H_2O$
3. the oxidative dehydrogenation of propane (ODP).
   $C_3H_8 + {}^1/_2\ O_2 \rightarrow C_3H_6 + H_2O$

Zinc oxide could be a good catalyst for the reactions above. Matsuura *et al.* reported ZnO doped with Li to be the most active one, among the tested alkali-doped ZnO catalysts [14]. Zhang and Giusti investigated the mechanism and the function of Li/ZnO as an OCM catalyst [15, 278]. The effect of chlorine in Li/ZnO was investigated by Wang and coworkers [279], and the ODP on ZnO by Wan *et al.* [280]. Spinicci investigated the properties of ZnO based catalysts with the help of transient response methods [285]. He reported that the results indicate that the surface oxygen species which could desorb at the highest temperature is the most basic species $O^{2-}$, and could lead to the formation of $C_2$ products. The less basic species, $O^-$ and $O_2^{2-}$, should lead to the formation of total oxidation products.

Recently the synthesis of pure and Li doped ZnO from single source precursors has been developed and published [281, 273, 274]. This procedure allows the preparation of solid compounds in a reproducible way and with controlled features on a molecular level. These compounds have been tested by Arndt *et al.* [272]. The results of the materials prepared from single source precursors were similar to zinc oxides prepared via mixed milling and a severe deactivation was observed.

Kim *et al.* studied ZnO supported on $\gamma$-$Al_2O_3$ with and without the addition of alkali halides in the oxidative coupling of methane. It was found that the optimal loading of ZnO was 60 wt% and the specific surface area was not related to the activity and promotion with LiCl increased the performance [286, 287].

For any practical application the stability of the catalyst is crucial, especially for the applications at higher temperatures such as C-H activation of methane, ethane and propane. But this fact has been neglected in the literature, only Arndt and co-workers denoting a stability problem for ZnO. Detailed studies of ZnO on different support materials for a high temperature application, their stability and activity under reaction conditions are missing in the literature. In this publication, we report about ZnO supported on $ZrO_2$, $TiO_2$, $\gamma$-$Al_2O_3$ and $SiO_2$ the catalytic activity and the stability under reaction conditions.

The C-H activation reactions were the oxidative coupling of methane and the oxidative dehydrogenation of ethane and propane. These three reactions allow the investigation of C-H activation for similar hydrocarbons over a broad temperature range.

## 6.2 Experimental Part

### 6.2.1 Catalyst Preparation

To the support material (origin and specific surface area are shown in Table 6.1), a solution of $Zn(NO_3)_2$ (Fluka, $Zn(NO_3)_2 \times 6\,H_2O$, $\geq 99.0\,\%$) in deionised $H_2O$ was added dropwise and stirred until a thick paste formed. The paste was dried at room temperature for 24 hours and then heated, with a heating rate of 7.5 K/min to 450 $^{\circ}C$ under air. The temperature was held at 450 $^{\circ}C$ for 3 hours. This procedure was adapted from Choilett and co-workers [288]. The obtained material was crushed and sieved and only the fraction below 200 $\mu m$ was used.

Table 6.1: The origin and specific surface area of the used support materials.

| **Support** | **Origin of Support** | **BET surface area [$m^2$/g]** |
|---|---|---|
| $ZrO_2$ | Aldrich, 3 % Y stabilized | 106.1 |
| $TiO_2$ | BASF, Ti11000E | 126.1 |
| $\gamma$-$Al_2O_3$ | Alfa Aesar | 105.3 |
| $SiO_2$ | BASF, D11-10 | 101.1 |

The prepared ZnO loadings for each catalyst were 5, 10, 15 and 20 wt%. The loading was calculated according to Equation 6.1. Commercial, pure ZnO was obtained from Fluka with a purity higher than 99.0 %.

$$\text{ZnO [wt\%]} = \frac{\text{ZnO [g]}}{\text{Support [g]}} \times 100\% \tag{6.1}$$

### 6.2.2 Catalyst Characterization

#### 6.2.2.1 Atomic Absorption Spectroscopy

The Zn content of the different samples was quantified via atomic absorption spectroscopy (AAS), using an AAS NovAA 400 G device from Analytik Jena via flame and graphite furnace. A summary of the calculated and measured loadings is given in Table 6.2.

Table 6.2: Prepared supported ZnO catalysts and their actual ZnO loading, determined with AAS.

| Catalyst | ZnO targeted | ZnO measured |
|---|---|---|
| 5 wt% ZnO/$ZrO_2$ | 5 wt% | 3 wt% |
| 10 wt% ZnO/$ZrO_2$ | 10 wt% | 9 wt % |
| 15 wt% ZnO/$ZrO_2$ | 15 wt% | 13 wt% |
| 20 wt% ZnO/$ZrO_2$ | 20 wt% | 20 wt % |
| 5 wt% ZnO/$TiO_2$ | 5 wt% | 3 wt% |
| 10 wt% ZnO/$TiO_2$ | 10 wt% | 7 wt % |
| 15 wt% ZnO/$TiO_2$ | 15 wt% | 11 wt% |
| 20 wt% ZnO/$TiO_2$ | 20 wt% | 19 wt % |
| 5 wt% ZnO/$\gamma$-$Al_2O_3$ | 5 wt% | - |
| 10 wt% ZnO/$\gamma$-$Al_2O_3$ | 10 wt% | 4 wt% |
| 15 wt% ZnO/$\gamma$-$Al_2O_3$ | 15 wt% | 7 wt% |
| 20 wt% ZnO/$\gamma$-$Al_2O_3$ | 20 wt% | 26 wt% |
| 5 wt% ZnO/$SiO_2$ | 5 wt% | 4 wt% |
| 10 wt% ZnO/$SiO_2$ | 10 wt% | 10 wt% |
| 15 wt% ZnO/$SiO_2$ | 15 wt% | 12 wt% |
| 20 wt% ZnO/$SiO_2$ | 20 wt% | 19 wt% |

#### 6.2.2.2 BET

The specific surface area was determined by a Micromeritics Gemini III 2375 Surface Area Analyzer, using nitrogen adsorption at -196 $^{\circ}C$. Before measuring, the supported samples were degassed at 300 $^{\circ}C$ and 0.15 mbar at least for 30 minutes, however unsupported ZnO was outgassed at 120 $^{\circ}C$. The surface areas were calculated by the method of Brunauer, Emmett and Teller (BET).

#### 6.2.2.3 XRD

The powder diffractograms were performed on a PANalytical X'Pert PRO MPD Diffraktometer instrument using CuK$\alpha$ radiation ($\lambda$ = 1.5418 Å) and a position sensitive-detector (PSD) in the 2$\Theta$ range from 10° to 90° with 0.015° step. The diffractorgrams were analyzed with the program STOE WinXPOW.

### 6.2.3 Catalytic Testing

#### 6.2.3.1 Set-Up

The catalytic experiments were carried out in a packed-bed, U-shaped, tubular reactor made of quartz glass. The outer diameter was 8 mm and the inner diameter

6 mm. For each catalytic run, the catalyst was diluted with approximately 3 ml quartz sand for proper heat transfer (quartz sand: purchased from Merck, already washed with HCl and calcined, approximately 60 % of the particles have the size 0.2 - 0.8 mm). The reactor behaves like a plug flow tubular reactor. The length of the catalytic bed was approximately 90 - 100 mm. Below and above the catalyst bed, a small amount of pure quartz sand was placed to ensure proper heat transfer. The particle size of the catalyst was below 200 $\mu$m in each experiment to exclude internal mass transfer effects. The amount of catalyst loaded into the reactor was calculated that always approximately 19 mg of ZnO was in the reactor as active component.

The gas was fed to the reactor using mass flow controllers of Brooks, 5850 TR series. The alkane ($CH_4$, $C_2H_6$ or $C_3H_8$) and synthetic air, as oxygen source (20.5 % $O_2$ in $N_2$), were fed into the reactor. The exact feed gas composition is shown in Table 6.3. Before entering the reactor, the reactants passed a pre-heater, heated to 180 $^{\circ}C$. The reactor was heated with an electric furnace (LK 1000-20-310-1 from HTM Reetz Berlin); isothermal conditions were insured. The reactor was heated to the desired reaction temperatures, as shown Table 6.3, applying a heating rate of 20 K/min. 19 minutes after the desired reaction temperature was reached, the first data point was measured. The same test protocol was applied for every experiment.

Table 6.3: The reaction conditions for the different catalytic test reactions.

| **Reaction** | **Alkane : $O_2$ : $N_2$** | **Temperature** | **Gas Flow** |
|---|---|---|---|
| OCM | 4 : 1 : 4 | 700 $^{\circ}C$ | 60 [ml/min] |
| ODE | 2 : 1 : 4 | 600 $^{\circ}C$ | 30 [ml/min] |
| ODP | 2 : 1 : 4 | 450 - 500 $^{\circ}C$ | 30 [ml/min] |

The analysis was performed with a gas chromatograph Agilent 7890 A, equipped with a flame ionization detector (FID), a thermal conductivity detector (TCD), a HP-PLOT/Q and a HP Molsieve column. The analyzed compounds were $O_2$, $N_2$, CO, $CO_2$ via TCD and the hydrocarbons via FID. $N_2$ was used as internal standard. The reproducibility of conversion (X) and selectivity (S) is sufficient. The conversion and selectivity has been calculated from a mass balance based on the inlet and outlet concentration of reactants and products, see Equations 6.2 and 6.3. The carbon balance was always above 95 %.

$$X = \frac{\sum(\text{Reaction Products})}{\sum(\text{Reaction Products}) + \text{unconverted Reactant}} \tag{6.2}$$

$$S = \frac{\text{Desired Product}}{\sum(\text{All Reaction Products})} \tag{6.3}$$

The reaction conditions have been chosen such, that for the case of full $O_2$ conversion, the possible alkane conversions are:

1. for the OCM
   (a) 12.5 % for total oxidation to $CO_2$,
   (b) 100 % for 100 % selectivity[1]
2. for the ODE
   (a) 14.3 % for total oxidation to $CO_2$,
   (b) 100 % for 100 % selectivity
3. for the ODP
   (a) 12.5 % for total oxidation to $CO_2$,
   (b) 100 % for 100 % selectivity

The desired reaction products of the oxidative coupling of methane are $C_2H_4$ and $C_2H_6$. The selectivity of these two products is discussed as a sum, the $C_2$-selectivity. Higher reaction products, especially $C_3H_8$ and $C_3H_6$, have not been detected in the OCM, although the applied method was suitable for their detection.

In order to determine the degree of thermal dehydrogenation, blank experiments with pure quartz sand were conducted under reaction conditions. For methane and propane, no conversion was observed. For ethane, the thermal dehydrogenation was 0.3 % ethane conversion at 74 % ethylene selectivity.

#### 6.2.3.2 Screening

For a fast and approximate determination of the activity for all catalyst, a screening protocol was developed. With one loading one data point was measured. The order was first ODP, then ODE and finally OCM activity was determined to avoid unwanted changes of the catalyst at higher temperatures.

#### 6.2.3.3 Stability Tests

For a determination of the long term stability, OCM, ODE and ODP was measured always with fresh catalyst in a separate experiment. In case of ODP, the activity was measured for 7 hours at 450 $^\circ C$, then the temperature was raised to 475 $^\circ C$ and the activity was measured for another 7 hours. Subsequently, the temperature was raised to 500 $^\circ C$ with further 7 hours of measurements. The aim of this experiment was to find out at what temperature the deactivation starts.

[1] In this specific calculation, the selectivity is confined to the selectivity towards $C_2H_6$.

## 6.3 Results and Discussion

### 6.3.1 Screening

For all catalysts, the same test protocol regarding reactor temperature, gas flow and time was applied. This was done to ensure the same conditions for each catalyst because a possible deactivation of the catalysts is not considered in these experiments. The screening results of pure commercial ZnO and supported ZnO are shown in Figure 6.1 for the oxidative coupling of methane, in Figure 6.2 for the oxidative dehydrogenation of $C_2H_6$ and in Figure 6.3 for the oxidative dehydrogenation of $C_3H_8$. These figures show a conversion selectivity diagram in which each catalyst is included. The colored symbols represent one support material and the actual loading is given next to each data point.

In the oxidative dehydrogenation of propane, pure ZnO exhibits a rather low conversion at a selectivity comparable to the other catalysts. However, in the oxidative dehydrogenation of ethane, and even more in the oxidative coupling of methane, it exhibits rather high conversions at comparatively good selectivities. The reason for this different behavior could be that in the ODP, the specific surface area does play an important role, while for reactions at higher temperatures, ODE and OCM, the importance of the specific surface area of the catalyst decreases. That there might be an optimal specific surface area in the oxidative coupling of methane, is discussed in the OCM literature [62].

$ZnO/ZrO_2$ and $ZnO/TiO_2$ show comparable conversions for all three test reactions. However, the selectivities are rather low; total oxidation activity is dominating. $ZnO/ZrO_2$ shows slightly higher selectivities at comparable conversions compared to the $ZnO/TiO_2$. Lower loadings of ZnO result in higher conversions for all reactions and both catalysts, indicating that a higher dispersion increases the activity. This effect is especially prominent in the case of ODP, see Figure 6.3. The data points of pure ZnO and $ZnO/ZrO_2$ and pure ZnO and $ZnO/TiO_2$ lie on one straight line. Drawing a straight line is also possible for the ODE and OCM, although the deviation is higher. The 5 wt% ZnO loading has for both catalysts the highest activity, being significantly higher than for the 10 wt% loading. For Cu supported on $TiO_2$ (rutile and antase) and $SiO_2$, the same dispersion effect has been reported [289].

That the differences in the activity $ZnO/ZrO_2$ and $ZnO/TiO_2$ cannot only be attributed to the different amount of catalyst loaded into the reactor can be seen at the data points for $ZnO/\gamma\text{-}Al_2O_3$ and $ZnO/SiO_2$. They are within a very narrow region, irrespective of the ZnO loading or of the amount of catalyst in the reactor. The 5 wt% $ZnO/SiO_2$ can be considered as an outlier. A dispersion effect can not be observed. The high conversion and low selectivity of $ZnO/\gamma\text{-}Al_2O_3$ could be attributed to the total oxidation activity of $\gamma\text{-}Al_2O_3$, which was also observed by

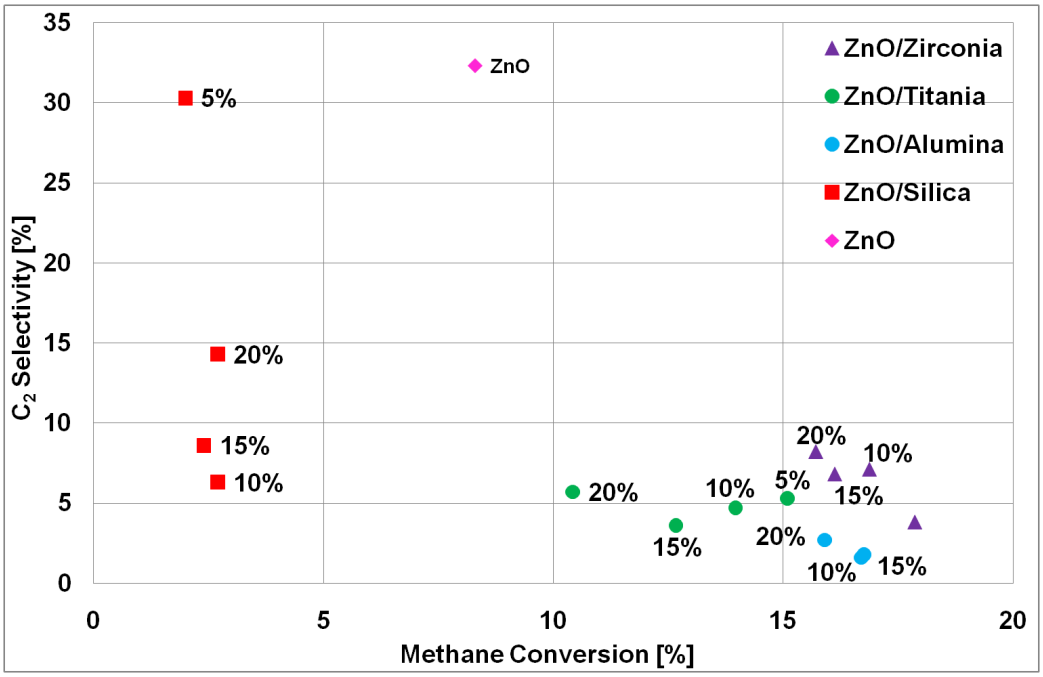


Figure 6.1: Different ZnO loadings on the different support materials and pure ZnO are compared in an X-S diagramm for the oxidative coupling of methane. The color indicates the support material and the loading is given next to the data point. Reaction conditions: gas flow 60 ml/min, 700 $^{\circ}C$.

other researchers [289]. The low conversion and high selectivity of $ZnO/SiO_2$ in comparison to pure ZnO could also be due a support effect.

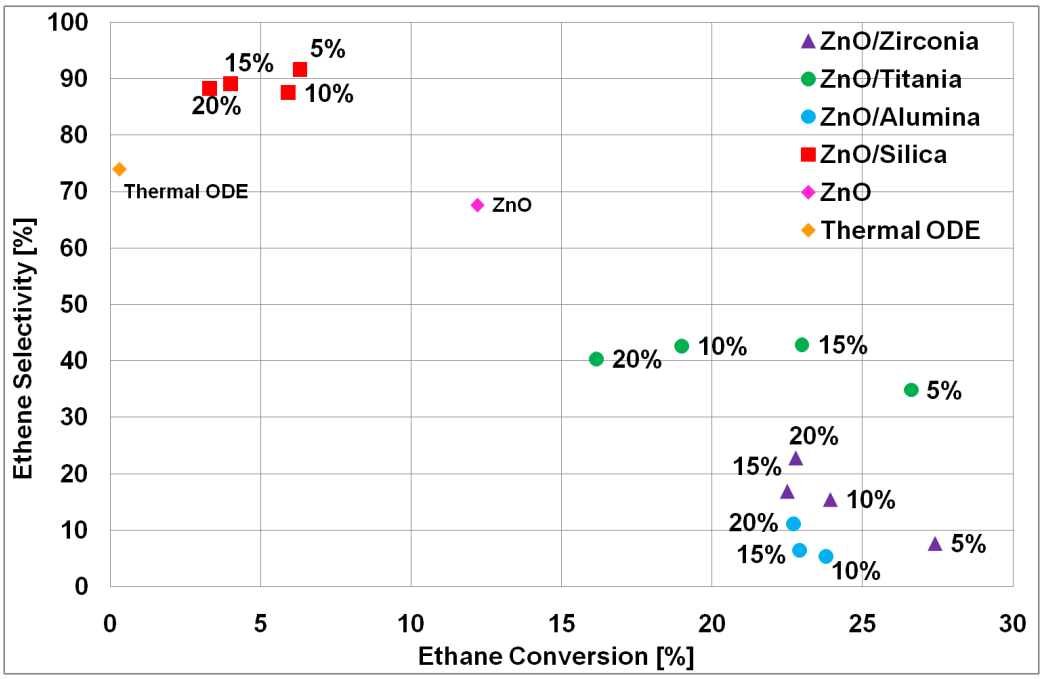


Figure 6.2: Different ZnO loadings on the different support materials and pure ZnO are compared in an X-S diagramm for the oxidative dehydrogenation of ethane. The color indicates the support material and the loading is given next to the data point. Reaction conditions: gas flow 30 ml/min, 600 °*C*.

The screening results of the prepared catalysts for the different test reactions show that the differences due to the different ZnO loading are small in comparison to the differences due to the different support material, which seems to be the crucial factor determining the conversion and selectivity and not the loading of ZnO. The effect that the support is the determining factor for the catalytic activity is also reported for other metal oxides, such as V and Mo [290, 291, 292].

### 6.3.2 Stability of the Catalyst under Reaction Conditions

The BET surface area of the catalysts was measured before and after the screening tests, with the oxidative coupling of methane as last test reaction in the screening protocol. The loss of specific surface area and the relative loss in % are shown Table 6.4. For clarification, the relative loss of the BET surface area of the different catalyst as a function of the ZnO loading is shown in Figure 6.4. It is evident

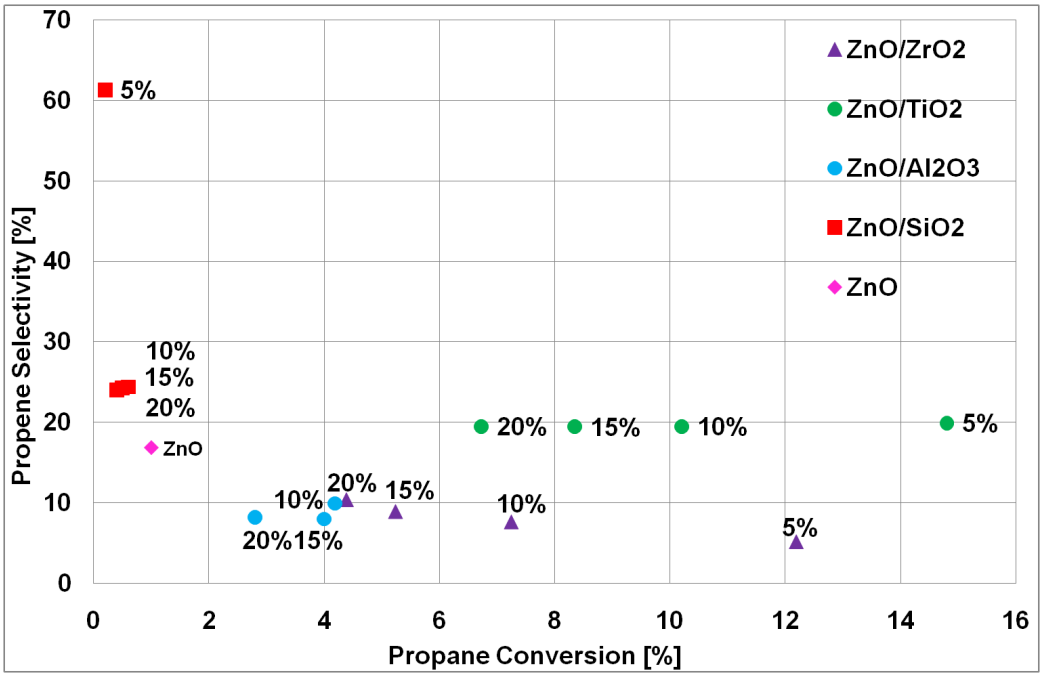


Figure 6.3: Different ZnO loadings on the different support materials and pure ZnO are compared in an X-S diagramm for the oxidative dehydrogenation of propane. The color indicates the support material and the loading is given next to the data point. Reaction conditions: gas flow 30 ml/min, 450 °*C*.

that with higher loadings of ZnO, the loss of BET surface area increases. ZnO/$\gamma$-$Al_2O_3$ losses approximately 50 % of the surface area, relatively independent of the loading. At a loading of 5 wt% ZnO on $SiO_2$, a loss 18 % can be observed, however, at higher ZnO loadings on $SiO_2$ a strong reduction of the surface area is observed. ZnO supported on $ZrO_2$ and $TiO_2$ suffers from a loss of BET surface area of nearly 100 %, irrespective of the ZnO loading. For pure ZnO the loss in BET surface area was nearly 100 %.

The question of interest is now: is the deactivation caused by sintering of the catalyst or caused by the reaction of the ZnO with the support material.

Table 6.4: BET surface area before and after the oxidative coupling of methane and relative loss.

| **Catalyst** | **before** | **after OCM** | **relative Loss** |
|---|---|---|---|
| ZnO | 5.8 $m^2/g$ | 0.0 $m^2/g$ | 100 |
| 5 wt% ZnO/$ZrO_2$ | 77.5 $m^2/g$ | 19.4 $m^2/g$ | 75 % |
| 10 wt% ZnO/$ZrO_2$ | 72.9 $m^2/g$ | 12.1 $m^2/g$ | 83 % |
| 15 wt% ZnO/$ZrO_2$ | 64.9 $m^2/g$ | 1.9 $m^2/g$ | 97 % |
| 20 wt% ZnO/$ZrO_2$ | 68.2 $m^2/g$ | 2.1 $m^2/g$ | 97 % |
| 5 wt% ZnO/$TiO_2$ | 104.2 $m^2/g$ | 16.1 $m^2/g$ | 85 % |
| 10 wt% ZnO/$TiO_2$ | 87.0 $m^2/g$ | 3.7 $m^2/g$ | 96 % |
| 15 wt% ZnO/$TiO_2$ | 82.4 $m^2/g$ | 1.2 $m^2/g$ | 99 % |
| 20 wt% ZnO/$TiO_2$ | 76.9 $m^2/g$ | 0.5 $m^2/g$ | 99 % |
| 5 wt% ZnO/$\gamma$-$Al_2O_3$ | 175.6 $m^2/g$ | - | - |
| 10 wt% ZnO/$\gamma$-$Al_2O_3$ | 93.7 $m^2/g$ | 66.3 $m^2/g$ | 29 % |
| 15 wt% ZnO/$\gamma$-$Al_2O_3$ | 89.1 $m^2/g$ | 52.1 $m^2/g$ | 42 % |
| 20 wt% ZnO/$\gamma$-$Al_2O_3$ | 86.3 $m^2/g$ | 39.4 $m^2/g$ | 54 % |
| 5 wt% ZnO/$SiO_2$ | 77.5 $m^2/g$ | 63.3 $m^2/g$ | 18 % |
| 10 wt% ZnO/$SiO_2$ | 65.7 $m^2/g$ | 22.4 $m^2/g$ | 66 % |
| 15 wt% ZnO/$SiO_2$ | 57.0 $m^2/g$ | 15.9 $m^2/g$ | 72 % |
| 20 wt% ZnO/$SiO_2$ | 54.8 $m^2/g$ | 9.6 $m^2/g$ | 83 % |

### 6.3.3 Stability of the Support Material

The specific surface areas of the support materials, after calcination at different temperatures for 6 hours, are shown in Figure 6.5. For $ZrO_2$ a constant decrease in the surface area over the temperature range can be observed. For $TiO_2$ however, up to 500 $^\circ C$ the material does not show a significant decrease of BET surface area. However, starting at 600 $^\circ C$, a strong and fast deactivation occurs. This can be attributed to a phase change of anatase-$TiO_2$ to rutile-$TiO_2$ [293], this phase

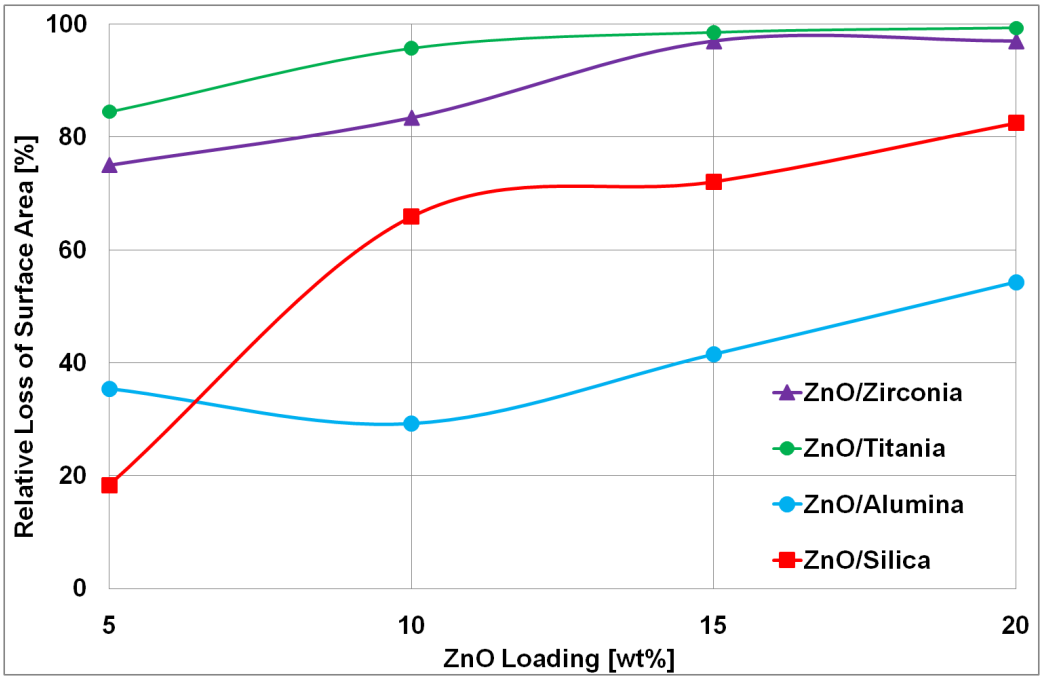


Figure 6.4: The relative loss of BET surface area as function of the ZnO loading.

change is further influenced by dopants or impurities [294]. For $\gamma$-$Al_2O_3$ and the $SiO_2$, no significant change in the BET surface area can be observed, after the calcination at different temperatures. Thus, these two support materials can be considered as stable.

For commercial ZnO, the loss of BET surface area starts between 300 to 400 °*C*, followed by a nearly linear decline until 800 °*C* and a BET surface area of smaller than 1 $m^2/g$. This has been previously reported [272].

### 6.3.4 Stability of the Catalyst without Reaction Conditions

To observe possible changes under reaction conditions, catalysts with loadings of 10 and 15 wt% ZnO were calcinated at 400, 600 and 800 °*C* in air. The XRD pattern were recorded and the specific surface areas were determined. Being a bulk method, the XRD is not able to detect small amounts of a certain compound; viz. the detection reflexes of compounds formed between the support and ZnO, as there are Zn-zirconates, Zn-titanates, Zn-aluminates and Zn-silicates indicate that they are present in distinctly more than only small amounts.

In the XRD patterns, the univocal reflexes for ZnO, the respective support material and the according Zn-zirconates, Zn-titanates, Zn-aluminates and Zn-silicates, are marked if present. However, many reflexes are superpositions of at

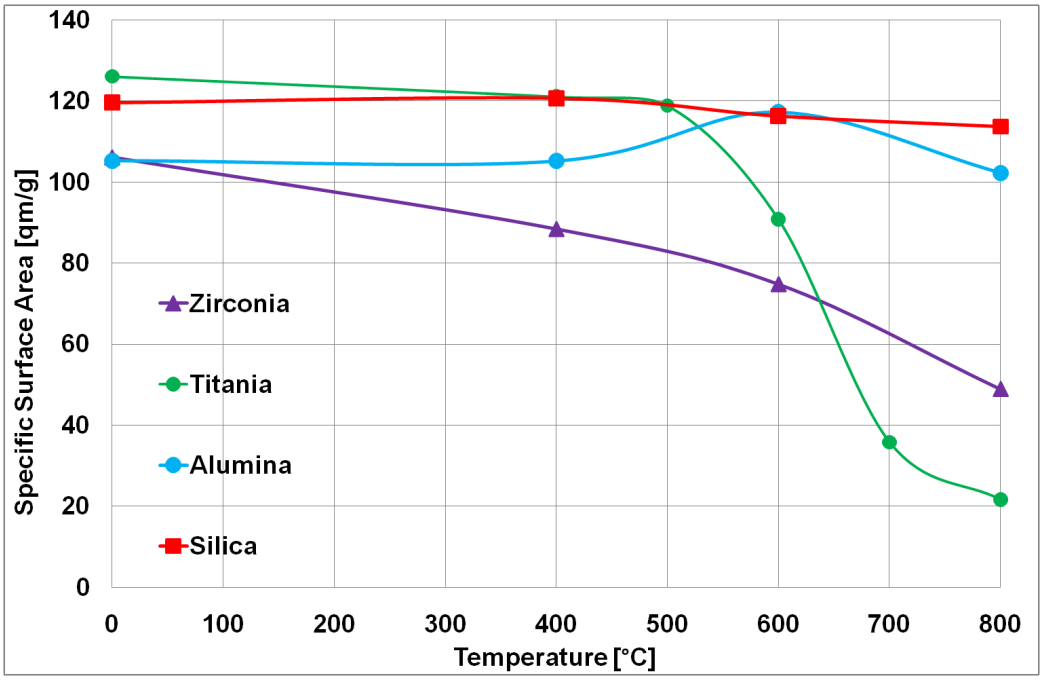


Figure 6.5: BET surface areas of the support materials after calcination at different temperatures for 6 hours, respectively.

least two of these three. In such cases, labeling was relinquished.

#### 6.3.4.1 ZnO on Zirconia

The XRD pattern for 10 and 15 wt% $ZnO/ZrO_2$ are shown in Figure 6.6. For both, the 10 and the 15 wt%, samples the formation of $ZnZrO_3$ is found already at 400 $^\circ C$. However, this compound should already form during the preparation procedure as a calcination temperature of 450 $^\circ C$ is applied. The intensity of the $ZnZrO_3$ increases with increasing calcination temperature showing that the amount increases. Reflexes for ZnO are also observed and their intensity increases slightly with increasing temperature. Overlapping of mixed reflexes of ZnO and $ZrO_2$ still exist at 800 $^\circ C$ indicating that the formation of the composed $ZnZrO_3$ phase is not strongly favored as on the titania support, see also paragraph 6.3.4.2. With growing calcinations temperature the formation of coarser crystals can be seen due to the sharpened reflexes. It is accompanied by the reduction of the BET surface as can be seen in Table 6.5. The drastic reduce in the BET surface area is evident, which is in accordance with the results obtained from the XRD measurements. Moreover, the loss of BET surface area after the screening, shown in Table 6.4 is more severe that after the calcination, although the applied reaction

temperature of 700 °$C$ is significantly lower than the highest temperature of the calcination experiment, which was 800 °$C$. This indicates that the instability of the catalyst is strongly affected by the reaction gas mixture.

Table 6.5: BET surface area for the $ZnO/ZrO_2$ samples after calcination at temperatures according to the XRD measurements.

| **Catalyst** | **10 wt% $ZnO/ZrO_2$** | **15 wt% $ZnO/ZrO_2$** |
|---|---|---|
| 400 °$C$ | 83.8 $m^2/g$ | 72.3 $m^2/g$ |
| 600 °$C$ | 48.2 $m^2/g$ | 51.1 $m^2/g$ |
| 800 °$C$ | 15.8 $m^2/g$ | 17.1 $m^2/g$ |

#### 6.3.4.2 ZnO on Titania

The XRD pattern for 10 and 15 wt% $ZnO/TiO_2$ are shown in Figure 6.7. For the 10 and 15 wt% $ZnO/TiO_2$ samples, reflexes for $ZnTiO_3$ can be found already at 400 °$C$, indicating that the formation occurs already during the preparation procedure, as calcination temperature is 450 °$C$. The intensity of the $ZnTiO_3$ is rather small, but the intensity increases at higher calcination temperatures. The reflexes for ZnO are also relatively small after calcination at 400 °$C$, with increasing intensity at higher temperatures. The reflexes are often relatively broad, indicating small crystal sizes and are growing with temperature. Reflexes become smaller and sharper with increase of temperature indicating a growing crystal size. For the 400 °$C$ calcined samples anatase as the $TiO_2$ phase is found. Yet for the 600 °$C$ calcined samples, an upcoming rutile phase can be found. This indicates a lowered transformation temperature for the anatase-rutil transformation due to the presence of ZnO as for pure TiO2 (800 - 1100 °$C$ transformation temperature). The specific surface area is shown for both samples in Table 6.6, showing a severe and drastic reduction in the surface area and therefore in the catalyst, which is in accord with the results of the XRD measurements. Alike for $ZnO/ZrO_2$, the loss of BET surface area after screening is more severe than after calcination at 800 °$C$, indicating that the instability is strongly affected by the reaction gas mixture.

Table 6.6: BET surface area for the $ZnO/TiO_2$ samples after calcination at temperatures according to the XRD measurements.

| **Catalyst** | **10 wt% $ZnO/TiO_2$** | **15 wt% $ZnO/TiO_2$** |
|---|---|---|
| 400 °$C$ | 91.3 $m^2/g$ | 87.4 $m^2/g$ |
| 600 °$C$ | 31.8 $m^2/g$ | 42.4 $m^2/g$ |
| 800 °$C$ | 2.6 $m^2/g$ | 6.4 $m^2/g$ |

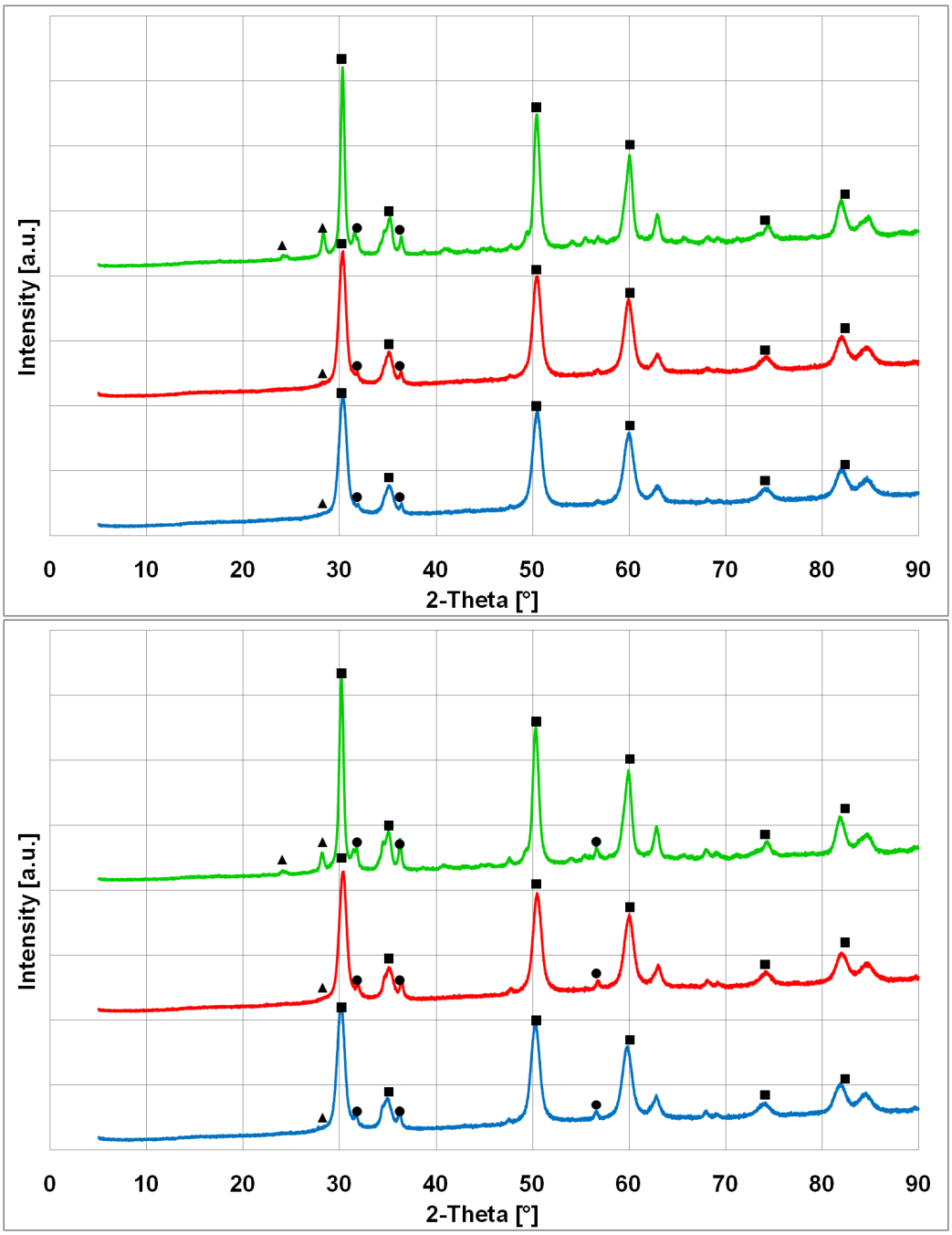


Figure 6.6: The XRD pattern for 10 wt% ZnO on $ZrO_2$ (above) and 15 wt% ZnO on $ZrO_2$ (below), calcinated at 400 °*C* (blue), 600 °*C* (red) and 800 °*C* (green). ● shows ZnO reflexes, ■ shows $ZrO_2$ and ▲ shows reflexes of $ZnZrO_3$.

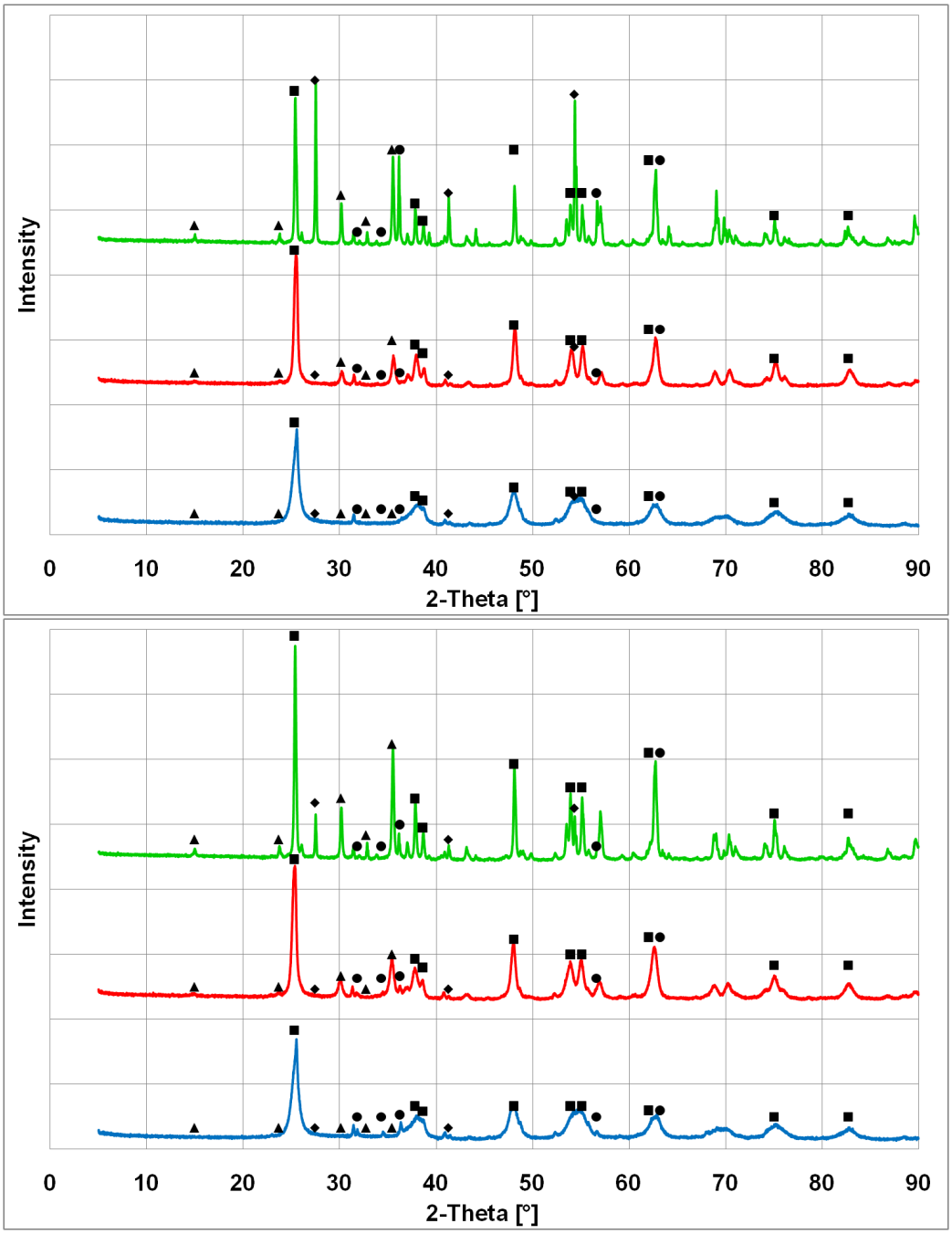


Figure 6.7: The XRD pattern for 10 wt% ZnO on $TiO_2$ (above) and for 15 wt% ZnO on $TiO_2$ (below), calcinated at 400 °*C* (blue), 600 °*C* (red) and 800 °*C* (green). ● shows ZnO reflexes, ■ shows anatase-$TiO_2$, ♦ shows rutil-$TiO_2$ reflexes and ▲ shows reflexes of $ZnTiO_3$.

#### 6.3.4.3 ZnO on Alumina

The XRD pattern for 10 and 15 wt% ZnO/$\gamma$-$Al_2O_3$ are shown in Figure 6.8. Reflexes with a relatively weak intensity indicate the formation of $ZnAl_2O_4$ already at 400 $°C$, i.e. it should already form during the preparation procedure. The reflexes for the spinel phase $ZnAl_2O_4$ are growing with temperature. This can be well seen for the reflexes at 32° and around 36°.Generally spoken the crystal size does not grow in the same manner as could be seen in the samples before. The growing and sharpening of reflexes is weaker and in the same way the reduction of BET surface is small, see Table 6.7, however, it is not as drastic as observed for ZnO on $ZrO_2$ or $TiO_2$. Alike for ZnO/$ZrO_2$ and ZnO/$TiO_2$, the reduction of BET surface area is much more severe under reaction conditions (see Table 6.4) than under calcination in air (see Table 6.7), indicating a strong impact of the reaction gas mixture.

The XRD patterns for the $\gamma$-$Al_2O_3$ indicate that the phase transformation from the $\gamma$ to the $\delta$ phase has started, which is in accordance to the literature [295].

Table 6.7: BET surface area for the ZnO/$\gamma$-$Al_2O_3$ samples after calcination at temperatures according to the XRD measurements.

| **Catalyst** | **10 wt% ZnO/$\gamma$-$Al_2O_3$** | **15 wt% ZnO/$\gamma$-$Al_2O_3$** |
|---|---|---|
| 400 $°C$ | 95.5 $m^2/g$ | 92.3 $m^2/g$ |
| 600 $°C$ | 91.3 $m^2/g$ | 88.1 $m^2/g$ |
| 800 $°C$ | 89.6 $m^2/g$ | 85.7 $m^2/g$ |

#### 6.3.4.4 ZnO on Silica

The XRD pattern for 10 and 15 wt% ZnO/$SiO_2$ are shown in Figure 6.9. The pattern for 10 wt% ZnO/$SiO_2$ is amorphous without any distinct reflexes, neither for ZnO nor for $SiO_2$. Structural changes due to the calcination at higher temperatures were not detected. The 15 wt% ZnO/$SiO_2$ is also amorphous after calcination at 400 and 600 $°C$. After calcination at 800 $°C$, however, new reflexes appear. They can be assigned to $SiO_2$ and to $Zn_2SiO_4$, indicating a restructuring of the support material and the reaction of the supported metal oxide with the support material. Strong ZnO reflexes could not be found due to the preferred formation of $Zn_2SiO_4$ instead of ZnO. A few reflexes are caused by the superposition of $SiO_2$ and $Zn_2SiO_4$, they are not specifically mentioned. The $SiO_2$ phase appears as $\alpha$-cristobalite. The BET surface area for 10 and 15 wt% ZnO/$SiO_2$ is shown in Table 6.8. There is no significant loss for the 10 wt% sample, which is congruent with the XRD, which also does not show a signifcant change. For the the 15 wt%

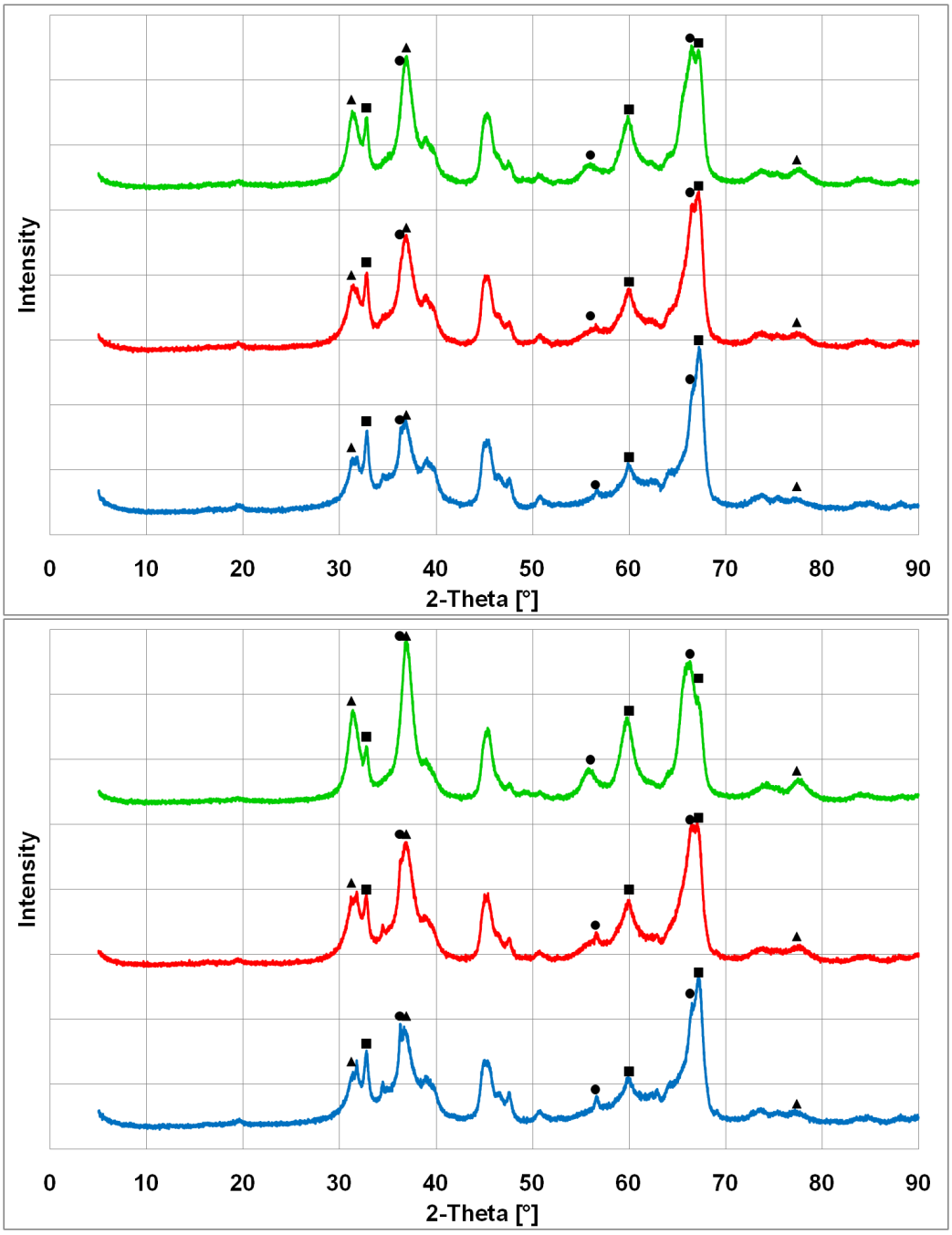


Figure 6.8: The XRD pattern for 10 wt% ZnO on $\gamma$-$Al_2O_3$ (above) and for 15 wt% ZnO on $\gamma$-$Al_2O_3$ (below), calcinated at 400 °*C* (blue), 600 °*C* (red) and 800 °*C* (green). ● shows ZnO reflexes, ■ shows $\gamma$-$Al_2O_3$ reflexes and ▲ shows reflexes of $ZnAl_2O_4$.

sample the decrease in specific surface area is small, indicating a rather high thermal stability of this catalyst. Unlike for the previous samples, the BET surface area obtained after the screening and after calcination in air does not differ significantly, indicating that the reaction gas mixture does not have a strong influence on the catalyst.

Table 6.8: BET surface area for the $ZnO/SiO_2$ samples after calcination at temperatures according to the XRD measurements.

| **Catalyst** | **10 wt% $ZnO/SiO_2$** | **15 wt% $ZnO/SiO_2$** |
|---|---|---|
| 400 $°C$ | 79.0 $m^2/g$ | 67.4 $m^2/g$ |
| 600 $°C$ | 80.7 $m^2/g$ | 68.4 $m^2/g$ |
| 800 $°C$ | 77.4 $m^2/g$ | 63.8 $m^2/g$ |

### 6.3.5 Discussion of the Active Component

For ZnO on $ZrO_2$ and $TiO_2$, the formation of Zn-zirconate and Zn-titanate should already occur during the preparation, as the applied calcination temperature of 450 $°C$ is already higher than the temperature required for their formation. For these two support materials, lower loadings of ZnO gave a higher conversion than higher loadings, especially in the ODP. This could be due to a high dispersions of ZnO and therefore also due to a high dispersion of the formed Zn-zirconate and Zn-titanate. This is well in agreement of the observed XRD patterns, as the intensity of the Zn-zirconate and Zn-titanate is small and width of the signals is broad. For the ODE and the OCM, the dispersion effect is not very distinct. However, at the temperatures applied for these reactions, further deactivation reactions occur, which can be considered having a stronger impact than the dispersion effect.

For $ZnO/\gamma$-$Al_2O_3$ the formation of Zn-aluminates is observed at 400 $°C$, indicating that it also forms during the preparation. However, the activity of the catalysts seems to be independent of the actual ZnO loading and of the amount of catalyst loaded into the reaction. The observed activity of $ZnO/\gamma$-$Al_2O_3$ can therefore be assigned to the activity $\gamma$-$Al_2O_3$.

A similar effect is found for $ZnO/SiO_2$. The observed conversion is independent of the ZnO loading and of the amount of catalyst in the reactor, indicating that the activity can also be attributed to the pure support. However, due to the amorphous XRD patterns, it remains unclear if $Zn_2SiO_4$ forms already at lower temperatures, as it does for the other materials.

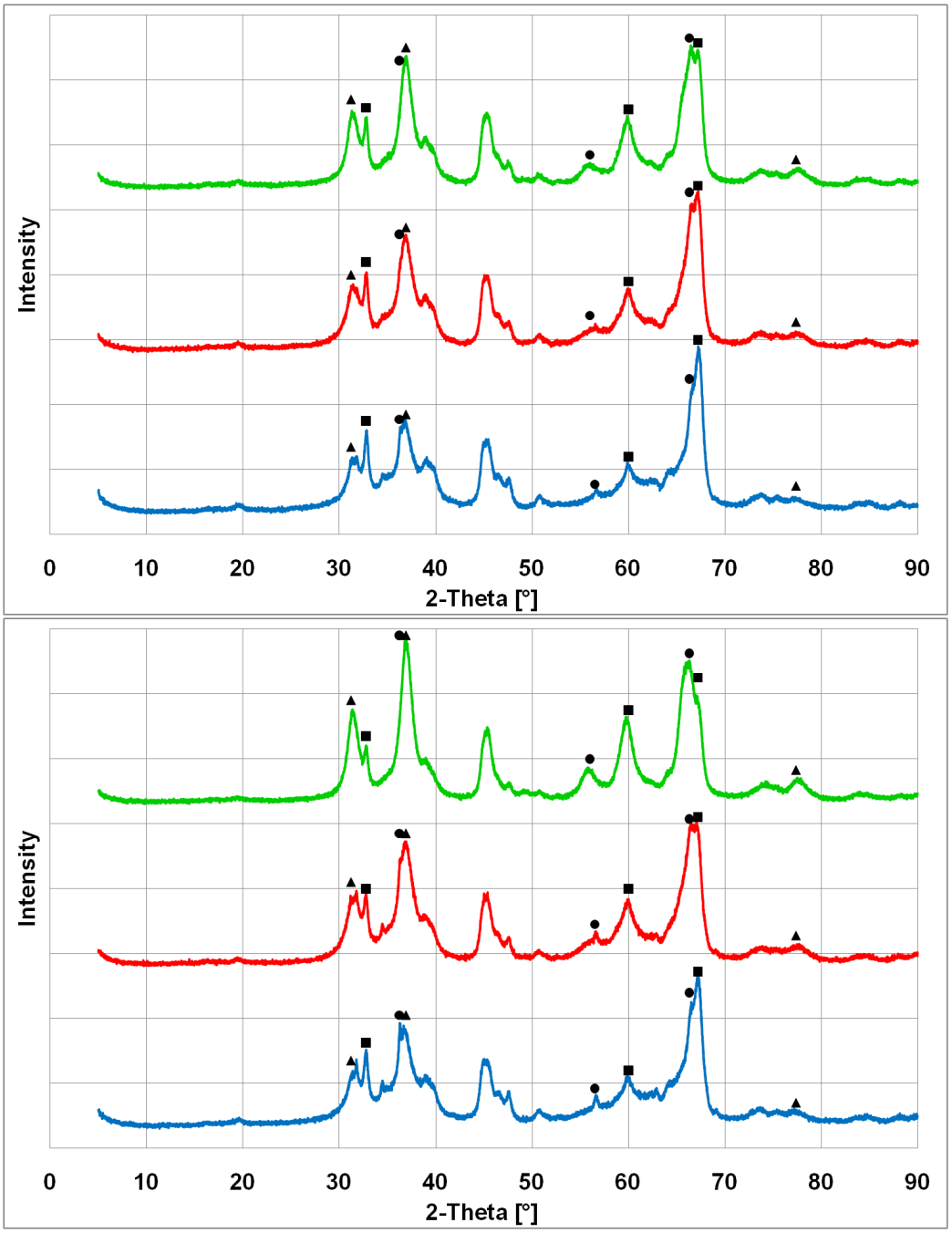


Figure 6.9: The XRD pattern for 10 wt% ZnO on $SiO_2$ (above) and for 15 wt% ZnO on $SiO_2$ (below), calcinated at 400 °*C* (blue), 600 °*C* (red) and 800 °*C* (green). The 10 wt% ZnO on $SiO_2$ sample is amorphous. However, for the 15 wt% ZnO on $SiO_2$, zinc silicate formation is found, the ▲ are reflexes of $Zn_2SiO_4$. The ● are ZnO reflexes, ■ are $SiO_2$ reflexes.

### 6.3.6 Longterm Stability

For any commercial application, the longterm stability is crucial and a comparison of the BET surface areas obtained after the screening and after calcination in air, indicate a strong impact of the reaction gas mixture on the deactivation. Therefore, time on stream experiments for 18 hours were conducted with one loading of each support material. However, the measured ZnO loading of the catalysts partly differ significantly from the calculated values. To ensure a good comparability of the results, the measured loading closest to 10 wt% ZnO was choosen for the stability experiment. The denomination remains unchanged and the loaded amount of catalysts is as described the experimental part. The used catalysts were

1. pure commercial ZnO,
2. 10 wt% $ZnO/ZrO_2$
3. 15 wt% $ZnO/TiO_2$,
4. 15 wt% $ZnO/\gamma$-$Al_2O_3$ and
5. 10 wt% $ZnO/SiO_2$.

#### 6.3.6.1 Oxidative Coupling of Methane

The results for the time on stream experiments for the oxidative coupling of methane are shown in Figure 6.10. It is evident, that the $CH_4$ conversion of pure ZnO is reduced from 10 % to nearly 2 % after 18 hours time on stream. The $C_2$ selectivity is the highest among all the tested catalysts. That no drastic change in $C_2$ selectivity is observed for ZnO indicates that only the number of active sites is being reduced and that no severe change of the catalysts occurs. $ZnO/\gamma$-$Al_2O_3$ and $ZnO/ZrO_2$ show a stable $CH_4$ conversion, the latter one with an inital activation period. However, their $C_2$ selectivity is very low, i.e. they are favor the total oxidation rather than the partial oxidation. $ZnO/TiO_2$ exhibits a signifcant reduce in $CH_4$ conversion and an increase in $C_2$ selectivity, indicating that the performance is not stable. Moreover, its main activity is the total oxidation of $CH_4$. $ZnO/SiO_2$ shows a relatively low conversion of $CH_4$ and strong deactivation, however, the selectivity raises constantly from 5 % at the beginning of the experiment until more than 15 % after 18 hours time on stream.

#### 6.3.6.2 Oxidative Dehydrogenation of Ethane

The results for the time on stream experiments for the oxidative dehydrogenation of ethane are shown in Figure 6.11. The results are similar to those observed for

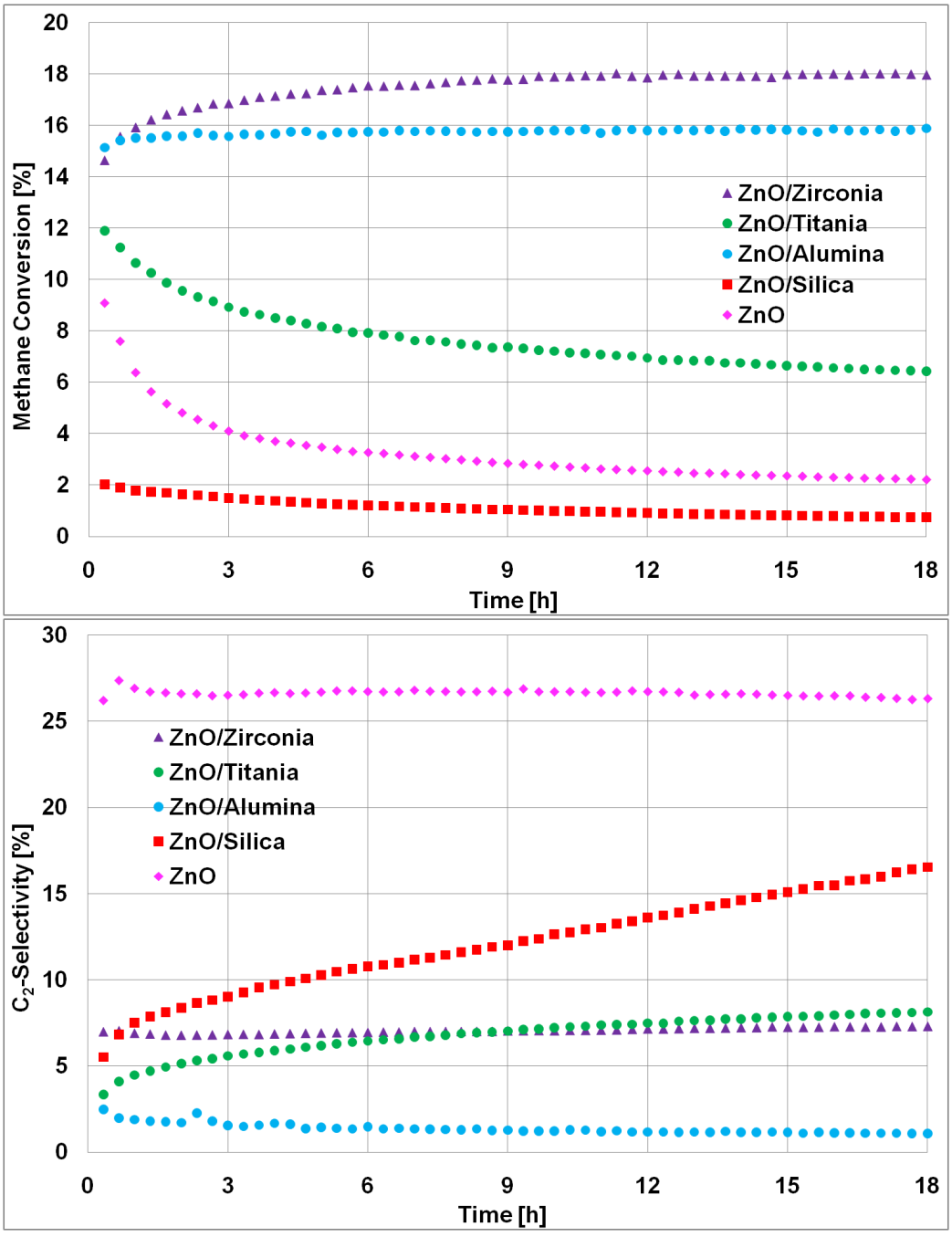


Figure 6.10: The $CH_4$ conversion (above) and $C_2$ selectivity (below) for the time on stream experiment for the OCM. Reaction conditions: gas flow 60 ml/min, 700 °*C*.

the oxidative coupling of methane, described in paragraph 6.3.6.1. ZnO/$\gamma$-$Al_2O_3$ and ZnO/$ZrO_2$ are stable catalysts, but their $C_2H_4$ selectivity is low. They are mainly total oxidation catalysts. ZnO/$TiO_2$ is also stable, with a $C_2H_4$ selectivity of approximately 30 %. Pure ZnO and ZnO/$SiO_2$ exhibit rather low conversions, at high selectivities. The gap in the selectivity trajectorie of ZnO is due to the small conversion. Alike for the OCM, ZnO/$SiO_2$ exhibits a significantly increasing selectivity with time on stream.

#### 6.3.6.3 Oxidative Dehydrogenation of Propane

The results for the time on stream experiments for the oxidative dehydrogenation of propane are shown in Figure 6.12. From 0 to 7 hours time on stream, the reactor temperature was 450 $^{\circ}C$. In this temperature range only pure ZnO and ZnO/$SiO_2$ were stable catalysts, however, at $C_3H_8$ conversions of 1 % and below. The other three catalysts exhibit a deactivation behavior, already at such a low temperature. The most significant reduce in $C_3H_8$ conversion is observed for ZnO/$TiO_2$, together with a relatively small increase in selectivity. Except for ZnO/$SiO_2$ and ZnO/$TiO_2$, all catalysts are more or less total oxidation catalysts.

Increasing the temperature to 475 $^{\circ}C$ after 7 hours time on stream and to 500 $^{\circ}C$ after 14 hours time on stream, leads to the same pattern, only at higher $C_3H_8$ conversions. Pure ZnO and ZnO/$SiO_2$ are again stable, at small $C_3H_8$ conversions and medium and high $C_3H_6$ selectivities, respectively. All the other catalysts suffer from deactivation, indicated by a reduced $C_3H_8$ conversion, accompanied by small increases of selectivity.

Remarkable, the dependency of the $C_3H_6$ selectivity on the reaction temperature is different for each catalyst.

## 6.4 Summary and Conclusion

ZnO was supported on commercial supports such as $ZrO_2$, $TiO_2$, $\gamma$-$Al_2O_3$ and $SiO_2$ and the activity for the C-H activation was methane, ethane and propane was tested. A screening of all prepared catalysts exhibited, that for ZnO on $ZrO_2$ and $TiO_2$ the dispersion dominates the activity. However, for ZnO on $\gamma$-$Al_2O_3$ and $SiO_2$, the support material seems to dominate the activity, with total oxidation activity for $\gamma$-$Al_2O_3$ and low conversions at high selectivities for $SiO_2$. Generally, the support material dominates the catalytic performance more than the loading of ZnO.

Moreover, XRD measurements after calcination of the prepared catalyst in air revealed, that zirconates, titanates, aluminates and silicates formed, giving evidence, that the ZnO reacts with the support material. For $ZrO_2$ and $TiO_2$, this

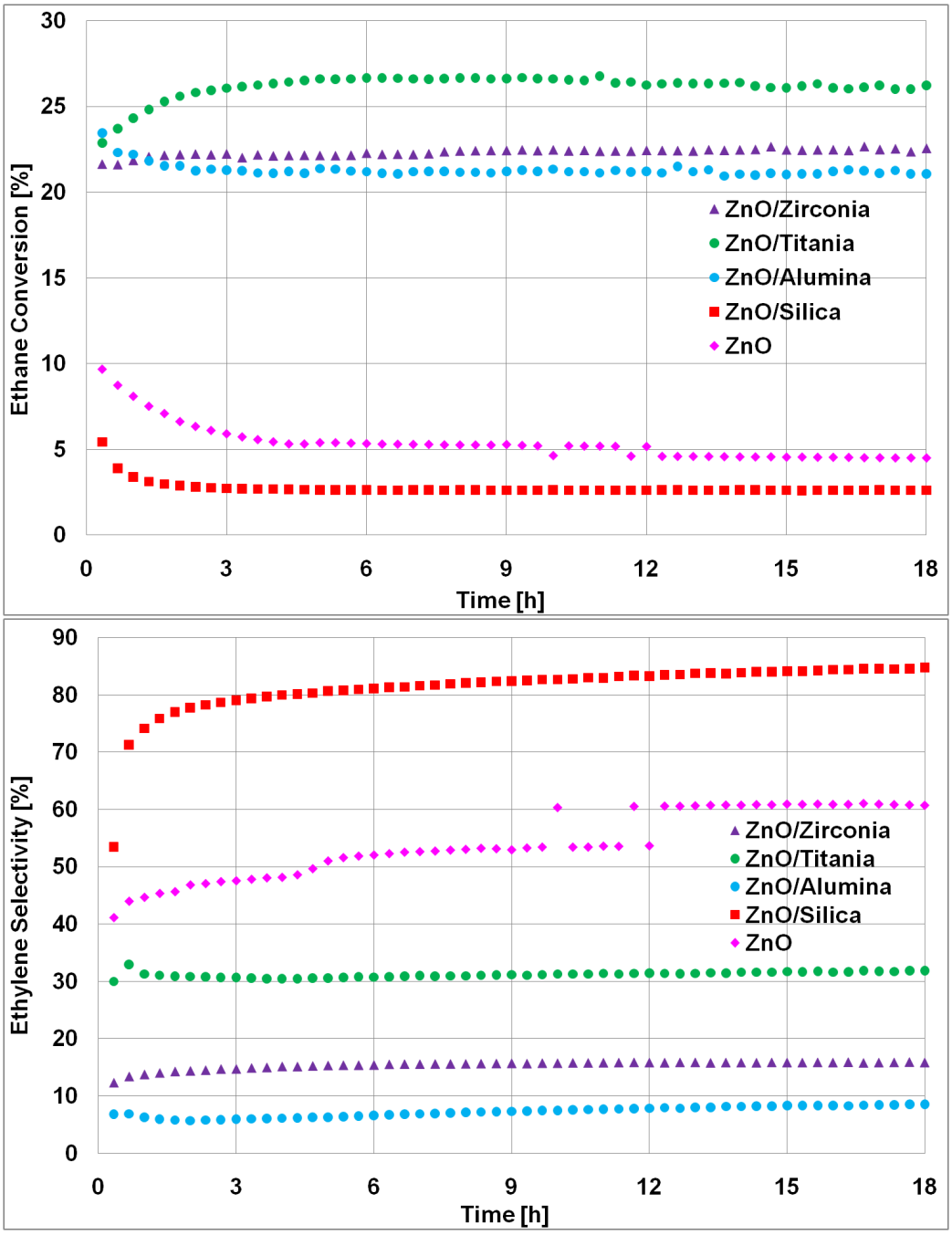


Figure 6.11: The $C_2H_6$ conversion (above) and $C_2$ selectivity (below) for the time on stream experiment for the ODE. Reaction conditions: gas flow 30 ml/min, 600 $^{\circ}C$.

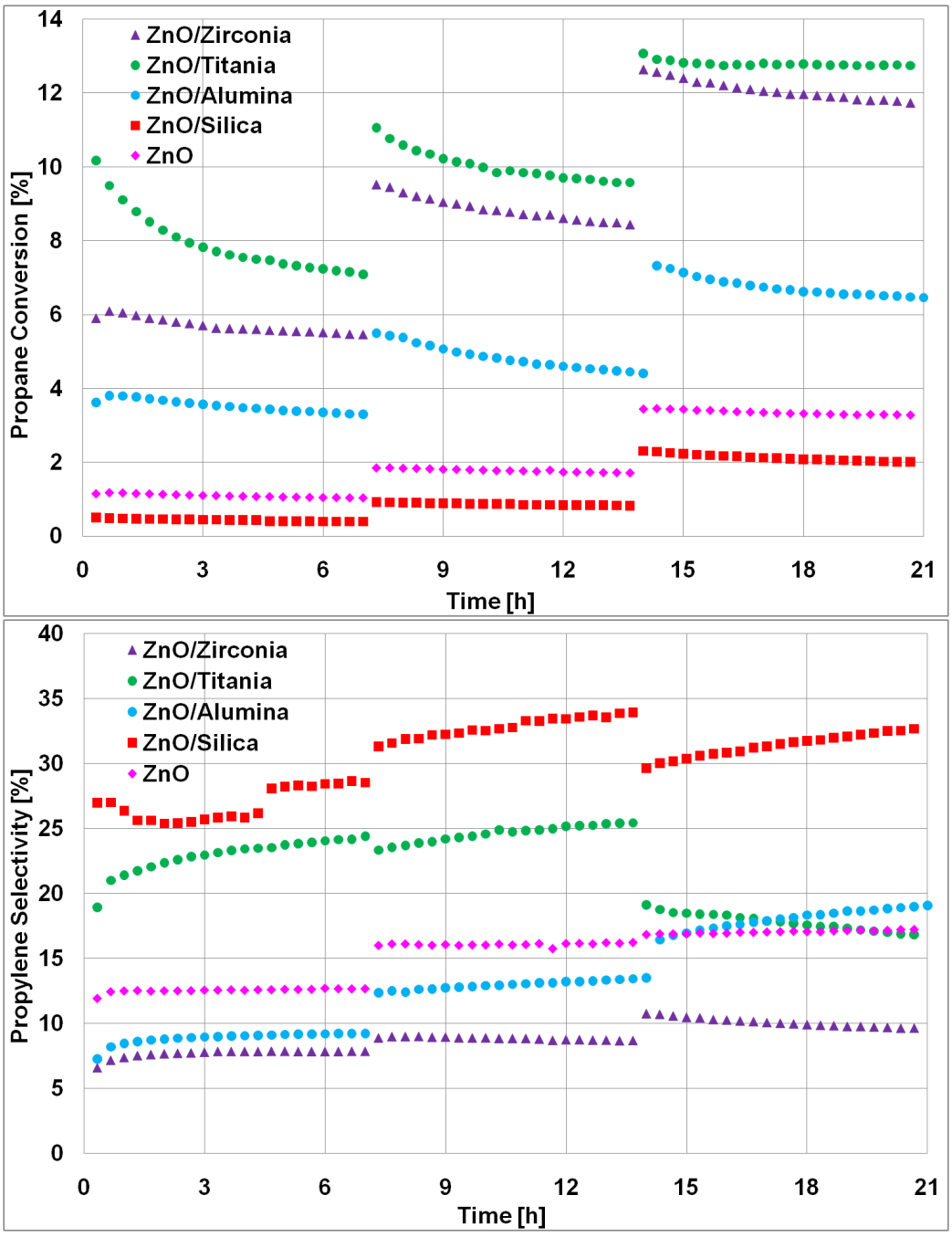


Figure 6.12: The $C_3H_8$ conversion (above) and $C_2$ selectivity (below) for the time on stream experiment for the ODP. After 7 hours the temperature is increased from 450 to 475 $^{\circ}C$, and after 14 hours from 475 to 500 $^{\circ}C$, at a gas flow of 30 ml/min.

reaction can be observed for temperatures that are below the required reaction temperatures. Since the zirconates, titanates, aluminates and silicates were detected via XRD, a bulk method, it can be concluded, that relatively large amounts must have formed.

Stability tests for selected catalysts for the oxidative coupling of methane and the oxidative dehydrogenation of ethane and propane revealed that even at low temperatures such as $450\,^{\circ}C$, a deactivation can be observed which is in agreement with the structural analysis. For ZnO on $\gamma$-$Al_2O_3$ and $SiO_2$, the deactivation is caused by the reaction gas mixture rather than sintering of the support or reaction of support and ZnO. For ZnO on $ZrO_2$ and $TiO_2$, the picture is not so clear because all three factors contribute, however, the dominating factor remains unknown.

The prepared catalysts are never ZnO on a support material. It is always, ZnO, support material and at least one mixed phase. This might very well be a general phenomenon for catalysis at elevated temperatures.

Preparing ZnO on thermally stable supports did therefore not lead to a thermally stable catalytic system. A possible solution for this specific problem, could be the preparation of ZnO-saturated support materials such as Zn-Silicates etc., with subsequent supporting of ZnO. On these kind of supports the ZnO should have no possibility to react with the support material. However, detailed work on the phase diagrams and the stability of the possible support materials is necessary.

# Chapter 7

# Conclusion

In this work, the stability and catalytic performance of Li/MgO as catalyst for the oxidative coupling of methane has been investigated. Due to reams of publications on Li/MgO, the existing literature has been critically reviewed and summarized. First of all, in many publications the stability has been neglected and the statements about the stability of Li/MgO which is crucial for any kind of practical application is inconsistent. Moreover, the reported catalytic activity differs severely. Therefore, catalysts with a loading of Li of 0, 0.5, 1, 2, 4, and 8 wt% were prepared via 4 different preparative routes, namely: decomposition of single source precursors, wet impregnation, precipitation and mixed milling. With a feed gas composition of $CH_4$:$O_2$:$N_2$ = 4:1:4 and a reaction temperature of 750 $^{\circ}C$, stability tests were performed for 40 hours time on stream. All materials suffered from a severe and drastic deactivation, especially at the beginning of the testing experiments, and none of the prepared catalysts were stable. Additionally, none of the catalysts reached a stable range during the experiment, indicating that the steady state is far beyond 40 hours time on stream. Stability experiments with different flow rates and at lower reaction temperatures exhibited the same deactivation phenomena.

Publications that reported Li/MgO as a stable catalyst always applied a large amount of inert dilutent in the feed gas. In contrast, publications dealing with the deactivation of Li/MgO did not make use of larger amounts of dilutents. Therefore, it can be concluded that the deactivation can be suppressed by using dilutents. However, under realistic conditions, the Li/MgO catalyst is unstable, irrespective of the preparation procedure and the reaction temperature. Therefore, Li/MgO is not a suitable catalysts for an industrial application.

The initial activity of the catalysts was strongly dependent on the preparation procedure. However, the residual activity after 40 hours time on stream did not scatter strongly anymore. It can be expected that in steady state the activity of all materials is approximately the same. In many publications the deactivation has

not been considered and the published catalytic performance was usually recorded within the first few hours time on stream. However, during this time the deactivation was observed to be the most severe and small differences in time lead to strong differences in recorded catalytic activity. This effect explains the vast difference in the published results.

For the materials with a Li loading of 0.5 wt%, structural analysis was done after 1, 3, 7, 14 and 24 hours time on stream. The major structural changes, such as loss of Li and particle growth, occurred within the first hour time on stream. After 3 hours time on stream only small structural changes occurred. Furthermore, a correlation between the change in catalytic activity and the physical properties of Li/MgO was not found, indicating that the deactivation follows a complicated mechanism which is not yet fully understood. However, experiments with different flow rates and temperatures showed that this mechanism is strongly influenced by the reaction conditions. The catalytic activity seems to be unaffected by the Li content, because within after approximately 3 hours time on stream the loss of Li is nearly completed, but the deactivation continuous.

The analysis of the Li content after 24 hours time on stream, showed a residual between 0.01 and 0.03 wt% Li, which Anderson and Norby determined to be the thermodynamic solubility of Li in the MgO [90]. The loss of Li and the residual content of Li appeared also to be independent of the preparation procedure. It remains unclear if the residual Li content is stable. One reason for the loss of Li is the formation of LiOH, during the reaction of Li compounds with the reaction product $H_2O$. But at longer periods of time on stream, the activity of the catalysts is usually very low so that hardly any $H_2O$ is formed. The effect of $H_2O$ has already been reported as detrimental to the catalyst stability, indicating a suicidal behavior of any active Li/MgO catalyst.

Lunsford *et al.* proposed $[Li^+O^-]$ as the active center of Li/MgO, based on the correlation of the intensity of the EPR signal at $g = 2.054$, which he assigned to $[Li^+O^-]$, increasing with increased loadings of Li and a concomitantly increased the formation rate of methyl radicals. This correlation was considered to be the evidence for $[Li^+O^-]$ as actice center [20, 21, 209]. In this work it was shown that Li/MgO is not a stable catalyst. Moreover, it was shown that the Li is not stable on or in the MgO and it is lost within a short period of time. Therefore, it is doubtful that the correlation between the intensity of the EPR signal, the Li loading and the methyl radical formation rate is reasonable. Thus, it can be concluded that $[Li^+O^-]$ is not the active center. This is further supported by the successful poisoning experiment with $H_2S$. This raises strong doubts if Li is really involved in the active center of Li/MgO, because Li cannot from stable sulfides. When $[Li^+O^-]$ is not the active center it can be concluded, that the reaction mechanism for the OCM as proposed by Lunsford (shown in Figure 2.8) is wrong. This conclusion additionally supported by the works of Yates

and Zlotin [150] shows that the gas phase contribution is large and the experiments with isotopic labeled reactants, indicating that the C-H bond breaking occurs in the gas phase [187, 193, 195, 184, 296] rather than on the catalyst as proposed by Lunsford.

Zinc oxide was considered to be an alternative for Li/MgO. The existing literature on ZnO in the activation of methane, ethane and propane is scarce. The stability of ZnO catalysts is also not described in the literature. Experiments with ZnO - pure and Li doped - revealed the instability of this material already at the rather low temperatures of the ODP, irrespective of the preparation procedure. The application of commercial supports such as $ZrO_2$, $TiO_2$, $Al_2O_3$ and $SiO_2$ did not lead to any improvements. The reasons were that the activity is mainly determined by the support. Moreover, except for ZnO on $SiO_2$, the total oxidation activity of the prepared materials was dominating. Stability tests outside the reactor showed that the ZnO reacts with the support materials. For $ZrO_2$ and $TiO_2$, the formation of Zn-zirconates and Zn-titanates was observed already $400\,^{\circ}C$, which is below the temperature required for the oxidative dehydrogenation of propane. The formation of Zn-zirconates and Zn-titanates was accompanied by particle growth and reduce in specific surface area, adding to the instability. All prepared catalysts suffered from a more severe deactivation when exposed to the reaction gas mixture compared to deterioration experiments in air. A solution for these problems could be the application of support materials that are saturated with ZnO, such as zinc silicate, zinc aluminate, etc., in order to prevent possible reactions of the zinc with the support material. However, the reaction of the supported catalyst with the support material could be a general problem, which is not limited to zinc oxide.

Reviewing the literature on OCM catalysts, it becomes evident that the stability of the catalysts, not only of Li/MgO is a neglected factor. The reaction temperature of the OCM is high, resulting in thermal stress on the catalyst. Additionally, the reaction gas mixture is reducing and it contains $H_2O$, also gnawing on the catalyst's stability as it has been shown for supported zinc oxide. Future research on the oxidative coupling of methane needs to investigate the stability of the catalyst under realistic conditions, prior to any other experiments; because in case of an instable catalyst the obtained data in kinetic and characterization experiments is only one point on the deactivation trajectory.

# Bibliography


[1] BP. Bp Statistical Review of World Energy June 2008. Online, 2008.

[2] J. Lunsford. *Catalysis Today*, 63:165–174, 2000.

[3] G. Keller and M. Bhasin. *Journal of Catalysis*, 73:9–19, 1982.

[4] W. Hinsen and M. Baerns. *Chemiker-Zeitung*, 107:223–226, 1983.

[5] E. Wolf, editor. Methane Conversion by Oxidative Processes - Fundamental and Engineering Aspects. Van Nostrand Reinhold, 1992.

[6] M. Bhasin and D. Slocum, editors. Methane and Alkane Conversion Chemistry. Plenum Press, 1995.

[7] E. Kondratenko and M. Baerns. Handbook of Heterogeneous Catalysis, chapter 13.17 Oxidative Coupling of Methane, 3010–3023. Wiley-VCH Verlag GmbH & Co. KGaA, 2 edition, 2008.

[8] M. Baerns. *Catalysis Today*, 1:357–363, 1987.

[9] M. Baerns and J. Ross. Perspectives in Catalysis, chapter Catalytic chemistry of methane conversion, 315–335. IUPAC International Union of Pure and Applied Chemistry, 1992.

[10] L. Mleczko and M. Baerns. *Fuel Processing Technology*, 42:217–248, 1995.

[11] A. Maitra. *Applied Catalysis A: General*, 104:11–59, 1993.

[12] C. Batiot and B. Hodnett. *Applied Catalysis A: General*, 137:179–191, 1996.

[13] S. Blanksby and G. Ellison. *Accounts of Chemical Research*, 36:255–263, 2002.

[14] I. Matsuura, Y. Utsumi, M. Nakai and T. Doi. *Chemistry Letters*, 11:1981–1984, 1986.

[15] H. Zhang, J. Wang, D. Driscoll and J. Lunsford. *Journal of Catalysis*, 112:366–374, 1988.

[16] H. Zhang, J. Wang, D. Driscoll and J. Lunsford. *Abstracts Of Papers Of The American Chemical Society*, 194:242–248, 1987.

[17] A. Maitra, I. Campbell and R. Tyler. *Applied Catalysis A: General*, 85:27–46, 1992.

[18] Z. Zhang, X. Verykios and M. Baerns. *Catalysis Reviews: Science and Engineering*, 36:507–556, 1994.

[19] T. Ito and J. Lunsford. *Nature*, 314:721–722, 1985.

[20] T. Ito, J. Wang, C. Lin and J. Lunsford. *Journal of the American Chemical Society*, 107:5062–5068, 1985.

[21] D. Driscoll, W. Martir, J. Wang and J. Lunsford. *Journal of the American Chemical Society*, 107:58–63, 1985.

[22] C. Lin, T. Ito, J. Wang and J. Lunsford. *Journal of the American Chemical Society*, 109:4808–4810, 1987.

[23] E. Iwamatsu, T. Moriyama, N. Takasaki and K. Aika. *Studies in Surface Science and Catalysis*, 36:373–382, 1988.

[24] E. Iwamatsu, T. Moriyama, N. Takasaki and K. Aika. *Journal of Catalysis*, 113:25–35, 1988.

[25] E. Iwamatsu and K. Aika. *Journal of Catalysis*, 117:416–431, 1989.

[26] V. Choudhary, S. Pataskar, M. Pandit and V. Gunjikar. *Thermochimica Acta*, 180:69–80, 1991.

[27] V. Choudhary, V. Rane and M. Pandit. *Journal of Chemical Technology & Biotechnology*, 68:177–186, 1997.

[28] S. Korf, J. Roos, N. de Bruijn, J. van Ommen and J. Ross. *Catalysis Today*, 2:535–545, 1988.

[29] I. Matsuura, Y. Utsumi and T. Doi. *Applied Catalysis*, 47:299–306, 1989.

[30] V. Choudhary, S. Chaudhari and M. Pandit. *Journal of the Chemical Society, Chemical Communications*, 1158–1159, 1991.

[31] J. Camino, M. Holgado and V. Rives. *Reaction Kinetics and Catalysis Letters*, 44:469–473, 1991.

[32] J. Camino, M. Holgado and V. Rives. *Reaction Kinetics and Catalysis Letters*, 45:35–39, 1991.

[33] M. Holgado, V. Rives and S. San Roman. *Reaction Kinetics and Catalysis Letters*, 48:455–460, 1992.

[34] V. Choudhary, S. Mulla, M. Pandit, S. Chaudhari and V. Rane. *Journal of Chemical Technology & Biotechnology*, 75:828–834, 2000.

[35] Y. Kuo, F. Behrendt and M. Lerch. *Zeitschrift für Physikalische Chemie*, 221:1017–1037, 2007.

[36] T. Lopez, I. Garcia-Cruz and R. Gómez. *Journal of Catalysis*, 127:75–85, 1991.

[37] T. López, R. Gómez, A. Ramírez-Solís, E. Poulain and O. Novaro. *Journal of Molecular Catalysis*, 88:71–84, 1994.

[38] R. Gómez, T. López, L. Herrera, A. Castro, O. Scelza, G. Baronetti, E. Lazzari, A. Cuan, M. Campos, E. Poulain, A. Ramirez-Solis and O. Novaro. *Studies in Surface Science and Catalysis*, 75:2213–2216, 1993.

[39] C. Trionfetti, I. Babich, K. Seshan and L. Lefferts. *Applied Catalysis A: General*, 310:105–113, 2006.

[40] C. Trionfetti, I. Babich, K. Seshan and L. Lefferts. *Topics in Catalysis*, 39:191–198, 2006.

[41] G. Roussy, E. Marchal, J. Thiebaut, A. Kiennemann and G. Maire. *Fuel Processing Technology*, 50:261–274, 1997.

[42] C. Chevalier, P. Ramirez de la Piscina, M. Ceruso, A. Choplin and J. Basset. *Catalysis Today*, 4:433–439, 1989.

[43] S. Heitz, Y. Aksu, C. Merschjann and M. Driess. *Chemistry of Materials*, 22:1376–1385, 2010.

[44] S. Heitz, J. Epping, Y. Aksu and M. Driess. *Chemistry of Materials*, 22:4563–4571, 2010.

[45] T. Berger, J. Schuh, M. Sterrer, O. Diwald and E. Knözinger. *Journal of Catalysis*, 247:61–67, 2007.

[46] G. Martin, P. Turlier, V. Ducarme, C. Mirodatos and M. Pinabiau. *Catalysis Today*, 6:373–380, 1990.

[47] H. Sarkas, S. Arnold, J. Hendricks, L. Kidder, C. Jones and K. Bowen. *Zeitschrift für Physik D Atoms, Molecules and Clusters*, 26:46–50, 1993.

[48] V. Choudhary, S. Mulla and B. Uphade. *Journal of Chemical Technology & Biotechnology*, 72:99–104, 1998.

[49] U. Zavyalova, F. Girgsdies, O. Korup, R. Horn and R. Schlögl. *Journal of Physical Chemistry C*, 113:17493–17501, 2009.

[50] U. Zavyalova, M. Geske, R. Horn, G. Weinberg, W. Frandsen, M. Schuster and R. Schlögl. *ChemCatChem*, Accepted, 2010.

[51] M. Baerns. Methane Conversion by Oxidative Processes, chapter 11. Basic Solids as Catalysts for the Oxidative Coupling of Methane, 382–402. Van Nostrand Reinhold, 1992.

[52] P. Käßner and M. Baerns. *Applied Catalysis A: General*, 139:107–129, 1996.

[53] A. Davydov, M. Shepotko and A. Budneva. *Catalysis Today*, 24:225–230, 1995.

[54] A. Davydov. *Chemical Engineering & Technology*, 18:7–11, 1995.

[55] S. Kus, M. Otremba, A. Tórz and M. Taniewski. *Applied Catalysis A: General*, 230:263–270, 2002.

[56] S. Kus and M. Taniewski. *Fuel Processing Technology*, 76:41–49, 2002.

[57] M. Bailly, C. Chizallet, G. Costentin, J. Krafft, H. Lauron-Pernot and M. Che. *Journal of Catalysis*, 235:413–422, 2005.

[58] C. Chizallet, G. Costentin, H. Lauron-Pernot, M. Che, C. Bonhomme, J. Maquet, F. Delbecq and P. Sautet. *Journal of Physical Chemistry C*, 111:18279–18287, 2007.

[59] C. Chizallet, H. Petitjean, G. Costentin, H. Lauron-Pernot, J. Maquet, C. Bonhomme and M. Che. *Journal of Catalysis*, 268:175–179, 2009.

[60] V. Choudhary, V.-H. Rane and S. Chaudhari. *Catalysis Letters*, 6:95–98, 1990.

[61] V. Díez, C. Apesteguía and J. Di Cosimo. *Catalysis Today*, 63:53–62, 2000.

[62] G. Martin and C. Mirodatos. Methane Conversion by Oxidative Processes, chapter 10. Morphological Aspects of Catalysts for Oxidative Coupling of Methane, 351–381. Van Nostrand Reinhold, 1992.

[63] G. Spoto, E. Gribov, G. Ricchiardi, A. Damin, D. Scarano, S. Bordiga, C. Lamberti and A. Zecchina. *Progress in Surface Science*, 76:71–146, 2004.

[64] V. Choudhary, V. Rane and R. Gadre. *Journal of Catalysis*, 145:300–311, 1994.

[65] V. Choudhary, S. Pataskar, V. Gunjikar and G. Zope. *Thermochimica Acta*, 232:95–110, 1994.

[66] V. Choudhary, S. Pataskar, G. Zope and P. Chaudhari. *Journal of Chemical Technology & Biotechnology*, 64:407–413, 1995.

[67] V. Choudhary and M. Pandit. *Applied Catalysis*, 71:265–274, 1991.

[68] S. Ardizzone, C. Bianchi and B. Vercelli. *Applied Surface Science*, 119:253–259, 1997.

[69] S. Ardizzone, C. Bianchi and B. Vercelli. *Applied Surface Science*, 126:169–175, 1998.

[70] I. Mellor, A. Burrows, S. Coluccia, J. Hargreaves, R. Joyner, C. Kiely, G. Marta, M. Stockenhuber and W. Tang. *Journal of Catalysis*, 234:14–23, 2005.

[71] J. Kimble and J. Kolts. *Chemtech*, 17:501–505, 1987.

[72] J. Lee and S. Oyama. *Catalysis Reviews: Science and Engineering*, 30:249–280, 1988.

[73] J. Kimble and J. Kolts. *Energy Progress*, 6:226–229, 1986.

[74] S. Korf, J. Roos, N. de Bruijn, J. van Ommen and J. Ross. *Applied Catalysis*, 58:131–146, 1990.

[75] J. Galuszka. *Catalysis Today*, 21:321–331, 1994.

[76] A. Turek, I. Wachs and E. DeCanio. *Journal of Physical Chemistry*, 96:5000–5007, 1992.

[77] G. Busca and V. Lorenzelli. *Materials Chemistry*, 7:89–126, 1982.

[78] M. Spencer, J. Lunsford, M. Roberts, J. Cunningham, R. Burch, O. Krylov, J. Moffat, G. Hutchings, R. Joyner, M. Ichi, A. Datye, J. Haber, E. Serwicka and J. Thomas. *Faraday Discussions of the Chemical Society*, 87:47–64, 1989.

[79] G. Hutchings, M. Scurrel and J. Woodhouse. *Catalysis Letters*, 5:301–308, 1990.

[80] J. Hargreaves, G. Hutchings and R. Joyner. *Catalysis Today*, 6:481–488, 1990.

[81] J. Hargreaves, G. Hutchings, R. Joyner and C. Kiely. *Catalysis Today*, 10:259–266, 1991.

[82] J. Hargreaves, G. Hutchings, R. Joyner and C. Kiely. *Journal of Catalysis*, 135:576–595, 1992.

[83] J. Hargreaves, G. Hutchings, R. Joyner and C. Kiely. *Catalysis Today*, 13:401–407, 1992.

[84] D. Lewis, R. Grimes and C. Catlow. *Journal of Molecular Catalysis A: Chemical*, 100:103–114, 1995.

[85] J. Lunsford, M. Cisneros, P. Hinson, Y. Tong and H. Zhang. *Faraday Discussions of the Chemical Society*, 87:13–21, 1989.

[86] V. Choudhary, A. Rajput, D. Akolekar and V. Seleznev. *Applied Catalysis*, 62:171–187, 1990.

[87] V. Choudhary, S. Sansare, A. Rajput and D. Akolekar. *Applied Catalysis*, 69:187–200, 1991.

[88] M. Sinev, V. Bychkov, V. Korchak and O. Krylov. *Catalysis Today*, 6:543–549, 1990.

[89] M. Taniewski, A. Lachowicz, R. Lachowicz, D. Czechowicz and K. Skutil. *Catalysis Letters*, 26:355–363, 1994.

[90] A. Anderson and T. Norby. *Catalysis Today*, 6:575–586, 1990.

[91] S. Mitoff. *Journal of Chemica Physics*, 41:2561–2562, 1964.

[92] J. Haggin. *Chemical & Engineering News*, 68:26–28, 1990.

[93] T. Norby and A. Anderson. *Applied Catalysis*, 71:89–102, 1991.

[94] I. Balint and K. Aika. *Journal of the Chemical Society, Faraday Transactions*, 93:1797–1801, 1997.

[95] I. Balint and K. Aika. *Applied Surface Science*, 173:296–306, 2001.

[96] M. Tardío, R. Ramírez, R. González and Y. Chen. *Physical Review B*, 66:134202, 2002.

[97] I. Balint and K. Aika. *Studies in Surface Science and Catalysis*, 81:177–186, 1994.

[98] I. Balint and K. Aika. *Journal of the Chemical Society, Faraday Transactions*, 91:1805–1811, 1995.

[99] M. Abraham, C. Butler and Y. Chen. *Journal of Chemical Physics*, 55:3752–3756, 1971.

[100] O. Schirmer. *Journal of Physics and Chemistry of Solids*, 32:499–509, 1971.

[101] M. Abraham, W. Unruh and Y. Chen. *Physical Review B*, 10:3540–3545, 1974.

[102] G. Rius and A. Herve. *Solid State Communications*, 15:399–402, 1974.

[103] Y. Chen, H. Tohver, J. Narayan and M. Abraham. *Physical Review B*, 16:5535–5542, 1977.

[104] Y. Chen, E. Montesa, J. Boldú and M. Abraham. *Physical Review B*, 24:5–10, 1981.

[105] J. Narayan, M. Abraham, Y. Chen and H. Tohver. *Philosophical Magazine A*, 38:247–257, 1978.

[106] J. Lacey, M. Abraham, J. Boldu, Y. Chen, J. Narayan and H. Tohver. *Physical Review B*, 18:4136–4142, 1978.

[107] J. Boldu, M. Abraham and Y. Chen. *Physical Review B*, 19:4421–4426, 1979.

[108] D. Olsen, V. Orera, Y. Chen and M. Abraham. *Physical Review B*, 21:1258–1263, 1980.

[109] Y. Chen, M. Abraham, J. Boldu and V. Orera. *Journal de Physique Colloques*, 41-C6:398–400, 1980.

[110] Y. Chen and M. Abraham. *Journal of Physics and Chemistry of Solids*, 51:747–764, 1990.

[111] R. González, Y. Chen and K. Tsang. *Physical Review B*, 26:4637–4645, 1982.

[112] R. González and Y. Chen. *Physical Review B*, 35:8202–8206, 1987.

[113] M. Anpo, M. Sunamoto, T. Doi and I. Matsuura. *Chemistry Letters*, 17:701–704, 1988.

[114] C. Padró, W. Grosso, G. Baronetti, A. Castro and O. Scelza. *Studies in Surface Science and Catalysis*, 82:411–418, 1994.

[115] H. Aritani, H. Yamada, T. Nishio, S. Imamura, S. Hasegawa, T. Tanaka and S. Yoshida. *Chemistry Letters*, 28:359–360, 1999.

[116] H. Aritani, H. Yamada, T. Nishio, T. Shiono, S. Imamura, M. Kudo, S. Hasegawa, T. Tanaka and S. Yoshida. *Journal of Physical Chemistry B*, 104:10133–10143, 2000.

[117] C. Trionfetti, I. Babich, K. Seshan and L. Lefferts. *Langmuir*, 24:8220–8228, 2008.

[118] P. Myrach, N. Nilius, S. Levchenko, A. Gonchar, T. Risse, K. Dinse, L. Boatner, W. Frandsen, R. Horn, H. Freund, R. Schlögl and M. Scheffler. *ChemCatChem*, 2:854–862, 2010.

[119] C. Mirodatos, V. Perrichon, M. Durupty and P. Moral. *Studies in Surface Science and Catalysis*, 34:183–195, 1987.

[120] E. Iwamatsu, T. Moriyama, N. Takasaki and K. Aika. *Journal of the Chemical Society, Chemical Communications*, 19–20, 1987.

[121] V. Perrichon and M. Durupty. *Applied Catalysis*, 42:217–227, 1988.

[122] C. Mirodatos, G. Martin, J. Bertolini and J. Saint-Just. *Catalysis Today*, 4:301–310, 1989.

[123] J. van Kasteren, J. Geerts and K. van der Wiele. *Studies in Surface Science and Catalysis*, 55:343–349, 1990.

[124] S. Korf, J. Roos, N. de Brujin, J. van Ommen and J. Ross. *Journal of the Chemical Society, Chemical Communications*, 1433–1434, 1987.

[125] H. Swaan, Y. Li, K. Seshan, J. van Ommen and J. Ross. *Catalysis Today*, 16:537–546, 1993.

[126] J. Roos, A. Bakker, H. Bosch, J. van Ommen and J. Ross. *Catalysis Today*, 1:133–145, 1987.

[127] G. Hutchings, M. Scurrel and J. Woodhouse. *Studies in Surface Science and Catalysis*, 36:415–419, 1988.

[128] S. Al-Zahrani, Q. Song and L. Lobban. *Industrial & Engineering Chemistry Research*, 33:251–258, 1994.

[129] S. Al-Zahrani, Q. Song and L. Lobban. *Industrial & Engineering Chemistry Research*, 34:1060–1073, 1995.

[130] S. Al-Zahrani and L. Lobban. *Studies in Surface Science and Catalysis*, 100:383–396, 1996.

[131] M. Taniewski, A. Lachowicz and K. Skutil. *Chemical Engineering Science*, 52:935–939, 1997.

[132] J. Roos, S. Korf, A. Bakker, N. de Bruijn and J. van Ommen. *Studies in Surface Science and Catalysis*, 36:427–432, 1988.

[133] X. Peng, D. Richards and P. Stair. *Journal of Catalysis*, 121:99–109, 1990.

[134] G. Hutchings, M. Scurrell and J. Woodhouse. *Journal of the Chemical Society, Chemical Communications*, 1388–1389, 1987.

[135] J. Aigler and J. Lunsford. *Applied Catalysis*, 70:29–42, 1991.

[136] Y. Bi, K. Zheng, Y. Jiang, C. Teng and X. Yang. *Applied Catalysis*, 39:185–190, 1988.

[137] A. Machocki. *Catalysis Letters*, 26:85–93, 1994.

[138] K. Asami, K. Omata, K. Fujimoto and H. Tominaga. *Journal of the Chemical Society, Chemical Communications*, 1287–1288, 1987.

[139] A. Ekstrom, R. Regtop and S. Bhargava. *Applied Catalysis*, 62:253–269, 1990.

[140] G. Lane and E. Wolf. *Journal of Catalysis*, 113:144–163, 1988.

[141] M. Pinabiau-Carlier, A. Ben Hadid and C. Cameron. *Studies in Surface Science and Catalysis*, 61:183–190, 1991.

[142] J. Edwards, R. Tyler and S. White. *Energy & Fuels*, 4:85–93, 1990.

[143] Q. Chen, P. Couwenberg and G. Marin. *AIChE Journal*, 40:521–535, 1994.

[144] Q. Chen, J. Hoebink and G. Marin. *Industrial & Engineering Chemistry Research*, 30:2088–2097, 1991.

[145] K. Parida and S. Rao. *Reaction Kinetics and Catalysis Letters*, 44:95–101, 1991.

[146] K. Aika, N. Fujimoto, M. Kobayashi and Iwamatsu. *Journal of Catalysis*, 127:1–8, 1991.

[147] J. Rynkowski, A. Kaźmierczak, A. Praźmowska-Wilanowski and T. Paryjczak. *Reaction Kinetics and Catalysis Letters*, 58:169–175, 1996.

[148] M. Abraham and Y. Chen. *Physical Review Letters*, 37:849–852, 1976.

[149] D. Driscoll, J. Martir, J. Wang and J. Lunsford. *Studies in Surface Science and Catalysis*, 21:403–408, 1985.

[150] D. Yates and N. Zlotin. *Journal of Catalysis*, 111:317–324, 1988.

[151] H. Liu, R. Liu, K. Liew, R. Johnson and J. Lunsford. *Journal of the American Chemical Society*, 106:4117–4121, 1984.

[152] M. Hatano, P. Hinson, K. Vines and J. Lunsford. *Journal of Catalysis*, 124:557–561, 1990.

[153] D. Yates and N. Zlotin. *Journal of Catalysis*, 124:562–565, 1990.

[154] D. Yates, N. Zlotin and J. McHenry. *Journal of Catalysis*, 117:290–294, 1989.

[155] Z. Kalenik and E. Wolf. Methane Conversion by Oxidative Processes, chapter 2. The Role of Gas-Phase Reactions during Methane Oxidative Coupling, 30–77. Van Nostrand Reinhold, 1992.

[156] G. Hutchings, M. Scurrel and J. Woodhouse. *Journal of the Chemical Society, Chemical Communications*, 253–255, 1988.

[157] G. Hutchings, M. Scurrell and J. Woodhouse. *Journal of the Chemical Society, Chemical Communications*, 1862–1863, 1987.

[158] J. Roos, S. Korf, R. Veehof, J. van Ommen and J. Ross. *Applied Catalysis*, 52:147–156, 1989.

[159] J. Roos, S. Korf, R. Veehof, J. van Ommen and J. Ross. *Applied Catalysis*, 52:131–145, 1989.

[160] J. Lunsford, P. Qiu, M. Rosynek and Z. Yu. *Journal of Physical Chemistry B*, 102:167–173, 1998.

[161] R. Nibbelke, J. Scheerová, M. de Croon and G. Marin. *Journal of Catalysis*, 106:106–119, 1995.

[162] K. Peil, J. Goodwin, Jr. and G. Marcelin. *Journal of Physical Chemistry*, 93:5977–5979, 1989.

[163] K. Peil, J. Goodwin, Jr. and G. Marcelin. *Studies in Surface Science and Catalysis*, 61:73–79, 1991.

[164] K. Peil, J. Goodwin, Jr. and G. Marcelin. *Journal of Catalysis*, 131:143–155, 1991.

[165] I. Dahl, K. Jens, S. Kvisle and Å. Slagtern. *Studies in Surface Science and Catalysis*, 61:81–87, 1991.

[166] V. Choudhary, V. Rane and S. Chaudhari. *Reaction Kinetics and Catalysis Letters*, 63:371–377, 1998.

[167] G. Keulks, N. Liao, W. An and D. Li. *Studies in Surface Science and Catalysis*, 75:2253–2256, 1993.

[168] S. Bhumkar and L. Lobban. *Industrial & Engineering Chemistry Research*, 31:1856–1864, 1992.

[169] M. Nakamura, H. Yanagibashi, H. Mitsuhashi and N. Takezawa. *Bulletin of the Chemical Society of Japan*, 66:2467–2472, 1993.

[170] G. Hutchings, M. Scurrel and J. Woodhouse. *Chemical Society Reviews*, 18:251–283, 1989.

[171] G. Hutchings and M. Scurrel. Methane Conversion by Oxidative Processes, chapter 7. Studies of the Mechanism of the Oxidative Coupling of Methane Using Oxide Catalysts, 200–258. Van Nostrand Reinhold, 1992.

[172] G. Hutchings and J. Woodhouse. *Journal of the Chemical Society, Faraday Transactions 1: Physical Chemistry in Condensed Phases*, 85:2507–2523, 1989.

[173] J. Cunningham and D. McNamara. *Catalysis Today*, 6:551–558, 1990.

[174] G. Hutchings, M. Scurrel and J. Woodhouse. *Journal of the Chemical Society, Chemical Communications*, 765–766, 1989.

[175] G. Hutchings, M. Scurrell and J. Woodhouse. *Catalysis Today*, 6:399–407, 1990.

[176] G. Hutchings, M. Scurrel and J. Woodhouse. *Applied Catalysis*, 38:156–165, 1988.

[177] C. Shi, M. Xu, M. Rosynek and J. Lunsford. *Journal of Physical Chemistry*, 97:216–222, 1993.

[178] H. Yamamoto, H. Chu, M. Xu, C. Shi and J. Lunsford. *Journal of Catalysis*, 142:325–336, 1993.

[179] A. Davydov, A. Budneva, S. Aliev and V. Sokolovskii. *Reaction Kinetics and Catalysis Letters*, 36:491–495, 1988.

[180] D. Wang, M. Xu, C. Shi and J. Lunsford. *Catalysis Letters*, 18:323–328, 1993.

[181] E. Morales and J. Lunsford. *Journal of Catalysis*, 118:255–265, 1989.

[182] M. Xu, C. Shi, X. Yang, M. Rosynek and J. Lunsford. *Journal of Physical Chemistry*, 96:6395–6398, 1992.

[183] K. Coulter and D. Goodman. *Catalysis Letters*, 20:169–178, 1993.

[184] N. Cant, C. Lukey, P. Nelson and R. Tyler. *Journal of the Chemical Society, Chemical Communications*, 766–768, 1988.

[185] J. Lapszewicz and X. Jiang. *Catalysis Letters*, 13:103–116, 1992.

[186] G. Martin and C. Mirodatos. *Journal of the Chemical Society, Chemical Communications*, 1393–1394, 1987.

[187] C. Mims, R. Hall, K. Rose and G. Myers. *Catalysis Letters*, 2:361–368, 1989.

[188] G. Martin, S. Bernal, V. Perrichon and C. Mirodatos. *Catalysis Today*, 13:487–494, 1992.

[189] J. Geerts, J. van Kasteren and K. van der Wiele. *Catalysis Today*, 4:453–461, 1989.

[190] K. Campbell and J. Lunsford. *Journal of Physical Chemistry*, 92:5792–5796, 1988.

[191] J. van Kasteren, J. Geerts and K. van der Wiele. *Catalysis Today*, 6:497–502, 1990.

[192] K. Campbell, E. Morales and J. Lunsford. *Journal of the American Chemical Society*, 109:7900–7901, 1987.

[193] P. Nelson, C. Lukey and N. Cant. *Journal of Physical Chemistry*, 92:6176–6179, 1988.

[194] P. Nelson and N. Cant. *Journal of Physical Chemistry*, 94:3756–3761, 1990.

[195] P. Nelson, E. Kennedy and N. Cant. *Studies in Surface Science and Catalysis*, 61:89–95, 1991.

[196] M. Utiyama, H. Hattari and K. Tanabe. *Journal of Catalysis*, 53:237–242, 1978.

[197] J. J. Hargreaves, G. J. Hutchings, R. Joyner and S. Taylor. *Applied Catalysis A: General*, 227:191–200, 2002.

[198] O. Buyevskaya, M. Rothaemel, H. Zanthoff and M. Baerns. *Journal of Catalysis*, 146:346–357, 1994.

[199] I. Balint and K. Aika. *Applied Catalysis A: General*, 196:209–215, 2000.

[200] J. van Kasteren, J. Geerts and K. van der Wiele. *Studies in Surface Science and Catalysis*, 61:139–146, 1991.

[201] G. Martin, A. Bates, V. Ducarme and C. Mirodatos. *Applied Catalysis*, 47:287–297, 1989.

[202] J. Roos, S. Korf, R. Veehof, J. van Ommen and J. Ross. *Catalysis Today*, 4:441–452, 1989.

[203] P. Nelson, C. Lukey and N. Cant. *Journal of Catalysis*, 120:216–230, 1989.

[204] N. Cant, C. Lukey and P. Nelson. *Journal of Catalysis*, 124:336–348, 1990.

[205] C. Mims, R. Mauti, A. Dean and K. Rose. *Journal of Physical Chemistry*, 98:13357–13372, 1994.

[206] C. Shi, M. Rosynek and J. Lunsford. *Journal of Physical Chemistry*, 98:8371–8376, 1994.

[207] J. Hargreaves, G. Hutchings and R. Joyner. *Studies in Surface Science and Catalysis*, 61:155–159, 1991.

[208] H. Swaan, A. Toebes, K. Seshan, J. van Ommen and J. Ross. *Catalysis Today*, 13:201–208, 1992.

[209] J. Wang and J. Lunsford. *Journal of Physical Chemistry*, 90:5883–5887, 1986.

[210] M. Wu, C. Truong and D. Goodman. *Physical Review B*, 46:12688 – 12694, 1992.

[211] M. Wu, C. Truong, K. Coulter and D. Goodman. *Journal of the American Chemical Society*, 114:7565–7567, 1992.

[212] M. Wu, C. Truong, K. Coulter and D. Goodman. *Journal of Catalysis*, 140:344–352, 1993.

[213] M. Wu, C. Truong, K. Coulter and D. Goodman. *Journal of Vacuum Science & Technology A: Vacuum, Surfaces, and Films*, 11:2174–2178, 1993.

[214] K. Coulter and D. Goodman. *Catalysis Letters*, 16:191–196, 1992.

[215] K. Coulter, J. Szanyi and D. Goodman. *Catalysis Letters*, 35:23–32, 1995.

[216] R. Nelson and A. Tench. *Journal of Chemical Physics*, 40:2736–2737, 1964.

[217] C. Lin, K. Campbell, J. Wang and J. Lunsford. *Journal of Physical Chemistry*, 90:534–537, 1986.

[218] K. Aika and J. Lunsford. *Journal of Physical Chemistry*, 81:1393–1398, 1977.

[219] M. Iwamoto and J. Lunsford. *Journal of Physical Chemistry*, 84:3079–3084, 1980.

[220] E. Garrone, A. Zecchina and F. Stone. *Journal of Catalysis*, 62:396–400, 1980.

[221] Y. Takita and J. Lunsford. *Journal of Physical Chemistry*, 83:683–688, 1979.

[222] T. Ito, T. Tashiro, T. Watanabe, K. Toi and I. Ikemoto. *Chemistry Letters*, 16:1723–1726, 1987.

[223] K. Zhen, S. Li, Y. Bi, X. Yang and Q. Wei. *Studies in Surface Science and Catalysis*, 91:691–698, 1995.

[224] K. Aika and T. Karasuda. *Studies in Surface Science and Catalysis*, 100:397–406, 1996.

[225] T. Karasuda and K. Aika. *Journal of Catalysis*, 171:439–448, 1997.

[226] T. Karasuda, K. Nagaoka and K. Aika. *Studies in Surface Science and Catalysis*, 119:283–288, 1998.

[227] D. McNamara, S. Korf, K. Seshan, J. van Ommen and J. Ross. *Canadian Journal of Chemical Engineering*, 69:883–890, 1991.

[228] S. Korf, J. Roos, L. Veltman, J. van Ommen and J. Ross. *Applied Catalysis*, 56:119–135, 1989.

[229] F. Larkins and M. Nordin. *Studies in Surface Science and Catalysis*, 81:249–251, 1994.

[230] F. Larkins and M. Nordin. *Journal of Catalysis*, 130:147–160, 1991.

[231] R. Mariscal, J. Soria, M. Pena and J. Fierro. *Journal of Catalysis*, 147:535–543, 1994.

[232] T. Kanno and M. Kobayashi. *Journal of Materials Science Letters*, 16:126–127, 1997.

[233] T. Kanno, J. Horiuchi and M. Kobayashi. *Reaction Kinetics and Catalysis Letters*, 70:73–80, 2000.

[234] J. Zhang, X. Yang, Y. Bi and K. Zhen. *Catalysis Today*, 13:555–558, 1992.

[235] S. Ramasamy, A. Rahman Mohamed and S. Bhatia. *Reaction Kinetics and Catalysis Letters*, 75:353–358, 2002.

[236] G. Hoogendam, A. van Keulen, K. Seshan, J. van Ommen and J. Ross. *Studies in Surface Science and Catalysis*, 81:187–192, 1993.

[237] G. Hoogendam, K. Seshan, J. van Ommen and J. Ross. *Catalysis Today*, 21:333–340, 1994.

[238] S. Korf, J. Ross, J. Vreeman, J. Derksen, J. van Ommen and J. Ross. *Catalysis Today*, 6:417–426, 1990.

[239] A. van Keulen, G. Hoogendam, K. Seshan, J. van Ommen and J. Ross. *Journal of the Chemical Society, Chemical Communications*, 18:1546–1547, 1992.

[240] E. Mallens, J. Hoebink and G. Marin. *Journal of Catalysis*, 160:222–234, 1996.

[241] K. Nagaoka, T. Karasuda and K. Aika. *Journal of Catalysis*, 181:160–164, 1999.

[242] R. Dittmeyer and R. Hoffmann. *Studies in Surface Science and Catalysis*, 81:241–247, 1994.

[243] S. Bartsch, J. Falkowski and H. Hoffmann. *Catalysis Today*, 4:421–431, 1989.

[244] S. Bartsch and H. Hoffmann. *Catalysis Today*, 6:527–534, 1990.

[245] S. Bartsch, H. Pirkl, W. Baumann and H. Hofmann. *Studies in Surface Science and Catalysis*, 61:147–154, 1991.

[246] K. Tiwari, T. Roy, S. Banerjee, S. Ganguly and D. Bhattacharyya. *Journal of Chemical Technology & Biotechnology*, 63:190–194, 1995.

[247] E. Ruckenstein and A. Khan. *Catalysis Letters*, 18:27–35, 1993.

[248] E. Ruckenstein and A. Khan. *Journal of Catalysis*, 141:628–647, 1993.

[249] H. Swaan, A. Toebes, K. Seshan, J. van Ommen and J. Ross. *Catalysis Today*, 13:629–634, 1992.

[250] S. Fuchs, L. Leveles, K. Seshan, L. Lefferts, A. Lemonidou and J. Lercher. *Topics in Catalysis*, 15:169–174, 2001.

[251] E. Mallens, J. Hoebink and G. Marin. *Studies in Surface Science and Catalysis*, 81:205–210, 1994.

[252] K. Otsuka, Q. Liu, M. Hatano and A. Morikawa. *Chemistry Letters*, 15:903–906, 1986.

[253] R. Burch, G. Squire and S. Tsang. *Applied Catalysis*, 46:69–87, 1989.

[254] R. Burch, S. Chalker and S. Hibble. *Applied Catalysis A: General*, 96:289–303, 1993.

[255] S. Conway and J. Lunsford. *Journal of Catalysis*, 131:513–522, 1991.

[256] P. Hinson, A. Clearfield and J. Lunsford. *Journal of the Chemical Society, Chemical Communications*, 1430–1432, 1991.

[257] J. Lunsford, P. Hinson, M. Rosynek, C. Shi, M. Xu and X. Yang. *Journal of Catalysis*, 147:301–310, 1994.

[258] D. Lewis and C. Catlow. *Topics in Catalysis*, 1:111–121, 1994.

[259] Q. Chen, P. Couwenberg and G. Marin. *Catalysis Today*, 21:309–319, 1994.

[260] J. Roos, S. Korf, J. Biermann, J. van Ommen and J. Ross. *Studies in Surface Science and Catalysis*, 55:381–392, 1990.

[261] Å. Slagtern, I. Dahl, K. Jens, E. Hansen and M. Seiersten. *Applied Catalysis A: General*, 91:13–25, 1992.

[262] M. Phillips and A. Eastman. *Catalysis Letters*, 13:157–174, 1992.

[263] A. Santos, C. Finol, J. Coronas, M. Menéndez and J. Santamaría. *Studies in Surface Science and Catalysis*, 81:171–176, 1994.

[264] A. Santos, M. Menéndez and J. Santamaría. *Studies in Surface Science and Catalysis*, 107:373–378, 1997.

[265] M. Miguel, J. Coronas, M. Meméndez and J. Santamaría. *Reaction Kinetics and Catalysis Letters*, 59:277–284, 1996.

[266] M. Taniewski, A. Lachowicz, K. Skutil and D. Czechowicz. *Chemical Engineering Science*, 51:4271–4278, 1996.

[267] N. Amin and S. Pheng. *Chemical Engineering Journal*, 116:187–195, 2006.

[268] G. Dai, Q. Yan, Y. Wang and Q. Liu. *Chemical Physics*, 155:275–284, 1991.

[269] S. Conway, J. Szanyi and J. Lunsford. *Applied Catalysis*, 56:149–161, 1989.

[270] Y. Aksu and M. Driess. *Angewandte Chemie International Edition*, 48:7778–7782, 2009.

[271] J. Ma, Y. Aksu, L. Gregoriades, J. Sauer and M. Driess. *Dalton Transactions*, 39:103–106, 2010.

[272] S. Arndt, Y. Aksu, M. Driess and R. Schomäcker. *Catalysis Letters*, 131:258–265, 2009.

[273] S. Jana, Y. Aksu and M. Driess. *Dalton Transactions*, 9:1516–1521, 2009.

[274] S. Polarz, A. Orlov, A. Hoffmann, M. Wagner, C. Rauch, R. Kirste, Y. Gelhoff, Y. Aksu, M. Driess, M. van den Berg and M. Lehmann. *Chemistry of Materials*, 21:3889–3897, 2009.

[275] R. Burch and M. Hayes. *Journal of Molecular Catalysis A: Chemical*, 100:13–33, 1995.

[276] R. Burch, D. Crittle and M. Hayes. *Catalysis Today*, 47:229–234, 1999.

[277] S. Håkonsen and A. Holmen. Handbook of Heterogeneous Catalysis, chapter 14.11.2 Oxidative Dehydrogenation of Alkanes, 3384–3400. Wiley-VCH Verlag GmbH & Co. KGaA, 2 edition, 2008.

[278] A. Giusti, S. Contarini, C. Flego, S. Palmery and G. Piro. *Catalysis Today*, 6:463–472, 1990.

[279] D. Wang, M. Rosynek and J. Lunsford. *Chemical Engineering & Technology*, 18:118–124, 1995.

[280] B. Wan and H. Chu. *Journal of the Chemical Society, Faraday Transactions*, 88:2943–2947, 1992.

[281] K. Merz, S. Block, R. Schoenen and M. Driess. *Dalton Transactions*, 17:3365–3369, 2003.

[282] K. Hauffe. *Angewandte Chemie*, 67:189–207, 1955.

[283] E. Molinari and G. Parravano. *Journal of the American Chemical Society*, 75:5233–5237, 1953.

[284] C. Gensch and K. Hauffe. *Zeitschrift für physikalische Chemie*, 196:427–437, 1950.

[285] R. Spinicci. *Studies in Surface Science and Catalysis*, 61:173–181, 1991.

[286] S. Kim, L. Erickson and E. Yu. *Journal of Hazardous Materials*, 41:327–340, 1995.

[287] S. Kim, S. Kim and E. Yu. *Applied Catalysis A: General*, 150:63–76, 1997.

[288] C. Chouillett, F. Villain, M. Kermarec, H. Lauron-Pernot and C. Louis. *Journal of Physical Chemistry B*, 107:3565–3575, 2003.

[289] S. Kim. *Journal of Hazardous Materials*, 91:285–299, 2002.

[290] I. E. Wachs. *Catalysis Today*, 100:79–94, 2005.

[291] K. Chen, A. Bell and E. Iglesia. *Journal of Catalysis*, 209:35–42, 2002.

[292] A. Dinse, B. Frank, C. Hess, D. Habel and R. Schomäcker. *Journal of Molecular Catalysis A: Chemical*, 289:28–37, 2008.

[293] R. Shannon and J. Pask. *Journal of the American Ceramic Society*, 48:391–398, 1965.

[294] R. Rodríguez-Talavera, S. Vargas, R.Arroyo-Murillo, R. Montiel-Campos and E. Haro-Poniatowski. *Journal of Materials Research*, 12:439–443, 1997.

[295] B. Lippens and J. de Boer. *Acta Crystallographica*, 17:1312–1321, 1964.

[296] N. Cant, E. Kennedy and P. Nelson. *Journal of Physical Chemistry*, 97:1445–1450, 1993.

# Abbreviations

| | |
|---|---|
| AAS | Atomic Absorption Spectroscopy |
| BET | Brunauer Emmer Teller |
| $C_2$ | Ethane + Ethylene |
| CVD | Chemical Vapor Deposition |
| DC | Direct Current |
| DFT | Density Functional Theory |
| DRIFTS | Diffuse Reflectance Fourier Transform Infrared Spectroscopy |
| ENDOR | Electron Nuclear Double Resonance Spectroscopy |
| EPR | Electron Paramagnetic Resonance |
| ESR | Electron Spin Resonance |
| eV | Electron Volt |
| FID | Flame Ionization Detector |
| FT | Fischer Tropsch |
| FT-IR | Fourier Transform Infrared Spectroscopy |
| FWHH | Full Width at Half Height |
| GC | Gas Chromatograph |
| HREELS | High Resolution Electron Energy Loss Spectroscopy |
| HR-TEM | High Resolution Transmission Electron Microscopy |
| IR | Infrared |
| KIE | Kinetic Isotope Effect |
| LC | Low Coordination |
| MAS | Magic Angle Spinning |
| MBOH | 2-methyl-3-butyn-2-ol |
| MFC | Mass Flow Controller |
| NMR | Nuclear Magnetic Resonance Spectroscopy |
| OCM | Oxidative Coupling of Methane |
| ODE | Oxidative Dehydrogenation of Ethane |
| ODH | Oxidative Dehydrogenation |
| ODP | Oxidative Dehydrogenation of Propane |
| PFTR | Plug Flow Tubular Reactor |
| S | Selectivity |

| | |
|---|---|
| SEM | Scanning Electron Microscopy |
| SSITKA | Steady State Isotopic Transient Kinetic Analysis |
| TAP | Temporal Analysis of Products |
| TCD | Thermal Conductivity Detector |
| TD | Time Dependent |
| TEM | Transmission Electron Microscopy |
| TPPM | Two Pulse Phase Modulation |
| TPD | Temperature Programmed Desorption |
| TPR | Temperature Programmed Reaction |
| UHF | Unrestricted Hartree-Fock |
| UHV | Ultra High Vacuum |
| X | Conversion |
| XANES | X-ray Absorption Near Edge Structure |
| XPS | X-Ray Photoelectron Spectroscopy |
| XRD | X-Ray Diffraction |

# Acknowledgement

I would like to thank Prof. Dr. Schomäcker for giving me the opportunity working on the interesting and challenging topic of C-H activation of lower alkanes, his interest in the research work and for the helpfull discussions. Moreover, I thank Prof. Dr. Baerns for being the second examiner.

I thank all the members of the research group, especially Gabriele Vetter, Torsten Otremba, Dr. Guillaume Laugel, Dr. Hary Soerijanto, Christa Löhr and Prof. Dr. Peter Hugo, for their support and discussions and the pleasant working atmosphere.

I am especially in dept to Mr. Torsten Otremba, whose automatisation of the experimental set-up enabled the performance of long-term experiments, and Mr. Axel Schiele and the workshop for their support with the equipment.

I thank Dr. Yilmaz Aksu, Stephan Heitz, Stephan Schutte, Burcu Uysal and Prof. Dr. Matthias Driess for their discussions and the preparation of various catalysts.

I thank Ulla Simon, Dr. Almuth Berthold, Dr. Oliver Görke, Manuel Harth and Prof. Dr. Helmut Schubert for their discussions, the preparation of various catalysts and their help with certain analytical procedures.

I thank Dr. Traugott Scheytt and his team for the performance of the AAS analysis. Dr. Nakhal for the $H_2S$ pretreatment of the Li/MgO catalyst.

I thank to Dr. Thomas Risse, Dr. Raimund Horn and Dr. Sergey Levchenko for their valuable advice and the discussions.

I thank my apprentices Mrs. Anna Paliszewska and Mr. Domenic Jelinski, who for their support with the sample preparation and analysation, and their hard work. I also thank my trainee Pauline Mazurkiewiez for her work.

I thank Prof. Dr. Arne Thomas for the permission to use his multi-sampling XRD machine and willingness to act as chairman. I thank Dr. Kamalakannan Kailasam for the XRD measurements.

I thank Mr. Reichert and his team for repairing and preparing used glas devices.

I thank Mr. Lenz from Agilent showing me the secrets of developing GC methods.

I thank the Helmholtz Center Berlin for the permission to use their electron microscope and the ZELMI (Zentrales Laboratorium für Elektronenmikroskopie, TU Berlin) for TEM analyses.

I thank like to thank the Deutsche Forschungsgemeinschaft for funding the Excellence Cluster “Unicat” (Unifying Concepts in Catalysis) and the IMPRS (International Max Planck Research School) of the Fritz Haber Institute of the Max Planck Society for financial support.

# Curriculum Vitae

**Personal Data**

| | |
|---|---|
| Name | Sebastian Arndt |
| Date of Birth | 31.10.1980 |
| Place of Birth | Meiningen |
| Nationality | German |

**Education**

| | |
|---|---|
| 1991 - 2000 | Gymnasium Bad Königshofen, Abitur |
| 2001 - 2003 | Study of Chemistry at Humboldt University of Berlin<br>Intermediate Exam August 2003 |
| 2003 - 2004 | Study of Chinese Language and Culture at Ocean University of China |
| 2004 - 2007 | Study of Chemistry at Humboldt University of Berlin<br>Final Exam for "Diplom Chemiker" in October 2006<br>Thesis in Physical Chemistry under Supervision of Prof. Dr. Rademann<br>Title: Investigation of the Conversion of Biomass under Supercritical Conditions - Hydropyrolysis of Model Compounds: Glucose, Alanine and Glycine |
| since 2007 | Ph.D. Student at the Institute of Chemistry, Technical University Berlin, under Prof. Dr. Schomäcker |

# Selbstständigkeitserklärung

Hiermit erkläre ich, dass ich die vorliegende Arbeit selbstständig und nur unter Verwendung der angegebenen Literatur und Hilfsmittel angefertigt habe.

Sebastian Arndt